

**Imperial College
London**

Imperial College London
National Heart and Lung Institute

**M6A RNA Methylation in Diabetes Induced
Endothelial Damage and Ischaemic Disease**

Walid Khalid Sweaad

Supervisor: Professor Costanza Emanuelli
Co-supervisor: Aránzazu Chamorro-Jorganes

This thesis is submitted to Imperial College London for the degree of
Doctor of Philosophy (PhD)

Declaration of Originality

I, Walid Khalid Sweaad, confirm that the work presented in this thesis is my own. Where information or contributions have been derived from other sources, I confirm that this has been indicated in the thesis.

Copyright Statement

The copyright of this thesis rests with the author, Walid Khalid Sweaad. Unless otherwise indicated, its contents are licensed under a Creative Commons Attribution-Non-Commercial-No Derivatives 4.0 International Licence (CC BY-NC-ND). Under this licence, you may copy and redistribute the material in any medium or format on the condition that; you credit the author, do not use it for commercial purposes and do not distribute modified versions of the work. When reusing or sharing this work, ensure you make the licence terms clear to others by naming the licence and linking to the licence text. Please seek permission from the copyright holder for uses of this work that are not included in this licence or permitted under UK Copyright Law.

بِسْمِ اللَّهِ الرَّحْمَنِ الرَّحِيمِ

For My Family.

Abstract

Diabetes mellitus exposes endothelial cells (ECs) to a chronic hyperglycaemic milieu, leading to dysfunction of the vascular endothelium. The resulting microvasculature rarefaction leads to tissue hypoperfusion and propagates the occurrence of ischaemic events, such as critical limb ischaemia and ischaemic heart disease. Moreover, hyperglycaemia impairs the angiogenic potential of ECs thereby compromising post-ischaemic reparative neovascularisation. N6-methyladenosine (m6A) is emerging as a new layer for fine-tuning gene expression. The functional importance of m6A has been revealed in a plethora of fundamental bioprocesses, while its dysregulation has been linked to several diseases including diabetes. However, our understanding of the precise roles of m6A in the cardiovascular system is still in its infancy and its significance in diabetes associated complications of the vasculature remains completely unexplored. This study elucidates a novel role for METTL3, the primary m6A methylase, in the regulation of angiogenesis. Loss and gain of function studies reveal METTL3 to be crucial in the modulation of EC processes that are conducive to angiogenesis *in vitro* and *in vivo*. Mechanistically, METTL3 modulates angiogenesis by mediating the endothelial bioprocessing of the angiogenic miRNAs let-7e and the miR-17-92 cluster. Expressional analysis revealed a dysregulation of m6A and METTL3 in human ECs exposed to diabetic and ischaemic mimicking conditions, ECs derived from a murine model of diabetic LI and in left ventricular tissue and ECs isolated from diabetic mouse hearts. The therapeutic potential of endothelial METTL3 was demonstrated using murine models of diabetic limb ischaemia and myocardial infarction. Here, the adenovirus mediated overexpression of METTL3 in ischaemic limb muscles improved post-ischaemic muscular neovascularisation. Additionally, infarcted hearts treated with Ad.METTL3 showed an increase in arteriole and capillary

densities while exhibiting improved contractile function. Thus, the findings in this thesis suggest that the modulation of METTL3 could represent novel therapeutic target for ischaemic complications in diabetic patients.

Publications arising from this thesis

Aránzazu Chamorro-Jorganes*, **Walid K Sweaad***, Rajesh Katare, Marie Besnier, Maryam Anwar, N Beazley-Long, Graciela Sala-Newby, Iñigo Ruiz-Polo, Dhananjie Chandrasekera, Alison A Ritchie, Andrew V Benest, Costanza Emanuelli. (2021) METTL3 regulates angiogenesis by modulating let-7e-5p and miRNA-18a-5p expression in endothelial cells. *Arteriosclerosis, Thrombosis, and Vascular Biology* 41 (6), e325-e337 ***Co-first author**

Walid Khalid Sweaad, Francesca Maria Stefanizzi, Aránzazu Chamorro-Jorganes, Yvan Devaux, Costanza Emanuelli. (2021) Relevance of N6-methyladenosine regulators for transcriptome: Implications for development and the cardiovascular system. *Journal of Molecular and Cellular Cardiology*. 160, pp. 56–70

Publications aside from the work in this thesis

Marie Besnier, Saran Shantikumar, Maryam Anwar, Parul Dixit, Aranzazu Chamorro-Jorganes, **Walid K Sweaad**, Graciela Sala-Newby, Paolo Madeddu, Anita C Thomas, Lynsey Howard, Sobia Mushtaq, Enrico Petretto, Andrea Caporali, Costanza Emanuelli. (2019) miR-15a/-16 inhibit angiogenesis by targeting the Tie2 coding sequence: therapeutic potential of a miR-15a/16 decoy system in limb ischemia. *Molecular Therapy-Nucleic Acids*. 17, 49-62

Sezin Aday, Inbal Hazan-Halevy, Aranzazu Chamorro-Jorganes, Maryam Anwar, Meir Goldsmith, Nicholas Beazley-Long, Susmita Sahoo, Navneet Dogra, **Walid K Sweaad**, Francesco Catapano, Sho Ozaki-Tan, Gianni D Angelini, Paolo Madeddu, Andrew V Benest, Dan Peer, Costanza Emanuelli. (2021) Bioinspired artificial exosomes based on lipid nanoparticles carrying let-7b-5p promote angiogenesis *in vitro* and *in vivo*. *Molecular Therapy*. 29 (7), 2239-2252

Selected Awards and Conferences

EU COST Action STSM Travel Grant (2020)

Diabetes UK Annual Conference, Glasgow, Scotland (2020)

The Chelmsford and District Diabetes UK Group £5000 Award (2019)

British Society for Gene and Cell Therapy, Sheffield, England (2019)

Acknowledgements

This accomplishment is a gift bestowed upon me from my colleagues, family and loved ones who supported me in different ways throughout this journey.

I would firstly like to express my sincere appreciation to the primary supervisor of this project, Professor Costanza Emanuelli. I am grateful for the opportunity to have been able to embark on this journey and the countless lessons learned which I will carry with me for a long time. Thank you. A very special thank you goes to Dr Aránzazu Chamorro-Jorganes, my secondary supervisor. It is rare in life that you encounter an individual who truly embodies their passion – Aran is one. Principled, diligent, forward thinking while encouraging new ideas and independent thought, Aran epitomizes a scientific mentor. I will always cherish the countless hours we spent together in the lab and the expertise I gained in this time. Today I am blessed to consider her a friend.

I am especially grateful to Dr Marie Besnier and the time she committed to thoroughly training me in the hindlimb ischaemia surgery and aiding in the experimental work outlined in chapter 4. Her tenacious and meticulous approach to science is contagious and I am blessed to have been exposed to it. I would also like to thank Professor Paolo Madeddu for allowing me to operate under his Project Licence. Thank you to Dr Graciela Sala-Newby for providing the crucial adenoviruses utilised in this study and her consistent willingness to share her vast expertise. I would like to express my gratitude to Professor Rajesh Katare, who kindly agreed to host me in his lab at the University of Otago while the COVID-19 pandemic impeded all animal-based studies in the UK. When this did not come to fruition, Rajesh ensured that key experiments composing the 6th chapter were performed. I would also like to thank Dr Andrew Benest for his collaboration on the Matrigel Plug model. A big thank you to the entire National Heart and Lung Institute for facilitating this project and a special thank you to

Tony Umelo for his kind support during my most difficult time. Lastly, I would like to thank Diabetes UK for funding my research and the proactive approach they maintain in supporting their beneficiaries.

A special thank you goes to Dr Graeme Birdsey. Although many years have passed since I was his Master's student, Graeme has remained a kind and nurturing presence throughout this PhD. Aside from my scientific and personal development, this 4-year journey has blessed me with the opportunity to connect with, and in some instances, form lifelong friendships with people from all walks of life, many of whom I would have never crossed paths with if not for our shared passion for science. Thank you to Dr Moumita Sarkar for her scientific expertise and more importantly her positive and motivational outlook. Thank you to Dr Fabiana Martino for the good vibes and to Natasha De Winter. A heartfelt thank you to soon-to-be Dr Pragati Pandey and Cathy Jenkins. Sharing the peaks and valleys of this adventure has been one of the highlights of my PhD. I am extremely blessed that our journeys crossed paths.

Most importantly, I would like to thank my Mother, Suad Mohamed Elghawi and my Father, Khalid Mohamed Sweaad. Their love and sacrifice is the foundation on which every accomplishment in my life is built on. I would like to thank my grandmother Hamida Yusef Shalabi for all her love and wisdom and my siblings Esrah, Sofian and Ismeel for always believing in me. I would particularly like to acknowledge my brother Sofian, who despite being younger in age, has unknowingly inspired me through his resilience in the face of adversity. I dedicate this achievement to the memory my loving grandfather Mohamed Bashir Elghawi.

Table of Contents

List of Figures	15
List of Tables	17
Abbreviations	18
1. Introduction	22
1.1 The Vascular System.....	22
1.1.1 The Endothelium in Vascular Homeostasis.....	23
1.1.2 Mechanisms of Angiogenesis	24
1.2 Diabetes Mellitus	29
1.2.1 Epidemiology and Pathophysiology of T2DM	29
1.2.2 Cardiovascular Complications of Diabetes	31
1.3 Therapeutic Angiogenesis.....	36
1.3.1 Methods and Approaches for Therapeutic Angiogenesis.....	38
1.4 Introduction to MicroRNAs	42
1.4.1 Biogenesis of miRNAs.....	43
1.4.2 Mechanisms of miRNA Mediated Gene Regulation	46
1.5 m6A RNA Methylation	46
1.5.1 M6A Regulatory Machinery – Writers	48
1.5.2 M6A Regulatory Machinery – Erasers	50
1.5.3 M6A Regulatory Machinery – Readers	52
1.6 Detection Methods of m6A.....	55
1.7 m6A in the Regulation of Different RNA Species.....	64
1.7.2 m6A Methylation of Primary miRNAs	68
1.8 Biological Impact of m6A RNA Modifications	70
1.8.1 Implications of m6A in Cardiac Homeostasis and Disease.....	70
1.8.2 Role of m6A in the Vasculature	75
1.8.3 m6A in Cardiovascular Disease Risk Factors	80
1.9 Study Rationale and Hypothesis	83
2. Materials and Methods.....	87
2.1 Cell Culture.....	87
2.1.1 HUVEC and HCMEC Culture.....	87
2.1.2 <i>In vitro</i> Diabetic and Ischaemic Mimicking conditions	87
2.2 Delivery of Short Interfering RNA and Mimic miRNA	88
2.3 Stable METTL3 Knockdown Generation	89
2.4 Adenoviral Transduction	90
2.5 EC Isolation from Murine Hearts and Limb Muscle	91

2.6 RNA Isolation from Cells or Mouse Tissue.....	92
2.7 cDNA Synthesis	92
2.8 Quantitative Real-Time PCR	93
2.9 Immunoblotting.....	95
2.9.1 Preparation of Whole Cell Lysates	95
2.9.2 Western Blotting	96
2.10 Quantification of m6A RNA Methylation	97
2.11 BrdU Incorporation Assay	99
2.12 Caspase-Glo Assay	99
2.13 Migration Assay	100
2.14 <i>In vitro</i> Matrigel Assay	100
2.15 Fibrin Bead Assay	101
2.16 Animal Studies.....	101
2.16.1 <i>In Vivo</i> Matrigel Plug.....	102
2.16.2 Induction of Type-1 Diabetes	103
2.16.3 Mouse Hind Limb Ischaemia Model.....	103
2.16.4 Myocardial Infarction (MI) Model	104
2.16.5 Echocardiography.....	105
2.17 Immunohistochemistry	106
2.18 Bioinformatic Analysis	108
2.19 Statistical Analysis	109
3. METTL3 Regulates Angiogenesis by Modulating let-7e-5p and miRNA-18a-5p Expression in ECs.....	111
3.1 Introduction.....	111
3.2 Results.....	114
3.2.1 METTL3 Depletion in ECs Impairs Key Angiogenic Processes <i>In Vitro</i>	114
3.2.2 METTL3 Overexpression in ECs Improves Angiogenesis <i>in vitro</i> ...	119
3.2.3 Endogenous METTL3 is Required for the Bioprocessing of let-7e and the miR-17-92 Cluster in ECs	123
3.2.4 METTL3 Modulates Tsp1 by Regulating miR-18a-5p and let-7e-5p Expression.....	127
3.2.5 METTL3 Overexpression Modulates the Expression of let-7e-5p, the miR-17-92 Cluster and Tsp1 Expression.....	131
3.2.6 The Overexpression of let-7e and miR-18a Restores the Angiogenic Capacity of METTL3 Depleted ECs <i>In Vitro</i>	133
3.2.7 Depletion of METTL3 in ECs Impairs Angiogenesis While its Overexpression Improves Angiogenesis <i>in vivo</i>	136
3.3 Discussion.....	141

4. Endothelial m6A and its Regulatory Components are Dysregulated in Diabetic Models <i>In Vitro</i> and <i>In Vivo</i>.....	147
4.1 Introduction.....	147
4.2 Results.....	151
4.2.1 Optimization of Timepoints for Expressional Analysis of m6A Regulatory Components	151
4.2.2 METTL3 and Total m6A RNA Levels are Dysregulated by High Glucose and Hypoxia in ECs.....	153
4.2.3 Expression of METTL3 in the Murine Model of Diabetic LI.....	157
4.2.4 Expressional Analysis of m6A and its Regulatory Components in Diabetic Murine Hearts	161
4.3 Discussion.....	164
5. Effects of METTL3 Overexpression in CLI Post-ischaemic Neovascularization and Blood Flow Recovery	174
5.1 Introduction.....	174
5.2 Results.....	179
5.2.1 The Rescue of METTL3 Using Ad.METTL3 Improves Angiogenesis in Pathogenic Conditions <i>In Vitro</i>	179
5.2.2 Optimization of Adenoviral Concentration for the Delivery of METTL3 to Ischaemic Limb Muscles.....	183
5.2.3 <i>In Vivo</i> Validation of Adenovirus Mediated METTL3 Overexpression in Ischaemic Limb Muscle ECs	185
5.2.4 Effects of METTL3 Overexpression on Post-LI Blood Flow Recovery	187
5.2.5 Ad.METTL3 Treatments Improve Post-LI Neovascularisation	190
5.2.6 Effects of METTL3 Overexpression on Toe Survival	193
5.3 Discussion.....	197
6. Effects of Exogenous METTL3 Supplementation on Post-myocardial Neovascularization and Cardiac Function	206
6.1 Introduction.....	206
6.2 Results.....	211
6.2.1 Validation of Adenovirus Mediated METTL3 Overexpression in the Ischaemic Myocardium.....	211
6.2.2 Exogenous METTL3 Supplementation Promotes Post-MI Neovascularisation	213
6.2.3 Post-MI Ad.METTL3 Treatments Reduces Cardiac Apoptosis	215
6.2.4 Post-MI Ad.METTL3 Treatments Attenuates Ischaemia Induced Loss of Cardiac Function	217
6.3 Discussion.....	222
7 Final Conclusions and Future Perspectives	229

7.2 Future Perspectives	236
References	239
Appendix 1	255
Appendix 2	256
Appendix 3	257

List of Figures

Chapter 1

- Figure 1.1 Overview of angiogenic process
Figure 1.2 Various micro- and macrovascular complications of diabetes
Figure 1.3 overview of the canonical miRNA biogenesis process
Figure 1.4A The m6A modification and it's regulatory machinery.
Figure 1.4B Conservation of m6A regulator proteins among species
Figure 1.5 m6A detection methods

Chapter 3

- Figure 3.1 METTL3 depletion in ECs impairs key angiogenic processes *in vitro*
Figure 3.2 METTL3 overexpression in ECs improves angiogenesis *in vitro*
Figure 3.3 METTL3 depletion in ECs decreases the levels of let-7e and miR-17-92
Figure 3.4 miR-18a-5p and let-7e-5p overexpression reduces Tsp1 expression while METTL3 depletion increases its expression
Figure 3.5 METTL3 overexpression increases the levels of let-7e and miR-17-92 and decreases Tsp1 expression
Figure 3.6 The overexpression of let-7e and miR-18a restores the angiogenic capacity of METTL3 depleted ECs *in vitro*
Figure 3.7 Depletion of METTL3 in ECs impairs angiogenesis while its overexpression improves angiogenesis in an *in vivo* Matrigel plug assay
Figure 3.8 Schematic summering the role of METTL3 mediated m6A in the regulation of angiogenesis

Chapter 4

- Figure 4.1 Establishing the optimal timepoint for the expressional analysis of m6A regulatory components in *in vitro* DM mimicking EC model
Figure 4.2 m6A and its regulators are dysregulated by high glucose and hypoxia in ECs
Figure 4.3A Schematic demonstrating experimental workflow
Figure 4.3B-E Expression of endogenous METTL3 is dysregulated in muscle-derived ECs after limb ischaemia in diabetic mice LI
Figure 4.4 *In vivo* and clinical expressional analysis of m6A machinery

Chapter 5

- Figure 5.1 METTL3 overexpression rescues the impaired angiogenic phenotype of "diabetic ECs *in vitro*"
Figure 5.2 Optimization of adenoviral concentration for the delivery of METTL3 to ischaemic limb muscles
Figure 5.3A Schematic demonstrating experimental workflow
Figure 5.3B-D Validation of human METTL3 overexpression in mouse muscle-derived ECs
Figure 5.4A Schematic demonstrating experimental workflow
Figure 5.4B-E Effects of METTL3 overexpression on post-LI blood flow recovery
Figure 5.5 METTL3 overexpression improves post-ischaemic angiogenesis
Figure 5.6A Toe necrosis visual score-based system
Figure 5.6B Effects of METTL3 overexpression on toe survival

Chapter 6

Figure 6.1A

Schematic demonstrating experimental workflow

Figure 6.1B

Validation of adenoviral mediated METTL3 overexpression in the ischaemic myocardium

Figure 6.2

Exogenous METTL3 supplementation promotes post-MI neovascularisation

Figure 6.3

3 Post-MI Ad.METTL3 treatments reduces cardiac apoptosis and fibrosis

Figure 6.4

Post-MI Ad.METTL3 treatments attenuates ischaemia induced loss of cardiac function

Chapter 7

Figure 7.1

General summary of thesis findings

List of Tables

Chapter 1

Table 1.1	Reported involvement of m6A regulators in CVS and CVD
-----------	---

Chapter 2

Table 2.1	List of siRNAs and miRNA mimics
Table 2.2	List of lentiviral constructs
Table 2.3	qRT-PCR cycling conditions
Table 2.4	Oligonucleotides used for qRT-PCR
Table 2.5	Antibodies used for Western blotting
Table 2.6	Animals used for <i>in vivo</i> studies
Table 2.7	List of antibodies utilised for IHC studies

Abbreviations

ACS	Acute coronary syndromes
Ad.METTL3	Adenoviral particles carrying METTL3
AGE	Advanced glycation end products
ALKBH5	Alpha-Ketoglutarate-Dependent Dioxygenase AlkB Homolog
ANG-1	Angiotensin-1
ANG-2	Angiotensin-2
AGO	Argonaute
BF	Blood flow
BMMSC	Bone marrow-mesenchymal stem cell
CVD	Cardiovascular disease
CVS	Cardiovascular system
CCS	Chronic coronary syndromes
CDS	Coding sequence
CM I	Consensus methylation motif I
Ad.Null	Control adenovirus
LV-CT-ShRNA	Control Short Hairpin RNA
CABG	Coronary artery bypass grafting
CAD	Coronary artery disease
CHD	coronary heart disease
CLI	Critical limb ischaemia
DART-seq	Deamination adjacent to RNA modification targets
DM	Diabetes mellitus
DGCR8	DiGeorge Critical Region 8
DVL1	Dishevelled 1
DO	Distraction Osteogenesis
ER	Endoplasmic reticulum
EVT	Endoscopic third ventriculostomy
EC	Endothelial cell
EPC	Endothelial progenitor cells
EHT	Endothelial-to-haematopoietic transition
ECM	Extracellular matrix
FTO	Fat-mass and obesity-associated protein
FFA	Free fatty acid
HSPC	Haematopoietic stem and progenitor cell
HNRNP	heterogeneous nuclear ribonucleoprotein
HG	High glucose
HFD	High-fat diet
HCMEC	Human cardiac microvascular endothelial cells
HUVEC	Human umbilical vein endothelial cells
HIF-1 α	Hypoxia Inducible Factor-1 α
H/R	Hypoxia/reoxygenation
IP	Immunoprecipitation
IR	Insulin resistance
IGF1	Insulin/insulin-like growth factor 1

ICAM-1	Intercellular adhesion molecule-1
I/R	Ischaemia/reperfusion
IHD	Ischaemic heart disease
LDI	Laser doppler imaging
LAD	Left anterior descending coronary artery
LV	Left ventricle
LVAW	Left ventricle anterior wall
LVEF	Left ventricle ejection fraction
LVFS	Left ventricle fractional shortening
LVID	Left ventricle intraventricular cavity
LV Vol	Left ventricle intraventricular volume
LVPW	Left ventricle posterior wall
db/db	Leprdb/db
LI	Limb ischaemia
lncRNA	long non-coding RNA
LDL	Low-density lipoproteins
m6A-CLIP	M6A cross-linking immunoprecipitation
miCLIP	M6A individual nucleoside resolution cross-linking and immunoprecipitation
MeRIP-seq	M6A RNA immunoprecipitation-seq
m6A-LAIC-seq	M6A-level and isoform-characterization sequencing
MAZTER-seq	M6A-sensitive RNA digestion and sequencing
MMP	Matrix metalloproteinase
MSC	Mesenchymal stem cell
METTL14	Methyltransferase-like 14
METTL16	Methyltransferase-like 16
METTL3	Methyltransferase-like 3
LV-METTL3-shRNA	METTL3 Short Hairpin RNA
miRNA	MircoRNA
MOI	Multiplicity of infection
MI	Myocardial infarction
m1A	N1-methyladenosine
m6Am	N6, 2-O-dimethyladenosine
m6A	N6-methyladenosine
NO	Nitric oxide
NF-kB	Nuclear factor-kB
OSC	Osmotic control
Ox-LDL	Oxidized low-density lipoprotein
PDX1	Pancreatic and duodenal homeobox 1
PAD	Peripheral artery disease
PA-m6A-seq	Photo-crosslinking-assisted m6A sequencing
PFU	Plaque forming units
pDNA	Plasmid DNA
PAI-1	Plasminogen activator inhibitor-1
PDGF-B	Platelet-derived growth factor B
PSC	Pluripotent stem cell

PGD2	Prostaglandin D2
PGH ₂	Prostaglandin H ₂
PKC	Protein kinase C
PHD	Proyl hydroxylase domain
ROS	Reactive oxygen species
rRNA	ribosomal RNA
REPIC	RNA EPItranscriptome Collection
m6A-REF-seq	RNA-endoribonuclease-facilitated sequencing
RISC	RNA-induced silencing complex
SAM	S-Adenosyl methionine
SCARLET	site-specific cleavage and radioactive-labelling
siRNA	Small interfering RNA
Tsp1	Thrombospondin-1
TXA ₂	Thromboxane A ₂
TIMP	Tissue inhibitors of metalloproteinases
tRNA	transfer RNA
TGF-β	Transforming growth factor-β
TNF-α	Tumor necrosis factor-α
T1DM	Type 1 diabetes mellitus
T2DM	Type 2 diabetes mellitus
UTR	Untranslated region
VCAM-1	Vascular cell adhesion molecule-1
VEGF	Vascular endothelial growth factor
VE-cadherin	Vascular endothelial-cadherin
VSMC	Vascular smooth muscle cell
VIRMA	Vir like m6A methyltransferase associated
VHL	Von Hippel-Lindau protein
VWF	von Willebrand factor
WTAP	Wilm's tumour 1 associated protein
YTHDC1	YTH domain-containing 1
YTHDC2	YTH domain-containing 2
YTHDF1	YTH N6-methyladenosine RNA-binding protein 1
YTHDF2	YTH N6-methyladenosine RNA-binding protein 2
YTHDF3	YTH N6-methyladenosine RNA-binding protein 3
αKG	α-ketoglutarate

Chapter 1
Introduction

1. Introduction

1.1 The Vascular System

The vascular circulatory system is comprised of the heart, blood and vessels and is the first organ system to form during embryonic development. The primary function of the vasculature is the delivery of oxygen and nutrients to peripheral cells, tissues and organs in line with their metabolic demand. The vascular system is also imperative for the removal and transport of waste, regulation of blood pressure and facilitating the deployment of immune responses. Dysfunctions in the vascular system therefore result in critical pathologies including tumour angiogenesis and cardiovascular diseases (CVD) such as atherosclerosis, hypertension, and ischaemic heart disease (IHD) [3].

The formation of the vascular system occurs through two main mechanisms, vasculogenesis and angiogenesis. Vasculogenesis is the de novo development of vessels from mesoderm-derived endothelial progenitor cells (EPCs) termed angioblasts which eventually differentiate into ECs. Angiogenesis is the complex process of forming new blood vessels from existing ones, regulated by a balance of pro-angiogenic and anti-angiogenic factors. It involves ECs proliferation, migration, differentiation, and extracellular matrix (ECM) remodelling [3]. The first vessels to form during embryogenesis through vasculogenesis are the cardinal vein and the dorsal aorta followed by the assembly of a primitive vascular labyrinth through the angiogenic process. The nascent vasculature is progressively expanded by the sprouting of new vessels from the pre-existing vasculature to form a highly organised network of larger vessels ramifying into smaller ones. This eventual hierarchical arrangement of arteries, veins and capillaries allows the vascular system to effectively function as a closed loop made up of distinct yet interconnected complex of arterial and venous

vessels. Functionally, the arteries which branch off into smaller arterioles and eventually capillaries deliver oxygenated blood and nutrients away from the heart and to tissues and organs around the body under high pressure. The veins return deoxygenated blood and waste products to the heart at low pressure with pulmonary system of vessels being the exception [9].

1.1.1 The Endothelium in Vascular Homeostasis

Both arteries and veins are composed of distinct yet closely interacting cell types. ECs line the lumen of every blood vessel wall and exhibit diverse phenotypes and functions depending on the class of vessel they line. Second are mural cells which encompass pericytes or vascular smooth muscle cells (VSMCs) in the macrovasculature. These cells sheath the outer walls of blood vessels, providing mechanical support to the pulsatile flow-induced wall shear stress and transmural pressure. Communication between mural cells and the endothelium also ensures synchronization of endothelial-mural functions along the vascular wall by sending signals through paracrine pathways and direct physical contact. This is facilitated by the vessel basement membrane—a specialized ECM layer that separates ECs from the mural cells. The basement membrane consists of a complex network of proteins, notably collagen, laminin, and proteoglycans. It primarily functions to provide structural support, regulate vessel permeability, and influence cellular processes including migration, proliferation, and differentiation [9].

A crucial factor released by the endothelium is nitric oxide (NO), originally identified as endothelium derived relaxing factor. Prostacyclin and bradykinin are other endothelium derived vasodilators. Prostacyclin acts in synergy via NO to inhibit platelet aggregation while bradykinin promotes the production of tissue plasminogen activator and thus regulates fibrinolysis. Vasoconstricting factors are also produced by

the endothelium and include endothelin, reactive oxygen species (ROS), prostaglandin H₂ (PGH₂), angiotensin-2 (ANG-2) and thromboxane A₂ (TXA₂) [7]. Damage to the endothelial layer results in the disruption of the delicate balance between vasodilation and constriction thus promoting or exacerbating a number of pathologies.

Although a simple monolayer, the endothelium is vital to the maintenance of homeostasis in the vascular system by functioning as the direct interface between circulating blood and the rest of the body. This therefore allows the endothelium to function as a physical barrier to regulate the movement of materials into and out of the bloodstream and as a signal transducer for circulating vasoactive factors and physical signals. ECs respond to these prompts and signals by producing active substances or through physical responses to promote or offset a plethora of crucial processes such as vascular permeability, inflammation, vascular tone and most relevant to this project, angiogenesis.

1.1.2 Mechanisms of Angiogenesis

Angiogenesis is a highly complex and regulated process whereby neo-vessels are formed from the pre-existing vasculature. Although numerous modes of vessel formation and restructuring have been described, such as the aforementioned vasculogenesis, intussusception and vessel co-option by tumour cells, sprouting angiogenesis accounts for the largest proportion of vessel growth and is the focus of this project. The developed vasculature is said to be quiescent and rarely forms new vessels, despite this ECs retain high plasticity to respond to proangiogenic signals. This is important for a number of physiological processes such as wound healing and the menstrual cycle. The mechanisms of angiogenesis are considered as a series of

sequential steps which are directly and indirectly regulated by numerous cytokines and growth factors.

Oxygen levels surrounding a tissue bed are detected by enzymes known as prolyl hydroxylase domain (PHDs) which set off a cascade of events leading to the formation of a new blood vessel upon stimulation by hypoxic conditions. Under normoxic conditions the cytoplasmically synthesised Hypoxia Inducible Factor-1 α (HIF-1 α) are quickly hydroxylated by PHDs and are subsequently degraded by the von Hippel-Lindau protein (VHL) [1]. Hypoxia impairs PHD-enabled hydroxylation, leading to the accumulation of HIF-1 α in the cytoplasm. The subsequent translocation of HIF-1 α to the nucleus results in the upregulation of pro-angiogenic factors, most predominate of which is the Vascular Endothelial Growth Factor (VEGF) family of proteins. VEGF-A plays the most active role in the progression of angiogenesis where it binds to the endothelial specific tyrosine kinase receptor VEGF receptor 2 (VEGFR-2) in the neighbouring vasculature. This in turn activates the quiescent endothelium to initiate a molecular and cellular cascade required for the formation of a new blood vessel and ultimately oxygenate the surrounding hypoxic tissue [2]. The first morphological change is the destabilisation of the vessel through the proteolytic degradation of the surrounding basement membrane by matrix metalloproteinases (MMPs) and the subsequent detachment of the surrounding mural cells in response to Angiopoietin-2 signalling. An angio-competent microenvironment is established by the loosening of endothelial junctions and vessel dilation to increase permeability and enable the extravasation of plasma proteins and deposit of a transient ECM [3].

To prevent ECs moving en masse towards the angiogenic signal, a single EC known as the tip cell is selected. The process of tip and stalk cell specification is regulated by the NOTCH pathway in a cell-cell contact dependant manner [4]. The tip cell acquires

a motile and invasive phenotype and leads the outgrowth of the vessel sprout through the ECM and towards a VEGF gradient [5]. Tip cells are equipped with emanating processes heavily endowed with VEGF receptors known as filopodia to sense surrounding guidance cues such as VEGF, ephrins and semaphorins. Contractions of actin filaments pull the tip cell towards guidance cues to ensure organised vessel growth [6]. ECs in close proximity to the selected tip cell assume subsidiary positions as stalk cells which exhibit an increased rate of proliferation stimulated by the NOTCH pathway, Wingless/integrated (WNTs), placental growth factor and fibroblast growth factor to elongate the trailing stalk.

The perfusion of vessels with a lumen is established in a process known as tubulogenesis and is an important step in the formation of a functional vessel. The exact morphogenic mechanisms and the underlying molecular pathways that ensure the formation of a lumen are not yet fully elucidated. A number of models have been proposed over the years and include intracellular vacuole coalescence [7], intercellular vacuole exocytosis [8] and apical membrane repulsion [9].

Anastomosis is the process by which adjacent tip cells fuse to form a new vessel and has been reported to be enabled by macrophages which act as cellular chaperones to promote initial contact [10]. Vascular endothelial (VE)-cadherin then establishes adhesion junctions at the ends of filopodia and along the extending interface of the connecting cells [11]. The maturation and stability of a newly formed vessel is a crucial step in ensuring proper functionality. The dynamics of the endothelium need to be altered from that of an active state in order to resume quiescence. Gene expression and downstream signalling pathways that promote the proliferation and migration of ECs are downregulated and replaced with homeostatic signals to stabilise the newly formed vessel. Protease inhibitors known as tissue inhibitors of metalloproteinases

(TIMPs) and plasminogen activator inhibitor-1 (PAI-1) ensure the deposition of a basement membrane and tight and adhesion junctions are re-established to maintain a barrier between ECs and ensure optimal flow distribution. Signals such as platelet-derived growth factor B (PDGF-B), transforming growth factor- β (TGF- β), ephrin-B2 and NOTCH ensure mural cells are recruited to surround the nascent vessel. This provides structural stability and ensures delivery of vascular stabilisation factors such as angiotensin-1 (ANG-1), leading to decreased VEGFR2 expression [9].

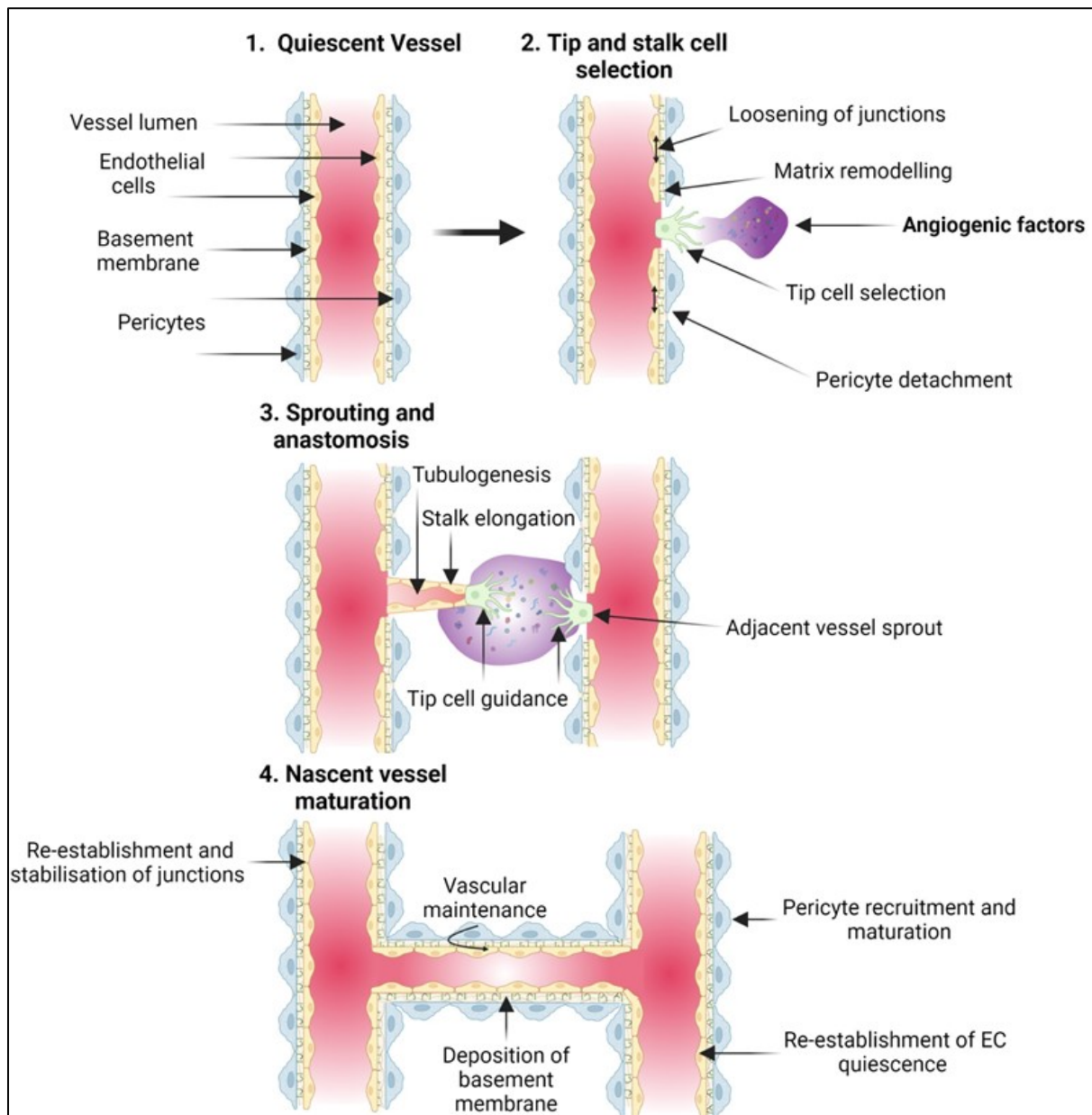


Figure 1.1 Schematic representation of angiogenic process (1) Quiescent blood vessel. (2) Endothelial activation by pro-angiogenic factors initiates a cascade of events resulting in the detachment of pericytes, detachment of EC junctions and basement membrane degradation. Determination of tip and stalk cells is dependent on Notch signalling between neighbouring ECs at angiogenic front. (3) Tip cells rely on their migratory phenotype to guide the growing sprout in the direction of a VEGF gradient while the trailing stalk cells proliferate to drive sustained sprout elongation. The fusion of the tip cells on adjacent growing sprouts establishes new cell to cell junctions along the extending interface of these cells. Tubulogenesis establishes the perfusion of the newly formed vessel. (4) For a newly formed vessel to be functional it must undergo a maturation process where junctions between ECs are re-established and stabilised, pericytes are recruited, a basement membrane is deposited, and pro-quiescent signalling ensues. Schematic modified from [3].

1.2 Diabetes Mellitus

Diabetes mellitus (DM) is a group of heterogeneous and complex chronic metabolic disorders characterised by hyperglycaemia, inadequate insulin secretion or excessive glucagon secretion. Over the past few decades, the worldwide prevalence of DM has reached epidemic proportions and is estimated to increase to 4.4% by 2030 [12]. An estimated 415 million individuals live with DM worldwide and an additional 193 million are undiagnosed [13]. DM imposes significant socioeconomic pressures on the individual and considerable costs to global health economics estimated at \$825 billion per year [14]. The three major groups of DM are type 1 (T1DM); an autoimmune disorder resulting in the destruction of pancreatic beta cells. Type 2 diabetes (T2DM) which is primarily a result of the progressive impairment of glucose regulation due to a combination of insulin resistance and dysfunctional pancreatic beta cells and gestational diabetes which can develop during pregnancy. There are also a number of other less common forms of DM which affect about 2% of the diabetic population and include cystic fibrosis-related DM, different types of monogenic DM and DM caused by rare syndromes. T2DM is the most common form of the disease accounting for more than 90% of patients with DM and will be the primary focus of this thesis.

1.2.1 Epidemiology and Pathophysiology of T2DM

The global rise in obesity, sedentary lifestyles, energy dense diets and aging populations have resulted in an unprecedented increase in the incidence and prevalence of T2DM. The International Diabetes Federation (IDF) estimates 382 million individuals aged 20–70 years worldwide have T2DM, with 80% of those affected living in low- and middle-income regions. This number is expected to rise to 592 million by 2035 which poses additional challenges in effective treatment at a global

scale [15]. Additionally, poor nutrition *in utero* and in early life combined with overnutrition in adult years, can contribute to the accelerated trajectory of the T2DM epidemic, especially in populations undergoing rapid nutrition transitions. Individuals with T2DM have a 15% increased risk of all-cause mortality compared with non-diabetics. The full disease burden of T2DM is likely underrepresented as upwards of 30% of diabetics, equivalent to 230 million people, are underdiagnosed [12]. T2DM is characterised by dysregulation of carbohydrate, lipid and protein metabolism as a result of pancreatic beta-cell dysfunction leading to impaired insulin secretion and/or insulin resistance (IR) in target organs. Briefly, insulin is a hormone that facilitates glucose uptake by cells and promotes its storage as glycogen, thereby lowering blood glucose levels. Overt hyperglycaemia is preceded by prediabetes, a condition that predisposes individuals to the development of T2DM characterised by an impairment in glucose tolerance, fasting glucose levels and an increase in glycated haemoglobin A1c levels [15]. Impairment in insulin secretion is a progressive process and its development involves glucose toxicity and lipotoxicity which in turn lead to accumulation of ROS in β -cells, with subsequent damage to cellular components and when left untreated is known to decrease β -cell mass and atrophy of the pancreas [16].

The progressive impairment of insulin secretion by β -cells usually takes place upon a background of pre-existing IR in the liver and skeletal muscle. IR is a condition in which secreted insulin does not exert sufficient action proportional to its blood concentration. IR pathways affect the action of insulin in each of the major insulin target tissues, leading to increased circulating fatty acids and the hyperglycaemia of diabetes. IR not only develops in the major target organs such as liver and skeletal muscle but also in the vasculature, adipose, kidney and brain tissues and worsens prior to onset of T2DM

by several years [17]. IR in adipocytes accelerates lipolysis and increased plasma free fatty acid (FFA) levels, both of which aggravate IR in muscle and the liver and contribute to β -cell failure. IR is influenced by known genetic factors including polymorphisms on insulin receptor and insulin receptor substrate (IRS)-1 genes that directly affect insulin signals and polymorphisms of “thrifty genes” such as the uncoupling protein (UCP) and the β 3 adrenergic receptor genes which are associated with obesity and promote insulin resistance [17].

T2DM is a complex chronic disorder that requires continuous self-management and multifactorial risk reduction strategies to normalize blood glucose levels, lipid profiles and blood pressure, crucial to minimizing acute and long-term microvascular macrovascular and nerve complications. T2DM should be viewed and treated as a heterogeneous condition with varying susceptibility to complications and responses to therapeutic intervention. Future therapeutic strategies for T2DM will require the elucidation of its molecular aetiology and effective interventions to combat the obesity epidemic.

1.2.2 Cardiovascular Complications of Diabetes

Cardiovascular complications represent the leading cause of morbidity and mortality in diabetic patients, accounting for up to 80% of deaths [18, 19]. Although the underlying aetiology differs between the types of DM, the majority of the resulting complications are similar. Alterations in endothelial homeostasis results in accelerated vessel occlusion, induction of microangiopathy and compromised native neovascularization responses essential for tissue reperfusion following an ischaemic event. The overall result is microvascular rarefaction and tissue hypoperfusion which manifests in the form of a number of macrovascular and microvascular diseases. Macrovascular complications involve atherosclerotic obstructions and lead to cerebral,

coronary and peripheral artery diseases (PADs). Microvascular pathologies include neuropathy, retinopathy and nephropathy; however the brain, myocardium, skin and other tissues/organs are also affected. While endothelial dysfunction is a key antecedent and modulator for both macro- and microvascular complications, this thesis will primarily focus on the aetiology and underlying pathogenic pathways related to critical limb ischaemia (CLI) and IHD.

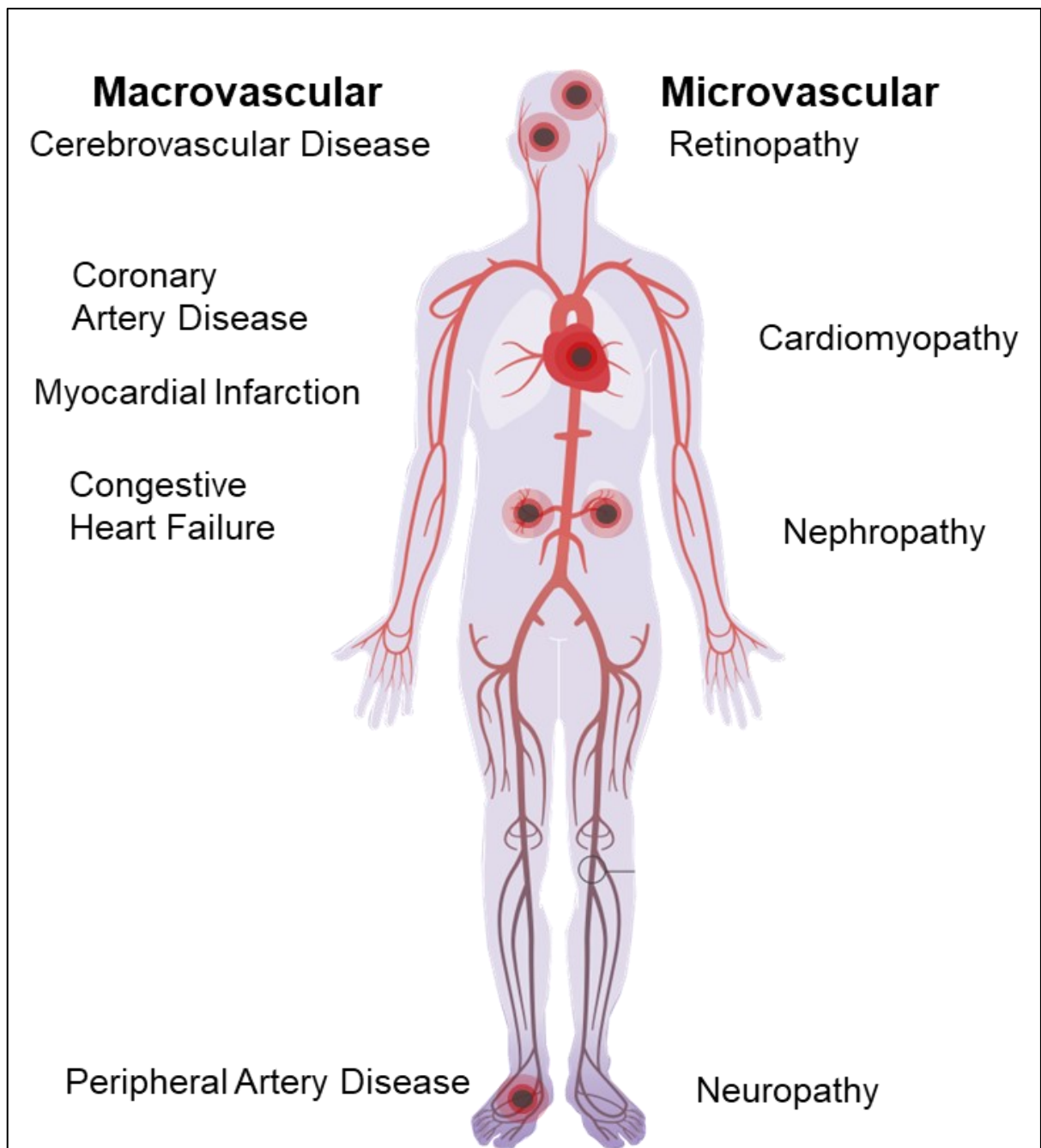


Figure 1.2 Schematic representation of the various micro- and macrovascular complications of diabetes.

DM-induced macrovascular disease of larger conduit arteries is the result of a confluence of intricate cellular and molecular pathophysiological factors that collectively create a "perfect storm" conducive to the development of atherosclerosis. These factors include chronic hyperglycemia, dyslipidemia, endothelial dysfunction, oxidative stress, inflammation, and impaired coagulation, all of which synergistically contribute to the initiation and progression of atherosclerotic plaques in individuals with DM [23]. Depending on the afflicted vasculature, this can lead to myocardial infarction (MI), stroke, and PAD. T2DM patients exhibit a greater atherosclerotic plaque burden, higher atheroma volume and smaller coronary artery lumen diameter in comparison with non-DM individuals [20]. IR is present prior to the onset of prediabetes or T2DM and is exacerbated over time, whereas elevated glucose levels develop in prediabetes and worsens with the development of T2DM. Both systemic and tissue-specific vascular IR, dysfunctional insulin signalling, hyperinsulinemia and elevated glucose levels contribute to numerous processes, including advanced glycation end (AGE) products, elevated FFA, protein kinase C (PKC) activation, oxidative stress, mitochondrial dysfunction and epigenetic modifications. These augment the dysfunction of the endothelium and inflammation to activate ECs, VSMCs and immune cells thereby contributing to the development and complexity of atherosclerosis and plaque vulnerability [21].

Oxidized low-density lipoproteins (LDLs) are exhibited in higher concentrations and are more atherogenic in DM [22]. LDL cholesterol particles are retained in the sub-endothelial layer of vulnerable vascular regions. This results in the recruitment and migration of circulating monocytes and other inflammatory cells through the endothelium and into the vascular smooth muscle layer of the intimal media. These monocytes differentiate into macrophages or dendritic cells, engulfing retained LDLs

to form lipid-laden foam cells, which along with other immune cells increase the production of cytokines and chemokines, including tumour necrosis factor- α (TNF- α) and interleukins. Atherosclerotic lesions also contain T-cells, which in DM patients exhibit a predominance of the proinflammatory Th-1 phenotype [23]. In addition to the pro-inflammatory effects of LDLs, aggregated cholesterol crystals within atherosclerotic regions activate endoplasmic reticulum (ER) stress and inflammasome complex formation to upregulate the transcription of NF- κ B-regulated gene products and interleukin-1 β . This propagates the proliferation of macrophages and their activation while resulting in a phenotypic switch of VSMCs to increase the rate of proliferation, migration and dedifferentiation [24]. These immune responses therefore create a feed-forward cycle to promote atherosclerotic lesion progression within the inflammatory milieu [23, 25]. Greater calcification is also observed in the arterial media in patients with T2DM compared with non-DM patients [26]. Additionally, individuals with T2DM are more thrombogenic and are shown to exhibit higher levels of von Willebrand factor (VWF), PAI-1 and fibrinogen, which are further dysregulated in line with poor glycaemic control [27]. Elevated glucose levels are also related to higher concentrations of coagulation factors and lower anticoagulants thereby contributing to atherothrombosis in DM [28]. In response to atherogenic injury to the vessel, VSMCs form a fibrous cap to promote the stability of the plaque. However, thinning of the fibrous cap and impaired phagocytic clearance of apoptotic lipid laden macrophages leads to a necrotic core which in turn further propagates inflammation and thrombosis. The result is an atherosclerotic lesion that is vulnerable to sudden expansion from thrombus formation, platelet thrombosis, haemorrhage of atherosclerotic plaque microvessels and breach of the fibrous cap [24].

Unlike renal and retinal microvascular disease, there is no distinct “pathological fingerprint” for the atherosclerotic plaque in the diabetic setting. However, studies indicate that DM drives faster lesion initiation and progression to more advanced atherosclerotic injury [26]. Prolonged exposure of the vasculature to hyperglycaemic conditions is in most cases the initial trigger to a complex cascade leading to various CVDs. Optimal glycaemic control has led to prevention and amelioration of numerous microvascular diseases, particularly retinopathy and nephropathy. Unfortunately, progress in hyperglycaemic management does not fully address the mechanisms that exacerbate the major causes of morbidity and mortality in T2DM patients, which include IHD, ischaemic stroke, PAD and congestive heart failure. The complex interactions between the metabolic, vascular and inflammatory pathways involved makes the long-term treatment of DM associated cardiovascular complications challenging. There is an urgent need for a better understanding of these individual pathways and their inter-relationships while also addressing the underlying complications to the microvasculature.

1.3 Therapeutic Angiogenesis

Perturbations from the angiogenic process, whether excessive or deficient can contribute to or cause pathologies such as cancer, diabetic retinopathy and ischaemic diseases. Angiogenesis is therefore a putative target for therapy, with significant efforts being made in recent decades toward the development of strategies to induce, augment and control the host angiogenic response. Despite many patients benefitting from the introduction of anti-angiogenic drugs, efficacy issues remain a major concern. In addition, efforts to stimulate angiogenesis therapeutically using pro-angiogenic factors have not had the expected results, where the spectacular efficiency of angiogenic therapy exhibited in preclinical studies not being translated into clinics [29].

Due to the complex nature of the angiogenic process, revascularisation of ischaemic tissue must be tightly controlled and effectively coordinated to mitigate adverse events, such as the formation of immature and leaky vessels and uncontrolled angiogenesis.

In addition to angiogenesis, postnatal growth of the vasculature is also mediated by arteriogenesis and vasculogenesis, which have been investigated as mechanisms to stimulate therapeutic revascularisation. Arteriogenesis is triggered by the rise in shear stress in an occluded vessel to induce the remodelling of collateral vessels 20–100µm in diameter with a fully developed tunica media to support distal portions of the afflicted organ. These vessels have a greater blood-carrying capacity than capillaries produced through angiogenesis where arteriogenesis may restore 30-40% of basal blood flow following critical stenosis and thrombosis [30]. The efficacy of arteriogenic response is however reduced with aging and disease; most notably in the context of DM induced ischaemia which greatly limits arteriogenesis, resulting in critical levels of ischaemia and tissue loss [31]. Vasculogenesis occurs when angioblasts accompanied by circulating bone-marrow derived progenitor cells proliferate and associate to form primitive vessels. Although once thought limited to early embryonic development, ischaemic conditions are also known to stimulate postnatal vasculogenesis through the mobilization of EPCs. These cells will integrate into existing blood vessels and differentiate into mature ECs or modulate existing ECs via paracrine mechanisms [32]. Angiogenesis, arteriogenesis and vasculogenesis share common growth factors, ECM components, enzymes, EC activation and numerous additional mediators. For adequate function, therapeutic angiogenesis must effectively target both medium/large arteries that provide influx of blood and smaller capillaries that deliver to cell beds. A greater understanding into the synergy between the angiogenic process

and arteriogenesis, the function of circulating EPCs and the interplay between de novo or remodelled collateral vessels and pre-existing capillaries is crucial for therapeutic angiogenesis to have an enduring impact.

1.3.1 Methods and Approaches for Therapeutic Angiogenesis

Experimental and clinical evidence curated over the last two decades establishes a proof of concept for therapeutic angiogenesis as a treatment option for “no-option” patients suffering from ischaemic conditions, including IHD and CLI. Despite this, the ideal vehicle that will stimulate the angiogenic effect remains elusive with numerous studies investigating protein delivery, gene therapy, cell therapy, microvesicles/exosome therapy and tissue engineering as solutions for the induction of vessel growth. Initially, protein-based therapeutics were explored as an ‘off-the-shelf’ treatment due to our vast fundamental knowledge of their actions and ease of production, administration and testing of their translational value. However, targeting and maintaining angiogenic activity at the site of interest posed a significant challenge while most of the injected peptides are rapidly cleared by the mononuclear phagocyte system [33]. Early clinical studies yielded results that were as valuable as they were disappointing and suggested that gene therapy with its local sustained expression of the desired protein as a more suitable alternative [34].

A gene therapy approach involves a gene or genes encoding the angiopeptides of interest delivered in a viral vector affording high transduction efficiency or non-viral vectors such as recombinant plasmid DNA (pDNA). The therapeutic gene or a combination of genes can be delivered in bicistronic or polycistronic vectors directly to cells present at the ischaemic site allowing for localised angiopeptide expression. Hundreds of studies have been published since the first experiments indicating the possibility of *in vivo* gene transfer in the early 90s [35].

Initially, adenoviral vectors were employed for gene delivery due to their high transduction efficiency, allowing for effective distribution of therapeutic genes to target cells. This is particularly advantageous in the context of ischaemic disease, where a high level of gene expression is often required to induce a robust angiogenic response due to the hostile microenvironment [36]. Adenoviral vectors can also infect a wide range of cells, including both dividing and non-dividing. This allows them to transduce various cell types within the ischaemic tissue, including ECs, mural cells, fibroblasts and immune cells, which collectively contribute to the angiogenic process. Although the transient nature of adenovirus-mediated gene expression may be advantageous in cases where sustained overexpression of angiogenic factors may lead to abnormal vessel growth – stable gene expression is generally a preferred approach in ischaemic disease [29]. Additionally, scalable production methods, including suspension cultures and bioreactors, ensure the feasibility of adenoviral vector manufacturing for clinical applications. However, the clinical translation of adenoviral vectors has been hindered by several limitations. Adenoviral treatments can be immunogenic, particularly at high doses, leading to the development of neutralizing antibodies and inflammatory responses. Moreover, limited cargo capacity poses challenges when larger or multiple therapeutic genes are to be delivered [36].

To overcome these challenges, pDNA vectors emerged as a non-viral alternative. pDNA vectors are circular, double-stranded DNA molecules containing an expression cassette with a promoter driving transcription of the transgene encoding the therapeutic protein. The ability of pDNA vectors to accommodate large DNA inserts allows for the delivery of multiple therapeutic genes or regulatory elements, thereby enabling the targeting of various aspects of ischaemic pathophysiology simultaneously [35]. pDNA vectors allow for localized gene expression and can be delivered directly

to target tissues via various routes, including local injection, systemic administration, or *in situ* gene transfer, allowing for a wide range of clinical applications. Additionally, the large-scale production of pDNA can be achieved using readily available and cost-effective techniques. Plasmid-based gene therapy has shown promise in preclinical studies, but its translation to clinical settings has been hindered by challenges in achieving efficient transfection and sustained gene expression [35].

Recent advancements have seen the emergence of adeno-associated viral (AAV) vectors as promising tools for therapeutic angiogenesis. AAV vectors combine the benefits of viral and non-viral vectors, offering high transduction efficiency and long-term gene expression, while exhibiting a favourable safety profile. Advancements in vector engineering have allowed the development of AAV serotypes with enhanced tissue specificity, enabling targeted gene delivery to specific cell types [30]. A major limitation remains to be the considerably lower transduction efficiency of available vectors in human target tissues compared to levels attainable in smaller mammals used to generate the preclinical data [36]. Additionally, it can be challenging to find a precise balance between relevant signals and fine tune the longevity of expression offered by viral vectors to avoid the indefinite overproduction of angiogenic factors and the resulting unpredictable long-term consequences. Although rapid progress has been made in recent years in the area of vector platform technology, there is currently no translatable solution to these challenges in ongoing clinical trials for CVDs.

Cell-based therapies are a promising tool for regenerative medicine, leveraging progenitor or stem cells' capacities to self-renew, differentiate, proliferate and colocalize with vessel components to mediate tissue repair. EPCs and bone marrow-mesenchymal stem cells (BMMSCs) are the most extensively studied cell types for therapeutic angiogenesis with the majority of clinical trials focused on MI, coronary

heart disease (CHD) and CLI, with pre-clinical studies indicating improved blood perfusion and cardiac function [29]. EPCs mobilize in response to hypoxia and are able to integrate into the sprouting vasculature to differentiate into ECs, VSMCs or pericytes thereby acting as the building blocks for revascularisation [37, 38]. While BMMSCs also exhibit the potential to differentiate, both BMMSCs and EPCs are able to potentiate angiogenesis through paracrine mechanisms. The acquisition of a sufficient number of cells remains a challenge and their *in vivo* viability remains low with the majority of cells failing to integrate with the host tissue. Studies exploring induced pluripotent stem cells (PSCs) produced by activating key transcription factors provide an attractive prospect. Here, terminally differentiated cells are reprogrammed to an embryonic like state and re-differentiated into the required cell type under precise culture conditions [39, 40]. Although the use of autologous cells circumvents limitations in cell sourcing, immune rejection as well as ethical concerns it is important to note that *in vitro* culturing of cells results in an altered cell phenotype, characteristics and angiogenic potential. A combination of cell based, and gene therapies may bolster the efficacy of using autologous cells by overexpressing therapeutic factors or cell homing factors, and its translation relies largely on safe and effective methods to deliver genes into stem cells.

The paracrine effects of stem cells play a crucial role in their therapeutic potential in the context of ischaemic diseases. There is much interest in cells that participate in post-ischaemic regeneration as a source of extracellular vesicles for use as delivery systems in pro-angiogenic therapies. Exosomes are nanovesicles that harbour biologically active cargo including proteins, lipids and RNA molecules. Their intracellular exchange is known to elicit angiogenic, proliferative and anti-inflammatory cascades in CVD [41]. MircoRNAs (miRNAs) are particularly enriched in exosomes

where they have been associated with improved post-MI cardiac repair and the reduction of fibrosis [42]. Additionally, exosomes derived from mesenchymal stem cells (MSCs) [43-48], embryonic stem cells [49, 50], cardiac progenitor cells [51-54] and human pericardial fluid [55] improve capillary density and overall cardiac function in various disease models. The novelty of the exosome-based approach means there is a lack of standardization of exosome and microvesicle isolation techniques. While the safety of exosome treatments has been established in human clinical trials for cancer immunotherapy and as diagnostic agents [56, 57], the use of exosomes as nanocarriers in the context of therapeutic angiogenesis has yet to be studied in the clinical context. Additionally, cell senescence dramatically decreases their rate of exosome release and although studies into artificially engineered exosomes aim to bypass this caveat to ensure stable exosome production the field is currently in its nascent stages [58].

1.4 Introduction to MicroRNAs

MicroRNAs are a subset of endogenous small non-coding RNAs approximately 22-nucleotides in length that play a key role in the post-transcriptional modulation of gene expression. miRNAs exert their actions by silencing target mRNAs through the partial or full complementarity of the seed sequence in their 5' untranslated regions (5'UTRs) with sequences on mRNAs referred to as miRNA response elements predominantly located in the 3'UTRs. Alternatively, miRNAs are also able to bind to the coding sequence (CDS) region of mRNAs [59]. The ability of miRNAs to target mRNAs through partial complementarity allows a single miRNA to bind to hundreds of different mRNAs, collectively resulting in the regulation of more than half of the protein coding genes in humans [60]. It therefore comes as no surprise that the dysregulation of miRNA expression has been associated with numerous disease conditions

including those of the cardiovascular system. Modulating the expression of miRNAs with inhibitors or mimics has become an area of interest for researchers as a viable therapeutic option in CVD. Additionally, miRNAs offer a unique opportunity as biomarkers and targets for early disease detection to improve diagnosis and surveillance of complex multi-factorial pathologies [61].

1.4.1 Biogenesis of miRNAs

The canonical pathway of miRNA biogenesis is the principal pathway by which miRNAs are processed. This pathway is initiated by the transcription of miRNA genes by RNA polymerase II/III (RNA Pol II/III) into long primary miRNA transcripts (pri-miRNA) [62, 63]. These pri-miRNAs typically consist of a ~35 base pair stem, a terminal loop and single-stranded 5' and 3' segments. The sequence for several miRNAs is often contained in a single pri-miRNA. The pri-miRNA is endonucleolytically cleaved by the microprocessor protein complex, composed of the RNase III enzyme Drosha and the DiGeorge Critical Region 8 protein (DGCR8) [62]. The RNase domains of Drosha cleave the 5' and 3' segments [64], while DGCR8 directly interacts with the target pri-miRNA and acts as a molecular anchor to determine the exact cleavage sites [65]. This interaction produces a ~70-nucleotide stem-loop precursor miRNA (pre-miRNA), which is subsequently recognised and transported to the cytoplasm by the transport receptor Exportin-5 and RanGTP-binding protein [65, 66]. In the cytoplasm, the RNase III endonuclease known as Dicer cleaves the pre-miRNA near the terminal loop, releasing a mature miRNA duplex [67]. A single strand of the generated duplex, known as the active or guide strand, is then loaded into an Argonaute protein (AGO 1-4) in an ATP dependent process to form the basic core of the effector complex known as the RNA-induced silencing complex (RISC). This

complex mediates the post transcriptional silencing of mRNAs through the partial or full complementarity with sequences on mRNA 3'UTR response elements [68].

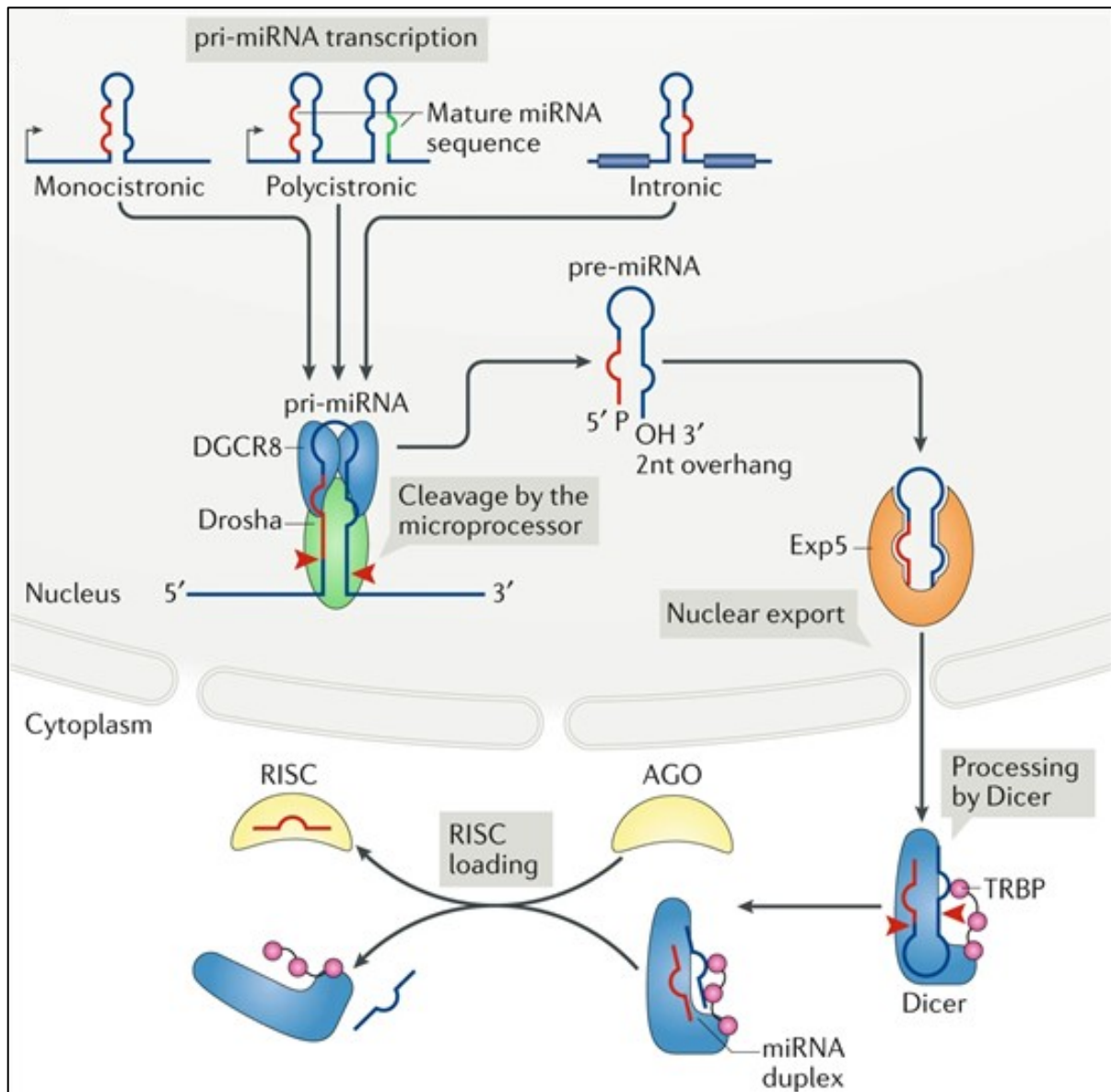


Figure 1.3 Schematic presenting an overview of the canonical miRNA biogenesis process. Red arrow heads indicate cleavage sites. miRNAs are encoded as monocistronic, polycistronic or in introns of host genes. Pri-miRNA transcripts are cleaved by the microprocessor complex composed of DGCR8 dimer and Drosha at the stem of the hairpin structure. The resulting precursor miRNA (pre-miRNA) exhibits characteristic 3' hydroxyl group (OH), overhangs of 2 nucleotides (nt) and a 5'phosphate (P). Exportin-5 facilitates the cytoplasmic export of pre-miRNAs where they are cleaved by Dicer to release a miRNA duplex intermediate. The guide strand of this duplex is loaded into the AGO protein which assembles with Dicer and trans-activation-responsive RNA-binding protein to form RISC. Schematic adapted from [69].

1.4.2 Mechanisms of miRNA Mediated Gene Regulation

Targets exhibiting perfect complementarity are cleaved through the endonuclease activity of AGO2. However, in cases where the mRNA target exhibits partial complementarity, the AGO protein recruit cofactors known as the GW182 protein family. These proteins function as a scaffold to bridge the interaction between the RISC complex and downstream effectors, including the poly(A)-binding protein (PABPC) and the poly(A)-deadenylase complexes PAN2-PAN3 and CCR4-NOT, which catalyse the deadenylation of the target mRNA [70, 71]. Subsequent decapping is accelerated by decapping protein 2 (DCP2) followed by the exoribonuclease1 (XRN1) mediated rapid 5'-3' degradation [72]. Additionally, miRNA mediated silencing has also been shown to occur through translational repression. Although the exact mechanisms are yet to be fully elucidated, emerging evidence suggests the interference of miRNAs with the assembly of the eukaryotic initiation factor 4F complex [71].

1.5 m6A RNA Methylation

RNA modifications are types of co-transcriptional and/or post-transcriptional regulations that can affect all aspects of RNA molecules lifecycle including stability, translation and degradation of the RNA. To date, the MODOMICS database identifies and reports 172 different types of RNA modifications, among which 72 include methyl groups [73]. Various types of RNA including mRNA, transfer RNA (tRNA), ribosomal RNA (rRNA), miRNA and long non-coding RNA (lncRNA) have been shown to harbour methyl modifications. The biological impact and exact functions of the numerous RNA modifications can vary greatly depending on the biogenesis, the target RNA molecule and the specific nucleotide modified.

The N6-methyladenosine (m6A) has been identified as the most abundant internal modification in mRNAs and lncRNAs accounting for more than 80% of all RNA base methylations. The amount of m6A in isolated RNA was approximated to constitute 0.1-0.4% of all adenosine nucleotides (approx. 3–5 m6A sites per mRNA) in mammals [74, 75]. Although first identified in the 70's [76, 77], interest in the biological relevance of m6A was rekindled in the last decade as a result of two primary advancements. The first of which is the discovery of fat-mass and obesity-associated protein (FTO) as the first demethylase enzyme, confirming that the m6A modification is indeed reversible and dynamic, and thus can be implicated in regulatory processes [78]. The second advancement was the development of an m6A RNA immunoprecipitation approach followed by high-throughput sequencing (m6A-seq or MeRIP-seq) to determine the positions of m6A at a transcriptome-wide level at ~100 nucleotides resolution. This offered the first view of the m6A epitranscriptome in mRNAs and lncRNAs [79, 80]. These studies identified over 12,000 m6A sites distributed in 7,000 mRNA and 300 non-coding RNA with an average frequency of 1 m6A per 2000 ribonucleotides. Indeed, m6A generally occurs in the highly conserved RNA consensus motif DRACH (D=A/G/U; R= A/G; H=A/U/C) and exhibits preferential enrichment within pre-mRNA internal long exons, 3'UTR or around the stop codon [79, 80]. The enrichment of m6A within introns also suggests that this modification can occur prior to or in concurrence with RNA splicing events.

The structure of target RNAs can be altered by the presence of m6A by forcing the rotation of the methylamino group into an anti-conformation position, thereby resulting in the destabilization of the thermodynamics of the RNA duplex by 0.5-1.7 kcal/mol [81]. These subtle alterations in structure make the target RNA accessible to the binding of RNA proteins in a mechanism dubbed “the m6A switch” [82].

Specialised proteins are able to insert (“writers”), interact with (“readers”) or remove (“erasers”) m6A in a dynamic manner, thereby determining the abundance and functions of the m6A modification. This dynamic post-transcriptional modification is emerging as a new layer of regulation of gene expression by effecting stability, translation or splicing processes [83-85].

1.5.1 M6A Regulatory Machinery – Writers

Methyltransferases that modify and insert the m6A mark on target RNA molecules are referred to as “writers” (figure 1.4). These enzymes function as a multicomponent nuclear complex composed of a core methyltransferase-like 3 (catalytic domain) and -14 (METTL3 and METTL14) heterodimer, METTL16, the Wilm’s tumour 1 associated protein (WTAP) and several auxiliary proteins including vir like m6A methyltransferase associated (VIRMA, commonly referred to as KIAA1429), RBM15 and ZC3H13. METTL3 has been established as the primary catalytic component of this complex. METTL3 is ubiquitously expressed in human tissues and its knockdown in different cell types resulted in marked reductions in total m6A levels and an increase in apoptosis through the activation of the p53-mediated pathway. Furthermore, genetic deletion of METTL3 resulted in a near-complete abrogation of total m6A [86]. Two functional domains responsible for the methylation activities of METTL3 have been identified, including the consensus methylation motif I (CM I), which represents the S-Adenosyl methionine (SAM) binding domain and the methylation catalytic residue containing CM II [87].

METTL3’s homologue METTL14 is crucial for its allosteric activation, thereby facilitating METTL3’s catalytic actions [88-90]. METTL14 manifested methyltransferase activities slightly higher than that of METTL3 and the combination of both resulted in significantly enhanced methylation activity, suggesting that

METTL14 is a distinct writer of m6A [91, 92]. However, recent crystallization studies demonstrated that METTL3, not METTL4, bound to the methyl donor SAM and is responsible for catalysing the formation of m6A [88, 90]. METTL3-METTL14 heterodimer crystal structure analysis revealed a non-functional degenerated SAM-binding domain on METTL14. Instead, METTL14 was shown to be important in facilitating the catalytic action of METTL3 by forming a continuous substrate binding surface to allow for RNA binding and by the stabilisation of the methyl group.

An important constituent of the methyltransferase complex, WTAP, was initially identified as a splicing factor that binds to Wilms' tumour 1 protein [93]. Interactions between METTL3 and WTAP were observed by studies both *in vitro* and *in vivo* [91, 94, 95]. Although it was found that WTAP alone does not display any catalytic activity, Liu et al., demonstrated a dramatic reduction in m6A levels as well as METTL3 and METTL14 degradation upon the knockdown of WTAP [96][91]. Characterisation of WTAP revealed its importance in the guidance and localisation of the METTL3-METTL14 heterodimer complex in nuclear speckles to efficiently methylate target RNAs.

The catalytic actions of the most recently identified m6A methyltransferase METTL16 have been shown to be specific for the targeting of adenosine bases in secondary structures or loops outside the consensus DRACH motif [97]. METTL16 crystal structures of the N-terminal methyltransferase domain and a post-catalytic S-adenosylhomocysteine bound complex reveals structural elements unique to METTL16. Indeed, RNA target specificity of METTL16 is likely conferred by a recently revealed extensive positively charged groove [98]. Furthermore, unlike the heterodimerizing METTL3 and METTL14, METTL16 has been shown to form a homodimer while the N-terminal methyltransferase domain exists as a monomer,

suggesting that the C-terminal domain confers protein dimerization [98]. Studies investigating crystal structures of METTL16-MATA2 3' UTR Hairpins describe the structural basis of METTL16 specificity [99].

1.5.2 M6A Regulatory Machinery – Erasers

The m6A mark is dynamically removed by the demethylase proteins or “erasers”. The identification of FTO as the first m6A eraser protein was hugely significant in rekindling interest in the study of m6A RNA methylation [78, 100]. This discovery suggested that m6A modifications could be implicated in biological and cellular processes due to the possibility that the m6A mark is dynamic and reversible. A second demethylase, Alpha-Ketoglutarate-Dependent Dioxygenase AlkB Homolog 5 (ALKBH5) has since then been identified. FTO was initially identified in genome wide association studies (GWAS) which strongly linked a single nucleotide polymorphism in the first intron of FTO with body mass index and obesity [101-103]. The actions of FTO as a demethylase were first demonstrated in the demethylation of N3-methylthymidine in single stranded DNA (ssDNA) [104] and N3-methyluridine in ssRNA [105]. In the context of m6A demethylation, Jia et al., demonstrated the actions of FTO both *in vitro* and *in vivo* where silencing of FTO resulted in increased total m6A levels and the over expression of FTO substantially decreased m6A levels on RNA [78]. The knockdown of ALKBH5 in human cell lines resulted in not only increased total m6A levels on polyadenylated RNA but also impacted several RNA processing steps. Zheng et al., demonstrated the cytoplasmic localization of mRNA in ALKBH5-deficient cells in contrast to the nuclear accumulation observed in cells with ALKBH5 [106]. Additionally, the overexpression of wildtype ALKBH5 could rescue this accelerated mRNA export, highlighting a demethylation dependant role of ALKBH5 in the

regulation of mRNA export. Furthermore, ALKBH5 demethylation activity was also shown to affect the rate of mRNA synthesis, splicing and global RNA stability [106].

Although both enzymes are members of the α -ketoglutarate (α KG)-dependent dioxygenase subgroup of enzymes, FTO and ALKBH5 differ significantly in their expression profiles and localisation. While ALKBH5 expression is predominately prevalent in the testis where it carries out a pivotal role in spermatogenesis [106, 107], FTO is shown to be expressed widely in all tissues [108-110]. FTO and ALKBH5 also display distinct substrate specificity which seems to be determined by a variety of factors. The first of which is the two proteins distinct subcellular localisation where FTO shuttles between the cytoplasm and the nucleus [111], whereas ALKBH5 expression is mainly restricted to the nucleus [106]. Secondly, the presence of the m6A mark itself incites a conformational change in the structure of the target RNA resulting in preferential recognition by one of the demethylases over the other [112]. Lastly, while the actions of ALKBH5 have been shown to primarily effect m6A, FTO is also able to demethylate N1-methyladenosine (m1A) and N6 2-O-dimethyladenosine (m6Am) modifications. In fact, studies indicate FTO's catalytic preference for m6Am over m6A [113, 114]. FTO regulates the demethylation of internal m6A and cap m6Am of polyadenylated RNAs while exhibiting differential substrate preferences in the nucleus compared to the cytoplasm and varying expression patterns in different cell types [115]. More specifically, FTO's catalytic actions have been shown to demethylate internal m6A and cap m6A, internal m6A in UB RNA, internal and cap m6Am small nuclear RNA and m1A in transfer RNA. FTO-mediated demethylation was also reported to have a greater effect on the transcript levels of mRNAs modified with an internal m6A mark and can directly inhibit translation by mediating m1A tRNA demethylation [115].

Furthermore, crystallographic analysis of FTO's catalytic pocket suggests that its substrate preference is dependent on the sequence and tertiary structure of the RNA rather than the varying ribose rings of m6A and m6Am [116]. Studies also reveal a C-terminal domain with a distinct novel fold in an active domain that is otherwise similar to that observed in other members of AlkB family, indicating additional functions unique to FTO [105, 117]. FTO's well established association with an increased risk to obesity makes it a potential drug target and as a result FTO inhibitors targeting the nucleotide-binding pocket have been developed [118-120]. Although crystallographic analysis of ALKBH5 describes conserved structural elements with FTO, a number of differences have been reported. The most distinct of which is the orientation of a shared extra loop needed for single stranded RNA binding in ALKBH5 compared to FTO [121, 122]. Further understanding of target recognition specificity of FTO and ALKBH5 through relevant structural analysis would offer a framework for the development of specific inhibitors.

1.5.3 M6A Regulatory Machinery – Readers

A final crucial component of the m6A regulatory machinery are the 'reader' proteins. These reader proteins recognise and bind to m6A sites to mediate specific downstream functions. Numerous m6A readers have been identified with the most well-characterised of which belonging to the highly evolutionary conserved YTH family of proteins. YTHDF1 (YTH N6-methyladenosine RNA-binding protein 1) enhances the translation efficiency of methylated mRNAs by recognising and binding to the m6A mark [123] while YTHDF2 binds to m6A and recruits the CCR4-NOT deadenylase complex which in turn accelerates the degradation of methylated transcripts [124]. The translation or degradation actions of YTHDF1 and YTHDF2 are facilitated through their direct interactions with YTHDF3 [124, 125]. YTHDC1 (YTH domain-containing 1)

is primarily localised in the nucleus and has been shown to regulate pre-mRNA splicing through the promotion of exon inclusion [126] while also regulating the nuclear transport of m⁶A modified mRNA [127]. Conversely, YTHDC2 expression is predominantly localised in the cytoplasm and is suggested to enhance the translation efficiency of methylated target mRNAs by directly interacting with the small ribosomal subunit [128, 129]. The study of YTHDC2 is still in its early stages and it is not fully understood how this mechanism is coordinated, however the presence of other putative binding domains in addition to its YTH domain, including protein-protein interaction and RNA-protein domains indicates complex functions for this protein [129].

A second family of m⁶A readers is the heterogeneous nuclear ribonucleoproteins (HNRNPs) and the most well characterised of which are HNRNPA2B1 [130], HNRNPD [131], HNRNPG [132] and HNRNPC [132]. Contrary to readers belonging to the YTH family, HNRNPs are thought to exert their actions on RNA substrates through an “m⁶A switch” rather than binding directly to m⁶A sites.

All components of the m⁶A machinery are highly evolutionary conserved with a 97% average protein identity among mammals (refer to figure 1.4B). The most conserved among the methylases are METTL3 and METTL14 sharing 51% and 28% protein homology with *Saccharomyces cerevisiae*. Aside from homologues of the YTHDC1 and YTHDC2 reader proteins existing in *Anopheles gambiae* and *Drosophila melanogaster*, no other homologues eraser and reader proteins are known to exist in invertebrates. This has led researchers to hypothesise that m⁶A is not a dynamic process in lower eukaryotes or perhaps other non-conserved proteins carry out similar functions.

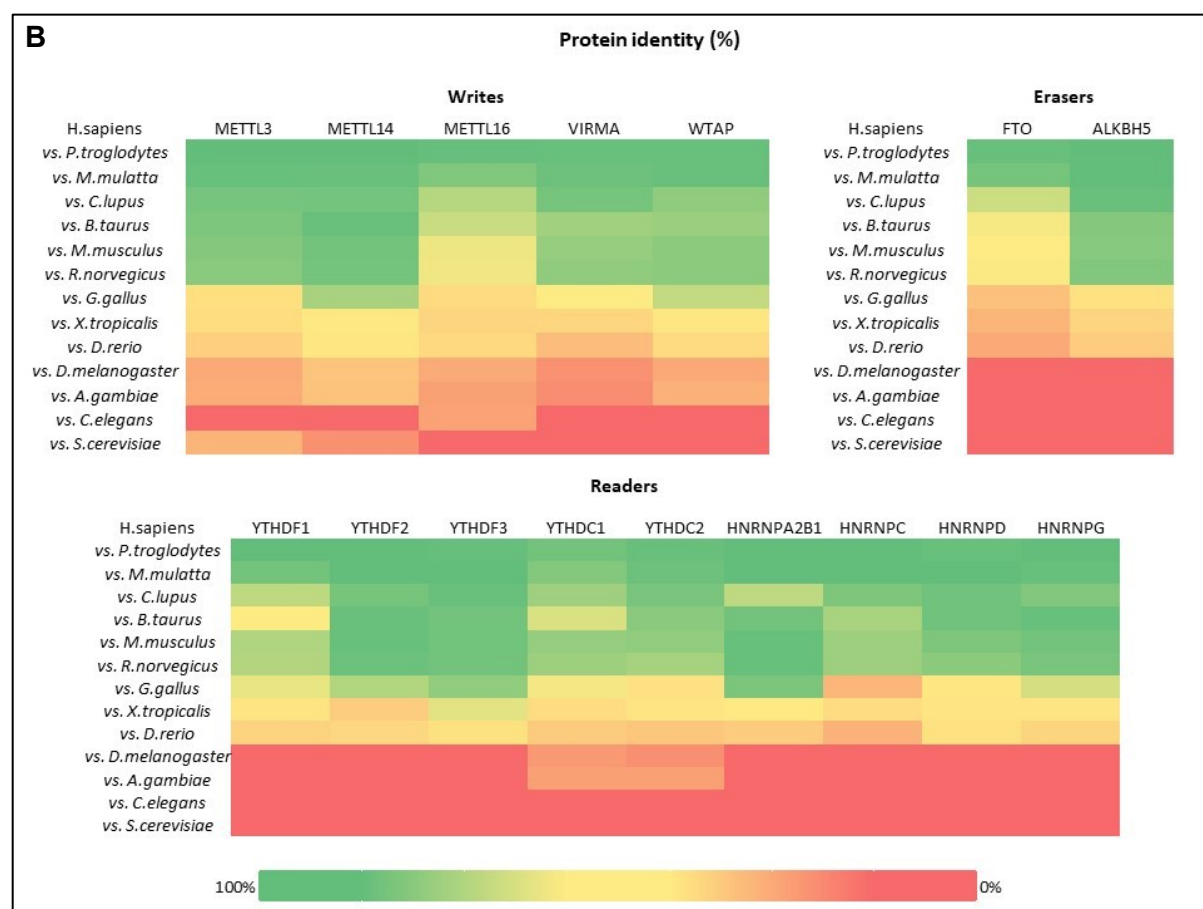
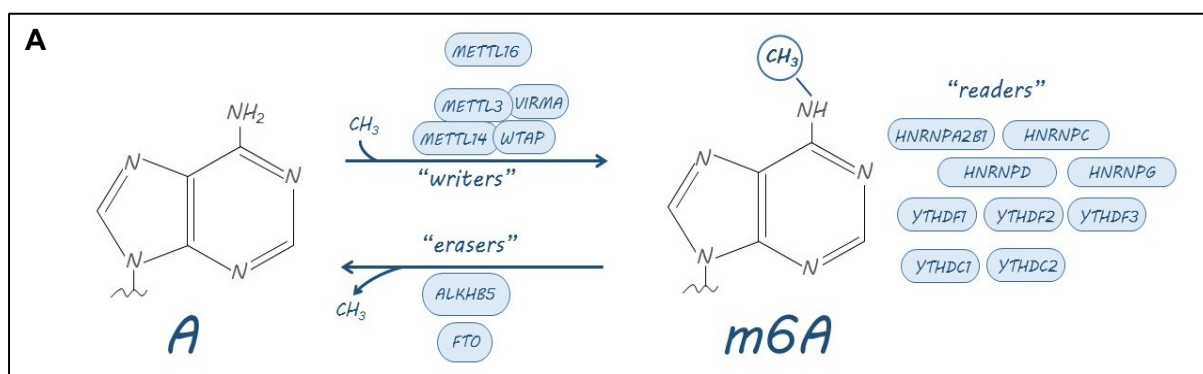


Figure 1.4 (A) Representation of the reversible m6A modification and its regulatory machinery. A heterodimer complex of METTL3-METTL14 catalyses the formation of the m6A modification. These methyltransferases are assisted by WTAP which is required for their localisation into nuclear speckles. M6A is dynamically reversed by the demethylases ALKBH5 and FTO. Reader proteins recognise and bind to m6A marks to mediate downstream biological functions. **(B)** Conservation of m6A regulator proteins among species. Human amino acid sequence of each component was utilised as a template for BLAST search. Percentage of homology among species is represented as a colour gradient where green represents the highest degree of homology and red represents the lowest. BLASTP version 2.9 from Uniprot database was used for analysis. Figure adapted from Sweaad et al. *J Mol Cell Cardiol* [133].

1.6 Detection Methods of m6A

The emergence of high-throughput sequencing methods enabled researchers to map and analyse the m6A modification at a transcriptome wide level. This in turn facilitated major breakthroughs in understanding the functions of m6A (figure 1.5). In 2012, Meyer et al. and Dominissini et al. described the first methods for the transcriptome-wide profiling of m6A in individual RNAs in the form of techniques respectively called m6A-seq and MeRIP-seq [79, 80]. These studies identified upwards of seven thousand mammalian genes harbouring m6A sites. The m6A mark was also shown to exhibit global enrichment in the 3' UTR near stop codons and long internal exons along with site, cell and tissue specificity thereby suggesting a unique m6A-derived transcriptome topology. These studies also describe m6A sites in some RNAs being highly conserved between human and murine species. The m6A-seq and MeRIP-seq techniques involve the random fragmentation of RNA into approximately 100 nucleotide sequences and m6A-specific anti-body-based RNA immunoprecipitation (IP), followed by next generation sequencing [79, 80]. Bioinformatical analysis then generates m6A peaks corresponding to m6A sites from immunoprecipitated RNA relative to input RNA (figure 1.5.a). Although these methods represent the most commonly utilised approaches for the mapping of m6A, they indeed present limitations. Firstly, the amount of required starting material is extremely high with a recommended minimum of 250µg of total RNA. In this regard, an MeRIPSeq approach optimised by Zeng et al., based on the removal of ribosomal cDNA allows for m6A profiling with as low as 500ng of total RNA [134]. Secondly, the resolution is limited to the size of RNA fragments, with no objective way of pinpointing exactly where in the fragment the m6A site is positioned. Locating DRACH motifs in close proximity to the peak of interest is commonly used to predict the position of the m6A site. This however

presents its own complications as m6A sites commonly exist in clusters corresponded by wider peaks which makes it difficult to detect the methylated residue. Additionally, different DRACH motifs may be present underneath a peak [80, 135]. Finally, analytical challenges and anti-body-based bias mean these techniques also face reproducibility issues [135]. Upwards of 10 million peaks from published MeRIP-Seq and m6A-seq datasets in over 60 cell types and tissues have been curated by the RNA EPItranscriptome Collection (REPIC) database [136]. REPIC also integrates DNase-seq and Chromatin IP (ChIP) data with available MeRIP-Seq and m6A-seq datasets, thereby offering a concise and extensive atlas of m6A binding sites, chromatin accessibility regions and histone modification sites. Research has indeed uncovered a link between m6A modifications and histone markers or promoters, indicating potential mechanisms by which m6A may fine tune the regulation of gene expression [136].

M6A sites were more accurately defined by UV crosslinking the m6A specific antibody to RNA, in line with principles of the crosslinking and immunoprecipitation (CLIP) protocol. The first of which is a photo-crosslinking-assisted m6A sequencing strategy (PA-m6A-seq) used to overcome the resolution limitation faced by the MeRIP-Seq and m6A-seq techniques (figure 1.5.A) [137]. Briefly, this technique involves the treatment of cells with a photoactivatable ribonucleoside, 4-thiouridine (4SU) which is incorporated into RNA. This is followed by an IP using a m6A-specific antibody in which full length RNA is used rather than fragmented molecules. Cross-linking is then initiated by treating with 365 nm UV light followed by digestion of RNA to fragments of 30 nucleotides. Prior to library preparation samples are treated with proteinase K to remove bonded peptides. Cross-linked 4SU leads to the T-to-C transition during

reverse transcription step in PCR allowing for the pinpointing of m6A sites with a 23-nucleotide resolution [137].

A further two approaches were simultaneously developed by Linder et al., and Ke et al., respectively termed m6A individual nucleotide resolution cross-linking and immunoprecipitation (miCLIP) and m6A cross-linking immunoprecipitation (m6A-CLIP) (figure 1.5.A) [138, 139]. Here, full length RNA is ultraviolet light-induced cross linked with an m6A specific antibody and immunoprecipitated followed by digestion with proteinase K, leaving an amino acid adduct attached to the RNA base. During library preparation, the reverse transcriptase either reads through this cross-linked adduct, resulting in a substitution or deletion mutation or is stopped, causing cDNA truncation. Linder et al., found that m6A specific antibodies differed in their propensities to induce a mutation and truncation in the positions of these signals in relation to the modified adenosine base. Both studies were able to achieve single nucleotide resolution, offering a more precise mapping technique of m6A sites [138, 139].

Furthermore, a technique coined m6A-level and isoform-characterization sequencing (m6A-LAIC-seq) provides a method to quantitatively differentiate between the proportion of m6A modified versus unmodified transcripts for each gene [140]. This protocol relies on anti-m6A IP of full-length transcripts prior to the addition of ERCC spike-in control to input, m6A+ and m6A- fractions, followed by sequencing of the intact RNA (figure 1.4.A) [140].

A challenge faced by the antibody-based detection methods described thus far is the promiscuity of m6A antibodies as they also may react with m6Am [139]. Furthermore, quantitative analysis of the m6A mark in certain conditions at single nucleotide resolution is greatly limited by antibody approaches. Additionally, methods dependent

on mutations induced by cross-linking as the read out are increasingly susceptible to changes in gene expression as higher read coverage to call sites is required. Finally, for all antibody-based approaches, variability is increased in experimental design due to the required integration of multiple control datasets (RNA input, methyltransferase depletion etc.) resulting in reduced statistical power to call sites.

To circumvent the limitations of these approaches, several antibody-free methods have been developed. The first of which is termed site-specific cleavage and radioactive-labelling followed by ligation-assisted extraction and thin-layer chromatography (SCARLET). This was developed to ascertain the stoichiometry of m6A sites or the ratio of modified to unmodified adenosine bases at a specific locus [96]. This quantitative approach directly measures the precise location and modification fraction, both important considerations in elucidating the cellular dynamics of the m6A modification. Briefly, SCARLET is based on site-specific RNase H or DNAzyme cleavage. A chimeric DNA oligonucleotide anneals to target RNA in close proximity to the candidate modification site. The sites to be cut are radiolabelled and splint-ligated to DNA oligonucleotides using DNA ligase. The radiolabelled m6A containing residue is subjected to thin layer chromatography following nuclease digestion to determine presence of m6A and the modified fraction. Although a highly informative approach, SCARLET is not applicable to high-throughput applications and can be very time-consuming [96].

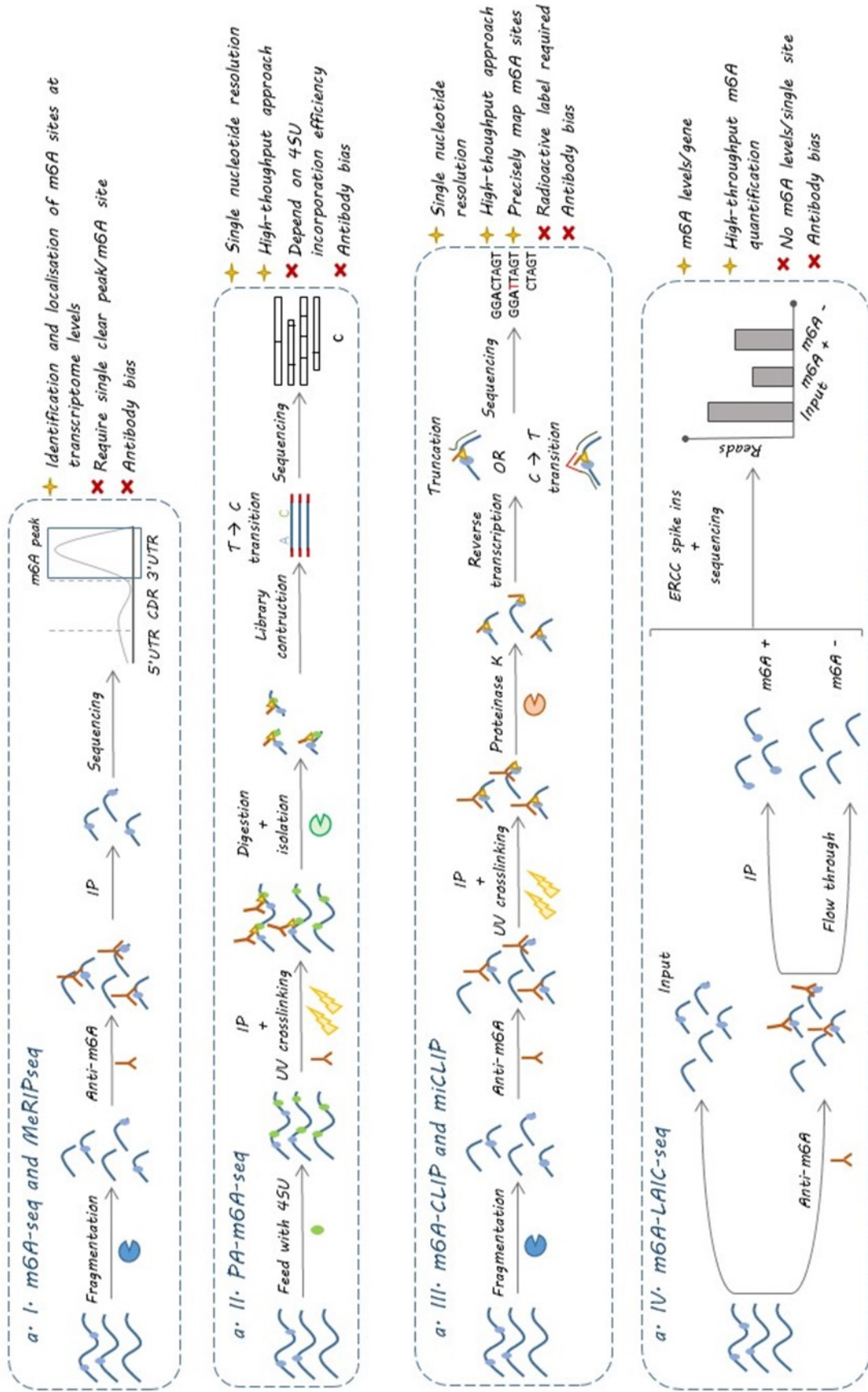
A study by Imanishi et al., describes the MazF endoribonuclease capabilities to cleave RNA within an ACA sequence motif, which is part of the m6A DRACH consensus motif, however, does not cleave upstream of M6A-CA. Thus, m6A sites can be detected as a reduction in MazF cleavage efficiency. Two recently developed methods known as RNA-endoribonuclease-facilitated sequencing (m6A-REF-seq) [141] and

m6A-sensitive RNA digestion and sequencing (MAZTER-seq) [142] utilise the bacterial RNase MazF to map m6A at single nucleotide resolution at 16-25% of all methylation sites (figure 1.5.B). In both approaches RNA is treated with MazF, leaving the fragments with a 5' ACA site and ending before the next ACA motif in the transcript. Following the sequencing step, any ACA sequences within a read suggest an uncut end and hence an m6A methylated site, thereby providing stoichiometric information on m6A based on uncut or cut ratio of reads for every ACA site [141, 142]. Notable limitations of these techniques arise due to extensive filtering requirements in order to remove any ACA sequences that are too close to one another to be accurately measured. This means that these methods alone cannot provide a whole transcriptome wide map of m6A. Nonetheless, m6A-REF-seq and MAZTER-seq represent valuable approaches to validate previously identified m6A sites, uncover new sites and elucidate m6A stoichiometry at a focused set of sites [141, 142]. Another antibody-free approach is deamination adjacent to RNA modification targets or DART-seq, a technique developed by Meyer et al., [143]. This utilises the *in vivo* expression of the m6A-binding YTH domain fused with the cytidine deaminase APOBEC1 to induce cytosine to uracil editing at positions adjacent to m6A sites, followed by next generation sequencing. The most notable advantage of this technique is the low starting material requirements with as little as 10ng of total RNA used to make libraries. Furthermore, this technique in theory should identify more relevant m6A sites due to its reliance on targeting m6A by a predominate m6A reader. Finally, library preparation is less complex as no RNA treatment is required to identify the m6A signal following extraction due to the fact that the TYH-APOBEC1 construct can be expressed transiently [143]. The past decade has seen hugely significant advancements in the methods for detecting and analysing the m6A modification.

Despite this, numerous challenges remain; a particular pain point is the ability to elucidate the status of various m6A sites on a unique RNA sequence. This will allow researchers to determine whether the modification of these sites can influence the others or whether each single site can produce varying downstream effects.

a. Antibody-based approaches

✦ = Advantages ✖ = Disadvantages



b. Non-antibody based approaches

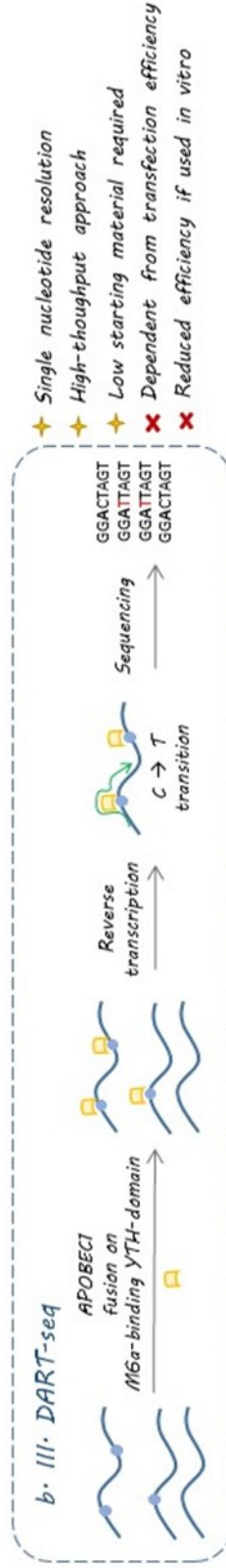
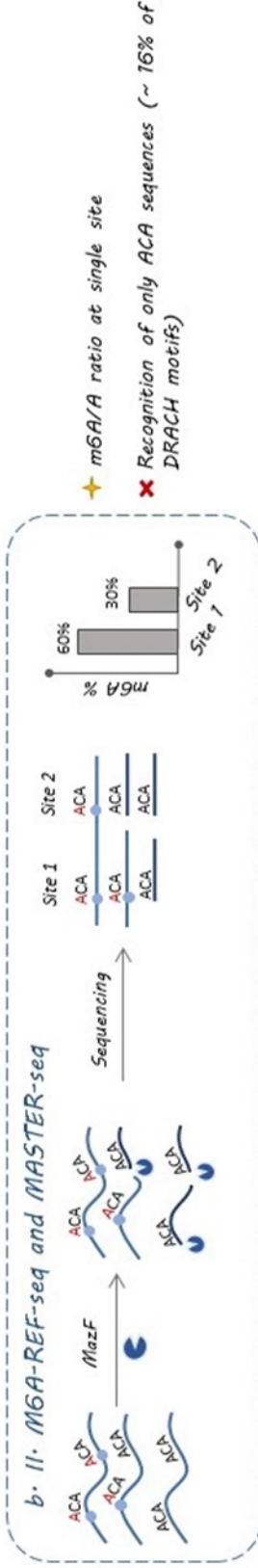
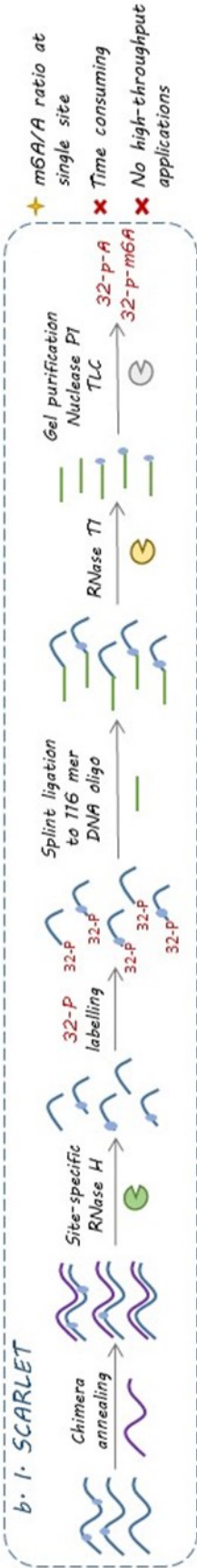


Figure 1.5 Schematic outlining m6A detection methods. **(A)** Antibody-based approaches: (I) m6A-seq and MeRIPseq; (II) PA-m6A-seq; (III) m6A-CLIP and miCLIP (IV) m6A-LAIC-seq. **(B)** Antibody free methods: (I) SCARLET); (II) M6A-REF-seq and MAZTER-seq; (III) DART-seq. Figure adapted from Sweaad et al. J Mol Cell Cardiol. 2021.

1.7 m6A in the Regulation of Different RNA Species

1.7.1 Lifecycle and Cellular Fate of m6A Modified mRNA

The deposition of the m6A mark on mRNA transcripts serves to fine tune gene expression through the mediation of almost every step of mRNA metabolism, from nuclear maturation to translation and eventual decay [144]. The m6A RNA methylation process is crucial for the mediation of early mRNA processing and maturation. Initial studies provide evidence linking the m6A mark as a regulator of splicing where a significantly higher enrichment of m6A is reported in nuclear pre-mRNA compared to mature mRNAs. Additionally, cells treated with methylation inhibitors exhibited an accumulation of unspliced transcripts in the nucleus [144-146]. In line with these findings, more recent investigations utilising photoactivatable-ribonucleoside-enhanced crosslinking and immunoprecipitation (PAR-CLIP) report an enrichment of METTL3 binding sites in introns of pre-mRNAs and a confined expression of m6A regulatory components in nuclear speckles [78, 95, 106]. Additionally, the analysis of the m6A methylome demonstrates a preferential deposition of the m6A mark in exons and UTRs of multi-isoform genes and alternatively spliced exons rather than single spliced isoform mRNAs. This indicates that the role m6A plays in splicing events is linked to the regulation of alternative splicing and in turn isoform diversity [79]. The demethylase protein FTO directly contributes to the regulation of mRNA splicing through the erasure of the m6A mark surrounding splice sites, thereby effecting the ability of SR protein family 2 (SRSF2), a pre-mRNA splicing factor, to bind to its target RNA molecule [147]. The nuclear reader protein YTHDC1 recognises and binds to the m6A mark to promote exon inclusion through the recruitment of the pre-mRNA splicing factor SRSF3 while limiting the access of SRSF10 to binding regions of targeted mRNAs [126]. The processing of methylated transcripts is also regulated by the

HNRNP family of m⁶A reader proteins where the HNRNPA2B1 protein functions in conjunction with METTL3 to co-regulate splicing of pre-mRNAs. The HNRNPC and HNRNPG members of the family contribute to the regulation of splicing events by recognising and attaching to introns of target transcripts as a direct result of m⁶A dependent changes in RNA structures [82, 132]. Studies that initially developed the aforementioned m⁶A-LAIC-seq technique uncovered the m⁶A regulation of alternative polyadenylation (APA). The authors describe widespread differences in the use of tandem APA sites by m⁶A modified and unmodified transcript isoforms and a strong bias for modified transcripts to be coupled with more proximal APA sites, leading to shortened 3' UTRs. While 1000s of methylated transcripts exhibited this bias, for 100s of transcripts the converse was true. Suggesting many genes generate at least two pools of transcripts with distinct metabolic fates dependent on a differing m⁶A methylation status coupled with differential binding of RNA proteins and miRNAs in UTR regions [140].

The export of mature mRNA from the nucleus to the cytoplasm is a vital process in the modulation of gene expression, linking nuclear transcription and maturation of mRNAs to translation in the cytoplasm. The inhibition of m⁶A RNA methylation through the depletion of METTL3 is reported to decrease RNA processing efficiency of transcripts related to the regulation of the circadian clock. Fustin et al., reveal an increase in RNA nuclear retention as a result of a delay in the export of mature mRNAs from the nucleus in METTL3 silenced models [148]. The demethylase activity of ALKBH5 was also shown to actively regulate mRNA export where its depletion results in aberrant subcellular distribution of nascent mRNAs through an acceleration of mRNA nuclear export [106]. The mechanism by which the m⁶A modification mediates the nuclear to cytoplasmic mRNA transport relies on the recognition and attachment of the nuclear

YTHDC1 reader protein to m6A methylated transcripts. YTHDC1 was reported to propagate methylated mRNA export through its association with the SRSF3 protein, thereby allowing for the incorporation of m6A methylated mRNA to export receptor NXF1. This mechanism indirectly results in the subsequent increase in translation due to increasing the cytoplasmic abundance of target mRNAs [127].

Initiation of translation is typically the rate limiting step in effective protein production, interestingly several distinct mechanisms by which the m6A mark mediates the translation of mRNA transcripts have been identified in recent years. The binding of the YTHDF1 reader protein to m6A methylated mRNA actively promotes translation by facilitating the coupling of m6A marked transcripts with cellular translation machinery. More specifically, YTHDF1 enables the recruitment of the translation initiation complex through its association with the eukaryotic initiation factor 3 thereby driving the rate of translation [123]. Interestingly, the primary m6A catalytic component METTL3 is reported to regulate translation efficiency in a role independent of its methyltransferase activities, the YTHDF1 mediated pathway and other known co-factors. Here, METTL3 improves target mRNA translation efficiency via its interaction with cellular translational machinery and subsequent recruitment of the eukaryotic initiation factor 3 [123, 149]. The insulin-like growth factor 2 mRNA-binding proteins (IGF2BPs) were also reported to preferentially recognise m6A modified mRNAs to promote the stability and translation of 1000s of target mRNAs in a m6A dependent manner [150]. The translation process typically begins with the recruitment of the 43S ribosomal complex to the 5' cap of mRNAs by a cap-binding complex. In many cases however, transcripts can be translated in alternative cap independent mechanisms. The presence of m6A in the 5' UTR was reported to regulate cap independent translation through the direct binding of the eukaryotic initiation factor 3 which facilitates

ribosome loading via recruitment of the 43S complex to initiate translation. Diverse cellular stresses induce transcriptome-wide redistribution of m6A and increased numbers of transcripts with 5' UTR m6A, suggesting a role for m6A in promotion of translation under stress conditions [151].

Evidence also implicates m6A methylation in the destabilisation and degradation of target transcripts to reduce half-life and accelerate the rate of decay of these mRNAs. The m6A binding protein YTHDF2 is shown to interact with methylated transcripts to deliver the YTHDF2-mRNA complex from the translatable pool to mRNA decay sites, such as cellular processing bodies [152]. A study by Du et al., elucidates the underlying mechanisms by which the YTHDF2 protein mediates the degradation of mRNAs. Evidence suggests that the YTHDF2 protein recruits the CCR4-NOT deadenylase complex by interacting directly with the superfamily homology (SH) domain of CNOT1, the scaffolding subunit of the complex. This in turn initiates deadenylation and decay of m6A marked mRNAs [153]. A spatiotemporal interplay between YTHDF3 and both YTHDF1 and YTHDF2 regulates the cytoplasmic metabolism of m6A methylated mRNA. YTHDF3 is reported to promote translation in synergy with YTHDF1 while regulating methylated mRNA decay through the YTHDF2 protein [124]. The m6A methylation of mRNA transcripts ensures an additional layer of regulation beyond what is offered by primary sequences or secondary structures. This allows for rapid and dynamic responses to an increase or decrease in demand for protein synthesis and subsequent removal of transcripts. The m6A modification also acts as a mechanism for the sorting of 100s of individual transcripts with diverse translation efficiencies and stabilities for coordinated processing and decay.

1.7.2 m6A Methylation of Primary miRNAs

An association between m6A RNA methylation and miRNA function was first described in 2012 where a strong correlation between m6A and miRNA binding sites in the 3'UTRs of target mRNA transcripts. M6A-seq analysis revealed that 67% of 3' UTRs containing m6A peaks also contain a minimum of 1 miRNA binding site [80]. Notably, a reverse pattern of localization of miRNA response elements and m6A peaks was elucidated where miRNA sites were highly enriched at the 3' end of 3' UTRs, while sites for m6A exhibited a higher abundance near the stop codon and are reduced along the 3' UTR. More highly expressed miRNAs were also shown to exhibit a much greater proportion of target mRNA transcripts abundant with m6A peaks than that of lower expressed miRNAs. Despite the exact underlying reasons for these apparent correlations not being fully elucidated, the authors hypothesise that miRNA binding could contribute to the modulation of the methylation landscape of target mRNA 3' UTRs [80]. It has been long known that miRNA mediated suppression of mRNA targets is primary dependent on the translational repression or degradation of target transcripts, however the exact pathways by which miRNA mediated inhibition is determined are yet to be completely understood. It is therefore possible that the spatial proximity of m6A sites to miRNA response elements could play a role in determining miRNA mediated inhibition of mRNAs. Furthermore, the m6A modification of the adenosine base slightly destabilises the hydrogen bonds that constitute A-U pairing. It is therefore speculated that the presence of the m6A mark within the 3' UTR of miRNA target transcripts could reduce duplex stability and in-turn destabilise miRNA-mRNA binding.

A more recent study has implicated the m6A RNA modification as a crucial factor in the promotion of miRNA biogenesis. Pri-miRNA transcripts were found to be highly

enriched in m6A and the depletion of this modification resulted in a profound reduction in expression of 70% of mature miRNAs [154]. METTL3 mediated methylation of pri-miRNAs is crucial for the recognition and processing of target pri-miRNAs by DGCR8, a component of the microprocessor complex. METTL3 knockdown was reported to reduce the associations between the DGCR8 complex and substrate pri-miRNAs, this was correlated with the nuclear enrichment of unprocessed pri-miRNAs. Consistent with this, the overexpression of METTL3 and the subsequent increase in m6A enrichment enhances global miRNA maturation in a non-cell-type specific manner [154]. The co-transcriptional deposition of the m6A mark on pri-miRNAs is shown to be recognised by the HNRNPA2B1 reader protein, which subsequently recruits the DGCR8 protein and in turn promotes miRNA processing [155]. Interestingly, this study found that only half of the miRNAs dependent on the m6A mark for their maturation were targets of HNRNPA2B1, suggesting the existence of additional nuclear readers that mediate m6A-dependant miRNA processing as well as other possible nuclear processing events that involve m6A [155]. In summary, the deposition of m6A is crucial for the specific recognition and attachment of the DGCR8 component of the microprocessor complex to target pri-miRNAs, as opposed to other secondary structures that may resemble pri-miRNAs.

A number of subsequent studies have emerged in recent years further validating the crucial role played by the m6A RNA modification and its regulators in miRNA processing and maturation, most of which are predominately in the fields of cancer biology and development. The importance of miRNAs in cardiovascular homeostasis and disease have been studied in depth and with the unfolding relevance of m6A in this field, I predict the interactions between m6A miRNAs will be of great interest to researchers in coming years.

1.8 Biological Impact of m6A RNA Modifications

1.8.1 Implications of m6A in Cardiac Homeostasis and Disease

Despite recent advancements in the field and rapidly growing interest in the biological importance of the m6A modification, its role in maintaining cardiovascular homeostasis and its dysregulation in disease is only recently emerging. A key study by Dorn et al., identified a role for METTL3 in the maintenance of healthy cardiac function and hypertrophic stress responses [156]. An increase in m6A modification levels in cardiomyocytes was described in response to hypertrophic stress stimulus. The transcriptome-wide mapping of m6A revealed transcripts encoding for protein kinases exhibited the most increased levels of m6A under hypertrophic conditions. This is indeed in line with the well-defined role of protein kinase mediated pathways in hypertrophic growth [157]. Researchers also generated cardiomyocyte specific METTL3 knock-out and knock-in mouse models. Here, the knock-in mice exhibited elevated levels of m6A in cardiomyocytes in line with an increase in cardiac hypertrophic growth [156]. Interestingly, no histopathological changes were reported in these hearts and cardiac function was preserved at both baseline and under stress despite observed morphological changes. Furthermore, METTL3 KO mice demonstrated no signs of remodelling at both cellular and morphological levels, indicating that METTL3 is not crucial for postnatal cardiac development. It is however important to note that a decrease in overall heart function and structural abnormalities were observed in aged METTL3 KO mice, indicating progression towards heart failure. Follow up studies could provide key insights into the relevance of m6A and METTL3 in cardiac aging. Here METTL3 KO mice could be aged for longer and total RNA from cardiomyocytes could be subjected to m6A transcriptome wide analysis to investigate differential m6A enrichment. *In vitro* studies involving the small interfering RNA

(siRNA) mediated transient knockdown of METTL3 in cardiomyocytes demonstrated an obstruction of hypertrophy upon stimulation. Further *in vivo* studies describe an accelerated progression towards cardiac failure when METTL3 KO mice are subjected to transverse aortic constriction to induce pressure overload stimulation. On the other hand, application of milder cardiac stress in these mice did not affect heart function and led to eccentric cardiomyocyte geometry. These findings suggest a newly identified role of METTL3 and m6A in cardiac adaptation to stress [156].

There is currently no effective approach for adverse post-ischaemic cardiac remodelling where expression levels of key regulators in the right ventricles during heart failure are inconsistent. This therefore indicates a possible role for post-transcriptional regulation in failing hearts [158]. A key study recently demonstrated the m6A eraser FTO as a crucial regulator of cardiac contractile function and myocardial repair [159]. An increase in the levels of m6A RNA methylation was described in infarcted ischaemic hearts in human, pig and murine models. Failing hearts also demonstrated significantly reduced levels of FTO where its aberrant expression was linked to the transcriptome wide elevation of m6A levels. The depletion of FTO in cardiomyocytes was also shown to result in increased arrhythmic events, suggesting a role for FTO in contractile function. Conversely, FTO overexpression resulted in the attenuation of ischaemia associated elevation of m6A and cardiomyocyte dysfunction. A series of *in vivo* interventional studies reveal an improvement in cardiac function at a chronic stage of post-MI while alleviating fibrosis and enhancing angiogenesis at the peri-infarct boarder zone. The cardiac reparative functions of FTO were further corroborated when a more severe progression of heart failure accompanied by a lower ejection fraction was observed in FTO KO mice [159]. While these studies provide robust novel insights into an indispensable role of FTO in heart failure, the generation

of a cardiomyocyte specific KO model could offer further understanding into the importance of FTO in the cardiac setting and the exclusivity of its functions. Mechanistically, the authors reveal the preferential demethylation of cardiac contractile mRNA transcripts including SERCA2A, MYH6/7 and RYR2. This in turn enhances their stability by preventing m6A accelerated degradation under hypoxic conditions. Transcriptome wide analysis of m6A also reveals the selective targeting of pathways associated with fibrosis, angiogenesis and the targeting of long noncoding RNAs linked to hypertrophy and fibrosis. Thereby supporting observed reductions in scar size and improved angiogenesis in infarcted hearts overexpressing FTO [159]. Collectively, this study provides compelling evidence for the cardioprotective role of FTO mediated demethylation of m6A during heart failure. Finally, future investigations into whether the functional action of FTO in this setting is exclusive to the demethylation of m6A or also depends on m6Am demethylation would be of great interest.

A study by Kmietczyk et al., explored the role of the m6A modification in the setting of dilated cardiomyopathy where an increase in m6A methylation is observed in mRNAs. MeRIP-Seq studies in dilated cardiomyopathy hearts suggest the methylation of mRNAs involved in heart development, cell adhesion and transcription. Additionally, the transient depletion of METTL3 in neonatal rat cardiomyocytes resulted in the aggravation of hypertrophic responses upon stimulation, while the depletion of FTO blunted these responses. Contrary to the findings presented by the aforementioned Dorn et al., study, this investigation demonstrates an attenuation of cardiac hypertrophic growth and remodelling upon the cardiomyocyte overexpression of METTL3 in hearts subjected to transverse aortic constriction [160]. These contrasting findings may be explained by differences in study design where Dorn et al., utilised a

transgenic approach driven by alpha myosin heavy chain-promoter for METTL3 overexpression, whereas Kmietczyk et al., employed an adeno-associated virus-based approach for the overexpression of METTL3 in C57B16/N mice. Further studies are therefore needed to fully elucidate the novel role of METTL3 in response to hypertrophic stress.

In agreement with the findings presented by Dorn et al., and Mathiyalagan et al., a recent study has demonstrated an alteration in the m6A landscape due to cardiac hypertrophy and heart failure [161]. Transverse aortic constriction in mice was used to investigate m6A in heart failure progression where m6A-Seq studies and RNA sequencing revealed that the proportion of transcripts with significant alterations in m6A landscape exceeded that of differentially expressed genes. This was corroborated clinically in end-stage heart failure biopsies in which transcripts with differential methylation primarily encode for metabolic functions and cardiomyocyte processes. Further studies into whether the extent of alterations in methylation is correspondent to clinical aetiology and severity through the analysis of m6A in patient samples would be of great interest. Additionally, Berulava et al., elucidated a novel transcription-independent mechanism of translation through the regulation of transcript-ribosome occupancy by the m6A modification resulting in aberrant expression in the progression of heart failure. Proteomic analysis by means of mass spectrometry would capitalise on the comprehensive bioinformatic data presented by this study and provide further clarity into the novel mechanisms presented here. Berulava et al., also generated cardiomyocyte specific FTO KO mice which were subjected to transverse aortic constriction in order to further understand m6A in adaptation to cardiac stress. These studies revealed a higher degree of dilation in FTO KO mice and an overall acceleration in the progression of heart failure. When taking

the findings by Dorn et al., into consideration which suggest a compromised response to pressure overload as a result of METTL3 depletion, it can be speculated that deregulation of the m6A landscape in either direction is linked with eccentric heart function and remodelling. Finally, having generated a cardiomyocyte FTO KO mouse model, further studies characterising the role of FTO mediated m6A in the context cardiac development and aging would address a plethora of unanswered questions.

Reperfusion following myocardial ischaemia is indeed essential in mitigating permanent damage to the myocardium, however the recovery of blood flow may cause a paradoxical amplification of tissue damage in a phenomenon coined “reperfusion injury”. A recent report describes an abnormal upregulation of m6A in hypoxia/reoxygenated cardiomyocytes *in vitro* and ischaemia/reperfusion (I/R) treated mouse hearts [131]. This report also provides evidence of antipodal effects of METTL3 and the eraser ALKBH5 in cardiomyocyte autophagy, a process notably known to be negatively regulated by ischaemia/reperfusion. Impairment in autophagic flux and a subsequent increase in apoptosis was observed following the overexpression of METTL3 or the depletion of ALKBH5 in cardiomyocytes subjected to hypoxia/reoxygenation (H/R) treatment. Interestingly, METTL3 silencing resulted in impaired autophagic flux and inhibited apoptosis, suggesting that METTL3 may be a negative regulator of autophagy. Song et al., also reveal that the upregulation in METTL3 expression following H/R increases the m6A levels of transcription factor EB (TFEB), a master regulator of autophagy and lysosomal biogenesis [162]. This thereby renders the TFEB pre-mRNA more accessible to the reader HNRNPD and in turn decreases cardiomyocyte expression of TFEB [131]. Conversely, the actions of ALKBH5 reverses the H/R mediated hypermethylation of nascent TFEB transcripts.

Recent research by Li et al. identified the METTL3 mediated pro-fibrosis in the post-infarct myocardium [163]. Cardiac fibroblasts exposed to TGF- β 1 *in vitro* and fibrotic tissue from post-myocardial infarcted murine hearts expressed an increase in METTL3 levels. Furthermore, mice treated with lentiviral particles to deplete METTL3 2-weeks prior to the induction of MI demonstrated an amelioration in infarct border zone collagen deposition and improved heart function 4-weeks post-MI. Mechanistically, Li et al. demonstrate that the novel pro-fibrotic role of METTL3 is mediated, at least partially, through the Smad2/3 pathway.

1.8.2 Role of m6A in the Vasculature

Recent investigations into the relevance of the m6A modification in the vasculature has primarily been focused on cancer cell biology. In this context, m6A has indeed been implicated in the modulation of numerous known vasoactive factors. This section of the thesis will strictly focus on recent studies exploring the m6A modification in EC biology and in the vasculature.

The hemogenic endothelium directly produces the first definitive haematopoietic stem and progenitor cells (HSPCs) during embryogenesis in a process termed endothelial-to-haematopoietic transition (EHT). Recent studies have demonstrated the importance of the m6A RNA modification in HSPC fate determination in vertebrate embryogenesis [164, 165]. Zebrafish embryos deficient of METTL3 expressed a reduction in expression of HSPC markers and a decrease in haemogenic ECs and emerging HSPCs [164]. The authors also report that ECs depleted of METTL3 maintained endothelial identity while exhibiting compromised transition into HSPCs while the levels of arterial endothelial markers is upregulated. Notably, the endothelial overexpression of METTL3 rescued haematopoietic defects. Notch1, a known regulator of endothelial identity through HSPC programming repression, was shown

to be an m6A methylated transcript in ECs and the haemogenic endothelium. Interestingly, Notch signalling during EHT is repressed as a result of the m6A modification of Notch1. Furthermore, the depletion of the YTHDF2 reader led to phenotypic characteristics homogenous to those observed in *mettl3* morphants. Studies indicate that the deposition of the m6A mark on Notch1 and other arterial endothelial mRNAs results in YTHDF2-mediated decay and in turn facilitates HSCPC generation. The METTL3-Notch-YTHDF2 axis is corroborated in a follow up study which developed a METTL3 KO murine model, thereby demonstrating a crucial evolutionary conserved function of METTL3 modulated m6A in the specification of HSPCs [165]. Notably, several constituents of the Notch and VEGF pathways were discovered to be m6A methylated targets. Given the importance of this pathway in the modulation of endothelial homeostasis and the regulation of vital endothelial functions such as angiogenesis, it would be of particular interest for future studies to characterise the significance of m6A and its regulators in the mature vasculature in more depth.

The endothelium forms an interface between circulating blood and the rest of the tissues of the body. Due to this unique role, ECs play a central role in the progression of metabolic disorders, including obesity. Kruger et al., investigated the relevance of endothelial FTO in obesity induced metabolic and vascular alterations through the generation of an EC specific tamoxifen inducible FTO KO murine model [166]. Although the absence of endothelial FTO had no direct effect on the development of obesity, it did however offer protection against the progression of obesity-induced metabolic aberrations including IR, hypertension, hyperglycaemia and vascular resistance. The effects of FTO knockdown were described to occur as a result of the increase of AKT phosphorylation in ECs and subsequently in skeletal muscle. The

authors also reveal that the vasculoprotective effects observed following FTO depletion were mediated through the increase in prostaglandin D2 (PGD2) expression subsequent to an increase of m6A levels in synthase lipocalin-type prostaglandin D synthase (L-PGDS). Interestingly, the abrogation of the protective effects of FTO depletion was reported following the inhibition of PGD2 synthesis, while the addition of PGD2 in resistance arteries of high fat diet fed endothelial FTO-KO mice and obese human arteries recused myogenic tone [166].

Angiogenesis is a highly intricate and regulated composite process whereby new blood vessels are formed from the pre-existing vasculature. Yao et al., describe a novel role for m6A mediated through METTL3 in the modulation of the angiogenic process [167]. These studies revealed altered EC processes crucial for angiogenesis including proliferation, migration and tube formation following METTL3 depletion or over expression *in vitro*. The authors reveal that the mechanisms by which METTL3 exerts this novel angiogenic role involves the regulation of Wnt signalling. More specifically, METTL3 mediates the methylation of dishevelled 1 (DVL1) and LDL receptor related protein 6 (LRP6) components of this pathway and in turn enhances the efficiency of translation in a YTHDF1 dependent manner. Yao et al., reveal an upregulation in METTL3 expression resulting in an aberrant increase in m6A levels in ECs and mouse retinas exposed to hypoxic conditions. This study also generated an endothelial specific METTL3 KO murine model to reveal a decreased avascular area and pathological neovascular tufts in an oxygen-induced retinopathy model and inhibited alkali burn-induced corneal neovascularization.

Subsequent studies have emerged that further corroborated the novel crucial role for METTL3 mediated m6A in the regulation of angiogenesis and the associated cellular processes. Dong et al., set out to define the relevance of METTL3 on angiogenesis,

oxidized low-density lipoprotein (ox-LDL) induced endothelial dysfunction and atherosclerosis development [169]. The authors describe compromised cellular processes crucial for angiogenesis following METTL3 depletion in healthy and ox-LDL-exposed ECs and hindered angiogenesis in developing embryos. Interestingly, ox-LDL-induced ECs exhibited an increase in METTL3 expression and total m6A RNA levels while a murine model of atherosclerosis demonstrated reduced blood lipid burden and inhibited atherosclerotic plaque formation following METTL3 depletion. Mechanistically, the authors reveal that the knockdown of METTL3 hindered the progression of atherosclerosis by inhibiting the JAK2/STAT3 pathway through the actions of the m6A reader IGF2BP1 [169].

Successful Distraction Osteogenesis (DO) mediated bone regeneration is highly dependent on the angiogenic process. Jiang et al., investigated the importance of m6A in EPC mediated angiogenesis during DO [170]. In line with the aforementioned findings, the depletion of METTL3 in EPCs was associated with the impairment of proliferation, migration, network formation and chicken embryo chorioallantoic membrane (CAM) angiogenic activity. The overexpression of METTL3 had an opposite effect by improving EPC capabilities via the PI3K/AKT signalling pathway. These findings indicate that the targeting of m6A via METTL3 may be a viable approach to enhancing DO regeneration and EPC angiogenesis [170].

A study by Wang et al., investigating the importance of m6A in the aetiology brain arteriovenous malformations (AVMs) identified the writer WTAP as an independent regulator of angiogenesis. The authors reveal that the depletion of WTAP compromised EC network forming capabilities [171]. WTAP expression is reduced in lesions of brain AVMs, while MeRIP-seq analysis in WTAP-depleted ECs identified Desmoplankin, a primary constituent of desmosomes crucial for microvascular tube

formation [172], as a downstream target of WTAP and m6A. The IGF2BPs reader protein was shown to interact with m6A sites to mediate the stabilisation of Desmoplankin transcripts. Desmoplankin plays a key role in preserving the mechanical integrity of the myocardium [173]. Taking into consideration that Desmoplankin is a common target for METTL3 and WTAP, further studies into the activity of these methylases in the regulation of Desmoplankin in the setting of myocardial mechanical stress would be particularly interesting. Additionally, investigations adopting a gene therapy-based approach to manipulate endothelial expression of WTAP in available genetically engineered mouse models of brain AVM would provide valuable insights into the therapeutic potential of WTAP mediated m6A in the prevention or the progression of brain AVMs [174].

In line with previously described atherosclerotic role of m6A [169], a recent study implicated METTL14 mediated m6A in the pathogenesis of EC inflammation and the development of atherosclerosis [175]. METTL14 expression levels are increased in a stable TNF- α -instigated EC inflammation model while atherosclerotic lesions from APOE KO mice also demonstrated a significant upregulation in METTL14 expression. A METTL14/APOE KO murine model was utilised to demonstrate a reduction in atherosclerotic plaques when compared to APOE deficient mice. The transcriptome-wide analysis of m6A revealed an increase in methylation levels on the transcription factor forkhead box O1 (FOXO1), while the knockdown of METTL14 significantly decreased its methylation. The reader YTHDF1 recognises and binds to METTL14 dependent m6A sites on FOXO1 to promote the translational capacity of these transcripts thereby upregulating FOXO1 expression. The expression levels of FOXO1 targets, including the endothelial adhesion proteins intercellular adhesion molecule-1 (ICAM-1) and vascular cell adhesion molecule-1 (VCAM-1) are thereby increased.

This results in subsequent mononuclear-endothelial adhesion and ultimately the progression of atherosclerosis [175].

1.8.3 m6A in Cardiovascular Disease Risk Factors

Two Swedish population-based case-control studies associated a single nucleotide polymorphism (SNP) within FTO (rs9939609 T>A) with an enhanced susceptibility to CHD [179]. The association of this FTO SNP with coronary artery disease (CAD) and obesity was corroborated by a successive study performed in a Pakistani cohort [180]. A 19-year follow up of the Oulu Project Elucidating Risk of Atherosclerosis (OPERA) studied the relevance of FTO rs9939609 on cardiovascular events and death. FTO rs9939609 indeed predicts CHD, with the AA genotype exhibiting an increased risk of cardiovascular events and death. Additionally, this variant was also identified as an independent risk factor for atherosclerosis [176]. A second SNP within FTO (rs17817449) was correlated with an increased risk of rejection in heart transplant patients [177]. Furthermore, the YTHDF3 polymorphism rs4739066 demonstrated a weak association with MI in an ethnic Arab population [178].

Obesity has been well established as an independent risk factor for CVD with its prevalence reaching epidemic proportions over the past few decades [181]. SNPs within FTO associated with an increased risk to obesity have been identified by several GWAS [101, 103, 182, 183]. Consequently, considerable interest was kindled in understanding whether FTO or another gene in the same locus was responsible for the obesity association signal in these GWAS. The characterisation of an FTO-overexpressing murine model revealed an increase in fat mass and overall body weight while exhibiting decreased leptin levels and hyperphagia. These findings indicate that FTO overexpression may dysregulate the secretion of leptin from adipose tissue or its expression [184]. A reduction in adipose tissue as a consequence of

increased energy exposure was also reported in FTO deficient mice, suggesting a functional role in the regulation of energy expenditure [185]. The underlying mechanisms by which FTO modulates fat mass and body weight are dependent on its role in regulating the early stages of adipogenesis. Here, FTO contributes to the enhanced expression of the pro-adipogenic short isoform of Runt-related transcription factor 1 (RUNX1) [186]. A decrease in the expression of autophagy-related 5 (ATG5) and ATG7 has been reported as a result of FTO knockdown. This in turn attenuates autophagosome formation and inhibits autophagy and adipogenesis [187]. FTO has also been reported to regulate adipogenesis through the modulation of cell cycle progression in early adipocyte differentiation. FTO depletion results in enriched m6A methylation levels on the cyclin A2 (CCNA2) and cyclin dependent kinase 2 (CDK2) pre-mRNAs. The m6A mark is recognised by the YTHDF2 reader which in turn improves that rate of mRNA degradation and a subsequent delay of cell cycle progression and impeded adipogenesis [188]. A plethora of studies beyond the scope of this thesis have in recent years come to light, providing insights into the molecular processes by which m6A and its components modulate obesity. Altogether, these discoveries underline the potential of m6A, in particular its modulation by FTO, as a novel biomarker and possible therapeutic target for obesity.

The m6A RNA modification has also been associated with hypertension where a large-scale GWAS elucidated the m6A-SNPs rs9847953 and rs197922 as functional variants with the possibility to dysregulate gene expression related to blood pressure modulation [189]. Additionally, m6A analysis in microvascular pericytes from spontaneously hypersensitive rats reveal a decrease in m6A, indicating a possible involvement of alterations to the m6A landscape to the pathogenesis of hypertension [190].

Component of the m6A machinery	Reported cardiovascular system role	Reference
<i>METTL3</i>	cardiac function maintenance	[156]
	hypertrophic stress responses	[156, 160]
	heart development	[156]
	cardiac ageing	[156]
	heart failure	[156, 161]
	I-R treatment	[131]
	CM autophagy	[131]
	angiogenesis	[167, 168]
	cardiac fibrosis	[163]
<i>WTAP</i>	brain arteriovenous malformations	[171]
<i>METTL14</i>	atherosclerosis	[175]
<i>FTO</i>	coronary heart disease	[176]
	heart failure	[177]
	atherosclerosis	[176]
	heart transplant rejection	[177]
	myocardial infarction	[159]
	fibrosis	[159]
<i>ALKBH5</i>	CM autophagy	[131]
<i>YTHDF1</i>	angiogenesis	[167]
<i>YTHDF3</i>	myocardial infarction	[178]

Table 1.1 Reported involvement of individual components of the m6A machinery and associated reader proteins in cardiovascular processes and pathologies

1.9 Study Rationale and Hypothesis

Diabetes exposes the vascular endothelium to a chronic hyperglycaemic milieu, leading to EC damage and dysfunction. The resulting microangiopathy and rarefaction of the microvasculature leads to tissue hypoperfusion and propagates the occurrence of ischaemic events, with diabetic individuals demonstrating a higher incidence of CVD than those without [191]. Two such manifestations are CLI and IHD, with the former posing a significant risk of limb loss and cardiovascular death, while the latter represents the leading cause of mortality in the diabetic population [192]. The ability to reduce CVD rates in the diabetic population by glycaemic control with or without associated lipid lowering approaches, has remained elusive [24]. Furthermore, diabetes is not only a direct casual factor in the development of vascular complications but is also associated with the impairment of endogenous reperfusion of ischaemic tissue accomplished by reparative neo-vascularisation. There is an urgent and unmet clinical need for novel therapeutic approaches that promote local revascularisation in the setting of diabetic CLI and IHD. Angiogenesis is therefore a putative target for therapy, with significant efforts being made in the identification of novel regulatory pathways that may translate into new targets for treatment.

A plethora of cellular functions during development, homeostasis and disease are modulated by m6A associated enzymes. Most relevant to this study, emerging genetic, experimental and clinical evidence have provided clear associations between components of the m6A regulatory machinery, diabetes and CVD in varying contexts [156, 159, 161, 193]. Pilot data from the Emanuelli laboratory highlights the potential clinical relevance of m6A in the setting of both CLI and IHD. A reduction the primary m6A methyltransferase, METTL3, was observed in limb muscles of diabetic patients

with CLI compared to non-diabetic or non-CLI patients undergoing saphenous vein stripping. Additionally, RNA-sequencing studies were performed in left ventricular (LV) biopsies collected as part of Association of non-coding RNAs with Coronary Artery Disease and type 2 Diabetes (ARCADIA), a perspective observational clinical study [194]. This investigation revealed a trend towards a decrease in METTL3 transcripts in biopsies derived from diabetic and ischaemic hearts (CABG-DM), when compared with ischaemia alone (CABG) or with absence of ischaemia and DM. At the time of the initiation of this study, the role of m6A in angiogenesis was completely unexplored. The m6A RNA modification has been identified as a crucial factor in miRNA processing. More specifically, the METTL3 mediated co-transcriptional deposition of m6A on pri-miRNAs is recognised by a putative reader of this mark, known as HNRNPA2B1, which in turn, promotes miRNA processing through the recruitment of the microprocessor component DGCR8 [154, 155]. A further understanding into the regulatory interface between this single-nucleotide modification and cellular functions will pave the way towards the development of novel diagnostic, prognostic and therapeutic tools for the management of DM associated CVDs. Consequently, this study has been designed to investigate the following **scientific hypotheses:**

- METTL3 plays an essential role in EC function and angiogenesis, potentially through the modulation of miRNA processing
- Endothelial expression of regulatory machinery and m6A levels are dysregulated in the diabetic and ischaemic environment
- Exogenous supplementation of METTL3 via local gene transfer:
 - improves post-ischaemic muscular neovascularisation and blood flow recovery in the murine hindlimb ischaemia model

- promotes therapeutic angiogenesis and improves myocardial function in the murine MI model

Chapter 2
Materials and Methods

2. Materials and Methods

2.1 Cell Culture

2.1.1 HUVEC and HCMEC Culture

Pooled Human Umbilical Vein Endothelial Cells (HUVEC) (cat no.C-12203, Promocell) and single donor Human Cardiac Microvascular Endothelial Cells (HCMEC) (cat no. C-12285, Promocell) were routinely cultured in either EC Growth Medium 2 (EGM2) supplemented with EGM2 SupplementMix kit (cat no.C-39216, Promocell) or EC Growth Medium MV2 (EGM-MV2) supplemented with EGM-MV2 SupplementMix Kit (cat no.C-39226, Promocell). Cell culture conditions were maintained at 37°C in a humidified atmosphere containing 5% CO₂. Cells were initially cultured in T-25 flasks (Corning) pre-coated with 0.1% gelatin (cat no.9000-70-8, Sigma-Aldrich) before being transferred to T-75 flasks (Corning) and passaged every 3-4 days at a ratio of 1:4 by trypsinization: cells were washed twice with PBS, incubated with TrypLE (cat no.12604013, Gibco,) for 3 minutes at 37°C and 5% CO₂ and resuspended in complete EGM2 or EGM-MV2. HUVEC and HCMEC were used between passage 3-6.

2.1.2 *In vitro* Diabetic and Ischaemic Mimicking conditions

To mimic hyperglycaemic conditions, cells were cultured under a high concentration of glucose (high glucose, HG: 25 mM D-glucose) (cat no. G8270, Sigma-Aldrich), control conditions (normal glucose, NG: 5mM) or osmotic control (osmotic control, OSC: 25 mM L-glucose) (cat no.G5500, Sigma-Aldrich) for 48 hours. To mimic ischaemia, cells were cultured under hypoxic conditions (1% O₂) or normoxic conditions (20% O₂) for 48 hours. To mimic advanced ischaemia in diabetes, cells were exposed to a combination of HG and hypoxia for 48 hours.

2.2 Delivery of Short Interfering RNA and Mimic miRNA

Human METTL3 expression was inhibited using short interfering RNA (siRNA) oligonucleotides; denoted as METTL3 siRNA in the text (cat no.s32142 and s32143, Ambion, Life Technologies). In parallel, control siRNAs were used, and denoted as CT siRNA (cat no.4390843, Ambion, Life Technologies). Overexpression of let-7e-5p and mir-18a-5p was achieved through the delivery of hsa-miR-18a-5p (cat no.300487-05, Dharmacon) and hsa-let-7e-5p mimics (cat no.300479-05, Dharmacon) or miRNA mimic negative control (cat no.001000-01-05, Dharmacon). For siRNA and mimic miRNA delivery into HUVEC or HCMEC, cells were seeded 24 hours before transfection onto 0.1% gelatin coated 6-well plates at a density of 1.6×10^5 cells/well or in 96 well plates at a density of 5×10^3 cells/well in complete EGM-2 medium. Cells were incubated overnight to form 60-70% confluent cultures at time of transfection. Transfection mixture was prepared by adding either 30 nM of METTL3 siRNA [15 nM of METTL3 siRNA 1 and 15 nM METTL3 siRNA 2] or CT siRNA, and hsa-miR-18a-5p mimic, hsa-let-7e-5p mimic or miRNA mimic negative control (final concentration 30nM) with Oligofectamine Transfection Reagent (cat no.12252011, Invitrogen) in OptiMEM medium (cat no.31985070, Invitrogen) and incubated for 30 minutes at room temperature (RT). Transfection mixture was added to each well and incubated for 12 hours at 37°C in a humidified atmosphere containing 5% CO₂. EGM-2 medium was added to each well for a further 36 hours. Transfected cells were incubated for a total of 48 hours before use in experiments.

Description		Sequence	Catalogue Number
METTL3 siRNA 1	Sense	GAUCCUGAGUUAGAGAAGAtt	s32142
	Antisense	UCUUCUCUAACUCAGGAUCtg	Ambion, Life Technologies
METTL3 siRNA 2	Sense	GCAGUCCUGAAUUAGCUAtt	s32143
	Antisense	UAGCUAAUUCAGGAACUGCtg	Ambion, Life Technologies
CT siRNA	N/A		4390843 Ambion, Life Technologies
hsa-miR-18a-5p	UAAGGUGCAUCUAGUGCAGAUAG		300487-05 Dharmacon
hsa-let-7e-5p	UGAGGUAGGAGGUUGUAUAGUU		300479-05 Dharmacon
miRIDIAN miRNA mimic negative control	UCACAACCUCCUAGAAAGAGUAGA		001000-01-05 Dharmacon

Table 2.1 List of siRNAs and miRNA mimics

2.3 Stable METTL3 Knockdown Generation

Human METTL3 expression was knocked down using commercially available lentiviral (LVs) expressing Short Hairpin RNAs specific to METTL3 (cat no. TRCN0000034715 or TRCN0000034717, Sigma-Aldrich) (LV-METTL3-shRNA) or control (LV-CT-ShRNA) shRNA (cat no. SHC002, Sigma-Aldrich) (LV-CT-shRNA). HUVEC or HCMEC were seeded 24 hours before infection onto 0.1% gelatin coated 6-well plates at a density of 1.6×10^5 cells/well in complete EGM-2 medium. Cells were incubated

overnight at 37°C in a humidified atmosphere containing 5% CO₂ to form 60-70% confluent cultures. HUVEC or HCMEC were then infected with LV-METTL3-shRNA or LV-CT-shRNA and polybrene (4ug/mL) (cat no. TR-1003-G, Millipore). Positively infected HUVEC or HCMEC were then selected with puromycin (1µg/mL) (cat no. A1113803, Life Technologies) for one week.

Description	Clone ID	Sequence	Catalogue Number
METTL3 1: MISSION Lentiviral Transduction Particles	NM_019 852.2- 1063s1c 1	CCGGGCAAGTATG TTC ACTATGAAAC TCGAGTTTCATAG TGAACATACTTGC TTTTTG	TRCN0000034715, Sigma- Aldrich
METTL3 2: MISSION Lentiviral Transduction Particles	NM_019 852.2- 849s1c1	CCGGGCCAAGGA ACAATCCATTGTT CTCGAGAACAATG G ATTGTTCCCTGGC TTTTTG	TRCN0000034717, Sigma- Aldrich
MISSION shRNA Control Transduction Particles	N/A	N/A	SHC002V, Sigma-Aldrich

Table 2.2 List of lentiviral constructs

2.4 Adenoviral Transduction

The adenovirus utilised for the overexpression of human METTL3 in this study was provided by Dr Graciela Sala Newby (University of Bristol). Wildtype human METTL3 clone (Addgene [91]) was cloned into pDC-515IO vector to generate recombinant

adenovirus (Microbix). HUVEC or HCMEC were seeded 24 hours before infection on gelatin-coated 6-well plates at a density of 1.8×10^5 in 1 mL complete EGM2 or EGM-MV2. Cells were incubated overnight at 37°C in a humidified atmosphere containing 5% CO₂ to form 80% confluent cultures. Cells were infected for 12 hours with adenoviral particles carrying METTL3 (denoted as Ad.METTL3 in text) or control virus (Ad.Null) at a ratio of 50 viral particles per cell (50 multiplicity of infection, MOI [195]) in complete EGM2 or EGM-MV2 at 37°C in a humidified atmosphere containing 5% CO₂. Cells were then washed twice with PBS and medium was incubated with complete or serum free EGM2 or EGM-MV2 for a further 36 hours.

2.5 EC Isolation from Murine Hearts and Limb Muscle

Whole hearts or adductor muscles were collected from diabetic or non-diabetic mice or 3 days post-limb ischaemia induction (male CD1 mice, refer to table 2.6). Briefly, animals under terminal anaesthesia (Avertin) were perfused through the left ventricle (LV) with ice cold PBS followed by warm PBS, the whole heart or the ischaemic and contralateral adductor muscles were then harvested. Tissue was digested with collagenase II (20,000 units/ml) (cat no.17101015, Gibco) and DNase I (30,000 units/ml) (cat no.A3778, Applichem) using gentleMACS Dissociator (cat no.130-093-235, Miltenyi Biotech), following the manufacturers protocol. The samples were then centrifuged at 4°C and the supernatant was removed. Cell pellet was resuspended in Hanks' Balanced Salt Solution (HBSS) (cat no.14025092, Gibco) and filtered through a 70µm and 40µm cell strainer (cat no. CLS431751 and CLS431750, Sigma-Aldrich). Following another centrifugation step, cells were resuspended in MACS solution and ECs were sorted using an immunomagnetic CD146 antibody (clone ME-9F1) (cat no. 130-103-795, Miltenyi Biotech), as previously reported [195]. CD146+ cells were retrieved, and RNA was extracted as described in section 2.6.

2.6 RNA Isolation from Cells or Mouse Tissue

RNA was extracted from HUVEC, mouse muscle-derived ECs, whole hearts and adductor muscle tissue using the miRNeasy Mini Kit (cat no.217084, Qiagen), according to the manufacture instructions. Prior to RNA isolation, muscle tissue was homogenised in 2ml tube with TRIzol Lysis Reagent (cat no.15596026, Life Technologies) and a sterile metal bead. Samples were then placed in TissueLyser LT (cat no.85600 Qiagen) at 4°C for 3-5 minutes. RNA was eluted with RNase-free water, purity (measurement of A260/A280 ratio) and concentration were determined using a NanoDrop 2200c Spectrophotometer (Thermo Fisher Scientific).

2.7 cDNA Synthesis

First strand complementary DNA (cDNA) was synthesised using PrimeScript RT Enzyme Mix I (cat no.RR037A, Takara Bio). Total RNA was added to 5X PrimeScript Buffer, PrimeScript RT Enzyme Mix I, 50 µM Oligo dT Primer and 100 µM Random 6mers (cat no. RR014A, Takara Bio). The final volume of the reaction was made up to 10µl with DNase/RNase free water. The reaction mixture was heated to 37°C for 15 minutes and inactivated by heating to 85°C for 5 seconds.

For pri-miRNAs, cDNA was synthesized using High-Capacity cDNA Reverse Transcription Kit (cat no.4368814, Applied Biosystem). The reaction mixture was heated to 42°C for 1 hour, 95°C for 5 minutes and cooled for 30 minutes at 4°C. Mature miRNA cDNA was synthesised using miRNA TaqMan Assays and TaqMan MicroRNA Reverse Transcription Kit (cat no.4366596, Life Technologies). 10ng/µl of RNA sample was used per reaction. The reaction mixture was heated to 16°C for 30 minutes, 42°C for a further 30 minutes and inactivated by heating to 85°C for 5 minutes. All cDNA synthesis reactions were performed using a thermocycler (cat no.732-2548, VWR).

2.8 Quantitative Real-Time PCR

1 µl of template cDNA was amplified by quantitative real-time PCR (qRT-PCR) using TB Green Premix Ex Taq Kit (cat no.RR82WR, Takara) in triplicates. The cycling conditions are outlined in Table 2.3. 18S ribosomal RNA (rRNA) was used as the housekeeping gene.

For pri-miRNAs analysis, qRT-PCR was performed using TaqMan Pri-miRNA Assays for pri-miR-17 (recognizes miR-17-miR-18a-miR-19a stem loops) (cat no.4427012, Applied Biosystems), pri-miR-92 (recognizes miR-20a-miR-19b-miR-92a stem loops) (cat no.4427012, Applied Biosystems) and pri-miR-let-7e (cat no.4427012, Applied Biosystems). Mature miRNA levels were analysed using miRNA TaqMan Assays outlined in Table 2.4. The cycling conditions for pri-miRNA and mature miRNAs qRT-PCRs are presented in Table 2.3. Both pri- and mature miRNA qRT-PCR was performed in triplicates using TaqMan Universal Master Mix (cat no.4304437, Life Technologies). 18S rRNA or small RNA U6 was used for normalization, respectively. All qRT-PCR reactions were performed using QuantStudio 6 Flex Real-Time PCR System (cat no.4485691, Life Technologies).

Programme	Temperature (°C)	Time	Cycles
mRNA	95	30 secs	40
	95	15 secs	
	60	45 secs	
Pri-miRNA	50	2 mins	40
	95	10 mins	
	95	15 secs	
	60	1 min	
miRNA	95	10 mins	40
	95	15 secs	
	60	60 secs	

Table 2.3 qRT-PCR cycling conditions

Primers		Oligonucleotide sequence/probe reference
18S (Human)	Forward	5' GCTTAATTTGACTCAACACGGGA 3'
	Reverse	5' AGCTATCAATCTGTCAATCCTGTC 3'
TSP-1 (Human)	Forward	5' GTGACTGAAGAGAACAAGAG 3'
	Reverse	5' CAGCTATCAACAGTCCATTC 3'
METTL3 (Human)	Sequence not available, ref provided: Hs00219820_m1	
METTL14 (Human)	Hs00383340_m1	
WTAP (Human)	HS01695908_S1	
FTO (Human)	Hs0105745_m1	
ALKBH5 (Human)	Hs00539502_m1	
Mettl3 (Mouse)	Mm01316319_m1	
Wtap (Mouse)	Mm00808544_s1	
Fto (Mouse)	Mm00488756_m1	

Alkbh5 (Mouse)	Mm00841140_m1
Tsp-1 (Mouse)	Mm01335418_m1
18S	Hs99999901_s1
U6	Hs00984809_m1
Hsa-pri-let-7e	Hs03295173_pri
Hsa-pri-miR-17	Hs03295901_pri
Hsa-pri-miR-92	Hs03302603_pri
Hsa-let-7e-5p	UGAGGUAGGAGGUUGUAUAGUU
Hsa-miR-17	CAAAGUGCUUACAGUGCAGGUAG
Hsa-miR-18a-5p	UAAGGUGCAUCUAGUGCAGAUAG
Hsa-miR-19a	UGUGCAAUUCUAUGCAAACUGA
Hsa-miR-19b	AGUUUUGCAGGUUUGCAUUUCA
Hsa-miR-20	UAAAGUGCUUAUAGUGCAGGUAG
Hsa-miR-92a	GGGUGGGGAUUUGUUGCAUUAC

Table 2.4 Oligonucleotides used for qRT-PCR. Probe references are provided when sequences not available

2.9 Immunoblotting

2.9.1 Preparation of Whole Cell Lysates

Cells were washed twice with ice-cold PBS and whole cell protein lysates were collected using ice-cold RIPA buffer (cat no.R0278 Sigma-Aldrich) containing 1mM orthovanadate, 1 mg/mL of protease inhibitor cocktail (cat no.11697498001 Roche) and 0.25 mg/mL AEBSF (cat no.11429868001, Roche). Lysates were centrifuged for 15 minutes at 2000g at 4°C.

2.9.2 Western Blotting

15µg of total cell lysate was used for immunoblotting per lane. Protein concentration of lysates was determined using Precision Red (cat no.ADV02, Universal Biologicals) and the absorbance of the protein samples was measured at 600nm wavelength using Synergy HT spectrophotometer (BIO-TEK). Samples were added to NuPAGE® LDS Sample Buffer (4X) (cat no.NP0007, Invitrogen) containing 0.7 M 2-mercaptoethanol (cat no.125472500, Thermo Scientific) and heated for at 70 °C for 10 minutes.

SDS-polyacrylamide gel electrophoresis was used to separate proteins which were then transferred to a Immobilon polyvinylidene difluoride (PVDF) membrane (cat no.IPVH00010, Millipore). Blocking was performed with 3% bovine serum albumin (BSA) in TBS for 1 hour and probed with antibodies diluted in Tris-buffered saline (TBS) with 0.1% TBS-T Tween-20 Tris-buffered saline with Tween-20 overnight at 4°C.

Immunoblots were labelled using the following primary antibodies prepared in 3% BSA/TBS solution: rabbit recombinant anti-METTTL3 antibody (1:1000) (cat no.ab195352, Abcam), monoclonal anti-Thrombospondin-1 [A6.1] (1:1000) (cat no.SC-59887, Santa Cruz), mouse monoclonal HSP90 (1:3000) (cat no.610418, BD Bioscience) and monoclonal anti-β-Actin (1:3000) (cat no.SC47778, Santa Cruz). Primary antibodies were detected using the relevant fluorescently labelled secondary antibodies: IRDye 800CW Donkey anti-Mouse IgG (1:15000) (cat no.925-32212, LI-COR), 680RD Donkey anti-Rabbit IgG (1:15000) (cat no.925-68073, LI-COR). Secondary antibodies were prepared in TBST, casein (cat no. 1610782, Bio-Rad) and SDS solution (cat no.71736, Sigma-Aldrich) (refer to Table 2.5 for full list of antibodies used in this study). Visualisation of protein bands was performed using an Odyssey

Infrared Imaging System (LI-COR). Densitometry analysis of the gels was carried out using NIH ImageJ software (U. S. National Institutes of Health, Bethesda).

Target antigen	Working Conc.	Product Details
Rabbit recombinant anti-METTL3	0.2µg/mL (1:1000)	ab195352, Abcam
Monoclonal anti-Thrombospondin-1 [A6.1]	3.8µg/mL (1:1000)	SC-59887, Santa Cruz
Mouse monoclonal HSP90	0.25µg/mL (1:3000)	610418, BD Bioscience
Monoclonal anti-β-Actin	0.4µg/mL (1:3000)	SC47778, Santa Cruz
IRDye 800CW Donkey anti-Mouse IgG	1µg/mL (1:15000)	925-32212, LI-COR
IRDye 680RD Donkey anti-Rabbit IgG	1µg/mL (1:15000)	925-68073, LI-COR

Table 2.5 Antibodies used for Western Blotting

2.10 Quantification of m6A RNA Methylation

The m6A RNA methylation status in total RNA isolated from cells or mouse tissue was determined using the EpiQuik m6A RNA Methylation Quantification Kit (Colorimetric) (cat no.#P-9005, Epigentek). Total RNA was isolated using miRNeasy Mini Kit as described in section 2.6 and an optimal amount of 200ng per reaction was used as the input RNA. Before starting the experiment, all the relevant buffers (wash buffer and enhancer solution), antibodies (capture antibody, detection antibody) and positive control dilutions were prepared following the manufacturer's protocol. RNA was first bound to the provided assay wells by adding the binding solution, negative control, diluted positive control and 200ng of sample RNA into each appropriate well. The strip

plate was sealed and incubated at 37°C in a humidified atmosphere containing 5% CO₂ for 90 minutes. The binding solution was then removed by washing each well with the diluted wash buffer three times. To capture the m6A bound RNA, the diluted capture antibody was added to each well and the plate was incubated at room temperature for 60 minutes. The wells were then washed three times using the diluted wash buffer, the detection antibody was added to each well and the plate was incubated at room temperature for 30 minutes. The wells were then washed four times and the diluted enhancer solution was added to each well followed by a 30-minute incubation at room temperature. Wells were washed five times and the detection solution was added to each well. The plate was incubated for 1-10 minutes away from light while the colour change in the sample and control wells was monitored. Stop solution was added to each well to stop the enzyme reaction when the colour in the positive control wells turned medium blue. The absorbance was read at 450nm 5-10 minutes following the addition of the stop solution using a Bio-Tek Synergy HT microplate reader. To determine the relative m6A RNA methylation status of different RNA samples, the following calculation for the percentage of m6A in total RNA was used:

$$\text{m6A\%} = \frac{(\text{sample OD} - \text{NC OD}) \div S \times 100\%}{(\text{PC OD} - \text{NC OD}) \div P}$$

OD = Optical Density

NC = Negative Control

PC = Positive control

S = Amount of input sample RNA in ng

P = Amount of input positive control (**PC**) in ng

2.11 BrdU Incorporation Assay

Cell proliferation was determined *in vitro* using a BrdU proliferation ELISA kit (cat no.11647229001, Roche) according to the manufacturer's instructions. HUVECs were seeded at a density of 10,000 cells/well on a gelatin-coated 96-well plate and transfected with CT siRNA or METTL3 siRNA as described in section 2.2. Cells were labelled using 10 μ M BrdU per well and incubated for 24 hours at 37°C in a humidified atmosphere containing 5% CO₂. Culture medium was then removed, and the cells were fixed and made permeable by adding FixDenat reagent. Cells were incubated with monoclonal anti-BrdU peroxidase-conjugated antibody (anti-BrdU-POD) for 90 minutes at RT. The antibody conjugate was removed; the cells were washed and incubated with the substrate solution for 20-30 minutes at RT. Upon sufficient colour development for photometric detection, the reaction product was quantified by measuring the absorbance at 370 nm with a reference wavelength of 492 nm using a Bio-Tek Synergy HT microplate reader.

2.12 Caspase-Glo Assay

HUVECs were seeded at a density of 5000 cells/well on a gelatin-coated white walled 96-well plate and transfected with CT siRNA or METTL3 siRNA as described in section 2.2. Apoptosis was quantified 48 hours post-transfection by measuring caspase 3 and 7 activity using the Caspase-Glo assay, a luminescent cell death detection kit (cat no.G8090, Promega). Cells were allowed to equilibrate to RT for 30 minutes, after which Caspase-Glo 3/7 reagent was added to each well in a 1:1 ratio. Contents of wells were mixed by placing plate on a shaker at 300-500rpm for 30 seconds and incubated at RT of 2 hours. Bio-Tek Synergy HT multi-detection microplate reader was used to measure luminescence.

2.13 Migration Assay

Endothelial migration was determined *in vitro* using a scratch wound assay.

HUVEC were seeded 24 hours before CT siRNA or METTL3 siRNA transfection or infection with adenoviral vectors on gelatin-coated 6-well plates at a density of either 1.6×10^5 or 1.8×10^5 , respectively (refer to sections 2.2 and 2.4). At 36 hours post transfection, cells were serum starved overnight at 37°C in a humidified atmosphere containing 5% CO₂ in basal EBM2 supplemented with 0.1% BSA to arrest proliferation. The next day, a p200 pipette tip was used to create a uniform gap in the cell monolayer. An inverted phase-contrast microscope was utilised to visualize EC migration. Images were captured at 0, 6 and 12 hours. Wound closure was analysed using the migration plug in for ImageJ software.

2.14 *In vitro* Matrigel Assay

HUVEC or HCMECs were seeded 24 hours before CT siRNA or METTL3 siRNA transfection or infection with adenoviral vectors on gelatin-coated 6-well plates at a density of either 1.6×10^5 or 1.8×10^5 , respectively (refer to sections 2.2 and 2.4). At 48-hours post-transfection, pre-chilled 96-well plates were coated with 50 µl Growth Factor Reduced Matrigel Basement Membrane Matrix (BD Biosciences). Transduced HUVEC or HCMEC were detached from the 6-well plates and re-seeded at a density of 13,000 cells per well. Plates were incubated for 6-8 hours at 37°C in a humidified atmosphere containing 5% CO₂. Images were taken using an inverted phase-contrast microscope, using a 4x objective lens, with a digital microscope camera. Tube formation was measured by quantifying the following morphological parameters; number of branches, number of intersecting points and the number of meshes/loops. Quantification was performed using the “Angiogenesis analyser” plugin for Image J.

2.15 Fibrin Bead Assay

HCMEC were infected with Ad.METTL3 or Ad.Null or transfected with CT siRNA or METTL3 siRNA as described in sections 2.2 and 2.4. 1×10^6 HCMEC were mixed with 2500 Cytodex-3 Beads (cat no.GE17-0485-01, Amersham) in EGM2 for 4 hours at 37°C. Coated beads were transferred to T25 flask in 5mL of EGM2 and incubated overnight at 37°C in a humidified atmosphere containing 5% CO₂. The following day, the coated beads were resuspended in fibrinogen solution (2.0 mg/mL fibrinogen, 0.15 Units/mL of aprotinin) (cat no.F3879, Sigma-Aldrich) (cat no.10236624001, Roche) at a concentration of ~200 beads/mL. Thrombin (0.625 Units/mL) (cat no.T4648-1KU, Sigma-Aldrich) was added to each well of a 24-well plate before seeding 0.5 mL of the fibrinogen/bead suspension. The plate was then placed at 37°C in a humidified atmosphere containing 5% CO₂ for 20 min to generate a clot, and 1 mL of EGM2 was added to each well. HCMEC were allowed to undergo morphogenesis for 2-3 days. Angiogenic sprouting was quantified by measuring cumulative sprout length, branches, sprouts, and the number of detached cells using ImageJ software. Sprouting was defined as a vessel with length greater than or equal to the diameter of the bead. Branching was defined as a segment of a vessel that has branched off from the major vessel sprout. For each experiment, at least 10 spheroids per triplicate well and condition were analysed.

2.16 Animal Studies

All animal procedures were covered by project and personal licenses issued by the United Kingdom Home Office, performed in compliance with the Guide for the Care and Use of Laboratory Animals (Institute of Laboratory Animal Resources) and with the prior approval of the United Kingdom Home Office and the appropriate ethics

committees. All mice were housed under pathogen-free conditions and had free access to food and water.

Species	Background Strain	Study	Sex	Vendor
Mouse	CD1-Foxn1nu	<i>In vivo</i> Matrigel Plug	F/M	Charles River, UK
Mouse	CD1	Hind Limb Ischaemia Model	M	Charles River, UK
Mouse	C57BL/6J	Myocardial Infarction (MI) Model	M	Hercus, New Zealand

Table 2.6 Animals used for *in vivo* studies

2.16.1 *In Vivo* Matrigel Plug

Dr Andrew Benest and Alison Ritchie (University of Nottingham) were responsible for Matrigel plug implantation, maintenance of animals and plug collection steps of this protocol. Studies were performed under the project license (PPL) P435A9CF8. Matrigel plug assay with METTL3 depleted ECs: HUVEC were infected with LV-METTL3-shRNA or LV-CT-shRNA particles, as described in section 2.3. HUVEC at a density of 3×10^5 were resuspended in 100 μ L of EGM without FBS and mixed with growth factor reduced matrigel premixed with VEGF-A165 (cat no.293-VE, R&D Systems) and basic fibroblast growth factor (bFGF) (cat no.3718-FB, R&D Systems). Samples were injected subcutaneously into the flank region of 10-week-old immunodeficient male mice (CrI:CD1-Foxn1nu, Charles River UK) (N=8 mice per group).

Matrigel plug assay with METTL3 overexpressing ECs: HUVEC were infected overnight with Ad.METTL3 or Ad.Null at 50 MOI in EGM2 medium. Cells were prepared and inoculated as described above in immunodeficient male and female mice in equal proportion (N= 6 mice per group).

To study the functionality of the newly formed vessels, mice were injected with 150µL of biotinylated isolectin B4 (cat no.I21411, Molecular Probes) in the tail vein. This was allowed to circulate for 15 minutes before mice were sacrificed and plugs were collected. For the METTL3 depletion studies, mice were sacrificed at 21 days whereas for the METTL3 overexpression studies mice were sacrificed at 14 days post-implantation. Matrigel plugs were embedded in OCT prior to immunostaining.

2.16.2 Induction of Type-1 Diabetes

8-week-old male CD1 mice received intraperitoneal injections of streptozotocin (STZ) (cat no.S0130, Sigma-Aldrich) for 5 consecutive days (40 mg/Kg in 0.05 mol/L citrate buffer per day) [195]. Non-diabetic male CD1 mice to be used as controls were injected with citrate buffer. Glycaemia under fasting conditions and glycosuria were measured 14 days after the first STZ injection, and only the mice with consistently elevated fasting glucose levels (above 200 mg/dL) and overt glycosuria were included in the protocol. Normoglycemia and the absence of glycosuria was verified in the non-diabetic control mice.

2.16.3 Mouse Hind Limb Ischaemia Model

Surgeries and training for the mouse hindlimb ischaemia model was carried out by Dr Marie Besnier (University of Bristol) under the project licences PPL/30/2811 and PI/I77AD3F36. Depending on the protocol, unilateral limb ischaemia (LI) was induced in either 10-12-week-old male CD1 mice or in mice with 12 weeks of diabetes and in age-matched non-diabetic controls [59, 195]. Mice were anaesthetized (inhalation of

1.5-2.5% isoflurane) and maintained at 37°C on a heating pad. A 5 mm longitudinal incision was made at the origin of the inguinal crease along the femoral blood vessels visible through the skin. Subcutaneous fatty and connective tissue was dissected to expose the neurovascular bundle. The sheet of connective tissue between the femoral vein and artery was carefully lacerated to free the artery. Leaving the femoral nerve and vein untouched, the femoral artery was occluded using a double surgical knot with a 6-0 silk suture at two points. A second incision was made in line with the knee and the femoral vein and artery were again carefully separated by blunt dissection and a third ligation was made. Adenovirus (Ad)- mediated local delivery of METTL3 was achieved by injecting Ad.METTL3 or Ad.Null into the ischaemic adductor in 3 equidistant points along the projection of the femoral artery (10^8 Plaque Forming Units [PFU] in 50µl total volume). The primary incision was closed with a subcutaneous and an interrupted suture whereas the secondary incision was closed with an interrupted suture. Post-surgical analgesia (Vetergesic, 0.02 ml/30 g) was then administered subcutaneously to control ischaemic pain. Ischaemia was confirmed by measurement of the superficial blood flow of the ischaemic and contralateral foot immediately after surgery using a high-resolution laser colour Doppler imaging system (Moor LD12, Moor Instruments).

Mice with symptoms of severe limb ischaemia were excluded and humanly euthanized in compliance with the conditions of the Project Licence. Any data collected for the excluded mice was analysed up to the point of exclusion.

2.16.4 Myocardial Infarction (MI) Model

This protocol was performed at the University of Otago under the licence AEC10/14 by Dr Rajesh Katare and Dhananjie Chandrasekera. All studies were performed on 10-week-old male C57BL/6J mice [168]. Due to the reported effects of oestrogens on

the heart and cardiac miRNAs expression, only male mice were used to avoid potential effects of sex differences. Following anaesthesia (2,2,2 tribromo ethanol, 0.3gm/kg, i.p.) and artificial ventilation, the chest cavity was opened, and after careful dissection of the pericardium, the left anterior descending coronary artery (LAD) was located and permanently ligated using a 7-0 silk suture. Immediately after ligation, mice were randomized to receive either Ad.METTL3 or Ad.Null intracardiac injections into the peri-infarct border zone (10^8 PFU/mouse, N=10 each group). After confirming the absence of bleeding, the chest cavity was sutured in layers. Animals were allowed to recover for at least 4 hours before being returned to the housing unit. Mice were monitored twice a day for the first 5 days post-surgery, and once a day thereafter. All mice received analgesic and antibiotic prior to the surgery and then for 3 days post-operation. Cardiac function was assessed using echocardiography measurement at baseline (before MI) and at 14 days post-MI. At the end of the treatment period and following echocardiography, the heart was stopped under anaesthesia in diastole using KCl, and ventricular tissue was collected following 4% PFA perfusion-fixation using a perfusion pump set at 2 mL/min constant flow.

2.16.5 Echocardiography

2D echocardiography was performed using vevo770 system. Animals were kept under anaesthesia (~1.5-2% isoflurane) during recording. Care was taken to avoid compression of thoracic cage which might otherwise distort ventricular geometry or induce bradycardia. All images obtained were blinded and digitally recorded. Subsequent independent detailed off-line analysis is also blinded and performed using Vevo software. Ventricular dimensions and function were assessed from averaged measurements of at least 3 consecutive cardiac cycles, avoiding breath-associated artifacts, from short-axis images at mid-papillary level from left parasternal window.

Analysis was performed from satisfactory images and acceptable heart rate range (recommended range of 400-650 beats/min to be suitable for analysis). Variables are as follows:

Dimensions

LV anterior wall (LVAW; mm) at diastole and systole; LV intraventricular cavity (LVID; mm) at diastole and systole; LV posterior wall (LVPW; mm) at diastole and systole (mm).

Volumes

LV intraventricular volume (LV Vol; uL) at diastole and systole.

Function

Main cardiac function variables are calculated using the following formulas:

LV ejection fraction (EF) % = $100 * (LV\ Vol;d - LV\ Vol;s) / LV\ Vol;d$

LV fractional shortening (FS) % = $100 * ((LVID;d - LVID;s) / LVID;d)$

Stroke volume (ul) = $LV\ Vol;d - LV\ Vol;s$

Cardiac output (ml/min) = $(Stroke\ volume\ (ul) * HR) / 1000$

2.17 Immunohistochemistry

Explanted matrigel plugs were sectioned at a thickness of 15µm and stained using Rabbit anti-human CD31 (1:200) (cat no.Ab32457, Abcam) and Goat anti-rabbit Alexa Fluor 594 (1:200) (cat no.Ab150080, Abcam) to detect human capillary like structures. Perfused vessels stained with biotinylated Isolectin B4 (1:200) (cat no.I21411, Molecular Probes) were detected using Streptavidin Alexa Fluor 488 conjugate (1:200) (cat no.S11223, Molecular Probes). The number of human CD31+ structures per mm² and perfused vessels were quantified using ImageJ software in 12 randomly selected fields at 10X magnification per mouse (n=8 per group in METTL3 depletion and n=6

in METTL3 overexpression studies). The extent of vessel perfusion was expressed as the percentage of perfused vessels among total human capillary like structures.

For analysis of post-ischaemic limb vascularisation, adductor muscles were sectioned at a thickness of 7 μ m and stained with biotinylated Isolectin B4 (1:100) (cat no.I21411, Molecular Probes) and Streptavidin Alexa Fluor 488 conjugate (1:200) (cat no.S11223, Molecular Probes) to detect ECs lining capillaries. Muscle sections were stained using α -smooth muscle actin (1:400) (cat no.C6198, Sigma-Aldrich) to identify arterioles. The number of capillaries and arterioles per mm² was counted in 10 randomly selected high-power fields per mouse (40x magnification) captured using a fluorescent microscope (Zeiss Axio Observer).

For analysis of post-MI vascularization, left ventricular tissue was sectioned at a thickness of 7 μ m and stained with biotinylated Isolectin B4 (1:100) (cat no.B-1205-5, Vector Laboratories) and α -smooth muscle actin (1:400) (cat no.C6198, Sigma-Aldrich) to identify capillaries and arterioles respectively. Apoptotic capillaries were detected in myocardial sections using terminal deoxynucleotidyl transferase dUTP nick end labeling (TUNEL) staining following the manufacturer's instructions (cat no.C10617, Invitrogen). Sections were probed with biotinylated Isolectin B4 (1:100) (cat no.B-1205-5, Vector Laboratories) to label capillaries. The number of capillaries, arterioles and TUNEL+ capillaries per mm² was counted in 6 random images analysed from each sample (400X magnification), captured using a confocal microscope (Nikon).

Target antigen	Working Conc.	Product Details
Rabbit anti-human CD31	1µg/mL (1:200)	ab32457, Abcam
Biotinylated IsolectinB4	1µg/mL (1:200)	I21411, Molecular Probes
Biotinylated IsolectinB4	5µg/mL (1:10)	B-1205-5, Vector Laboratories
α-smooth muscle actin	3.25µg/mL (1:400)	C6198, Sigma-Aldrich
Streptavidin Alexa Fluor 488 conjugate	(1:200)	S11223, Molecular Probes
Goat anti-rabbit Alexa Fluor 594	2µg/mL (1:200)	Ab150080, Abcam

Table 2.7 List of antibodies utilised for IHC studies

2.18 Bioinformatic Analysis

A list of METTL3 methylated pri-miRNAs was extracted from published data obtained in a metastatic breast cancer line (MDA-MB-231) [154]. Target genes of the corresponding mature miRNAs with a reported role in the modulation of angiogenesis were then identified. MiRcode is a software that provides "whole transcriptome" human microRNA target predictions based on the comprehensive GENCODE gene annotation. MiRcode was used to scan the 3'UTRs of the identified mRNAs to find miRNA binding sites [196]. To filter the predicted targets, only the candidates that were conserved across vertebrates were considered. Since miRcode only provides target predictions for miRNA clusters, TargetScan was used to identify individual components of these clusters corresponding to the targets. DAVID was then utilised to identify Gene Ontology/KEGG pathways for the conserved targets [197]. Candidates that

corresponded to the term Angiogenesis with $P \leq 0.05$ were incorporated into experimental design and probed throughout the project.

2.19 Statistical Analysis

Data shown are representative of at least three experiments unless stated otherwise and are expressed as mean \pm S.E.M. Data were plotted and relevant statistical analyses (as indicated in figure legends) were performed using GraphPad Prism 9 software (GraphPad Software, CA, USA). P values $P \leq 0.05$ were considered statistically significant.

Chapter 3

METTL3 Regulates Angiogenesis by Modulating let-7e-5p and miRNA-18a-5p Expression in ECs

3. METTL3 Regulates Angiogenesis by Modulating let-7e-5p and miRNA-18a-5p Expression in ECs

3.1 Introduction

Postnatal angiogenesis is the physiological process by which neo-vessels are formed from the pre-existing vasculature. As described in Chapter 1 section 1.1.2, angiogenesis is a complex morphological process relying on the interplay between several distinct cellular functions including EC proliferation, survival, migration, cell-cell interactions and differentiation of ECs. These processes are regulated by the precise coordination of proangiogenic and antiangiogenic mediators and downstream gene expression.

A functional vascular system is crucial for proper maintenance of tissues and organs through the delivery of oxygenated blood and nutrients, removal of waste and transport of immune cells. The impairment of EC functions conducive for angiogenesis contributes to numerous pathological conditions, including tumour growth, ischaemic disease and vascular malformations. Angiogenesis is therefore a putative target for therapy, with significant efforts being made in recent decades in the development of strategies to induce, augment and control the host angiogenic response. With ischaemic diseases representing the leading cause of mortality worldwide, the field of therapeutic angiogenesis offers a particularly attractive prospect for tissue regeneration. Due to the complex nature of the angiogenic process, revascularisation of ischaemic tissue must be tightly controlled and effectively coordinated to mitigate adverse events. In addition to the refinement of an efficient delivery approach to stimulate an angiogenic effect in varying settings of ischaemic disease, deciphering the underlying regulatory mechanisms of vessel formation may translate into novel targets for treatment.

RNA species can be post-transcriptionally modified by a collection of more than 160 chemical modifications, the most abundant of which is the methylation of the RNA adenosine base at the nitrogen-6 position (m6A). Other characterised modifications include pseudouridine (Ψ), 5-methylcytosine (m5C), inosine (I), 2'-O-methylation, N1-methyladenosine (m1A), N7-methylguanosine (m7G), and many more. Each modification has its own specific regulatory mechanisms and functional consequences, contributing to the complexity of RNA biology [73][80]. The m6A modification is emerging as a new layer in the developing landscape of posttranscriptional regulation of gene expression. M6A RNA methylation is catalysed by a methyltransferase complex composed of a core METTL3 and METTL14 heterodimer [91, 198], the WTAP [93] and several auxiliary proteins including KIAA1429, RBM15, and ZC3H13. The m6A mark is dynamically reversed by the demethylase proteins, FTO and ALKBH5 [198]. Reader proteins, identified as members of the YTH domain-containing and HNRNP protein families, recognise and bind to m6A sites to mediate specific downstream functions [79, 152].

miRNAs have been shown to be crucial regulators of EC function under physiological and pathological settings. Briefly, miRNAs are a class of endogenous small non-coding RNAs approximately 22-nucleotides in length that play a key role in the repression of gene expression at the post transcriptional level. Most miRNAs genes are transcribed primarily by RNA polymerase II into long pri-miRNA transcripts, which are sequentially processed by the endonucleases Drosha-DGCR8 and Dicer into precursor and mature miRNAs, respectively [199]. Canonically, miRNAs repress gene expression at the post-transcriptional level in the RISC (RNA-induced silencing complex) complex by targeting mRNAs in their 3' UTRs, thereby promoting the degradation of mRNAs or translational repression or both. A single miRNA can target

hundreds of genes and can be involved in the regulation of a plethora of cellular processes, including angiogenesis [200]. The m6A RNA modification has been identified as a crucial factor in miRNA processing. More specifically, the METTL3 mediated co-transcriptional deposition of m6A on pri-miRNAs is recognised by a putative reader of this mark, known as HNRNPA2B1, which in turn, promotes miRNA processing through the recruitment of the microprocessor component DGCR8 [154, 155].

M6A RNA methylation has been shown to be crucial in the regulation of a number of biological processes and its dysregulation has been implicated in several diseases. Its role in EC function however remains unclear. ***I therefore hypothesize that METTL3 mediated m6A plays an essential role in EC function and angiogenesis potentially through the modulation of the expression of target miRNAs.***

The aims of the work described in this chapter are:

- Determine the functional relevance of the m6A-catalysing enzyme, METTL3, in the modulation of EC functions conducive to angiogenesis
- Investigate the physiological importance of METTL3 in the regulation of angiogenesis
- Elucidate the underlying mechanisms by which METTL3 exerts its regulatory role on the angiogenic process by investigating whether METTL3 levels effect the processing and functional activity of endothelial miRNAs involved in angiogenesis.

3.2 Results

3.2.1 METTL3 Depletion in ECs Impairs Key Angiogenic Processes *In Vitro*

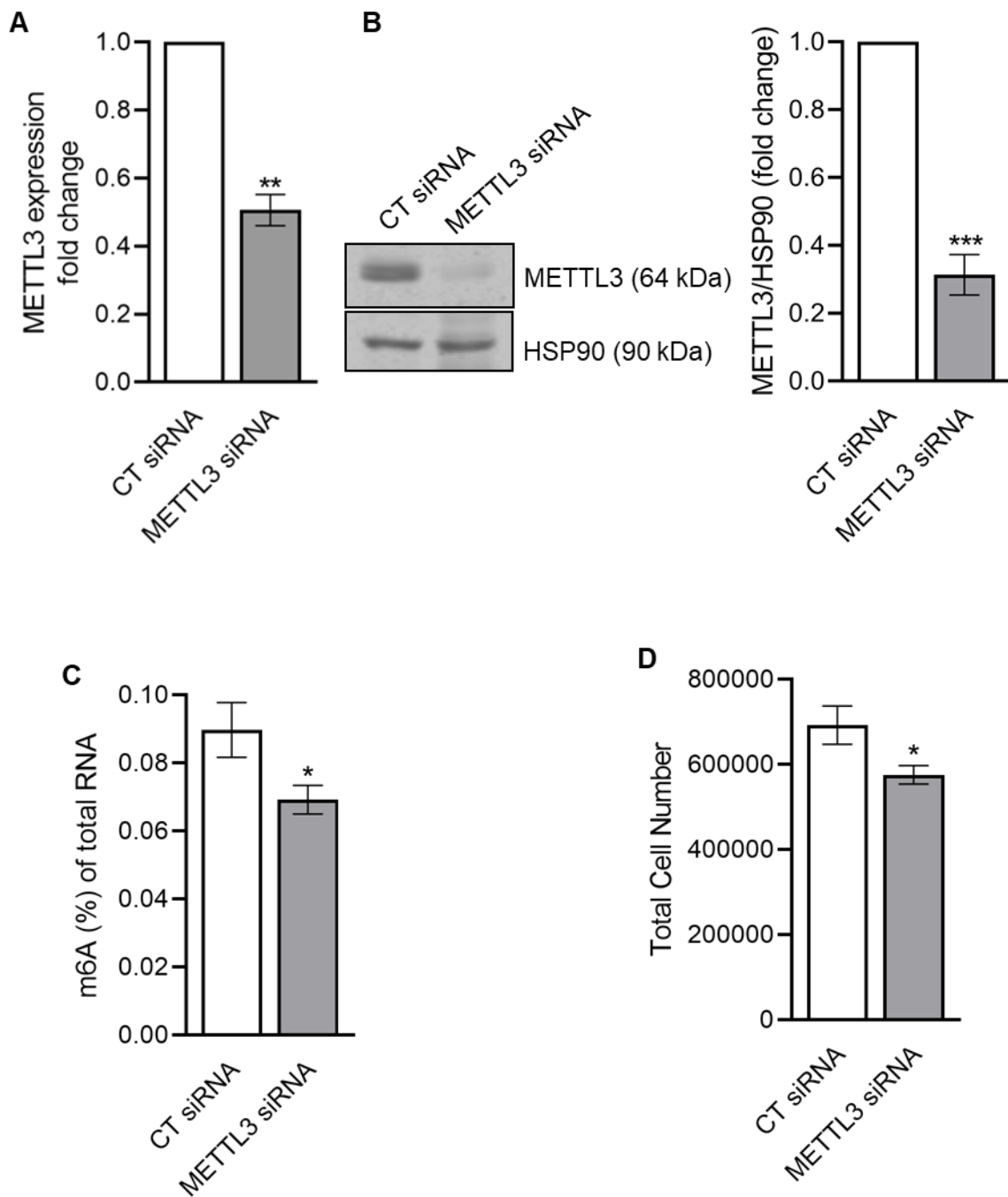
Angiogenesis is an intricate morphogenetic process relying on the interplay between several distinct cellular processes. To investigate the relevance of METTL3 on the capacity of ECs to develop an angiogenic programme, I performed a series of loss- and gain-of-function studies. Firstly, METTL3 was depleted in HUVEC using 2 independent siRNAs against METTL3. Validation experiments were performed to confirm a decrease in METTL3 expression at both mRNA and protein levels by RT-qPCR and Western blot analysis (figures 3.1A and B). The depletion of total endothelial m6A levels was also confirmed following the knockdown of METTL3 (figure 3.1C).

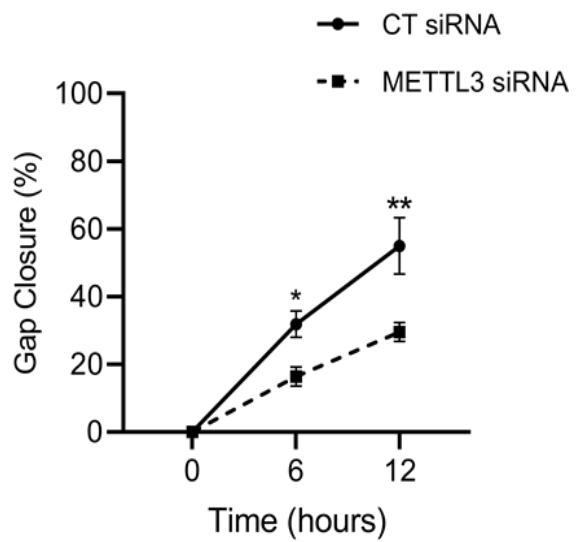
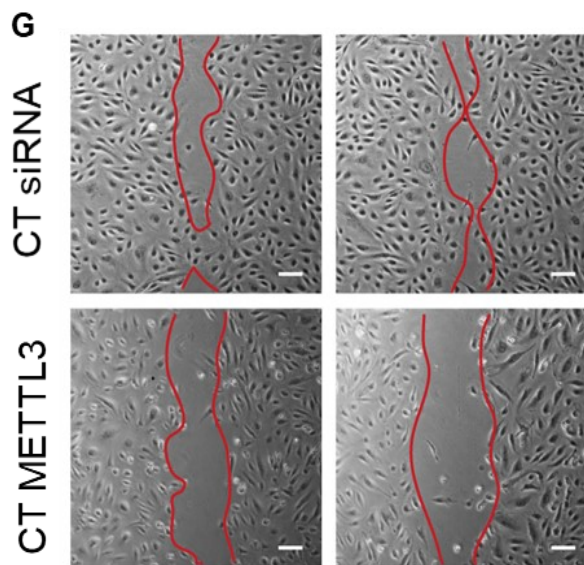
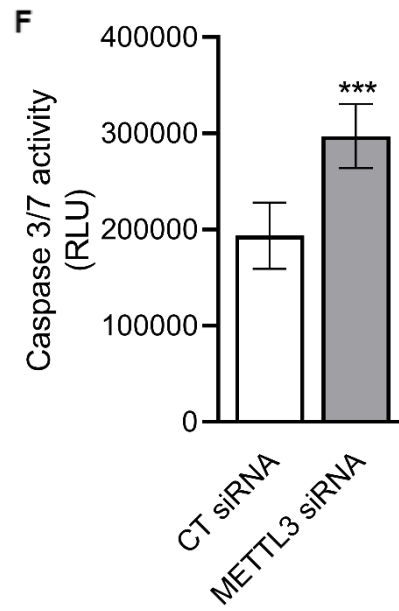
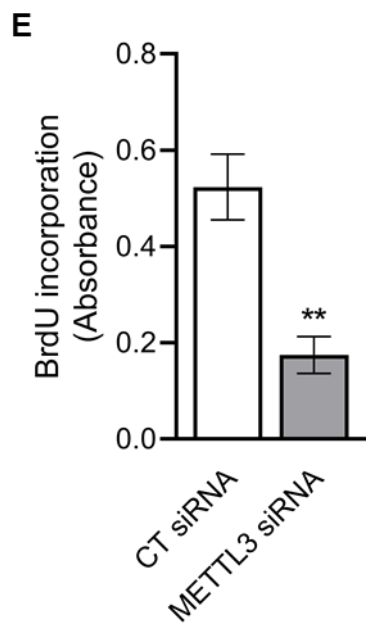
EC proliferation is a key step in the formation of a new sprout from existing vasculature during angiogenesis. To test whether METTL3 plays a role in the regulation of EC proliferation, cell number was quantified and a BrdU incorporation ELISA was utilised. The BrdU assay detects the incorporation of 5-bromo-2'-deoxyuridine into DNA during proliferation using an anti-BrdU antibody. The magnitude of absorbance for the developed colour is proportional to the amount of BrdU incorporated and can be directly correlated to cell proliferation. A significant reduction in cell number and a decrease in BrdU incorporation was observed 48 hours post METTL3 siRNA transfection compared to CT siRNA transfected cells (figure 3.1D and E). This reduction in EC proliferation maybe linked to changes in cell survival, a process previously shown to be regulated by METTL3 in various cell types [201]. To investigate this, apoptosis was measured by Caspase 3/7 Glo assay in CT siRNA and METTL3 siRNA transfected HUVEC. As shown in figure 3.1F, this analysis revealed an increase

in Caspase 3/7 cleavage in METTL3 deficient cells compared to CT siRNA treated HUVEC, indicating an increase in apoptosis.

EC migration is important for organised vessel growth during angiogenesis, where highly specialised 'tip cells' direct the migration of a new vessel sprouts toward a growth factor gradient. We aimed to study whether METTL3 regulates EC migration using an *in vitro* scratch wound assay. HUVEC were transfected with CT siRNA or METTL3 siRNA and a cell free gap was created on a confluent monolayer of cells. Cell proliferation was arrested to isolate the effects of cell migration without the confounding influence of cell division. Although this was achieved through serum starvation, another appropriate method is the addition of pharmacological inhibitors such as hydroxyurea [195]. Inhibition of METTL3 expression resulted in a significant defect in the ability of the cells to migrate into the 'wounded' area compared with the control (figure 3.1G).

Additionally, an *in vitro* Matrigel assay was used to elucidate the relevance of METTL3 in the regulation of tube formation. HUVEC or HCMEC transfected with CT siRNA or METTL3 siRNA were seeded onto growth factor reduced Matrigel. METTL3 depleted HUVEC and HCMEC exhibited an impaired capacity to develop an endothelial network, as indicated by a significant reduction in the number of branches, meshes, junctions and in the total length of the network (figures 3.1H and I).





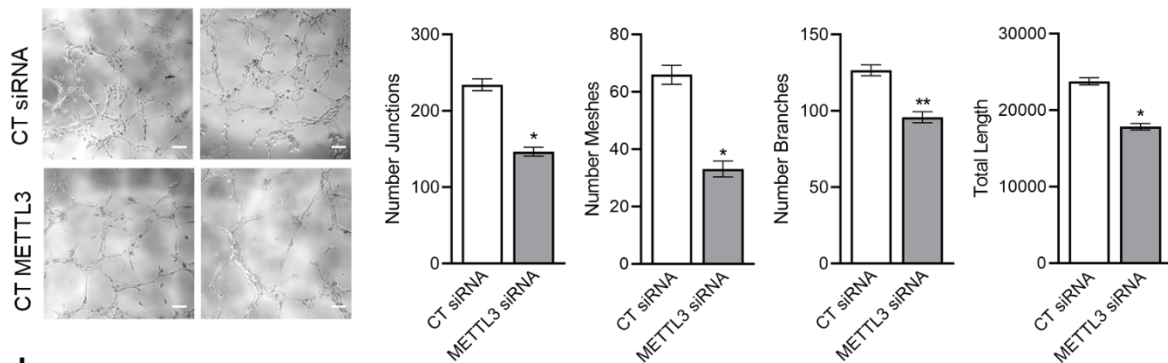
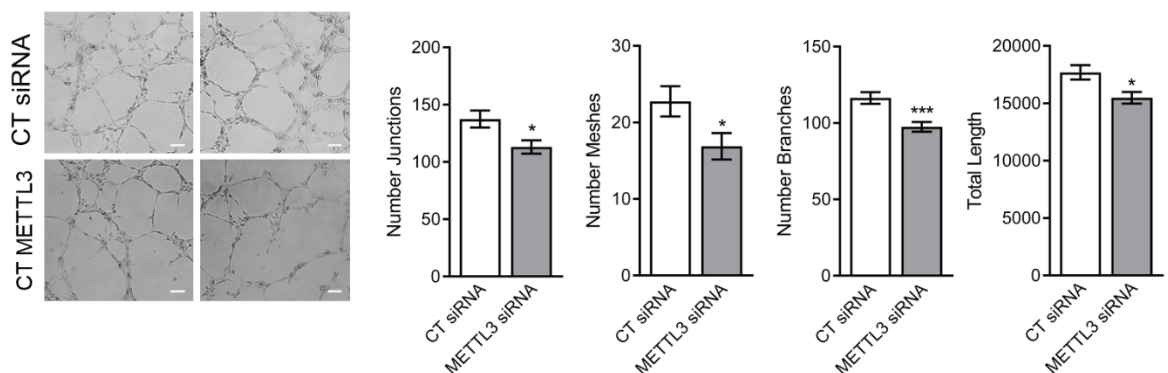
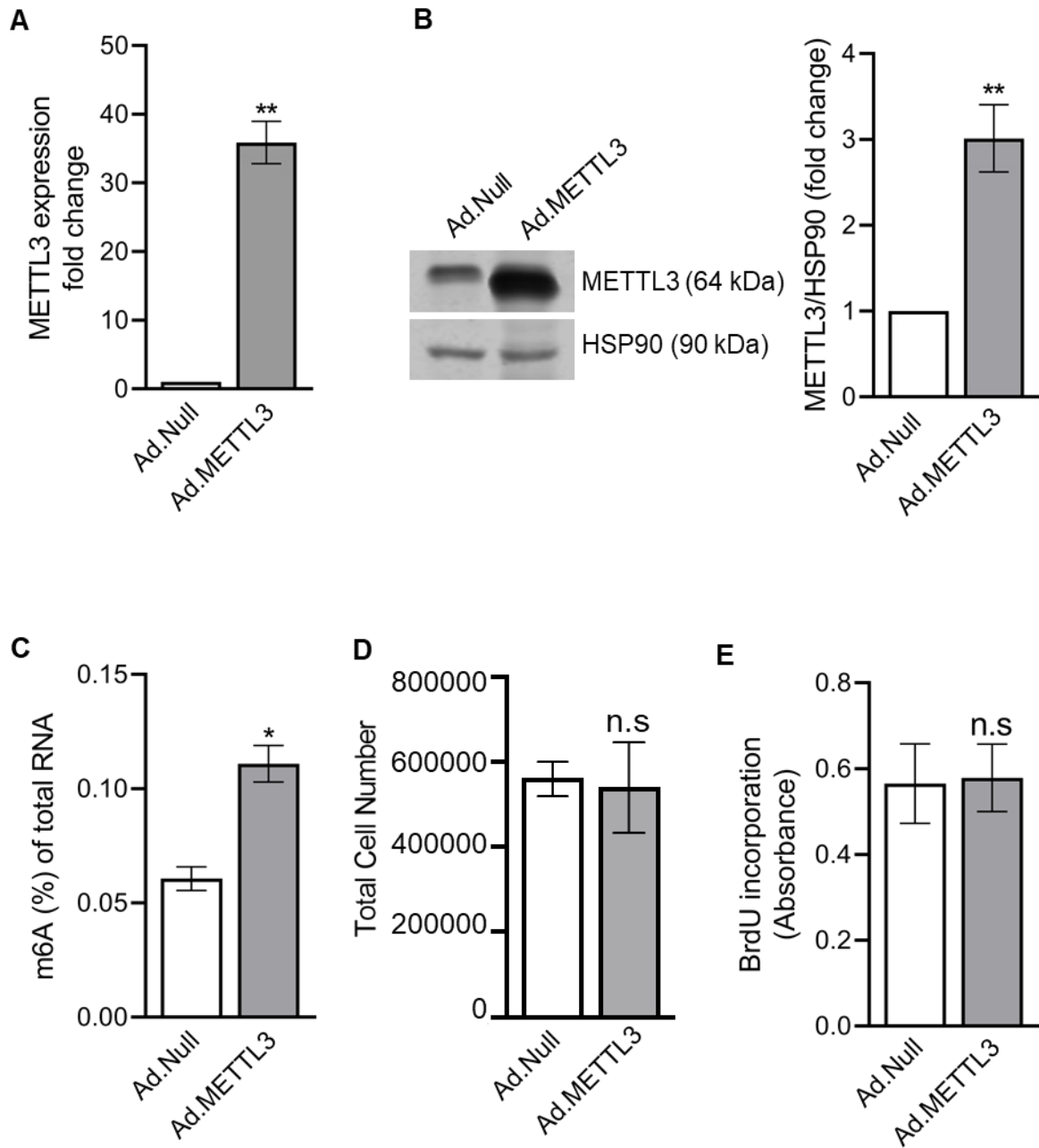
H**I**

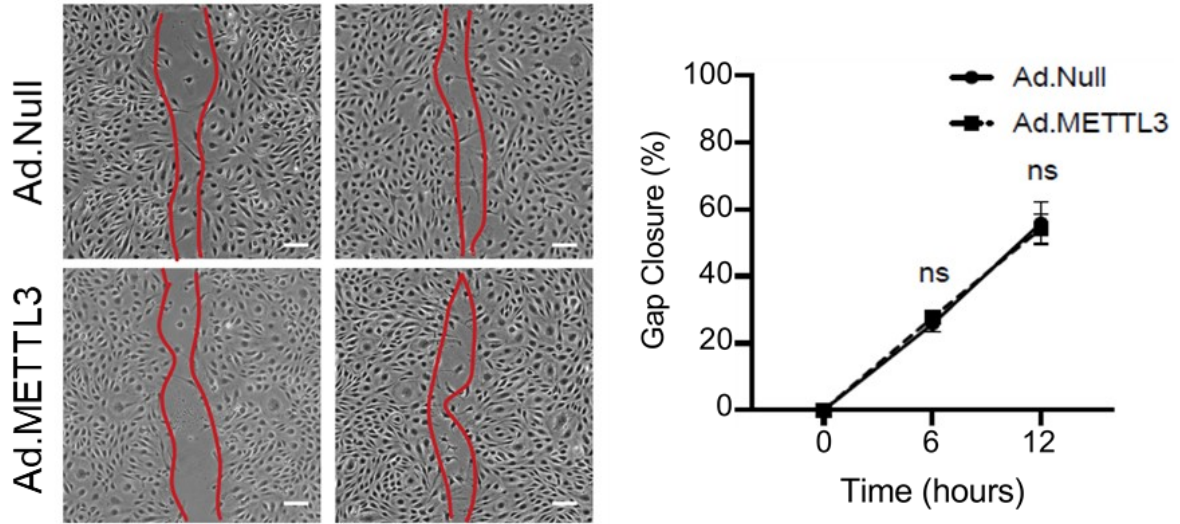
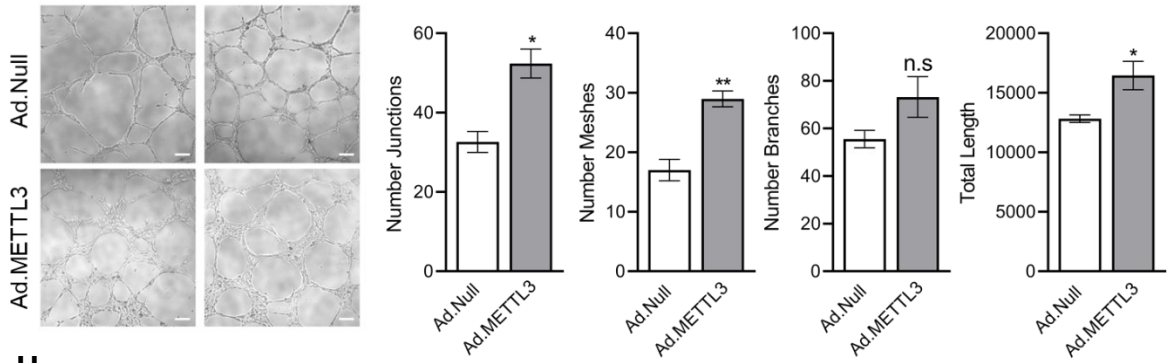
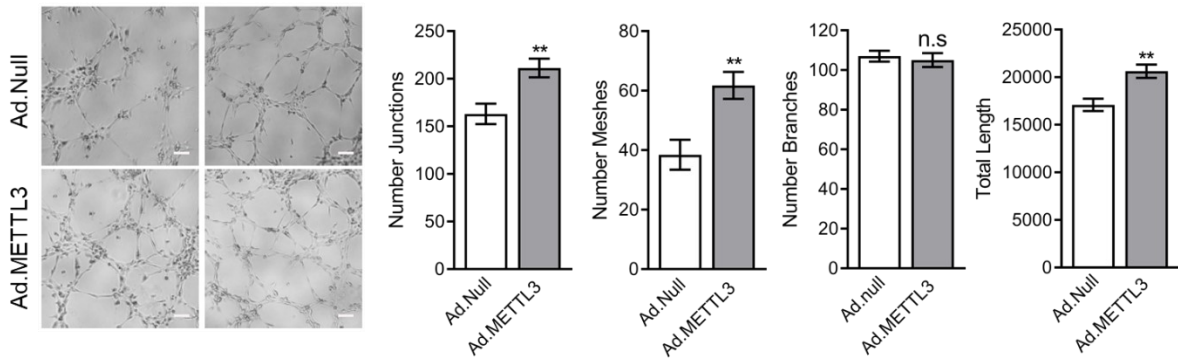
Figure 3.1 METTL3 depletion in ECs impairs key angiogenic processes *in vitro*. **(A-I)** HUVEC or HCMEC were transfected with 30 nM of control (CT) siRNA or METTL3 siRNA for 48 hours. **(A)** qRT-PCR analysis of METTL3 expression in HUVEC. 18s was used as housekeeping gene (n=3). **(B)** Quantification of METTL3 protein levels in HUVEC was performed by western blot analysis. Representative blots are shown, and western blot quantification is expressed as fold change vs CT siRNA (n=3). HSP90 was used as loading control [168]. **(C)** Global m6A RNA methylation levels in HUVEC were quantified using an ELISA based assay (n=2, performed in triplicates). **(D)** Quantification of total cell number (n=3). **(E)** Colorimetric assessment of BrdU incorporation (n=3). **(F)** Caspase 3/7 activity (n=3). **(G)** Representative microscopy images of scratch wound assay (4x magnification, scale bar 50µm) (n=3). EC migration was quantified as the percentage of gap closure at 0 hours, 6 hours and 12 hours following scratch formation. **(H-I)** Representative microscopy images of cord formation assay (4x magnification, scale bar 50µm) (n=4) in **(H)** HUVEC and **(I)** HCMEC. Angiogenesis was quantified by analysing the number of junctions, number of meshes, number of branches and total network length after 6 hours. Data are expressed as mean ± SEM. Results in **(A-F)** and **(H-I)** were assessed by unpaired Student's t-test. Results in **(G)** were assessed by two way ANOVA with Tukey's multiple comparison test applied. *P<0.05, **P<0.01, ***P<0.01, n.s non-significant vs cells transfected with CT siRNA.

3.2.2 METTL3 Overexpression in ECs Improves Angiogenesis *in vitro*

To further investigate the functional effects of METTL3 on angiogenesis, HUVEC or HCMEC were infected with an adenovirus (Ad.METTL3 or Ad.Null) to overexpress METTL3. These cells were then subjected to a battery of angiogenic assays. METTL3 overexpression was validated at both mRNA and protein levels (figures 3.2A and B). We also confirm an increase in m6A levels in total RNA following Ad.METTL3 infection (figure 3.2C).

The adenovirus mediated overexpression of METTL3 had no effect on EC proliferation as shown by cell number quantification and BrdU incorporation (figure 3.2D and E). Additionally, METTL3 supplementation had no significant effect on endothelial migration (figure 3.2F). However, its overexpression resulted in the formation of a more robust endothelial network as observed in an *in vitro* Matrigel assay in both HUVEC and HCMEC (figures 3.2G and H). Both cell types exhibited an increase in the number of junctions, meshes, branches and total length of the network. The angiogenic potential of METTL3 was further confirmed using a fibrin gel bead assay in HCMEC where I observed an increase in the number of sprouts and sprout length (figure 3.2I).



F**G****H**

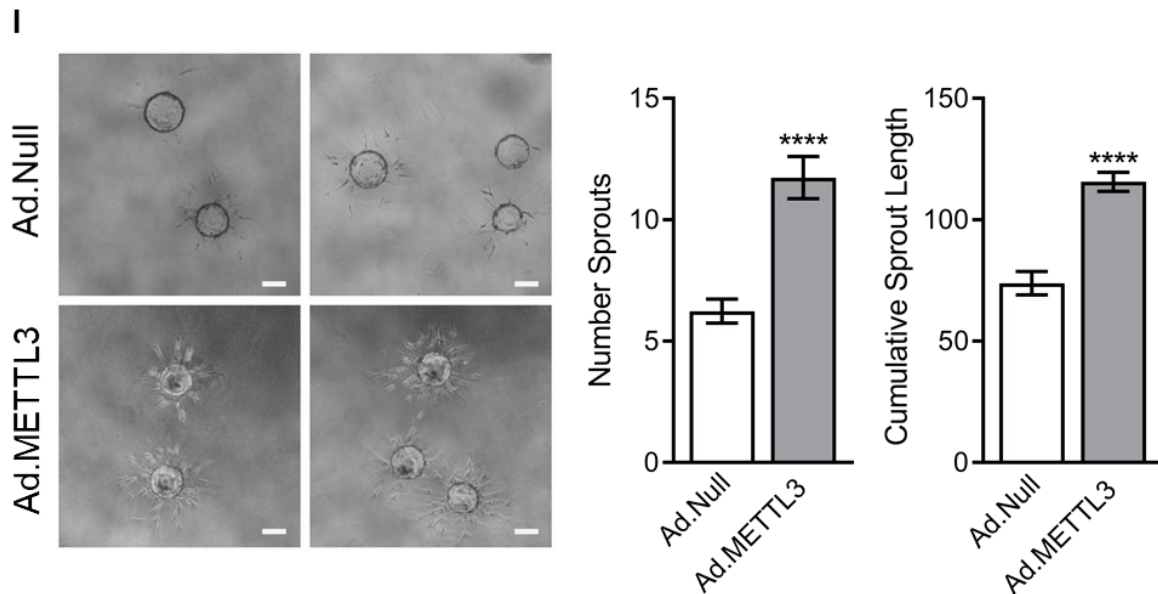
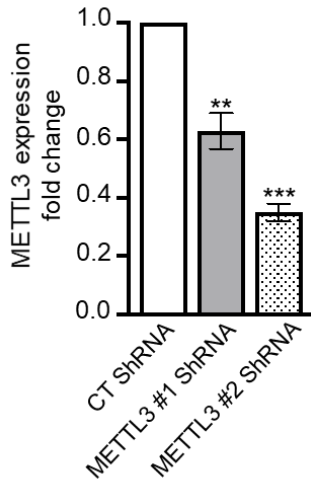
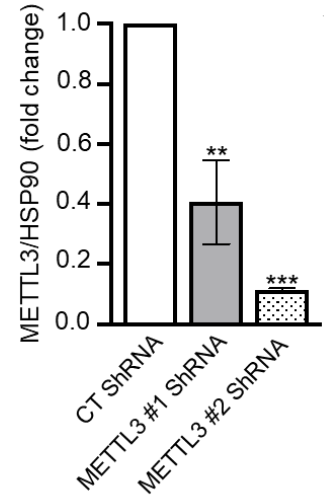
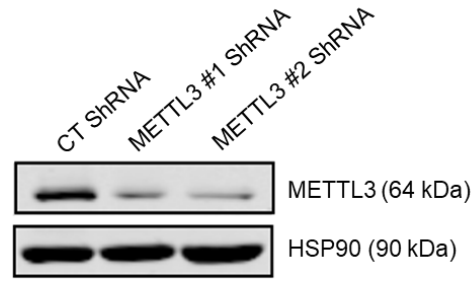
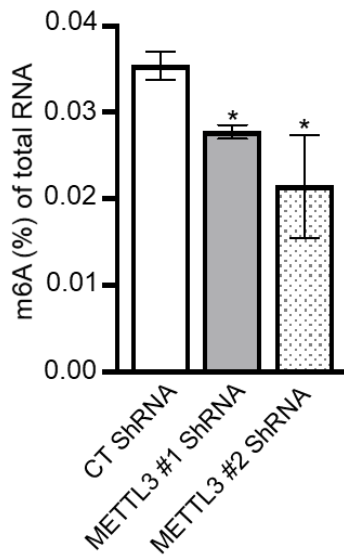
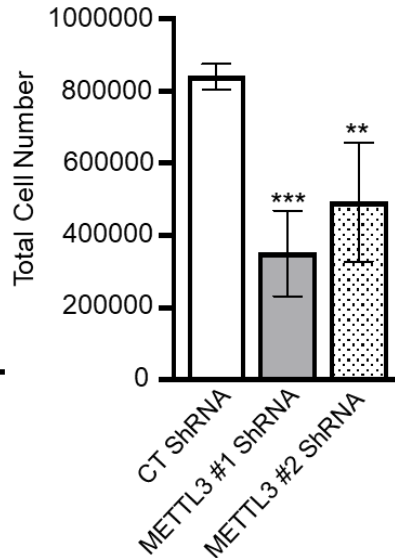
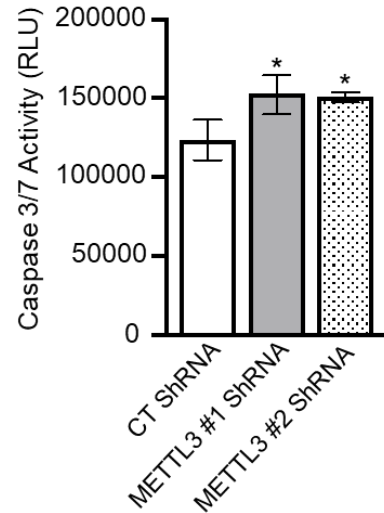


Figure 3.2 METTL3 overexpression in ECs improves angiogenesis *in vitro*. (A-I) HUVEC or HCMEC were infected with 50 MOI Ad.Null or Ad.METTL3 for 48 hours. (A) qRT-PCR analysis of METTL3 expression in HUVEC. 18s was used as housekeeping gene (n=3). (B) Quantification of METTL3 protein levels in HUVEC was performed by western blot analysis. Representative blots are shown and western blot quantification is expressed as fold change vs Ad.Null (n=3). HSP90 was used as loading control. (C) Global m6A RNA methylation levels in HUVEC were quantified using an ELISA based assay (n=2, performed in triplicates). (D) Quantification of total cell number (n=3). (E) Colorimetric assessment of BrdU incorporation (n=3). (F) Representative microscopy images of scratch wound assay (4x magnification, scale bar 50µm) (n=3). EC migration was quantified as the percentage of gap closure at 0 hours, 6 hours and 12 hours following scratch formation. (G-H) Representative microscopy images of cord formation assay in HUVEC (G) and HCMEC (H) (4x magnification, scale bar 50µm) (n=4). Angiogenesis was quantified by analysing the number of junctions, number of meshes, number of branches and total network length after 6 hours. (I) Representative microscopy images of HCMEC bead spheres used for fibrin bead assay (4x magnification, scale bar 50µm). HCMEC were allowed to undergo morphogenesis for 48 hours in the presence of EGM2. Quantification of angiogenesis was performed through the analysis of the number of sprouts and cumulative sprout length (n=3 experiments, 10 beads analysed per experiment). Data are expressed as mean ± SEM. Results in (A, B, C, D, E and G-H) were assessed by unpaired Student's t-test. Results in (F) were assessed by two way ANOVA with Tukey's multiple comparison test applied. *P<0.05, **P<0.01, ***P<0.01, n.s non-significant vs cells transfected with Ad.Null.

3.2.3 Endogenous METTL3 is Required for the Bioprocessing of let-7e and the miR-17-92 Cluster in ECs

We next aimed to elucidate the mechanisms underlying the newly identified functional role of METTL3 in angiogenesis. Previous studies in a metastatic breast cancer cell line (MDA-MB-231) suggest METTL3 plays a crucial role in the processing of primary miRNAs that contain RRACH motifs. We utilised these data to extract a list of EC expressed pri-miRNAs methylated by METTL3 [154]. This included pri-let-7e and the polycistronic pri-miR-17-92, which most importantly in their mature forms, are crucial regulators of angiogenesis [202-204]. To confirm the relevance of METTL3 in the bioprocessing of these miRNAs in ECs, METTL3 was depleted using two independent LV-METTL3-shRNAs (sequence #1 or #2) or LV-CT-shRNA. Successful knockdown of METTL3 expression was validated at both mRNA and protein levels by RT-qPCR and Western Blotting (figures 3.3A and B). Additionally, both METTL3-shRNAs significantly reduced m6A levels in total RNA (figure 3.3C). Consistent with our data thus far, these ECs demonstrated a decrease in proliferation and an increase in apoptosis (figure 3.3D and E). Interestingly, METTL3 deficient ECs exhibited an increase in the expression of both pri-let-7e and pri-miR-17-92 (figure 3.3F and G), while the levels of the mature forms of let-7e and the individual components of the miR-17-92 cluster were reduced (figure 3.3H and I). These data suggest METTL3 depletion results in a reduction in primary miRNA processing and a decrease in mature miRNA levels, including miRNAs endogenous to ECs that play a role in angiogenesis.

A**B****C****D****E**

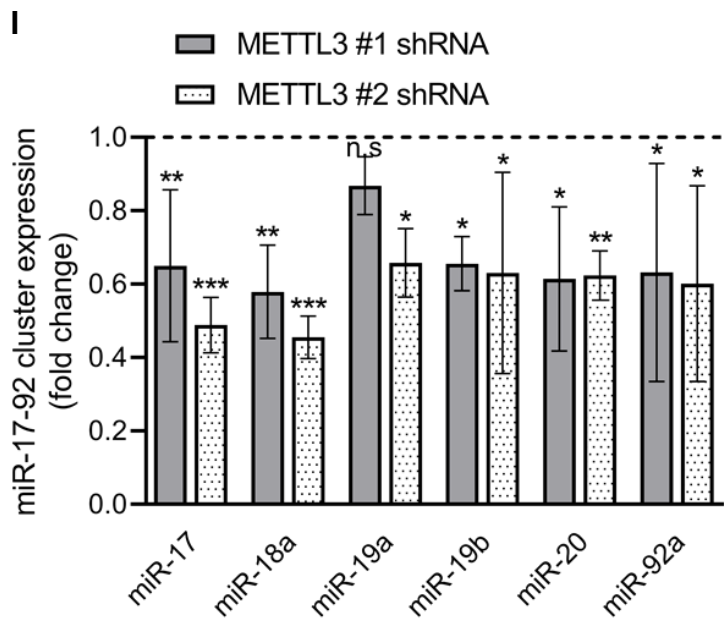
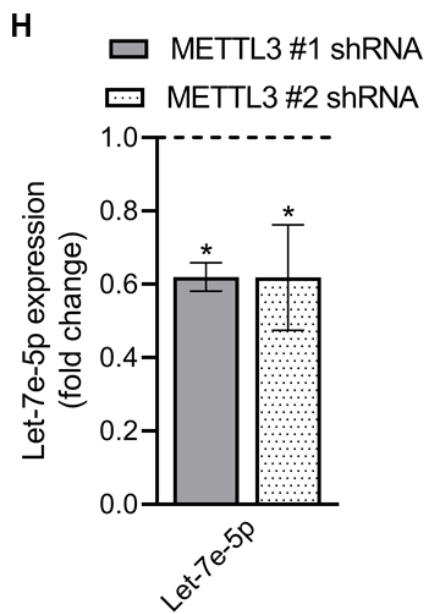
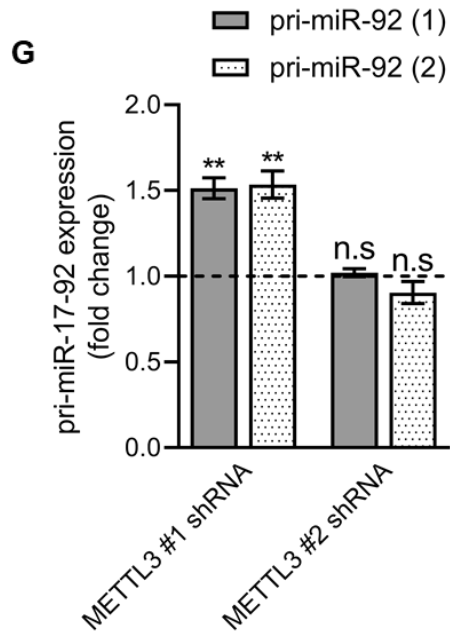
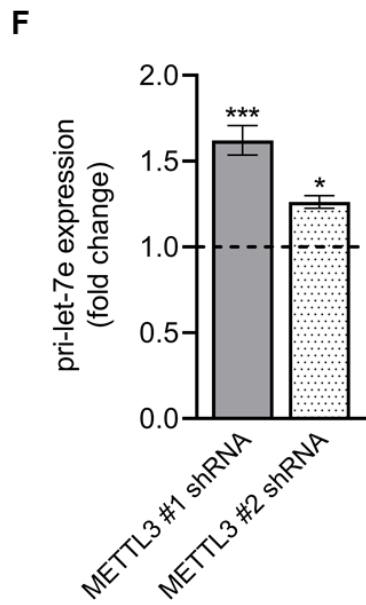
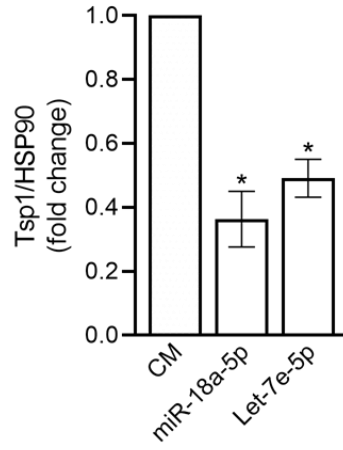
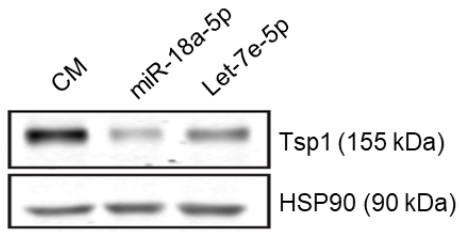
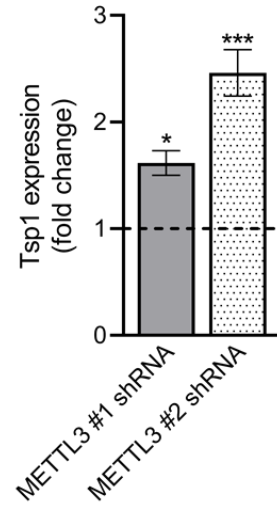
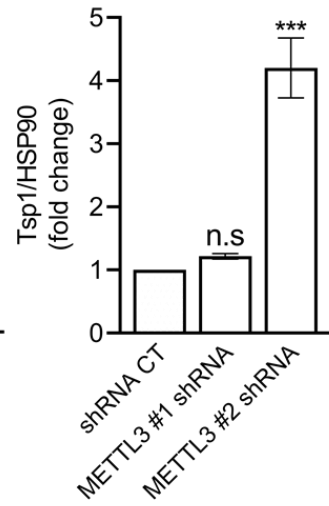
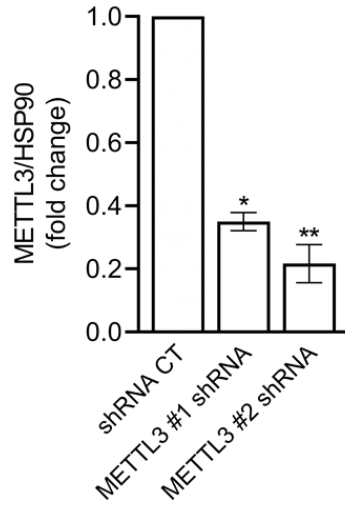
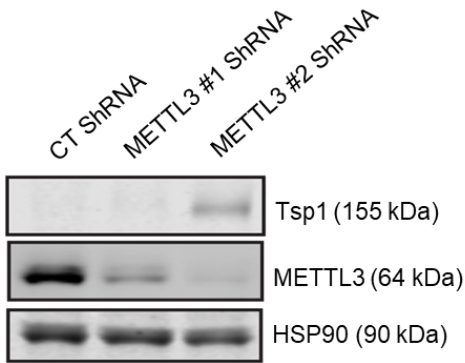


Figure 3.3 METTL3 depletion in ECs decreases the levels of let-7e and miR-17-92. (A-I) HUVEC were infected with two control (CT) shRNA or two different METTL3 shRNAs (#1 or #2) and selected with puromycin (1 µg/mL) for one week. **(A)** qRT-PCR analysis of METTL3 expression in HUVEC. 18s was used as housekeeping gene (n=4). **(B)** Quantification of METTL3 protein levels in HUVEC was performed by western blot analysis. Representative blots are shown, and western blot quantification is expressed as fold change vs CT shRNA (n=3). HSP90 was used as loading control. **(C)** Global m6A RNA methylation levels in HUVEC were quantified using an ELISA based assay (n=2, performed in triplicates). **(D)** Quantification of total cell number (n=3). **(E)** Caspase 3/7 activity to assess apoptosis (n=3). qRT-PCR analysis in METTL3 depleted ECs of **(F)** pri-let-7e, **(G)** pri-miR-17-92, **(H)** let-7e-5p and **(I)** miR-17-92 Data are expressed as mean ± SEM. Results were assessed by two way ANOVA (Tukey's post hoc test) . *P<0.05, **P<0.01, ***P<0.01, n.s non-significant vs cells transfected with CM or infected with CT shRNA.

3.2.4 METTL3 Modulates Tsp1 by Regulating miR-18a-5p and let-7e-5p

Expression

To understand the impact of METTL3 on the functional capacity of let-7e and the miR-17-92 cluster, I explored the effect of METTL3 modulation on the expression of genes targeted by these miRNAs. miRcode and TargetScan were used to identify common targets for let-7e and miR-17-92, and DAVID was used to identify potential targets relevant in angiogenesis. These studies allowed us to identify Thrombospondin-1 (Tsp1), a potent anti-angiogenic factor [205], as a common target for let-7e and the miR-18a component of the miR-17-92 cluster. Members of the let-7e family [206] and the miR-18a-5p component of the miR-17-92 cluster [207] have been shown to modulate Tsp1 expression in ECs. I firstly confirmed that overexpression of mimics of let-7e and miR-18a reduced Tsp1 protein levels in HUVECs (figure 3.4A). Consistently, I also show an increase in Tsp1 mRNA and protein levels following the shRNA mediated depletion of METTL3 in HUVEC and HCMEC (figure 3.4B-D). The overexpression of let-7e-5p and miR-18a-5p mimics in HUVEC depleted of METTL3 maintained Tsp1 expression at levels similar to that of the control cells (figure 3.4E and F).

A**B****C**

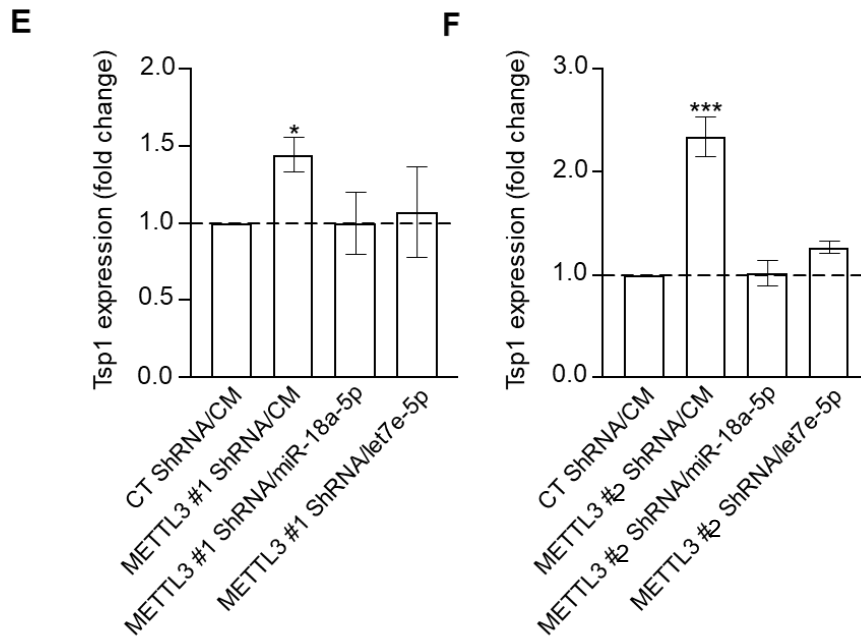
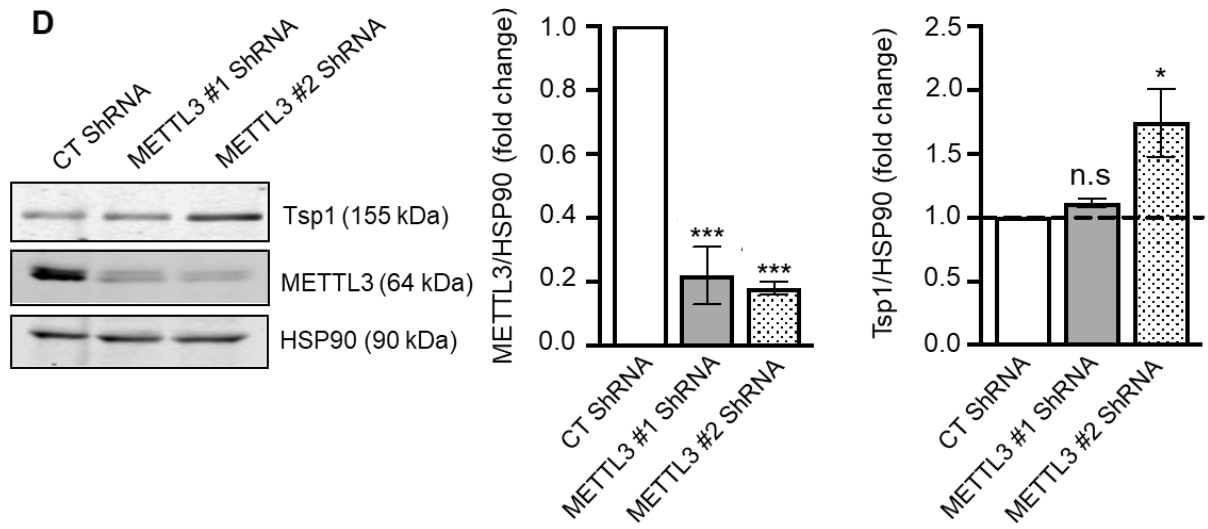


Figure 3.4 miR-18a-5p and let-7e-5p overexpression reduces Tsp1 expression while METTL3 depletion increases its expression. HUVECs (**B-C** and **E-F**) or HCMECs (**D**) were infected with two control (CT) shRNA or two different METTL3 shRNAs (#1 or #2) and selected with puromycin (1 μ g/mL) for one week. **(A)** Quantification of protein levels of Tsp1 in HUVEC transfected with 30 nM of miR-18a-5p mimic, or control miRNA (CM) by western blot analysis. Representative western blot is shown (N=3). Western blot quantification is expressed as fold change vs CM. HSP90 was used as loading control. **(B)** Quantification of METTL3 mRNA levels in HUVEC by qRT-PCR analysis of Tsp1 (n=3). **(C)** Quantification of protein levels of Tsp1 and METTL3 by western blot analysis. Representative western blot is shown (N=3). Western blot quantification is expressed as fold change vs CT shRNA. HSP90 was used as loading control. **(D)** Western blot analysis of METTL3 and Tsp1 in HCMEC (n=3). Representative western blot is shown (N=3). Western blot quantification is expressed as fold change vs CT shRNA. HSP90 was used as loading control. **(E-F)** qRT-PCR analysis of Tsp1 expression in cells infected with METTL3 shRNAs (E #1, or F #2) and co-transfected with mimic miR-18a-5p or let-7-5p, or control mimic (CM) (n=3). Data are expressed as mean \pm SEM. Results were assessed by two way ANOVA (Tukey's post hoc test) . *P<0.05, **P<0.01, ***P<0.01, n.s non-significant vs cells transfected with CM or infected with CT shRNA.

3.2.5 METTL3 Overexpression Modulates the Expression of let-7e-5p, the miR-17-92 Cluster and Tsp1 Expression

Next, METTL3 was overexpressed in ECs and the levels of let-7e-5p and the miR-17-92 cluster were assessed to further confirm the METTL3 mediated modulation of these angiogenic miRNAs. Here, I find that HUVECs infected with Ad.METTL3 exhibited significant increases in the expression of let-7e-5p and each individual component of the miR-17-92 cluster (figure 3.5A and B). I also report a dramatic reduction of Tsp1 at both an mRNA and protein levels (figure 3.5C and D).

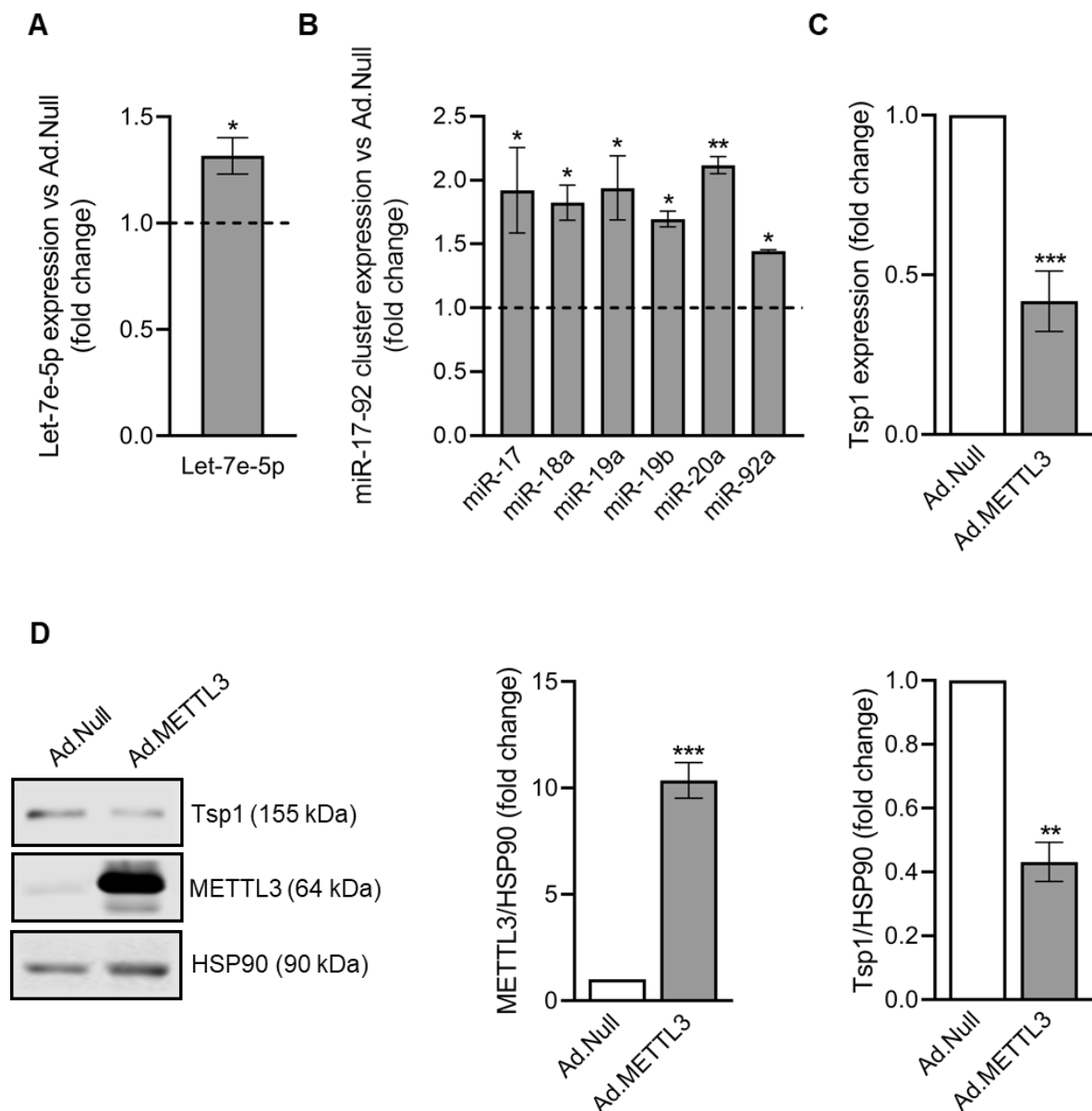
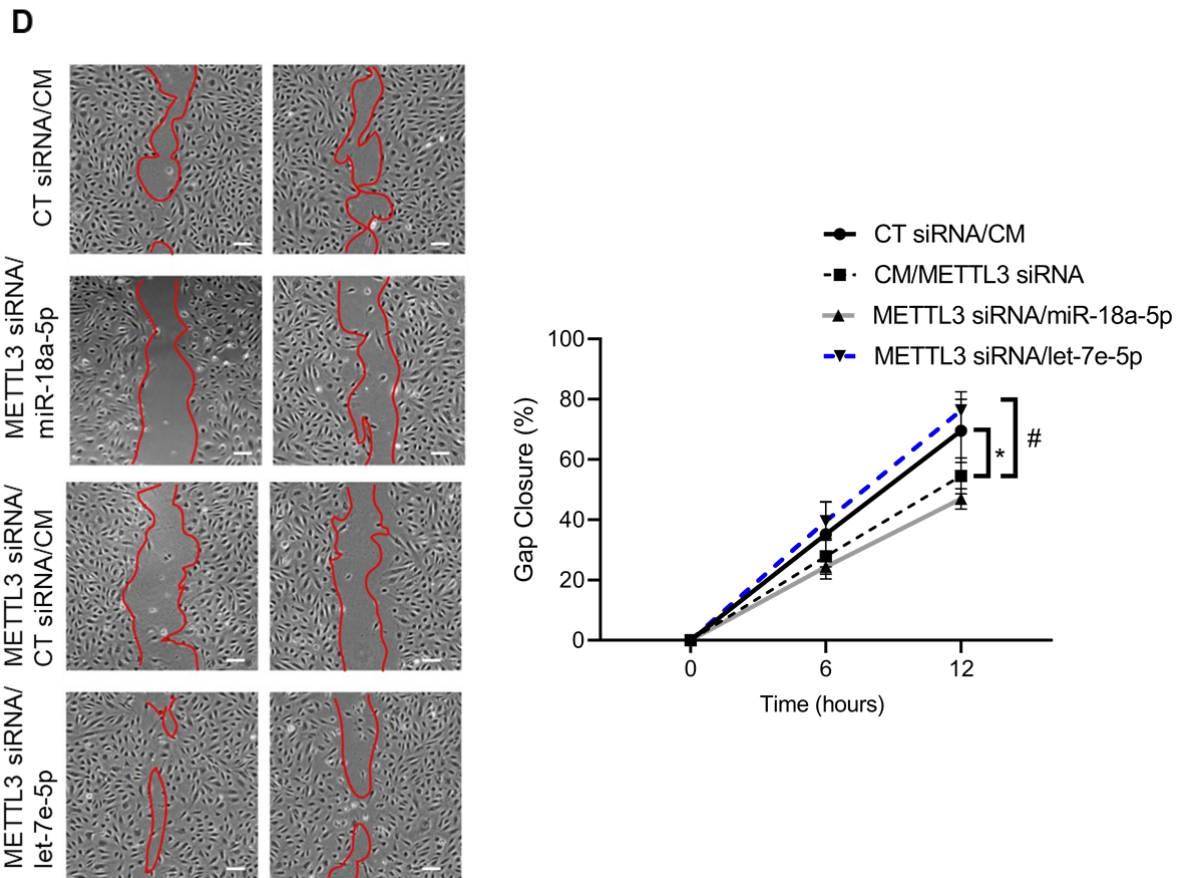
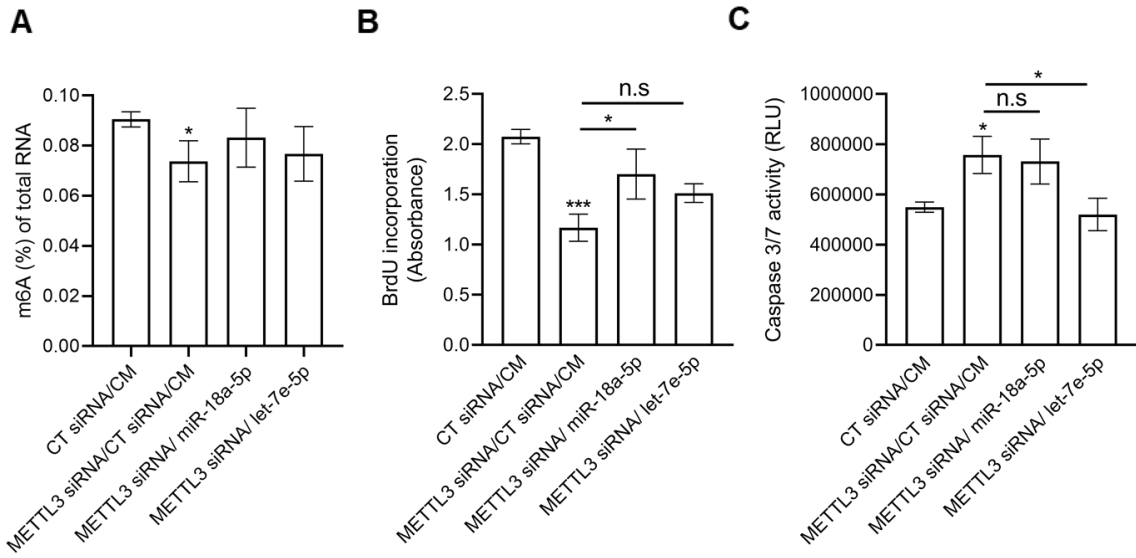


Figure 3.5 METTL3 overexpression increases the levels of let-7e and miR-17-92 and decreases Tsp1 expression. HUVEC were infected with 50 MOI of Ad.Null or Ad.METTL3 for 12 hours. qRT-PCR analysis of **(A)** let-7e-5p **(B)** miR-17-92 and **(C)** Tsp1 at 48 hours post infection (n=4). 18s was used as housekeeping gene. **(D)** Quantification of protein levels of Tsp1 and METTL3 by western blot analysis 48 hours post infection. Representative blots are shown (n=4). HSP90 was used as loading control. Data are expressed as mean \pm SEM. Results in **(A, C-D)** were assessed by unpaired Student's t-test, and **(B)** by one-way ANOVA (Tukey's post hoc test). *P<0.05, **P<0.01, ***P<0.001, n.s non-significant. vs Ad.Null infected cells.

3.2.6 The Overexpression of let-7e and miR-18a Restores the Angiogenic Capacity of METTL3 Depleted ECs *In Vitro*

The mechanistic data presented thus far suggests that METTL3 regulates key angiogenic processes in ECs through the bioprocessing of the angiogenic miRNAs let-7e-5p and miR-18-a-5p. A series of rescue experiments were performed to further corroborate these findings where endothelial METTL3 levels were depleted, and miRNA mimics were used to restore let-7e-5p and miR-18-a-5p expression. I firstly confirmed that the overexpression of let-7e-5p and miR-18a-5p in METTL3 depleted ECs did not affect the levels of m6A RNA methylation (Figure 3.6A). Interestingly, the overexpression of miR-18a-5p in METTL3 depleted ECs partially rescued the observed decrease in proliferation (figure 3.6B). While the overexpression of let-7e-5p abrogated the induction of apoptosis and restored the ability of METTL3 deficient cells to migrate (figure 3.6C and D). As expected, the depletion of METTL3 impaired the formation of an endothelial network using an *in vitro* Matrigel assay. However, the mimic induced rescue of both let-7e-5p and miR-18-a-5p restored the angiogenic capacity of these cells (figure 3.6E).



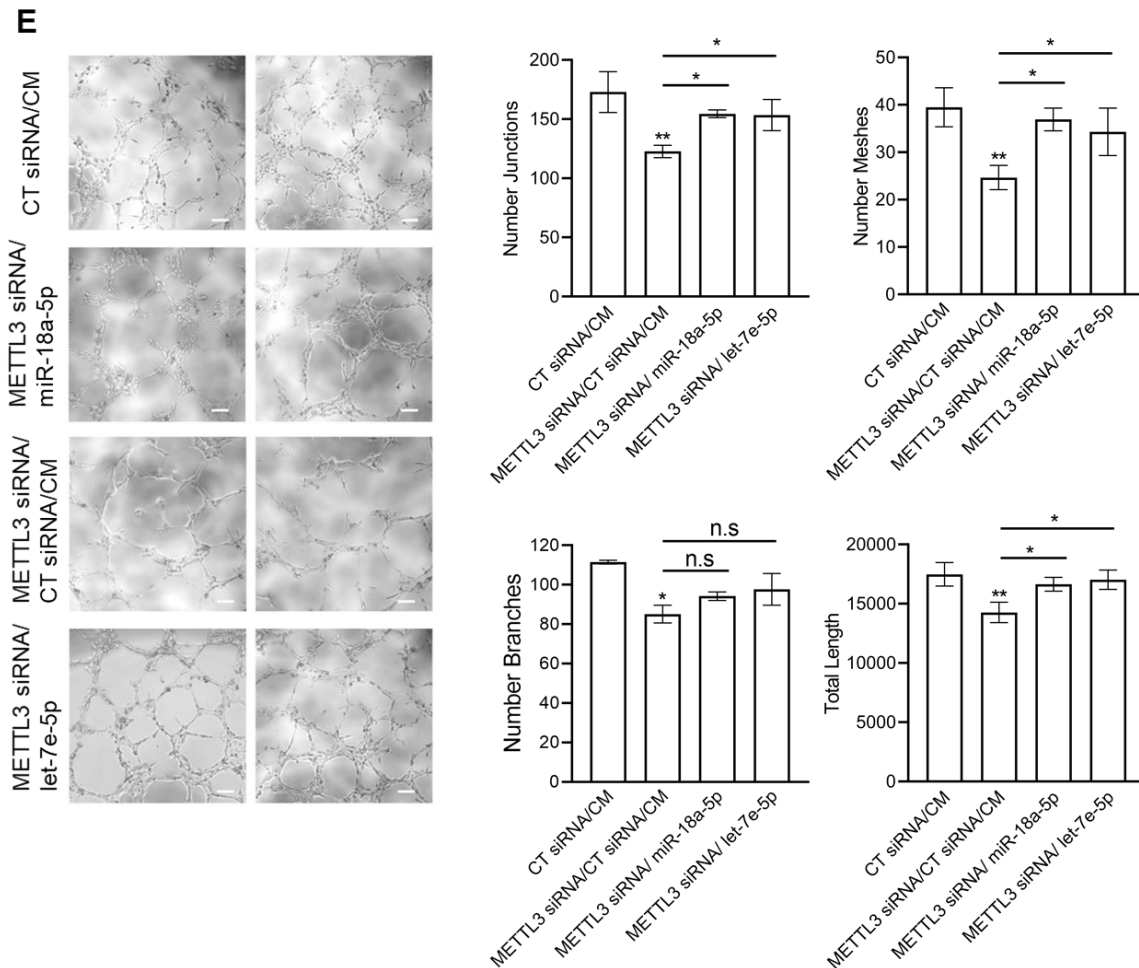


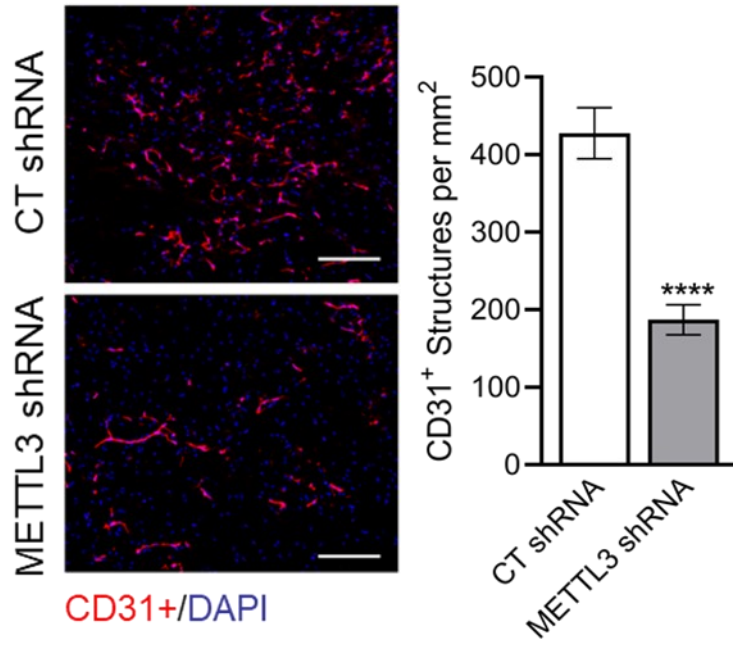
Figure 3.6 The overexpression of let-7e and miR-18a restores the angiogenic capacity of METTL3 depleted ECs *in vitro*. HUVEC were co-transfected with 30 nM of control (CT) siRNA and control mimic (CM) sequences (CT siRNA/CM), METTL3 siRNA in the presence of CT siRNA and CM (METTL3 siRNA/CT siRNA/CM), or METTL3 siRNA in the presence of mimic miR-18a-5p or let-7e-5p for 48 hours. **(A)** Global m6A RNA methylation levels in HUVEC were quantified using an ELISA based assay (n=3, performed in triplicates). **(B)** Colorimetric assessment of BrdU incorporation (n=3). **(C)** Caspase-3/7 activity assay (n=3). **(D)** Representative microscopy images of scratch wound assay (4x magnification, scale bar 50µm) (n=3). EC migration was quantified as the percentage of gap closure at 0 hours, 6 hours and 12 hours following scratch formation. **(E)** Representative microscopy images of cord formation assay. Angiogenesis was quantified by analysing the number of junctions, number of meshes, number of branches and total network length after 6 hours. (4X magnification, scale bar 50 µm) (n=4). Angiogenesis was quantified as number of junctions, meshes, branches and total length after 6 hours. Data are expressed as mean ± SEM. Results in **A-E** were assessed by one-way ANOVA (Tukey's post hoc test). *P<0.05, **P<0.01, ***P<0.01, n.s non-significant vs cells transfected with CT siRNA/CM or † P<0.05vs cells transfected with METTL3 siRNA/CT siRNA/CM.

3.2.7 Depletion of METTL3 in ECs Impairs Angiogenesis While its Overexpression Improves Angiogenesis *in vivo*

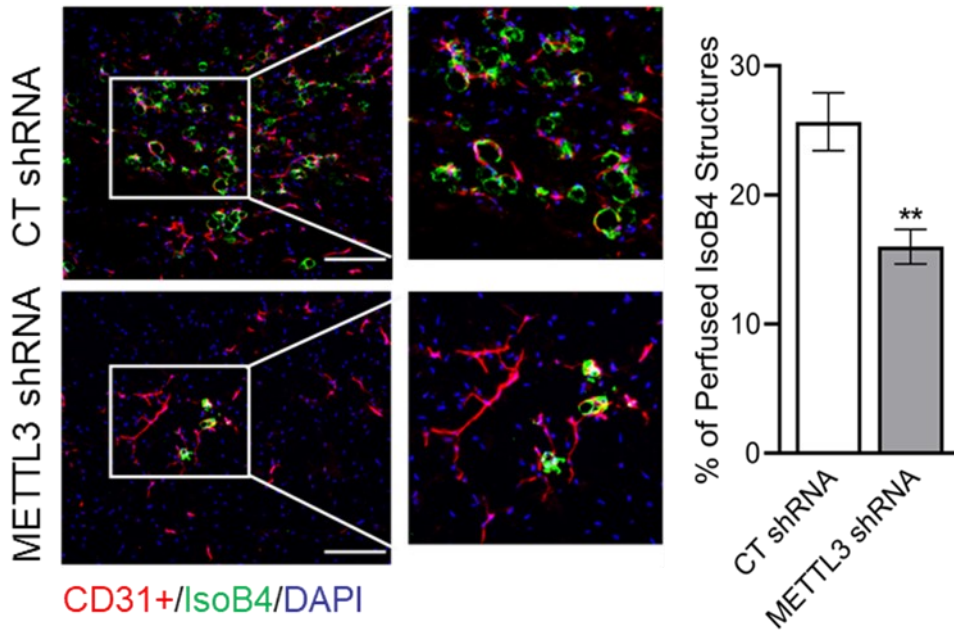
To gain an insight into the physiological significance of endogenous METTL3, an *in vivo* Matrigel plug assay was performed using HUVEC infected with lentiviral particles expressing shRNAs against METTL3 (LV-METTL3-shRNAs or LV-CT-shRNA). In these experiments, transduced cells were suspended in Matrigel and subcutaneously implanted into the flank region of immunodeficient mice for 21 days. To study the perfusion of newly formed vessels, mice were injected in the tail vein with biotinylated isolectin B4, which was allowed to circulate for 15 minutes before sacrifice. Plugs containing METTL3 depleted human ECs exhibited distinctly fewer CD31+ capillary-like structures (figure 3.7A) and a lower percentage of isolectin B4 perfused vessels compared to control plugs (figure 3.7B).

Additionally, a second experiment was performed using HUVEC infected with Ad.METTL3 to overexpress METTL3. These studies reveal an increase in the number of CD31+ capillary-like structures and a higher percentage of perfused vessels compared to Ad.Null treated plugs (figure 3.7C and D). As shown in figures 3.7E and F, the proangiogenic response elicited by the overexpression of METTL3 was equivalent in mice of both sexes. It's important to note that the statistical power of the analysis between both sexes may be limited due to the small sample size of only three mice per group.

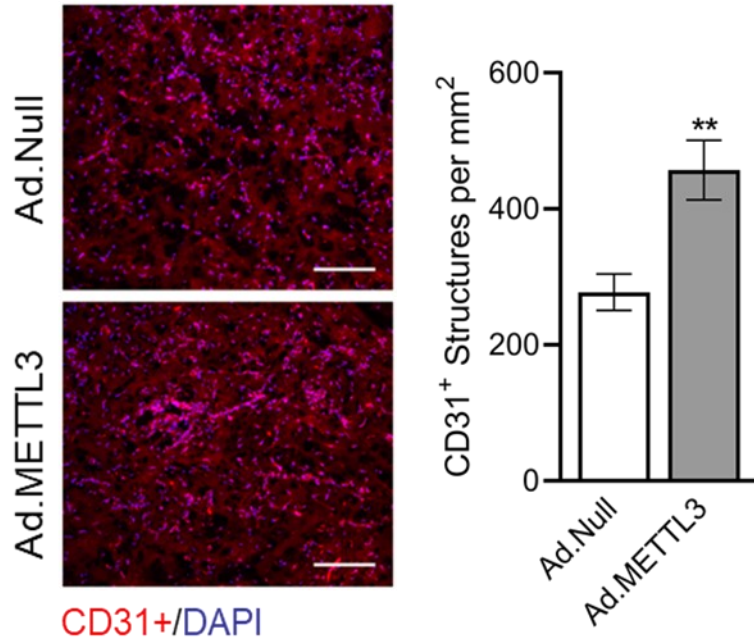
A



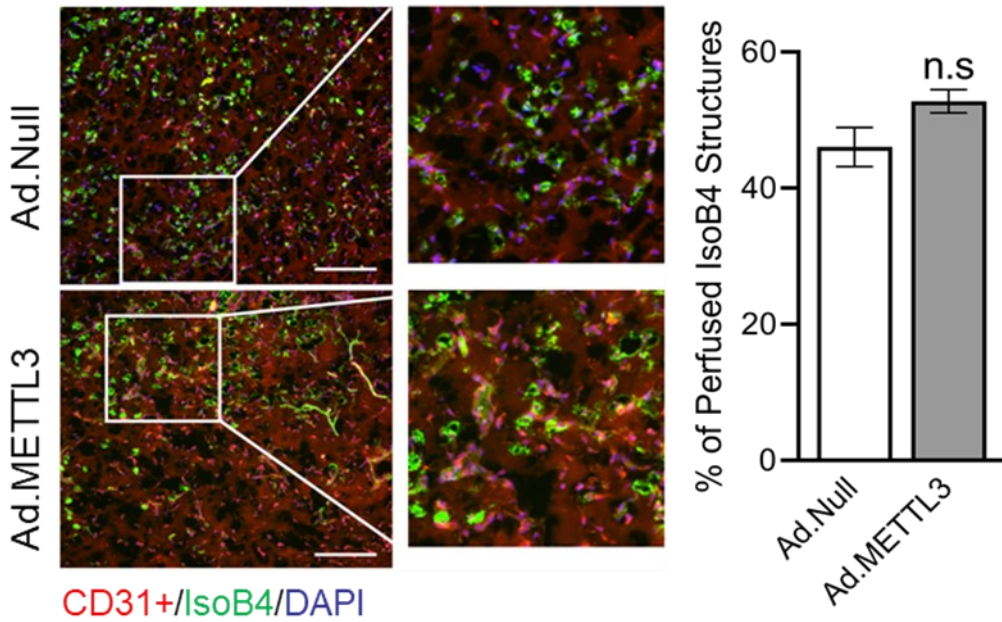
B



C



D



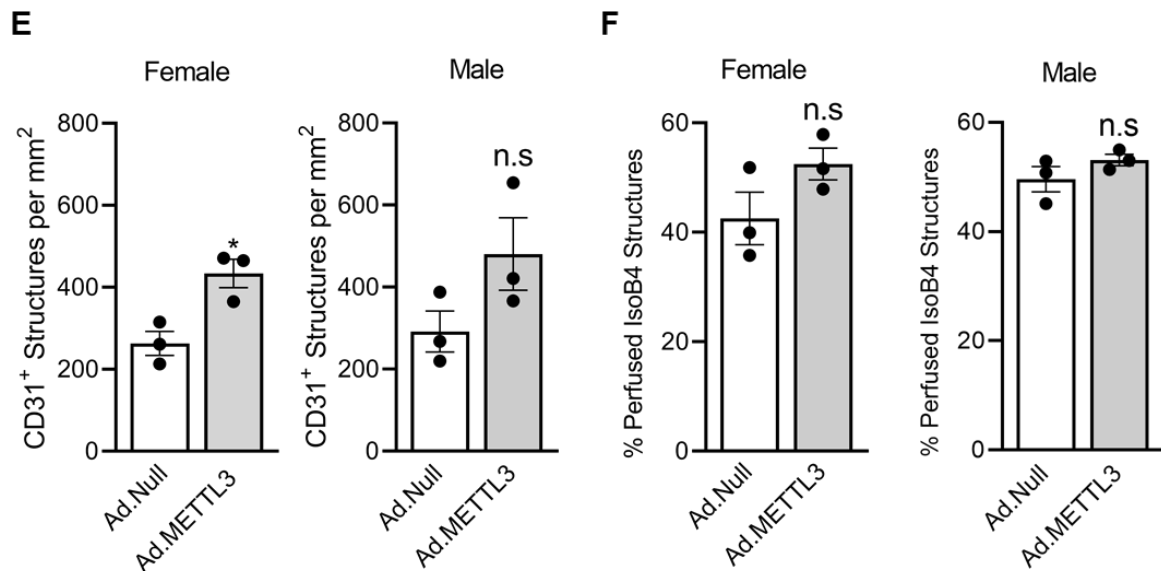


Figure 3.7 Depletion of METTL3 in ECs impairs angiogenesis while its overexpression improves angiogenesis in an *in vivo* Matrigel plug assay. (A-B) HUVEC were infected with control (CT) or METTL3 shRNA lentiviral particles and selected with puromycin (1 μ g/mL) for 1 week. Transduced cells were resuspended in Matrigel and injected subcutaneously into the flank region of 10-week-old immunodeficient male mice. Grafts from METTL3 or CT shRNA transduced cells were isolated three weeks after implantation (n=8 mice in each group). **(C-D)** HUVEC were infected with 50 MOI of adenoviral particles carrying human METTL3 (Ad.METTL3) or control adenoviral particles (Ad.Null) for 12 hours. Infected cells were resuspended and inoculated as described above in immunodeficient male and female mice. Grafts from Ad.Null or Ad.METTL3 were isolated 2 weeks after implantation (n=6 mice in each group, 3 male and 3 female). **(A-D)** Representative microscopy images showing vascular density in the study groups (10X magnification, scale bar 50 μ m). Angiogenesis was quantified in **A**, **C** and **E** as CD31⁺ structures. Perfused vessels were quantified as percentage of human vessels perfused with isolectin-B4 in **B**, **D** and **F**. Data are expressed as mean \pm SEM. Results in **A-F** were assessed by unpaired Student's t-test. *P<0.05, **P<0.01, ***P<0.01, n.s non-significant vs grafts from CT shRNA or Ad.Null transduced cells.

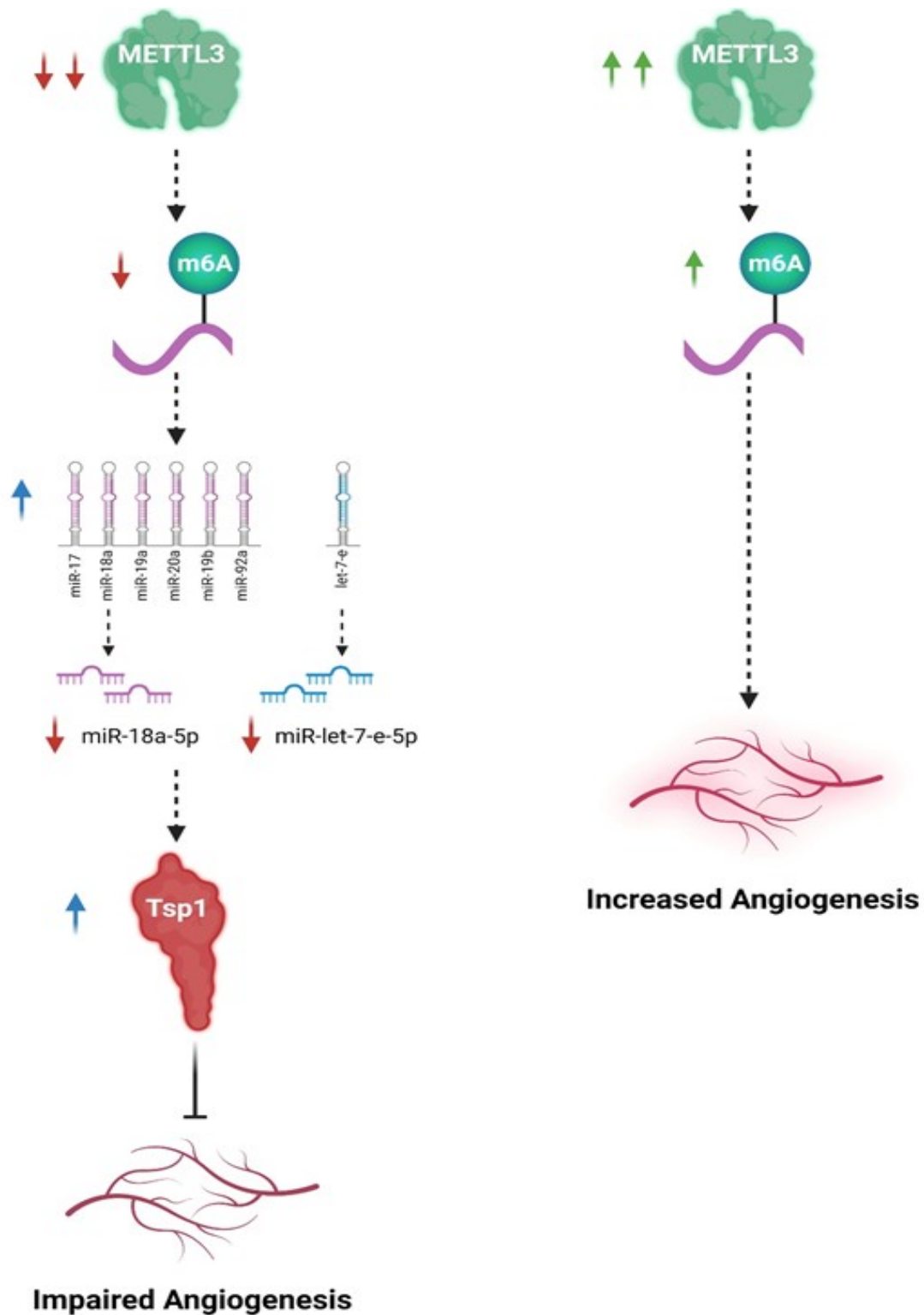


Figure 3.8 Schematic summarizing the role of METTL3 mediated m6A in the regulation of angiogenesis. METTL3 regulates the maturation of “angiomiRNAs”. More specifically, we showed that the depletion of METTL3 impairs the bioprocessing of the angiomiRNA let-7e-5p and miR-18a-5p (produced from the miRNA-17-92 cluster). This resulted in the nuclear accumulation of pri-let-7e and pri-miR-17-92, a reduction in the miRNA functional mature forms and the subsequent increase in their common anti-angiogenic target, thrombospondin 1 (Tsp1).

3.3 Discussion

The studies presented in this chapter provide the first insights into the functional relevance of METTL3 mediated m6A in the regulation of angiogenesis. We have shown that the repression of endothelial METTL3 expression results in the impairment of EC proliferation, migration and network formation capacities. In line with these findings, the overexpression of METTL3 in ECs improved angiogenesis *in vitro*. Additionally, the physiological significance of METTL3 in the regulation of angiogenesis was corroborated using an *in vivo* Matrigel plug model, where human ECs depleted from METTL3 exhibited distinctly fewer CD31+ capillary-like structures and a lower percentage of perfused vessels. The overexpression of METTL3 in this *in vivo* Matrigel model resulted in an increase in capillary like structures and a higher percentage of perfused vessels. Mechanistically, I demonstrate that METTL3 mediates the levels of m6A on total RNA in ECs and promotes the bioprocessing of let-7e-5p and miR-17-92 cluster, thereby improving the angiogenic capacity of ECs.

Previous studies suggest a crucial role for m6A RNA methylation in facilitating the first step in miRNA biogenesis, the Drosha-DGCR8 mediated processing of pri-miRNAs into mature miRNAs. The presence of m6A is suggested to facilitate the binding between pri-miRNA and the DGCR8 component of the microprocessor complex. These studies found that the depletion of METTL3 reduced m6A levels on pri-miRNAs and in turn decreased interactions between the microprocessor complex and target pri-miRNAs. Additionally, this same study described a number of RRACH motifs in pri-miRNA-let-7e and pri-miR-17-92. The authors also reveal that the depletion of METTL3 in a metastatic breast cancer cell line (MDA-MB-231) led to a decrease in mature let-7e and a nuclear accumulation of its unprocessed form [154]. In line with this data, I report an increase in the expression of pri-miR-let-7e and pri-miR-17-92,

and a reduction of their mature forms in ECs where METTL3 was knocked down and m6A levels were depleted. More importantly, this deregulation in the expression of let-7e-5p and the miR-18a-5p component of the miR-17-92 cluster was associated with an impairment in their functional capacity, as demonstrated by their inability to repress Tsp1 expression, a common anti-angiogenic target. This was supported by our findings that the restoration of let-7e-5p and miR-18-5p rescued the angiogenic capacity of METTL3 depleted ECs. Conversely, METTL3 overexpression resulted in an increase in the levels of let-7e-5p and individual components of the miR-17-92 cluster while reducing Tsp1 expression. It would be valuable to ascertain the direct binding of let-7e-5p and miR-18-5p to the 3'UTR of TSP1 by employing a luciferase reporter assay. This would allow us to quantitatively assess the impact of let-7e-5p and miR-18-5p on the translational efficiency of TSP1 mRNA, shedding light on the extent of their regulatory influence. Nonetheless, my data suggests that the underlying mechanisms by which METTL3 regulates key angiogenic processes and EC function involves the processing of angiogenic miRNAs.

Interestingly, a recent study by Van den Homberg et al., identified an alternative mechanism by which the m6A methylation of vasoactive miRNAs effects angiogenesis and vascular remodelling. The authors identified a particular set of miRNAs which were hypermethylated by METTL4, a methyltransferase of predominantly small nuclear RNAs, rather than METTL3 under hypoxic conditions. This increase in methylation did not affect the processing or expression of the identified miRNAs, but rather negatively modulated RISC-loading to alter target mRNA expression [208]. Consistent with our findings, recently published work demonstrated that the depletion of METTL3 in ox-LDL-treated HUVEC reduced EC proliferation, migration and tube formation. Although the underlying mechanisms were not considered, this study also

suggests that the knockdown of METTL3 results in impaired angiogenic activity *in vivo* utilising a chick chorioallantoic membrane assay [169].

The angiogenic front is a dynamic environment requiring precise spatial and temporal coordination of signalling pathways and downstream gene expression. One such mechanism is the Notch signalling pathway, an extensively studied mechanism with well-established functions in quiescent and angiogenic ECs. Lv et al., explored the relevance of METTL3 in the broader endothelial setting by demonstrating a link between m6A and the Notch signalling pathway to regulate haematopoiesis during mouse embryogenesis [165]. The study describes a mechanism by which expression of METTL3 in ECs drives the methylation of Notch1 transcripts and results in the repression of Notch activity during endothelial-to-hematopoietic transition. In line with our data, recent work also highlights a role of METTL3-mediated m6A in the regulation of angiogenesis [167]. METTL3 was shown to regulate angiogenesis through the methylation of dishevelled 1 (DVL1) and LRP6 components of the Wnt signalling pathway. More specifically, METTL3 enhances the rate of translation of DVL1 and LRP6 in a YTHDF1 dependent manner. Furthermore, the importance of METTL3 in the regulation of angiogenesis was reinforced by an additional study which demonstrated that the migratory ability of METTL3 deficient ECs was decreased. Moreover, the knockdown of METTL3 significantly inhibited formation of capillary-like structures. This study focused on Cerebral arteriovenous malformations (AVM), a condition in which abnormalities in angiogenesis is a key characteristic. RNA transcriptome profiling and MeRIP-seq were utilised to clarify the underlying mechanisms where they reveal DRX3L as a direct downstream target of METTL3. DRX3L was shown to synergise with DTX1 to modulate the Notch signalling pathway to regulate angiogenesis *in vitro* [209]. The discovery of these distinct METTL3-

dependent pathways is indeed in agreement with the overarching paradigm that the m6A mark is a complex and dynamic mechanism crucial for fine tuning the regulation of important biological processes such as angiogenesis.

WTAP is another key constituent of the m6A methyltransferase complex. In agreement with our findings, a recent investigation identified WTAP as a regulator of angiogenesis, where EC network forming capacities were compromised upon its depletion. WTAP is downregulated in lesions of AVMs, while a transcriptome-wide analysis of m6A in WTAP-deficient cells reveals Desmoplankin, a key component of desmosomes required for microvascular tube formation [172], as a downstream target of WTAP where IGF2BPs reader proteins bind to the m6A mark and stabilise Desmoplankin transcripts.

Our findings reveal METTL3 as a regulator of angiogenesis by modulating the processing and in turn the expression and function of let-7e and the miR-17-92 cluster. However, apart from miRNA processing, m6A RNA methylation also modulates the biogenesis and functional capacity of other non-coding RNAs, such as long noncoding RNAs and circular RNAs. Additionally, METTL3 regulates every step of mRNA metabolism, including alternative splicing, rate of export, RNA stability, translation and decay [210, 211]. Thus, endothelial levels of METTL3 also influence potential non-coding RNAs and mRNA transcripts involved in angiogenesis, as indicted by other studies described in this section. Furthermore, although METTL3 is the primary catalytic component responsible for the deposition of m6A, the levels of m6A are also highly influenced by other components, such as WTAP. Each of which may influence the angiogenic process through the regulation of independent and common targets. Further transcriptome wide profiling using ECs deficient of METTL3, WTAP and potentially other m6A regulators will allow further characterisation of downstream

targets of METTL3 relevant for angiogenesis. Aberrant angiogenesis, whether excessive or deficient is associated with numerous pathologies such as AVM, diabetic retinopathy and IHD. Thus, the therapeutic modulation of m6A and its regulators should be considered as a new approach for controlling angiogenic responses in different clinical settings.

Chapter 4

Endothelial m6A and its Machinery Components are Dysregulated by Diabetes *In Vitro* and *In Vivo*

4. Endothelial m6A and its Regulatory Components are Dysregulated in Diabetic Models *In Vitro* and *In Vivo*

4.1 Introduction

The incapacity of ECs to regulate glucose influx makes them especially susceptible to DM induced damage. Clinical and experimental evidence suggests that chronic intracellular hyperglycaemia causes endothelial dysfunction and microvascular rarefaction. Endothelial dysfunction is an umbrella term referring to the inability of the endothelium to regulate vascular homeostasis, leading to impairments in barrier functions, vasodilation, angiogenesis, disturbances in proliferative capacities and deterrence of leukocytes from adhesion and diapedesis. Chronic intracellular hyperglycaemia causes EC dysfunction by initiating a self-perpetuating cycle of oxidative stress and aberrant metabolic memory. Endothelial dysfunction represents an independent risk marker for cardiovascular events, while attenuation of endothelial function is a common factor in numerous DM associated vascular complications. Although the exact mechanisms of endothelial dysfunction remain unclear, multiple homeostatic disturbances have been identified alongside the typically described hyperglycaemia, indicating a multifactorial aetiology.

Prolonged exposure of the endothelium to hyperglycaemic conditions is now recognised as a major factor in the pathogenesis of DM induced vascular injury. The initial trigger whereby hyperglycaemia results in the dysfunction and damage of the endothelium is the reduction of NO bioavailability and the accumulation of ROS [212]. The hyperglycaemia induced generation of superoxide anion (O_2^-) inactivates NO to form the oxidant peroxynitrite which induces substrate nitration. The accumulation of intracellular glucose leads to the initiation of a secondary metabolic pathway in which the excessive flow of glucose leads to alterations in redox potential as a result of

NADPH depletion and an increase in NADH/NAD⁺ cytosolic rate. This imitates the effects of hypoxia and results in an acceleration of glycolysis and in turn increased de novo production of diacylglycerol from glycolytic intermediates and subsequent activation of protein kinase C (PKC) [213]. PKC interferes with the production of NO and is responsible for various structural and functional changes in the endothelium including aberrations in cellular permeability, angiogenesis, cell proliferation, ECM expansion and promotes inflammation through the activation of cytokines and adhesion molecules [214]. The overproduction of ROS also increases intracellular levels of AGEs which elicits activation of AGE receptors present on the surface of ECs, smooth muscle cells, monocytes and macrophages. This in turn activates hexoamine flux to enhance inflammation and decrease phagocytosis and NO production [212]. The resulting downstream activation of Nuclear factor- κ B (NF- κ B) induces the transcription of a number cytokines and growth factors including endothelin-1, thrombomodulin, VEGF, IL-1, IL-6 and TNF- α , which trigger an inflammatory and pro-coagulant state and endothelial activation [215].

Hyperglycaemia is not the sole factor responsible for EC dysfunction in DM, which can indeed precede the development of overt hyperglycaemia in T2DM [216]. In addition to its metabolic activities, insulin plays a vital role in maintaining endothelial function through its ability to stimulate the release of NO via a signalling cascade involving the activation of the PI3K-Akt axis. Insulin also stimulates the release of the vasoconstrictor ET-1, thus having multiple opposing hemodynamic actions. IR in the endothelium results in the disruption of PI3K and increased mitogen-activated protein kinase (MAPK) signalling and in turn decreased NO levels and elevated ET-1. Additionally, excessive release of FFAs due to insulin resistance leads to diminished

NO release [217]. FFAs also promote increased vascular inflammation and expression of NADPH oxidases, mitochondrial uncoupling and increased superoxide production.

Finally, inflammation is a crucial factor responsible for the dysfunction of the endothelium in DM. Obesity and DM are inflammatory conditions where a pro-inflammatory state is induced with oxidative stress. The upregulation of TNF- α and IL-6 associated with DM interferes with insulin action by impairing insulin signal transduction and therefore its anti-inflammatory actions. Elevated levels of glucose over prolonged periods exacerbates the inflammation associated with T2DM.

Evidence emerging in recent years suggests an important role for the m6A RNA modification and its regulators in the pathogenesis and progression of T2DM. The first clear association between T2DM and m6A was described by Shen et al., in a case-control study which revealed a decrease in total m6A contents in RNA from peripheral blood of T2DM patients compared with healthy controls [193]. This reduction was paralleled by a significant increase in FTO mRNA expression while correlation analysis showed that m6A was highly correlated with the risk of T2DM and FTO levels. Furthermore, receiver-operating characteristic analysis (ROC) indicates that T2DM can be characterised by the content of m6A RNA methylation, thereby suggesting m6A may also serve as a novel T2DM biomarker [193]. The negative association between m6A and T2DM was further validated in a subsequent study where a significantly higher increase in FTO was reported in patients with T2DM with hyperglycaemic emergency compared to those with hypoglycaemic emergency [218]. Hyperglycaemia induced endothelial dysfunction is an underlying factor in a number of DM associated cardiovascular complications, including CLI and IHD, despite this the role of m6A remains completely unexplored. Here, I set out to gain an initial understanding into the effects of the diabetic environment on endothelial m6A and its

regulators. ***I hypothesise that the endothelial levels of m6A and the expression of its regulatory machinery are dysregulated in the diabetic and ischaemic environment.*** The aims of the studies described in this chapter are:

- To determine whether diabetes regulates m6A and its machinery in ECs exposed to hyperglycaemic and ischaemic mimicking conditions
- To investigate the expression of m6A's regulatory components in ECs extracted from ischaemic limb muscles of diabetic mice.
- To elucidate the relevance of METTL3 and other m6A regulators in total heart tissue and ECs from diabetic mice

4.2 Results

4.2.1 Optimization of Timepoints for Expressional Analysis of m6A Regulatory Components

Numerous studies have elucidated an association between m6A and its regulators and DM, however this association remains completely unexplored in the endothelial setting. Here, I set out to assess the impact of diabetics mimicking conditions on m6A RNA methylation and the expression of its regulators in ECs *in vitro* using either HUVEC or HCMECs.

Initial experiments exposed HUVEC to HG for 24, 48 or 72 hours to determine the optimum timepoint in which the regulatory components of the m6A machinery were affected by hyperglycaemic conditions. To mimic hyperglycaemia, cells were cultured under normal (NG, 5mM D-glucose) or high glucose (HG, 25mM D-glucose) for the indicated time points. L-glucose is an enantiomer of D-glucose and is not used as an energy source by cells as it cannot be phosphorylated by hexokinase. An osmotic control was thereby established by culturing ECs in medium containing 20mM L-glucose and 5mM D-glucose (OSC). Across the tested components, which include the writers METTL14, METTL3 and WTAP and the eraser FTO, only METTL3 showed a significant downregulation at 48 hours under HG treatment (figure 4.1A). Although FTO showed a trend towards an increase in expression, these changes were not significant (figure 4.1D). The expression of tested components is not affected by osmotic pressure (OSC). All further experiments were therefore performed at the 48-hour timepoint. The expressional analysis of the demethylase ALKBH5 was omitted from these studies due to overwhelming evidence indicating the expression profile and localisation of ALKBH5 to be predominately prevalent in the testis where it carries out a pivotal role in spermatogenesis [107, 108].

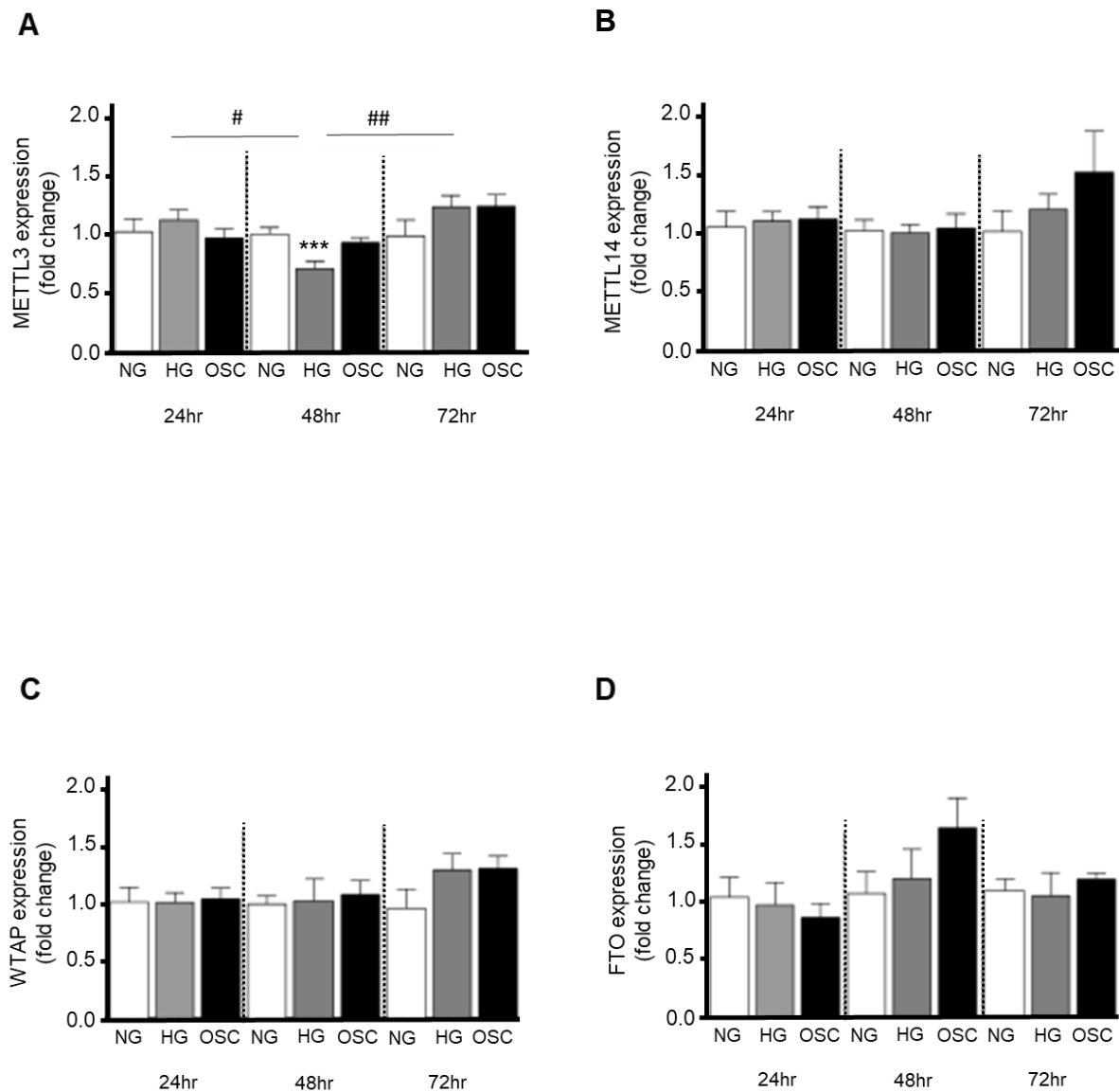


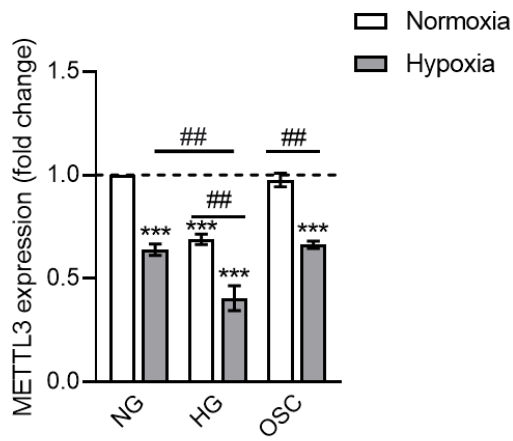
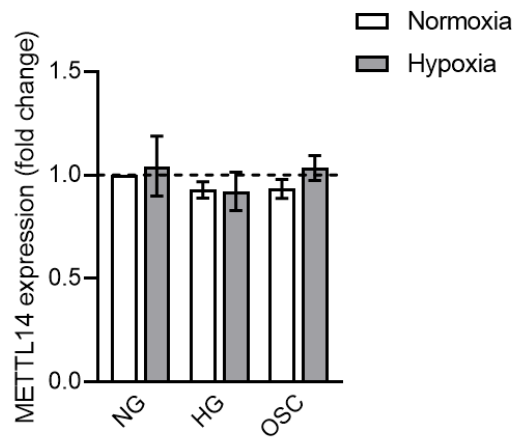
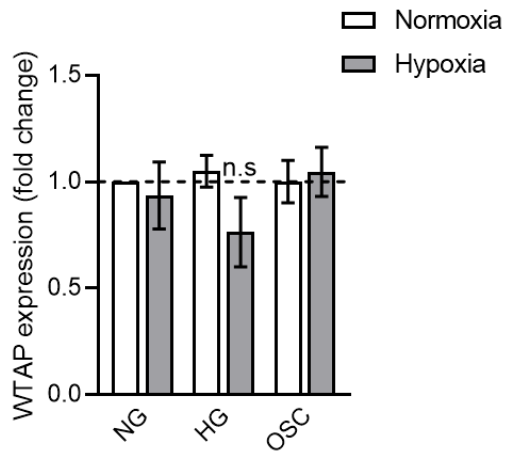
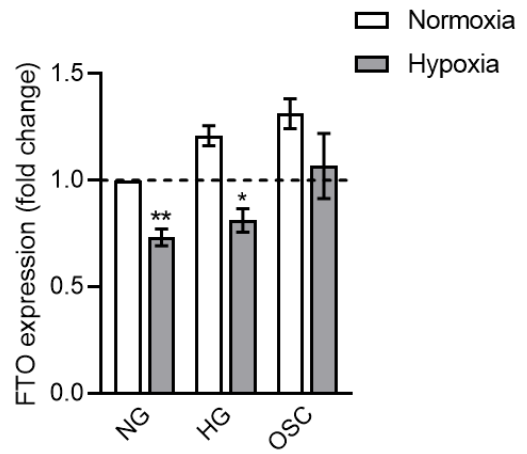
Figure 4.1 Establishing the optimal timepoint for the expressional analysis of m6A regulatory components in *in vitro* DM mimicking EC model. (A-D) HUVEC were cultured under normal glucose (NG) (concentration of 5mM D-glucose), high glucose (HG) (concentration of 25mM D-glucose) or under a concentration of 20mM L-glucose and 5mM D-glucose to establish an osmotic control (OSC) for 24, 48 and 72 hours. qRT-PCR was used for the expressional analysis of (A) METTL14, (B) METTL3, (C) WTAP and (D) FTO. 18s was used as the housekeeping gene (n= 6). Data are expressed as mean \pm SEM and one-way ANOVA with Turkey's multiple comparison test applied. *P<0.01 vs NG cells at 24 hours. HG at 48 hours #P<0.05 vs HG at 24 hours and ##P< 0.01 vs HG at 72 hours.**

4.2.2 METTL3 and Total m6A RNA Levels are Dysregulated by High Glucose and Hypoxia in ECs

In the more advanced stages of diabetes, the vascular endothelium is exposed to hyperglycaemia accompanied by oxygen deprivation. To gain an insight into the effects of this environment on the endothelial expression levels of the methyltransferase complex and total m6A RNA levels, HUVEC were cultured under HG or HG combined with hypoxia. To mimic hyperglycaemia, cells were cultured under normal (NG, 5mM D-glucose), high glucose (HG, 25mM D-glucose) or osmotic control conditions (20mM L-glucose and 5mM D-glucose). The ischaemic environment was modelled by culturing ECs in 1% O₂ for 48 hours. HUVEC cultured in NG under hypoxic conditions exhibited a significant down regulation of METTL3 expression. A more profound reduction in METTL3 mRNA levels was observed in HUVEC exposed to a combination of HG and hypoxia than those treated with HG alone (figure 4.2A). METTL14, a protein that acts as an RNA binding scaffold for METTL3, showed no changes in expression under HG or HG combined with hypoxia (figure 4.2B). While a decrease in WTAP mRNA levels were observed in HG and hypoxic conditions, this reduction was not of statistical significance (figure 4.2C). Contradictory to what we expected, expression of the m6A demethylase FTO was reduced under hypoxic conditions and in HG combined with hypoxia (figure 4.2D).

Similar studies were performed in HCMECs to gain an initial insight into m6A and METTL3 in the vasculature of the diabetic heart. In line with my data thus far, HCMECs exposed to hyperglycaemic conditions demonstrated a significant decrease in METTL3 expression (figure 4.2E). Interestingly and contrary to what was observed in HUVEC, FTO levels exhibited an increase in HCMECs cultured under HG (figure 4.2F).

I next explored the effects of hyperglycaemic conditions on the m6A RNA methylation status in both HUVEC (figure 4.2G) and HCMEC (figure 4.2H) by utilising a colorimetric based assay. Here, I demonstrate a significant reduction in m6A levels in both HUVECs and HCMECs.

A**B****C****D**

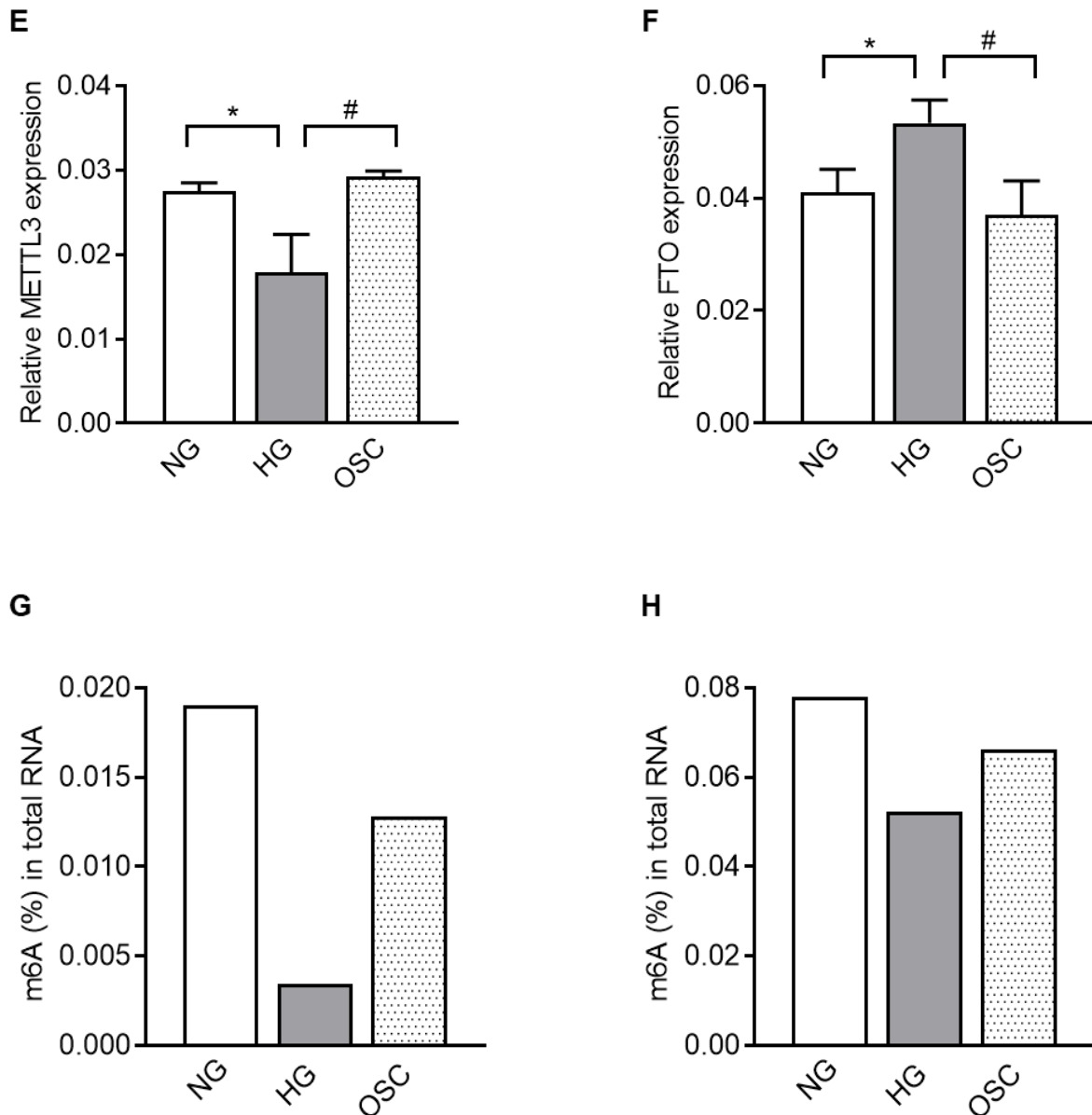


Figure 4.2 m6A and its regulators are dysregulated by high glucose and hypoxia in ECs. (A-D and G) HUVECs were cultured under normal glucose (NG) (concentration of 5mM D-glucose), high glucose (HG) (concentration of 25mM D-glucose) or under a concentration of 20mM L-glucose and 5mM D-glucose to establish an osmotic control (OSC) in the presence or absence of hypoxia (1% O₂) 48 hours. (E-F and H) HCMECs were cultured under NG, HG or OSC. qRT-PCR was used for the expressional analysis of (A and B) METTL3, (B) METTL14, (C) WTAP and (D and F) FTO. 18s was used as the housekeeping gene (n= 4). Colorimetric based m6A RNA Methylation Quantification Kit was used to assess m6A levels in (G) HUVEC and (H) HCMEC (n=1, performed in triplicates). All data are expressed as mean ± SEM. Results in (A-F) were assessed by two-way ANOVA with Tukey's multiple comparison test applied. *P<0.05, **P<0.01, ***P<0.01, n.s non-significant vs NG cells under normoxia (A-D) or NG (E-H) at 48 hours.

4.2.3 Expression of METTL3 in the Murine Model of Diabetic LI

Our lab is particularly interested in DM induced vascular damage in the context of CLI. I next set out to investigate whether endogenous endothelial METTL3 expression is regulated by DM and ischaemia utilising the murine hindlimb ischaemia model. Briefly, DM was induced in CD1 mice through the intraperitoneal injection of STZ for 5 consecutive days. STZ is a glucosamine-nitrosourea compound which exerts a toxic effect on pancreatic β cells, resulting in hypoinsulinemia and hyperglycaemia. Unilateral LI was then surgically induced through the occlusion of the femoral artery. Ischaemic and contralateral adductor muscles were harvested 3-days post-surgery from diabetic and control mice and ECs were separated using an immunomagnetic CD146 antibody (overview of experimental procedure in figure 4.3A).

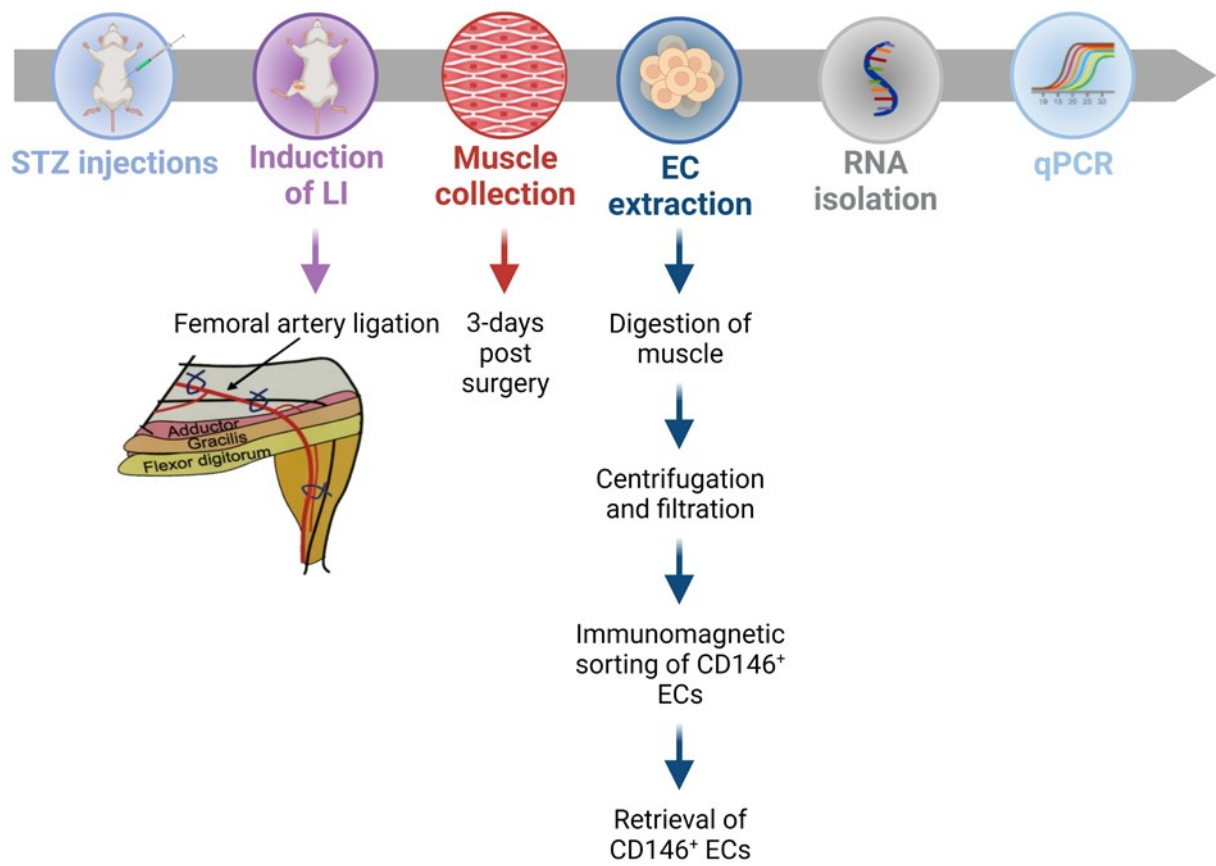
Endogenous METTL3 mRNA levels were measured in CD146+ ECs where no difference in expression was detected in ECs isolated from DM compared to non-DM contralateral adductor muscles. Moreover, no significant changes in METTL3 expression were observed in ECs from ischaemic limbs of non-DM mice in comparison with those from contralateral limbs. In line with our *in vitro* data, METTL3 expression was remarkably reduced in ischaemic ECs from DM mice compared to the control group, where a 50% decrease was observed. Interestingly, METTL3 expression in ischaemic and diabetic ECs were also significantly reduced when compared with non-DM ischaemic and diabetic contralateral ECs (figure 4.3B).

Endothelial analysis of WTAP revealed no changes in expression in cells isolated from DM and non-DM contralateral adductor muscles. WTAP expression is however reduced in ECs derived from ischaemic limb muscles of non-diabetic mice compared contralateral control muscles. Furthermore, WTAP expression in ischaemic and

diabetic ECs is profoundly reduced compared to contralateral limb derived ECs (figure 4.2C).

The expression levels of the m6A demethylases FTO and ALKBH5 were also analysed in this setting. No changes in FTO expression were observed in ECs derived from contralateral diabetic limbs compared to the contralateral controls. Additionally, no changes in FTO expression were observed in non-DM ischaemic limbs. FTO was significantly reduced in ECs isolated from ischaemic limbs of diabetic mice (figure 4.3D). Interestingly, ALKBH5 expression was found to be decreased in CD146+ ECs derived from limb muscles of diabetic mice compared to contralateral limbs. Further reductions in ALKBH5 expression were revealed in non-diabetic ischaemic adductor ECs and those derived from ischaemic muscles of diabetic mice (figure 4.3E).

A



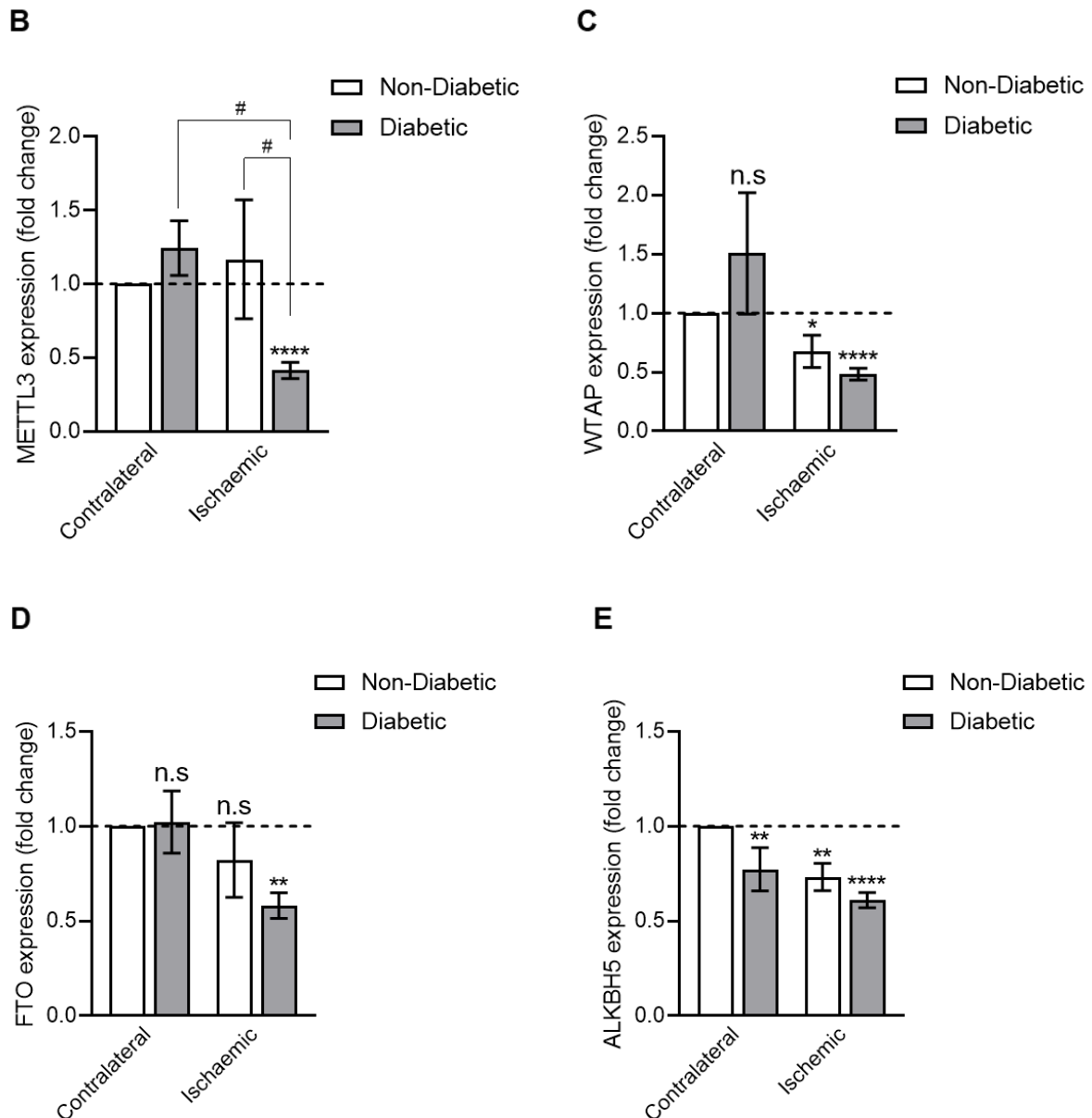
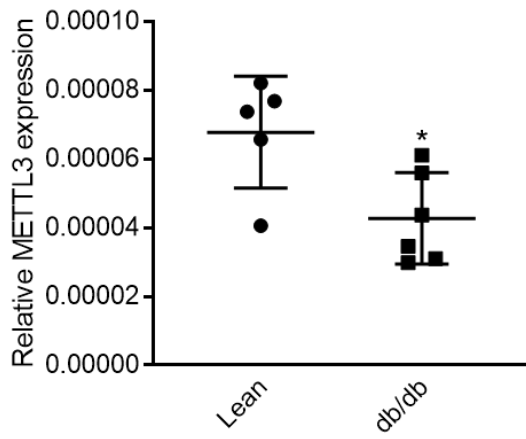
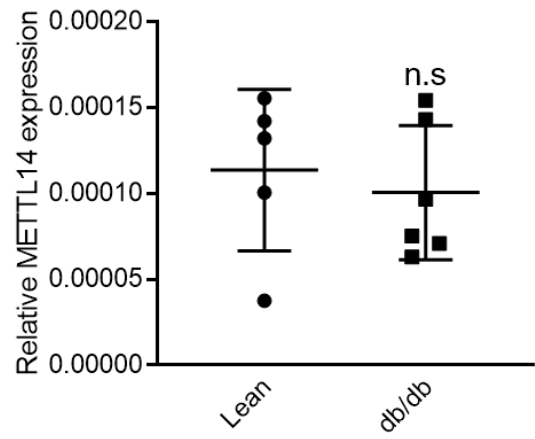
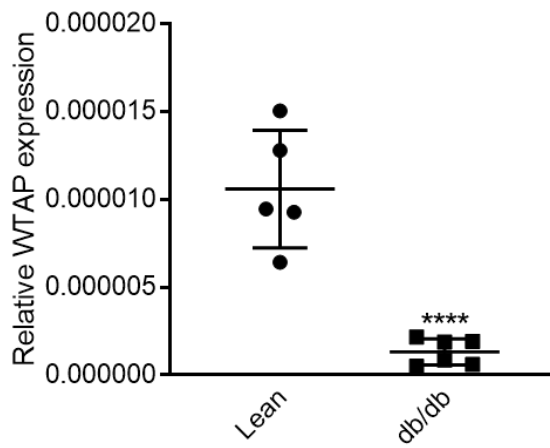
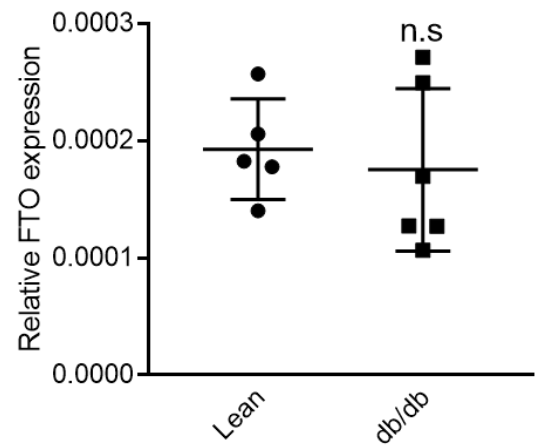
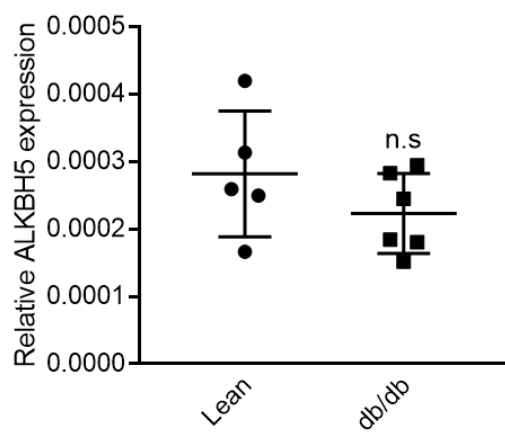


Figure 4.3 Expression of endogenous METTL3 is dysregulated in muscle-derived ECs after limb ischemia in diabetic mice LI. (A) Schematic demonstrating experimental workflow; mice received intraperitoneal injections of STZ (40mg/Kg in 0.05mol/L citrate buffer) for 5 consecutive days, glycaemia and glycosuria were measured 14 days after first STZ injection. Unilateral LI was induced, and ischemic and contralateral (control) adductor muscles collected from non-diabetic and diabetic mice 3 days post-surgery. CD146+ ECs were isolated from collected muscle samples and RNA was extracted. qPCR was used to quantify mRNA expression levels of (B) METTL3, (C) WTAP, (D) FTO, (E) ALKBH5. All graphical data presented as mean \pm SEM. Results were assessed by two-way ANOVA with Tukey's multiple comparison test applied. 18s was used as housekeeping gene. * $P < 0.05$, ** $P < 0.01$, *** $P < 0.01$, n.s non-significant vs cells derived from contralateral non-diabetic adductor muscles. Three mice pooled for $n = 1$. Total $n = 4$ per condition.

4.2.4 Expressional Analysis of m6A and its Regulatory Components in Diabetic Murine Hearts

Studies were performed to provide *in vivo* evidence into the relevance of the m6A modification in the setting of the diabetic heart. The *Leprdb/db* (*db/db*) mouse model is a commonly used murine model to study T2DM. These mice exhibit dysfunctional leptin receptor signalling, conferring susceptibility to obesity, insulin resistance and T2DM. *Db/db* mice develop hyperglycaemia at 6 weeks and microangiopathy from 16 weeks of age, leading to reduced myocardial microvascular density and tissue perfusion [219, 220]. qPCR analysis identified a reduction in the expression of METTL3 mRNA in left ventricular tissue isolated from hearts of 14-week-old *db/db* mice (figure 4.4A). METTL14 showed no significant change in mRNA levels while WTAP expression exhibited a profound decrease in this setting (figure 4.4B and C). Additionally, the demethylases FTO and ALKBH5 exhibited no significant changes in expression (figure 4.4D and E). Further expressional analysis was performed in ECs isolated from hearts of 9-week-old *db/db* mice where I show a reduction in the expression of METTL3 (figure 4.4F) while WTAP levels remained unchanged (figure 4.4G). Despite demonstrating a trend towards an increase in expression in a small sample size, no significant changes in FTO were observed (figure 4.4H). Moreover, analysis of m6A RNA methylation levels revealed a decrease in m6A in these ECs (figure 4.4I). These findings further demonstrate the potential importance of METTL3 mediated m6A in the diabetic cardiac vasculature.

A**B****C****D****E**

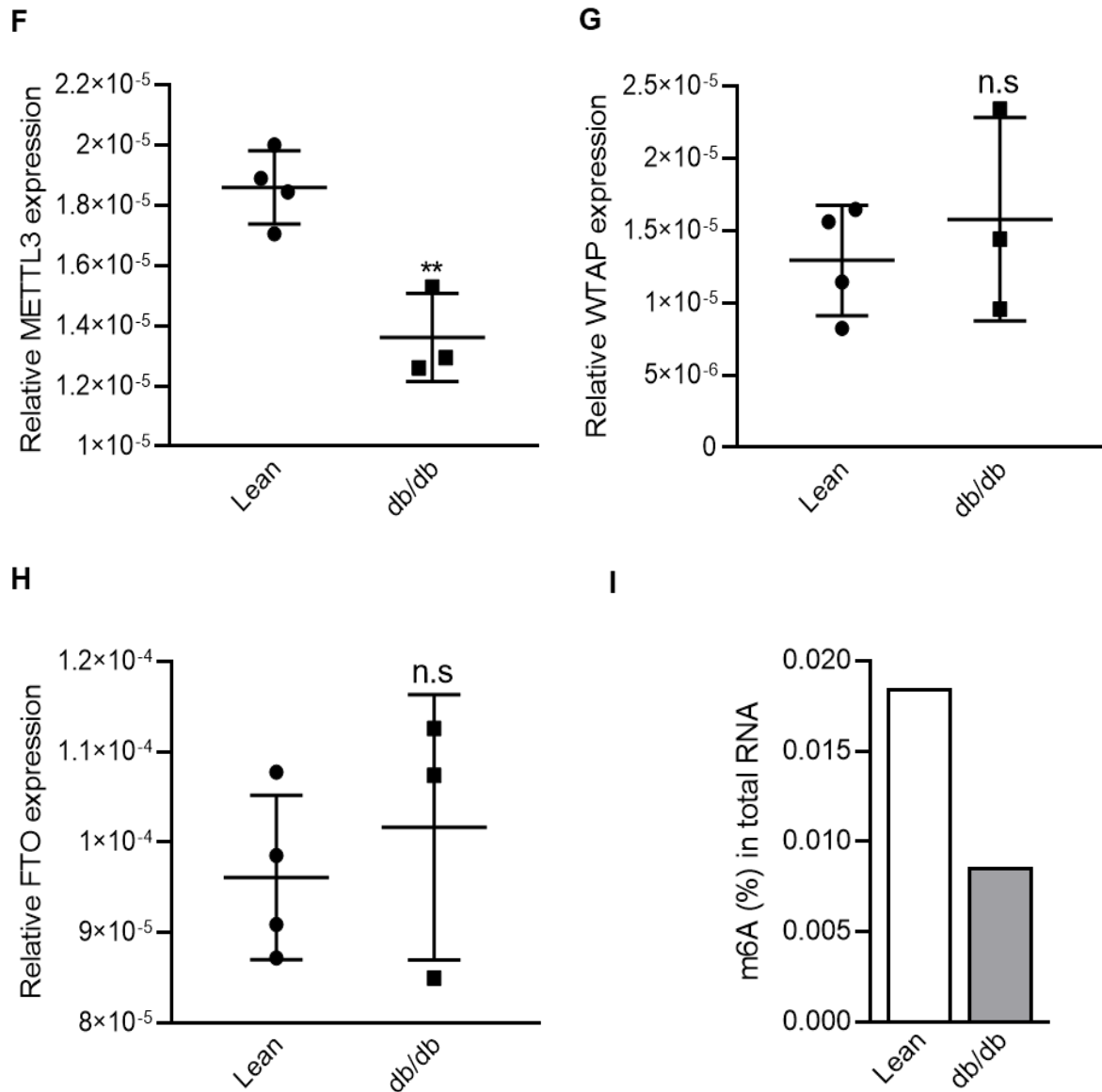


Figure 4.4 *In vivo* expressional analysis of m6A machinery. (A-C) qRT-PCR analysis of (A) METTL3, (B) METTL14, (C) WTAP, (D) FTO and (E) in whole hearts from 14-week-old db/db mice. (F) qRT-PCR analysis of METTL3, (G) WTAP and (H) FTO in ECs isolated from whole hearts of 9-week-old db/db mice. 18s was used as housekeeping gene. All graphical data presented as mean \pm SEM. Results were assessed by unpaired student t-test. *P<0.05, **P<0.01, ***P<0.01, n.s non-significant vs lean. (I) Colorimetric based m6A RNA Methylation Quantification Kit was used to assess m6A levels in ECs isolated from hearts of 9-week-old db/db mice, (N=1).

4.3 Discussion

Hyperglycaemic and hypoxic conditions that ECs are exposed to during DM are a direct causal factor of endothelial dysfunction, which in turn plays a dominant role in the development of debilitating cardiovascular complications. DM not only propagates vascular damage but also compromises native proangiogenic responses of the endothelium essential for tissue reperfusion following an ischaemic event. Having shown a clear role for METTL3 mediated m6A in the modulation of the angiogenic process (refer to Chapter 3) [168], the next step is to elucidate the effects of the diabetic milieu on endothelial m6A and its associated proteins. Although RNA methylation, in particular m6A is emerging as a new layer of gene expression regulation, its relevance in the context of diabetes associated vascular complications remains unexplored. The studies presented in this chapter utilised several *in vitro* and *in vivo* models of diabetes to analyse the global RNA deposition of m6A as well as the expression patterns of METTL3 and other components of the m6A machinery.

Large-scale clinical and epidemiological studies of DM patients suggest that the prolonged exposure to hyperglycaemia imprints a long-lasting effect on vascular cells. This progressively induces the development of vascular complications, which persist even following the achievement of glycaemic control. The same studies also demonstrated that effective glycaemic control could delay the onset of diabetic vascular complications [221, 222]. Regardless, both lines of evidence along with recent studies directly linking m6A to DM are compatible with an underlying implication of epitranscriptomic mechanisms. The RNA epitranscriptome is a complex system which ensures an additional layer of regulation beyond what is offered by primary sequences or secondary structures. The reversible deposition of the m6A marks and other forms of RNA modifications allows for rapid and dynamic responses to changes

in demand for protein synthesis and subsequent removal of transcripts. It is becoming apparent that this mode of gene regulation is of particular importance in harsh cellular environments, such as that imposed by hyperglycaemia and ischaemia.

Here, I provide the first evidence indicating a disruption of m6A levels in response to transient increases in glucose concentration in human vascular ECs (HUVEC and HCMEC). In line with this, our findings also indicate a dysregulation in endothelial m6A levels in the diabetic heart where I demonstrate a reduction in m6A in ECs derived from the left ventricles of db/db mice. These alterations to the m6A landscape would profoundly affect the processing of target transcripts and ultimately gene expression. Our findings are in agreement with previous research by Shen et al., which links DM to m6A dysregulation in RNA from peripheral blood of T2DM patients compared with healthy controls [193].

Additionally, the transcriptome wide analysis of m6A in human T2DM β -cells indicates a decrease in methylation levels in the mRNA transcripts of insulin/insulin-like growth factor 1 (IGF1)–AKT-pancreatic and duodenal homeobox 1 (PDX1), thereby resulting in impairment of cell-cycle progression and insulin secretion. This study also suggests that the m6A landscape more efficiently segregates human T2DM islets from controls than the transcriptome, further indicating that mRNA m6A modifications significantly contribute to the pathogenesis of T2DM [223]. It would indeed be of great interest for future studies to attempt the characterisation of the m6A methylome in diabetic ECs using MeRIP-seq. Defining the unique transcriptome-wide m6A distribution signatures in diabetic ECs would provide novel insights into the mechanistic functions of m6A in the setting of diabetes.

The data presented in this chapter also demonstrates a consistent disruption in the expression of the primary m6A methylase protein METTL3 across several *in vitro* and

in vivo models of diabetic vascular disease. I firstly show remarkable reductions in METTL3 expression in HUVEC and HCMECs cultured in high glucose to mimic hyperglycaemic conditions. I also demonstrate that hypoxic conditions alone are sufficient to deregulate METTL3 expression levels in human ECs. The effects of hypoxia were further confirmed in ECs cultured under osmotic control conditions where no changes in METTL3 expression were observed in ECs treated with L-glucose alone, while the incorporation of hypoxia significantly decreased the levels of METTL3. Additionally, I describe a more profound reduction in METTL3 expression when high glucose is combined with hypoxia to mimic a more advanced diabetic environment. This suggests a compounding effect and a further disruption in METTL3 and in turn m6A as the diabetic environment of the vasculature worsens. This is further supported by my data utilising the murine model of diabetic CLI. Here, I show that METTL3 is remarkably decreased in ECs isolated from ischaemic adductor muscles of diabetic mice while METTL3 levels remain unchanged in ECs derived from diabetic mice and those from ischaemic adductors of non-diabetic animals. Together, these data suggest that endogenous METTL3 mRNA expression in limb muscle ECs is decreased by the compounding effects of diabetes and ischaemia and that diabetes or limb ischaemia alone have no effect on the regulation of endothelial METTL3 expression at this timepoint. It would also be of great interest to study the m6A RNA methylation status in ischaemic and contralateral limb muscle ECs from non-diabetic and diabetic mice to determine whether this is in line with our METTL3 data. Despite pooling adductor muscles from three mice for each experiment, the number of extracted ECs remain low, resulting in an RNA yield which fell in the range of 12ng – 34ng/ul per sample. It was therefore not possible analyse the total m6A level in these samples, which would require a recommended amount of 200ng of total RNA per

reaction. These findings are also in agreement with unpublished pilot data from the Emanuelli lab which discerned a trend in METTL3 reduction in limb muscles of diabetic patients with CLI compared to non-diabetic or non-CLI patients undergoing saphenous vein stripping (Appendix 1). These unpublished data highlight the potential clinical relevance of METTL3. I had planned to further investigate the clinical importance of the m6A modification in the context of diabetic CLI through the analysis of METTL3 in RNA-sequencing studies and subsequent expressional analysis in addition to the assessment of the m6A methylation status in whole tissue and isolated ECs.

Our lab is also interested in DM induced vascular damage in the context of IHD. Initial *in vitro* studies in HCMECs revealed a significant downregulation in METTL3 expression in high glucose conditions. On the strength of these findings, I set out to investigate whether endogenous cardiac METTL3 is regulated by diabetes *in vivo*. The db/db murine model of T2DM leads to the development of hyperglycaemia at 6 weeks and microangiopathy from 16 weeks of age, leading to reduced myocardial microvascular density and tissue perfusion. Total heart tissue from 14-week-old db/db mice exhibited a decrease in METTL3 expression. These findings were further corroborated in ECs where I demonstrate a depletion in endogenous METTL3 as early as 9-weeks, only 3-weeks after the expected development of hyperglycaemia in this model. Importantly, these findings are in agreement with unpublished data from the Emanuelli lab where the RNA-seq analysis of LV biopsy samples confirm reduced METTL3 reduction in association with T2DM and ischaemic heart disease, thereby suggesting a clinical relevance of METTL3 in this context (Appendix 2). Taken together, these findings demonstrate a clear and consistent dysregulation in endothelial METTL3 associated with hyperglycaemic and ischaemic conditions across

several *in vitro* and *in vivo* models of DM, consistent with unpublished findings in a clinical context. It would be of particular importance for future studies to assess the levels of m6A and METTL3 expression in the infarcted myocardium. The experimental procedure would involve the induction of MI in diabetic mice, isolation of left ventricular ECs and subsequent expressional analysis of METTL3 and detection of m6A levels. The m6A mark has indeed been shown to be deregulated in cardiac tissue following MI induction in rats where Vasusort et al., observed an increase in m6A. The authors also considered m6A levels in peripheral blood samples of patients following an MI and found a significant decrease in patients who went on to develop heart failure compared to those who did not [224].

Although, to the best of our knowledge this is the first-time diabetes has been associated with perturbations in METTL3 levels in the vasculature, the direct involvement of METTL3 and its activity as an m6A methylase has indeed been shown to contribute towards the development of diabetes. A study by Wang and associates investigated the role of the m6A RNA modification in embryonic and early post-natal islet development [95]. Here, a mouse model in which METTL3/METTL14 is deleted in Ngn3⁺ endocrine progenitors was developed. These mice exhibited hyperglycaemia at 2-weeks of age and a decreased number and defected functional maturity of neonatal β -cells. RNA-seq and methylome analysis conducted in islets isolated from wildtype and METTL3/METTL14 KO mice suggests the depletion of the transcription factor MafA by modulating its transcript stability thereby impeding the functional maturity of β -cells. Additionally, m6A RNA methylation levels and METTL3 expression were consistently upregulated in liver tissue from T2DM patients. Hepatocyte specific METTL3 KO mice fed a high fat diet exhibited improved insulin sensitivity and reduced fatty acid synthesis, thereby averting obesity induced metabolic disorders.

Mechanistically, the deletion of METTL3 reduced the m6A methylation of fatty acid synthase and in turn its mRNA expression, thereby inhibiting fatty acid metabolism. Transcription inhibition assays also show that the RNA decay rates of fatty acid synthase transcripts increased with the overexpression of METTL3. These findings suggest that fatty acid synthase expression is regulated by METTL3 mediated m6A to regulate fatty acid metabolism and subsequent contribution to the progression of T2DM [225].

METTL3 functions in a complex composed of METTL14, WTAP and additional regulatory subunits while the alkylation repair homologs (ALKBH) proteins FTO and ALKBH5 reverse the deposition of the m6A mark. Although METTL3 is the primary focus of this thesis, this chapter also explored the endothelial expression of the additional methylases and demethylases under diabetic conditions in both *in vitro* and *in vivo* disease models to gain a more comprehensive understanding. Surprisingly, although a trend towards a decrease in METTL14 expression was observed in LV tissue of 14-week-old mice with T2DM, no significant changes in METTL14 expression were reported in any of the other disease models. Liu et al., investigated the relevance of the m6A modification in β -cell survival and function by generating a β -cell specific METTL14 KO mouse line [225]. Here, a crucial role for METTL14 was described in β -cell differentiation, survival and insulin production leading to glucose intolerance and T2DM. β -cells deficient of METTL14 exhibited increases cell death, aberrant differentiation, decreased cell mass and insulin secretion. RNA sequencing in islets indicated an increase in transcripts related to inflammation and cell death in METTL14 KO β -cells [225]. In a subsequent study, β -cell specific METTL14 KO mice exhibiting reduced m6A levels also mirror the islet phenotype in human T2DM with an early onset of diabetes due to reduced β -cell proliferation and insulin degranulation [223].

Although these studies link the methylase activities of METTL14 as a regulator of β -cells with a crucial role in the development of diabetes, our data suggests METTL14 cannot be implicated in the regulation of EC biology in the context of diabetes.

Data presented in this chapter also indicates that WTAP may play a specific role in DM induced CLI. In this context, I demonstrate a reduction in WTAP mRNA levels in ECs derived from ischaemic limb muscles of both diabetic and non-diabetic mice. This is indeed consistent with the unpublished CLI data from the Emanuelli lab which revealed a profound reduction in WTAP in limb muscles samples collected from diabetic patients with CLI (Appendix 1). Based on these findings, it would be interesting for future studies to explore the relevance of WTAP and its interaction with miRNAs in the context of diabetic CLI. This would allow for the elucidation of possible underlying mechanisms by which WTAP contributes to disease progression. Notably, a recent study investigated the expressional profile of several methyltransferases including METTL3, METTL14 and WTAP where they reveal an increase in their mRNA levels in T2DM patients, while METTL3, METTL14 and KIAA1429 were negatively correlated with m6A content. The authors of this study therefore suggest a possible regulatory mechanism that maintains the balance of adenosine and m6A in T2DM patients [218].

The demethylase protein FTO was the first m6A regulatory component to be directly linked to T2DM [193]. A follow up study by the same lab described a significantly higher increase in FTO in patients with T2DM and hyperglycaemic emergency compared to those with hypoglycaemic emergency [218]. High glucose treatments in HepG2 cells increased the expression of FTO, which induced the upregulation of key regulators of glucose and lipid metabolism including FOXO1, glucose-6-phosphatase catalytic subunit (G6PC) and diacylglycerol O-acyltransferase 2 (DGAT2). In line with

these findings, I also report a significant increase in FTO expression in HCMECs treated with HG and a trend towards an increase in both demethylase transcripts FTO and ALKBH5 in LV tissue from db/db mice. Interestingly I also report opposing effects in HUVECs exposed to hypoxic conditions. Here, FTO expression remains unchanged in HUVEC treated with HG, however FTO expression significantly decreases in those cultured under normal glucose and hypoxia and those treated under HG and hypoxia. These data indicate a hypoxia specific downregulation of FTO. To further support this, I report a decrease in FTO expression in ECs derived from ischaemic limb muscles of diabetic mice. In this setting, I also reveal a clear reduction in ALKBH5 in ECs derived from adductor muscles of diabetic mice, ischaemic muscles of non-diabetic mice and those of diabetic mice. It is becoming clear that, although the METTL3-containing methylase complex plays a ubiquitous role for the deposition of the m6A mark on RNA species, different ALKBH proteins have acquired some level of tissue specificity that remains to be fully understood, particularly in the diabetic cardiovascular system.

The m6A modification is part of a wider field of RNA epigenetics, a growing area of research that is only beginning to be explored in the context of diabetes and in the cardiovascular system. Similar to the deposition of epigenetic marks on DNA, methylation of RNA species can impact gene expressivity and define cell fates of subgroups of RNAs. This is particularly important for stress-response pathways required to react rapidly to environmental challenges, such as those involved in hyperglycaemia and ischaemia. The data presented in this chapter highlights the potential importance of METTL3 mediated m6A as a dynamic epigenetic mark that is disrupted by diabetes in ECs. Profiling the unique epitranscriptome of m6A in ECs under homeostatic and when exposed to hyperglycaemia and ischaemia mimicking conditions would provide a more comprehensive understanding of the mechanisms by

which the METTL3-m6A axis exerts its effects in the diabetic vasculature. More specifically and of particular interest to our lab, the use of the MeRIP-seq approach would be a practical method to decipher for the first time how diabetes affects m6A targeting of pri-miRNAs in ECs. It will also be imperative for future studies to corroborate the observed disruptions in METTL3 and other m6A regulators at a protein level. Furthermore, m6A recognition factors (or readers) have also been discovered and together with writers and erasers, contribute to the overall regulation of m6A-RNA biology. It would therefore be of interest to gain an understanding into their relevance in the context of diabetes-associated vascular complications.

Chapter 5

Effects of METTL3 Overexpression in CLI Post-ischaemic Neovascularization and Blood Flow Recovery

5. Effects of METTL3 Overexpression in CLI Post-ischaemic Neovascularization and Blood Flow Recovery

5.1 Introduction

PAD is caused by occlusive atherosclerosis in the lumen of peripheral arteries, with the lower extremity being the most common site for PAD [226]. The prevalence of PAD increases with age and affects an estimated 20% of individuals over 70 worldwide [227]. While it is projected that upwards of 200 million people suffer from PAD worldwide, most remain asymptomatic until the progression of typical manifestations of leg pain caused by an insufficient blood supply, known as intermittent claudication [228]. PAD is linked with risk factors including DM, aging, dyslipidaemia, smoking and hypertension. PAD is most prevalent in diabetic individuals due to associated metabolic alterations including rapid inflammatory progression, endothelial dysfunction and impairment of angiogenesis [229]. CLI represents the most severe manifestation of PAD, in which extreme tissue hypoperfusion results in chronic pain at rest, ischaemic ulcers or gangrene, a significant risk of limb loss and cardiovascular death in 20% of patients within the first year after diagnosis [192]. CLI is reported to have an annual incidence of 0.35% and an average prevalence of 1.33%, affecting 500-1000 per 1 million people in Europe and the United States [230]. CLI patients are classified following on internationally accepted consensus guidelines based on clinical criteria and hemodynamic parameters [231]. It is reported that 25-40% of patients face a risk of minor or major amputations and a mortality rate of 20% [192]. CLI patients suffer from a considerably diminished quality of life associated with a high dependence on caregivers, permanent local wound treatment, chronic use of pain relief medications and a negative impact on mental health [232].

The primary aims for current CLI therapies is to mitigate ischaemic pain and limb loss to improve wound healing, rate of survival and quality of life [233]. To achieve this, conjugational and less invasive approaches are desirable. Although not all CLI patients can be considered for conventional therapeutic approaches, these strategies can indeed be very beneficial for many patients. Surgical revascularisation strategies have been the dominant approach for CLI treatment with remarkable progress in techniques and devices applied in recent years. The two current methods to promote revascularisation of ischaemic tissues are bypass surgery and endoscopic third ventriculostomy (EVT, also referred to as balloon angioplasty). These surgical approaches are able to provide straight-line blood flow into the limb, improve wound healing and minimize the rate of amputation [234]. Despite this, the percentage of patients eligible for these treatments remains less than 45% and depends on various patient specific factors such as the distribution and progression of the arterial disease, anatomical lesions, presence of foot ulcers and infections, comorbidities and the patient's overall health status [235].

While surgical revascularisation remains the primary approach for CLI treatment, complementary non-invasive pharmacological approaches can improve the outcomes of CLI treatment following surgery or can be considered for non-eligible patients. Lipid lowering agents, primarily statins, are recommended as either initial treatments and in conjunction or alternatives to surgical approaches. Statins induce vasodilation by increasing the synthesis of NO, reduction of endothelin-1 synthesis and the hampering of vascular responses to angiotensin-2 [236]. Statin therapy can significantly reduce the incidence of further fatal and non-fatal cardiovascular events and improve the survival of patients who had undergone bypass graft surgery [237]. A relatively low number of clinical studies into the safety and efficacy of statin therapy in the setting

CLI raises concerns in regard to their therapeutic use. A study determining the predictors of the success of endovascular tibial artery interventions in patients with CLI found no correlation between limb salvage and statin-based therapies [238]. Prostanoids are also used as an alternative treatment for CLI patients in which surgical procedures have failed to reduce symptoms [239]. Despite their reported effectiveness in improvement of ulcer healing, pain relief and survival rates, studies also suggest a lack of long-term effectiveness and no changes in amputation or death rates [240-242]. Pharmacological agents with vasodilatory and antiplatelet aggregation properties are also used in combination with surgical procedures to minimise cardiovascular events, reduce the symptoms of CLI and increase pain free walking distance [192, 243, 244].

Limb amputations are a last resort when revascularisation strategies and medical therapies have failed to subdue severe ischaemic rest pain or tissue loss. In some instances, the progression of deep osteomyelitis and continued tissue damage due to unmanageable systemic infections may dictate the need for urgent amputation. Depending on the degree of amputation, these can be classified as minor or major. A minor amputation is defined as toe, metatarsal or transmetatarsal whereas major amputations are generally classified as above the ankle [245]. Minor amputations may form part of an overall limb salvage strategy where revascularisation surgery in tangent with minor amputations may preserve a patient's ambulatory status and overall quality of life. Generally, minor amputations do not limit functional dependence or require a prosthesis [234]. On the other hand, major amputations are associated with a significantly decreased quality of life, functional status and life expectancy with confounding factors such as DM playing an important role. A study by Jones et al., reported a mortality rate of 48.3% at one year and less than 30% of patients alive 3

years post-amputation with proximal amputations associated with a higher risk compared to more distal amputations [246]. Additionally, up to one-third of below the knee amputations may require further surgery or an above the knee amputation due to poor healing [247].

There is an urgent clinical need for the development of novel therapeutic strategies to locally promote angiogenesis and reperfusion for CLI patients who are not suitable for revascularisation [242]. In particular, the elucidation of several unknown aspects of DM associated CLI pathophysiology, such as genetic and epigenetic factors, SNPs or chemical modifications is an important step towards improved therapeutics. DM is not only a direct casual factor in the development of CLI but is also associated with the impairment of endogenous reperfusion accomplished by reparative neo-vascularisation following an ischaemic event. Angiogenesis is therefore a putative target for therapy, with significant efforts being made in the identification of novel regulatory pathways that may translate into new targets for treatment. The m6A RNA modification is emerging as a new determinant of fine-tuned gene expression regulation. Chapter 3 of this thesis provides evidence uncovering a novel role for METTL3-mediated m6A in the regulation of angiogenesis through the modulation of target miRNAs involved in angiogenesis. I also highlight a clear reduction in total m6A levels and METTL3 expression in diabetic and ischaemic human ECs, a downregulation in METTL3 levels in ECs derived from ischaemic murine limbs and those derived from LV tissue of db/db mice (chapter 4). ***On the strength of these evidence, I hypothesise that the exogenous supplementation of METTL3 via local gene transfer will improve post-ischaemic muscular neovascularisation and blood flow recovery in the mouse hindlimb ischaemia model.***

The aims of the work described in this chapter are to:

- Optimise the adenoviral concentration and ensure efficient delivery to limb muscle ECs
- Identify possible m6A-mediated mechanisms of impaired angiogenic responses in mouse LI model
- Explore the possibility of improving post-LI vascular repair and blood flow recovery by restoring METTL3 levels in ischaemic limb muscles

5.2 Results

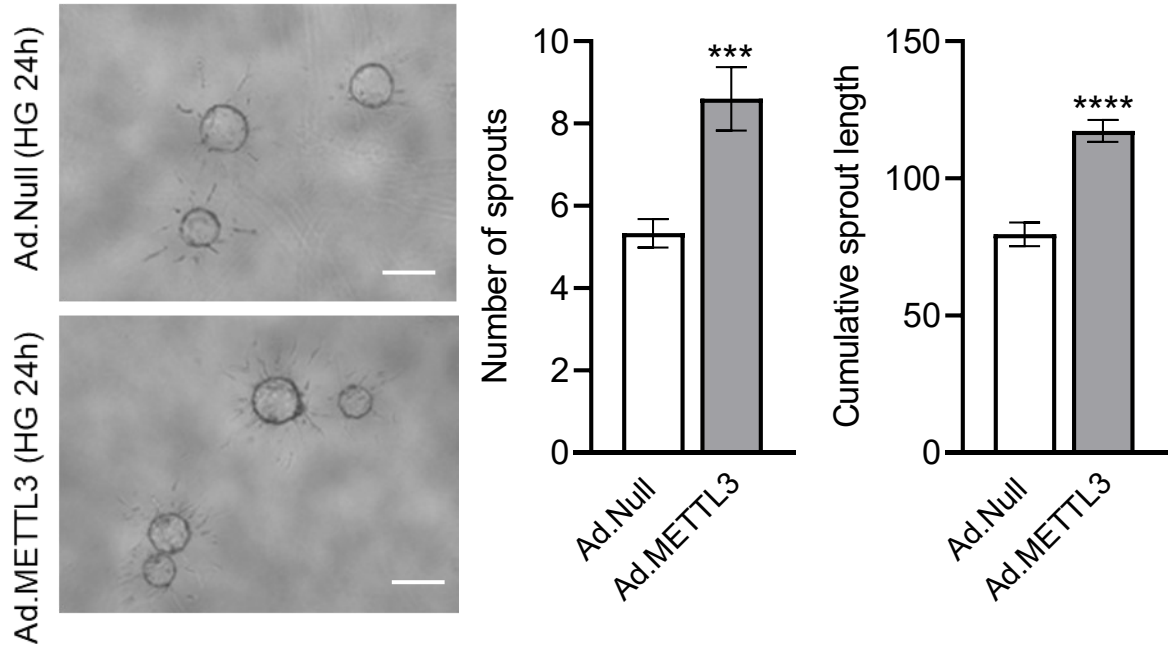
5.2.1 The Rescue of METTL3 Using Ad.METTL3 Improves Angiogenesis in Pathogenic Conditions *In Vitro*

Chapter 3 of this thesis provides novel evidence of METTL3 mediated regulation of angiogenesis, while chapter 4 highlights a clear dysregulation of endothelial METTL3 as a result of diabetes and ischaemia in several *in vitro* and *in vivo* models of CLI. Here, I aim to investigate whether the adenoviral (Ad-) mediated supplementation of METTL3 can restore the angiogenic capacity of human ECs cultured under *in vitro* disease conditions. These studies will provide insights into the potential of METTL3 in rescuing the impaired angiogenic phenotype of “diabetic ECs”, while providing an early proof of concept for further *in vivo* interventional studies investigating the therapeutic potential of METTL3 in the setting of diabetic CLI and MI (outlined in chapters 5 and 6 respectively).

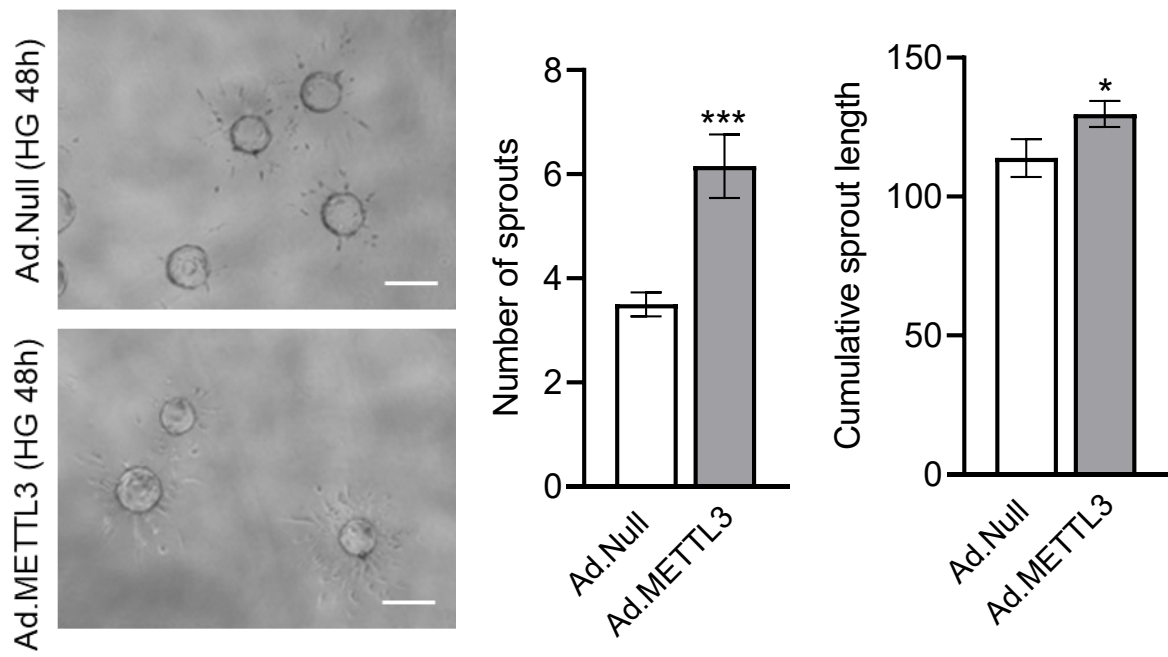
To this aim, HCMECs infected with 50 MOI of adenoviral particles carrying human METTL3 (Ad.METTL3) or control adenoviral particles (Ad.Null) were cultured under hyperglycaemic conditions (HG, 25mM D-glucose) for 24 or 48-hours. A fibrin bead assay was then performed where the number of sprouts and cumulative sprout length were quantified to assess the early stage angiogenic capacity of these cells. The overexpression of METTL3 resulted in an increase in the number of EC sprouts and sprout length formation compared to Ad.Null infected cells at both 24 and 48-hours of HG treatment (figure 5.1A and B). Next, HCMECs infected with Ad.METTL3 or Ad.Null were cultured under HG combined with hypoxia (1% O₂) for 48-hours. An *in vitro* Matrigel assay was then performed where the “diabetic and ischaemic” ECs were allowed to form a network of tubes for a period of 6-hours, after which several key angiogenic parameters were quantified. Here, I observed an increase in the number

of junctions, meshes, branches and an overall improvement in network formation in the Ad.METTL3 compared to the Ad.Null infected ECs (figure 5.1C).

A



B



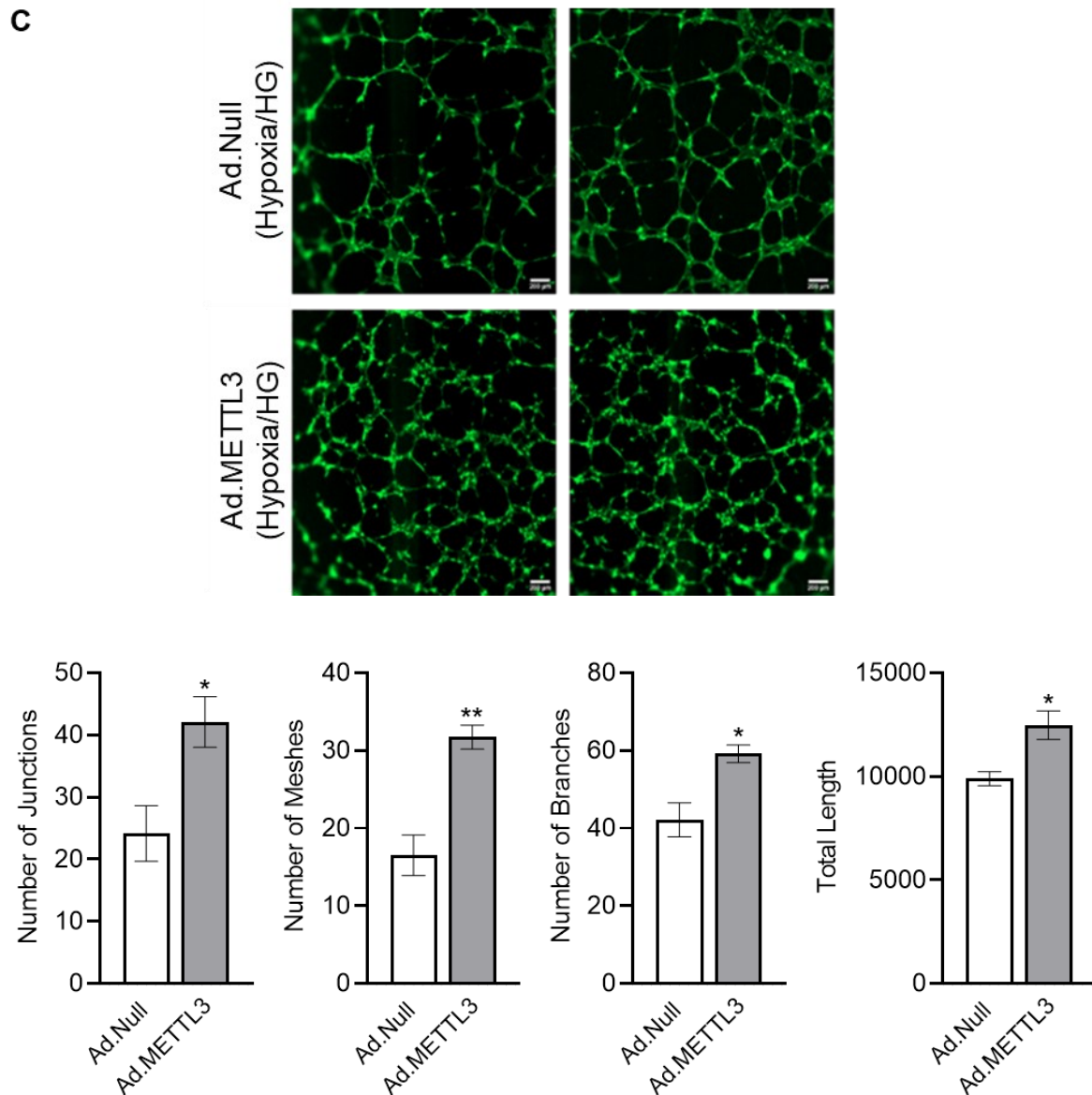


Figure 5.1 METTL3 overexpression rescues the impaired angiogenic phenotype of “diabetic ECs *in vitro*.” (A-C) HCMEC were infected with 50 MOI Ad.Null or Ad.METTL3 for 48 hours. (A-B) Representative microscopy images of HCMEC bead spheres used for fibrin bead assay (4x magnification, scale bar 50µm). HCMECs were treated with high glucose (HG) (25mM D-glucose) for (A) 24 or (B) 48 hours and allowed to undergo morphogenesis for 48 hours. Quantification of angiogenesis was performed through the analysis of number of sprouts and cumulative sprout length (n=1, 10 beads analysed per experiment). (C) Representative microscopy images of cord formation assay (4x magnification, scale bar 50µm) (n=3). HCMEC were cultured under a combination of HG and hypoxic conditions (1% O₂). Angiogenesis was quantified by analysing the number of junctions, number of meshes, number of branches and total network length after 6 hours. All data are expressed as mean ± SEM and assessed by unpaired Student’s t-test. *P<0.05, **P<0.01, *P<0.01, n.s non-significant vs cells transfected with Ad.Null.**

5.2.2 Optimization of Adenoviral Concentration for the Delivery of METTL3 to Ischaemic Limb Muscles

Future experiments described in this chapter will adopt a strategy where m6A is re-established by adenoviral mediated human METTL3 gene transfer to the ischaemic limb muscles of non-diabetic and diabetic mice. To evaluate the optimal concentration of Ad.METTL3 for these experiments, non-diabetic mice were injected with Ad.METTL3 at concentrations of 10^8 or 5×10^8 PFU directly into the adductor muscles at 3 equidistant points along the projection of the femoral artery. Adductor muscles were collected three days after injections and RNA was extracted from total muscle. RT-qPCR was utilised to assess human METTL3 overexpression levels following treatments with each viral concentration (experimental procedure outlined in figure 5.2A). Following treatment with Ad.METTL3 at a PFU of 10^8 , I observed a 7-fold increase in the expression of human METTL3, whereas the treatment with a higher concentration of 5×10^8 PFU resulted in a 25-fold increase (figure 5.2B). I next explored the efficiency of the different viral concentrations in modulating the total m6A methylation status in limb muscles. Interestingly, I observed a trend in which the muscles injected with the lower concentration of Ad.METTL3 (10^8 PFU) exhibited comparatively higher levels of m6A RNA methylation (figure 5.2C). However, it is important to note that this difference did not reach statistical significance. All further studies were therefore performed using a viral concentration of 10^8 PFU.

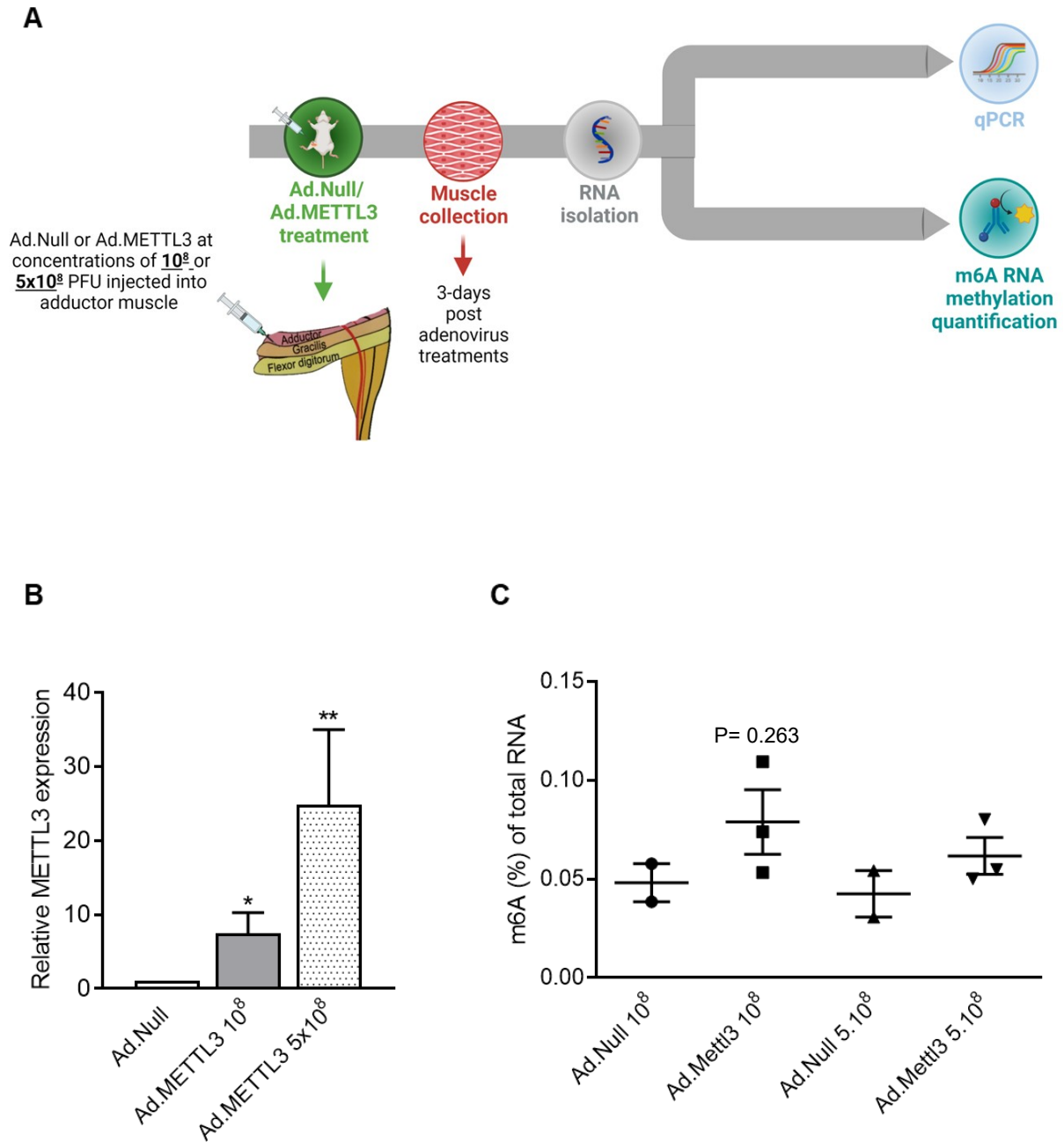


Figure 5.2 Optimization of adenoviral concentration for the delivery of METTL3 to ischaemic limb muscles. (A) Schematic demonstrating experimental workflow; mice received Ad.METTL3 injections in adductor muscles at a PFU of 10^8 or at 5×10^8 . Muscles were collected 3 days post-surgical induction of LI; ischemic adductor muscles were collected and the expression of human METTL3 was assessed by (B) qRT-PCR. 18s was used as the housekeeping gene ($n = 3$). (C) Colorimetric based m6A RNA Methylation Quantification Kit was used to assess m6A levels in whole ischemic adductor muscles. Results in were assessed by two-way ANOVA with Tukey's multiple comparison test applied. * $P < 0.05$, ** $P < 0.01$, n.s non-significant vs Ad.Null 10^8 and Ad.Null 5×10^8 .

5.2.3 *In Vivo* Validation of Adenovirus Mediated METTL3 Overexpression in Ischaemic Limb Muscle ECs

I next set out to validate the efficiency of the adenovirus mediated METTL3 gene transfer by analysing the human METTL3 expression levels and m6A RNA methylation in limb muscle ECs. Briefly, non-diabetic mice were induced with unilateral LI through the occlusion of the femoral artery. Immediately after surgery, animals were randomized to receive either Ad.METTL3 or Ad.Null injections in the ischaemic adductor muscle at the optimised concentration of 10^8 PFU. Ischaemic and adductor muscles were harvested 3 days post-femoral artery ligation and ECs were isolated and separated using CD146+ MicroBeads (refer to figure 5.3A for overview of experimental procedure). The expression of human METTL3 mRNA was assessed by RT-qPCR where a 10-fold increase was observed in ischaemic limb ECs injected with Ad.METTL3 compared to those injected with Ad.Null (figure 5.3B). The overexpression of human METTL3 also resulted in a significant increase in total RNA m6A levels in ischaemic limb ECs compared to those treated with Ad.Null (figure 5.3C). Finally, qRT-PCR analysis of endogenous METTL3 expression from Ad.METTL3 or Ad.Null treated ischaemic adductor muscles was performed (figure 5.3D). These studies reveal no significant changes in endogenous Mettl3 levels, indicating that our treatments are able to overexpress human METTL3 while causing in no detectable changes in native Mettl3 levels, thereby suggesting that the observed increase in m6A RNA methylation are indeed a result of exogenous METTL3.

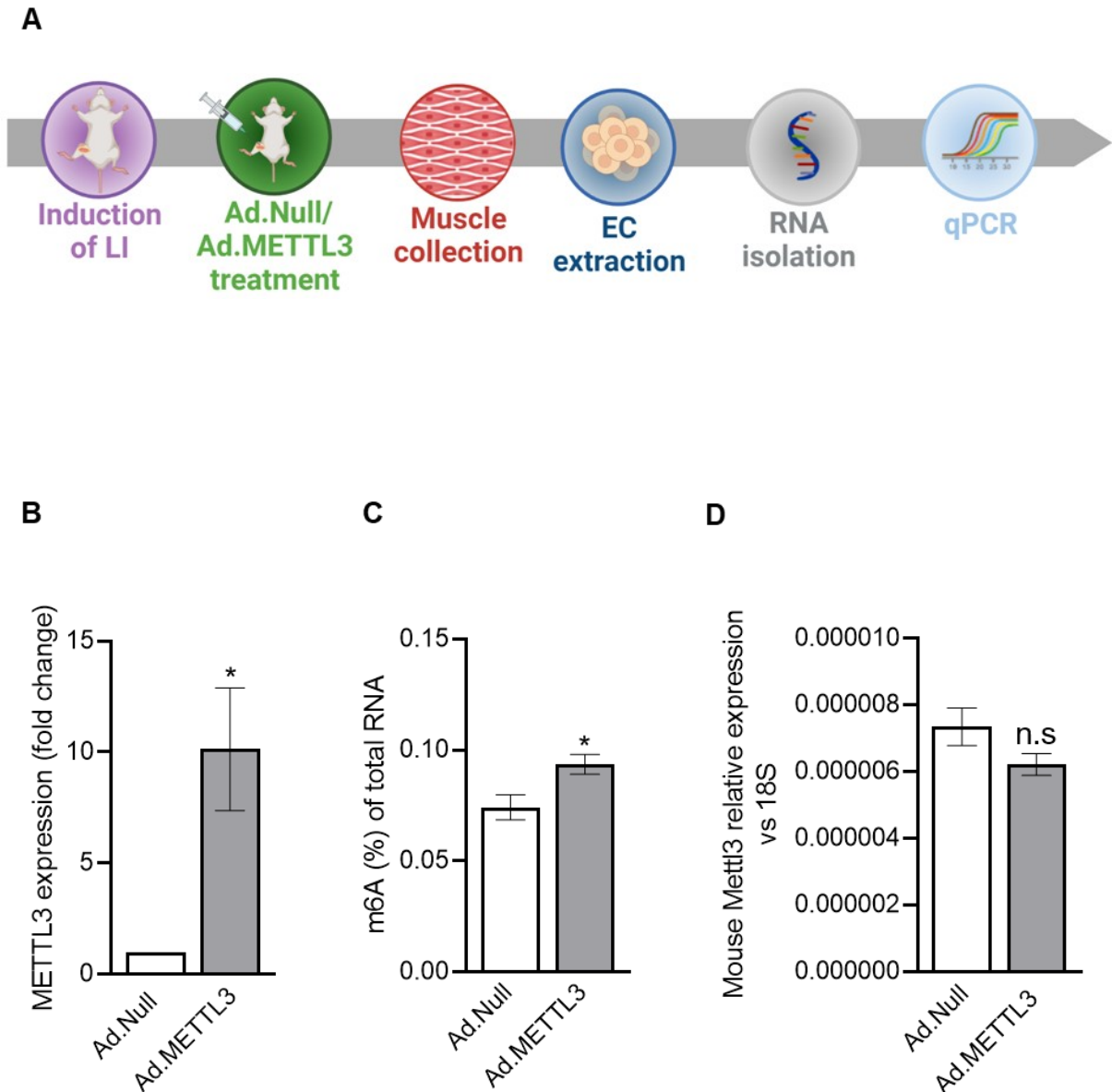
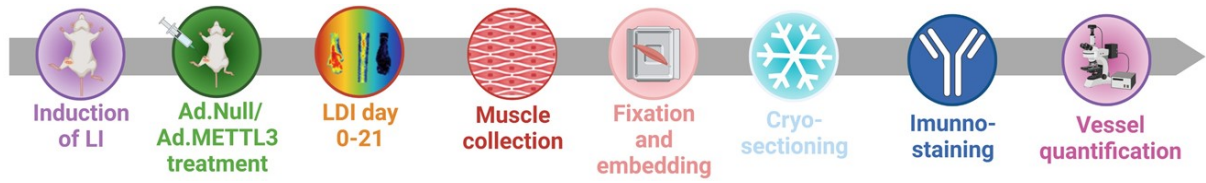
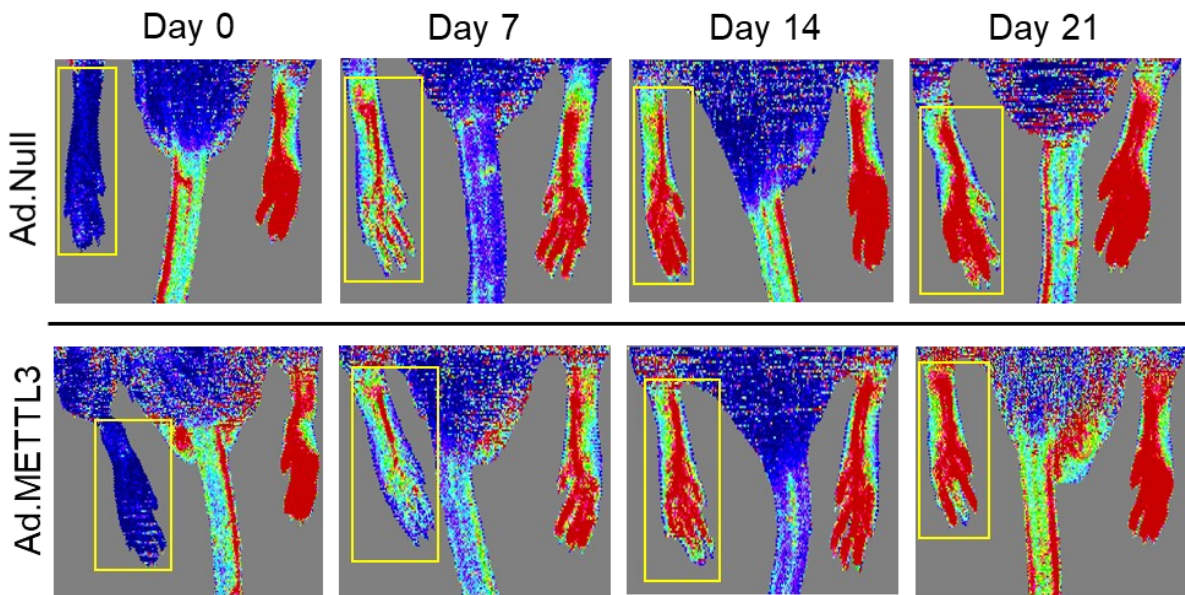
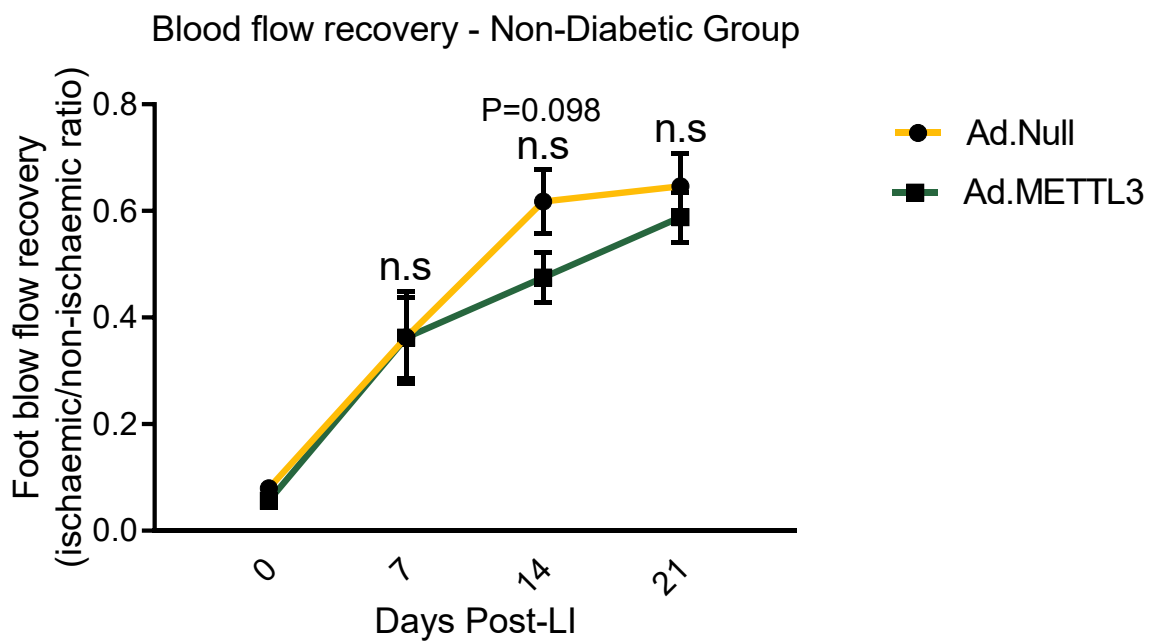


Figure 5.3 Validation of human METTL3 overexpression in mouse muscle-derived ECs. (A) Schematic demonstrating experimental workflow; limb ischemia was surgically induced in male CD1 mice, immediately after ligation, the mice were randomized to receive either Ad.METTL3 or Ad.Null injections (10^8 plaque-forming units [PFU]/mouse) into the adductor muscles. 3 days post-surgery, muscles were collected, CD146+ ECs were isolated, and RNA was extracted. qRT-PCR was used for the expressional analysis of (B) human METTL3 and (D) endogenous Mettl3. 18s was used as the housekeeping gene (C) Colorimetric based m6A RNA Methylation Quantification Kit was used to assess m6A levels in muscle derived CD146+ endothelial cells. Adductor muscles from three mice were pooled for n=1, 12 mice used in total to gain n=4. Results were assessed by unpaired student t-test. * $P < 0.05$, ** $P < 0.01$, *** $P < 0.001$, n.s non-significant vs Ad.Null.

5.2.4 Effects of METTL3 Overexpression on Post-LI Blood Flow Recovery

I next investigated the therapeutic potential of Ad.METTL3 in the mouse hindlimb ischaemia model by studying the effects of METTL3 replacement on post-ischaemic blood flow (BF) recovery in ischaemic limbs of non-diabetic and diabetic mice. Briefly, hindlimb ischaemia was induced in cohorts of non-diabetic and diabetic mice followed by Ad.Null or Ad.METTL3 injections directly into the adductor muscles along the projection of the femoral artery. Limb BF was measured by colour Laser Doppler Imaging (LDI) immediately after surgery to confirm successful ligation of the femoral artery and at 7-, 14- and 21-days to monitor the gradual reperfusion of the limb post-ischaemia (overview experimental procedure is provided in figure 5.4A). LDI uses a low power Helium-Neon laser to scan living tissue where moving blood cells give rise to Doppler shifts in the reflected light. These are recorded and converted into perfusion values as the magnitude and frequency distribution of the Doppler-shifted light is directly proportional to perfusion of the upper 200-300 μ m of the skin. In our studies, the region of interest (ROI) was precisely confined to the plantar sole in order to limit the influence of fur, skin pigmentation and motion artifacts. Tissue perfusion was quantified relative to the non-ligated contralateral limb. Interestingly, I reveal no improvements in post-ischaemic BF recovery in limbs treated with Ad.METTL3 compared to Ad.Null in both non-diabetic and diabetic cohorts, as shown in colour-coded doppler images (figures 5.4B and D) and line graphs demonstrating the time course of post-ischaemic BF recovery (figures 5.4C and E).

A**B****C**

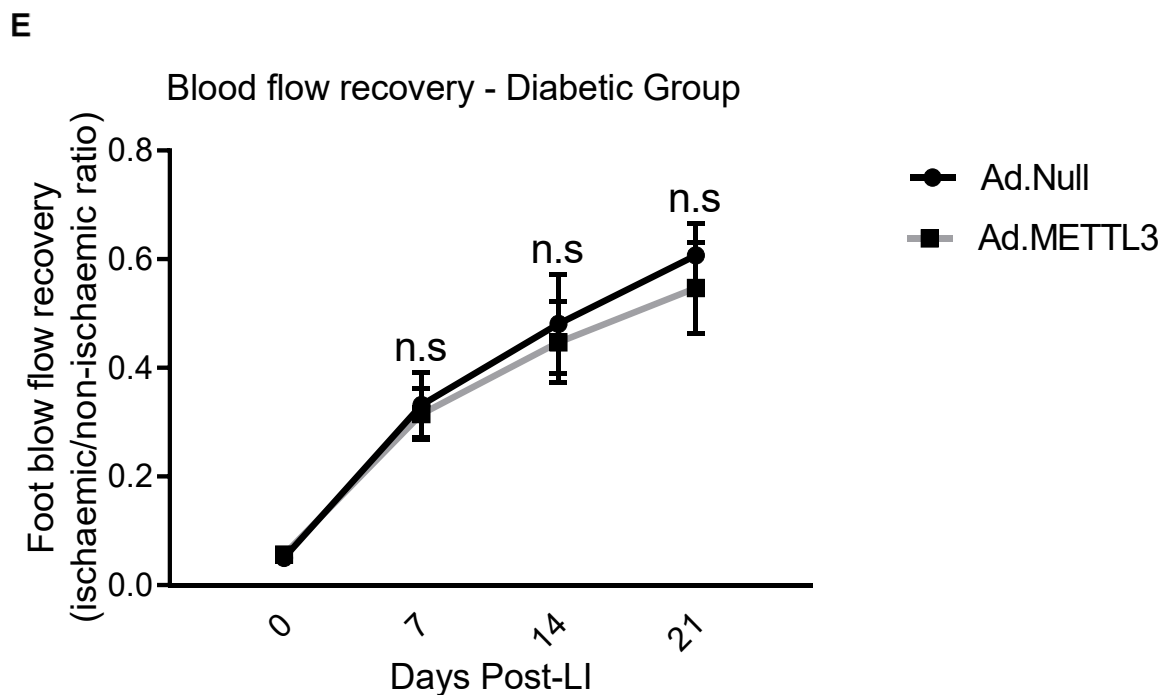
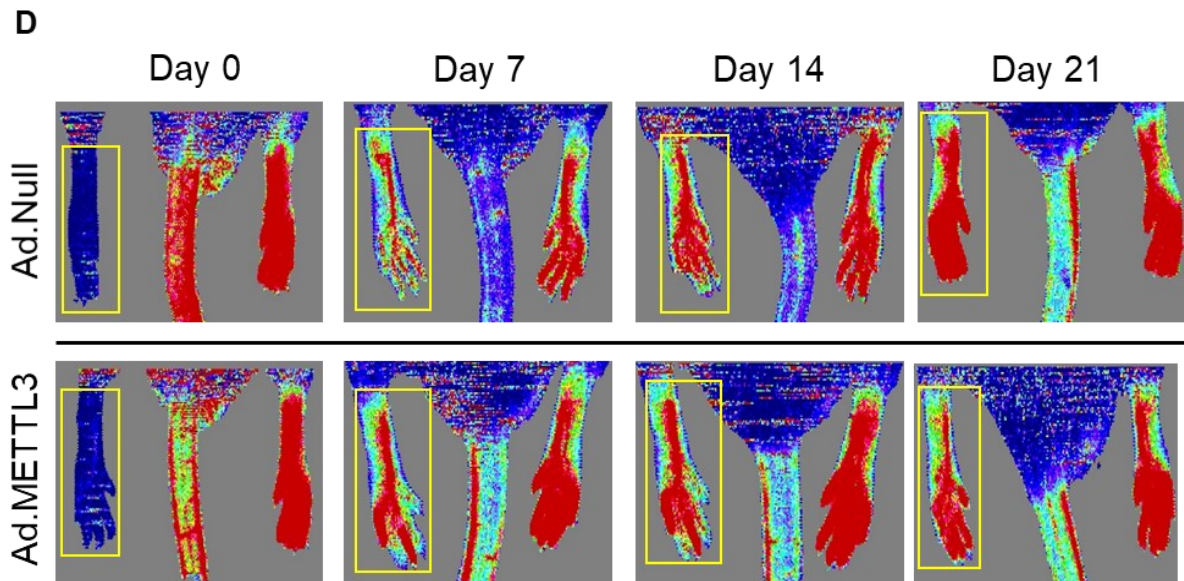


Figure 5.4 Effects of METTL3 overexpression on post-LI blood flow recovery. (A) Schematic demonstrating experimental workflow; limb ischemia was surgically induced in male non-diabetic or diabetic CD1 mice by occlusion of the left femoral artery. Immediately after ligation, mice were randomized to receive either Ad.METTL3 or Ad.Null injections into adductor muscle (10^8 plaque-forming units [PFU]/mouse). (B and D) representative colour laser Doppler images of (B) non-diabetic and (D) diabetic cohorts taken at days 0, 7, 14, and 21 post-ischemia. Yellow frames show the analysed region of interest on ischemic foot. (C and E) Line graph shows the time course of post-ischemic blood flow recovery (calculated as the ratio between ischemic foot and contralateral foot BF) in (C) Non-diabetic and (E) diabetic cohorts injected with Ad.Null or Ad.METTL3. Data are presented as mean \pm SEM. Results were assessed by Mann-Whitney test. * $p < 0.05$, ** $p < 0.01$ versus time-matched Ad.Null condition (n=12 mice per group).

5.2.5 Ad.METTL3 Treatments Improve Post-LI Neovascularisation

To understand the relevance of the METTL3 mediated m6A modification in post-ischaemic neovascularisation, non-DM and DM cohorts of mice were sacrificed at day 21 post-LI induction and the adductor muscle was collected and processed for immunohistochemical analysis of capillary and arteriole densities (refer to figure 5.4A for experimental overview). The capillaries were visualized by immunofluorescent staining with a fluorochrome-coupled isolectin B4 to stain ECs and the capillary density was assessed relative to the area of muscle fibres per high power field area. The local delivery of Ad.METTL3 improved reparative angiogenic responses in the ischaemic limb muscles of both non-DM and DM cohorts of mice as demonstrated by 36.3% and 48.8% increases in capillary densities of each respective group (figures 5.5A and C). I have previously described the impact of METTL3 on the functional capacity of let-7e and the miR-17-92 cluster in ECs through the modulation of Tsp1. Tsp1 is a matricellular protein with well-characterised angiostatic properties which plays a deleterious role in CLI (refer to Chapter 3, section 3.2.4) [168, 248]. In order to gain preliminary mechanistic insights into the observed increase in angiogenesis, Tsp1 expression was assessed in ischaemic limb muscles where I observe a reduction at an mRNA level in Ad.METTL3 compared to Ad.Null treated muscles was observed (figure 5.5E).

Arterioles were visualised by immunolabelling of α -smooth muscle actin (α -SMA) as a marker of VSMCs that line the tunica media of arterioles. Surprisingly, I report a significant decrease of small arteriole density (lumen diameter <20 μ m) in ischaemic limb muscles receiving post-LI Ad.METTL3 compared to Ad.Null treatments (figure 5.5B and D).

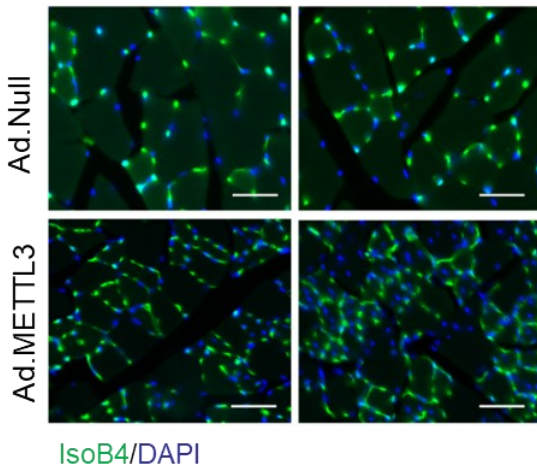
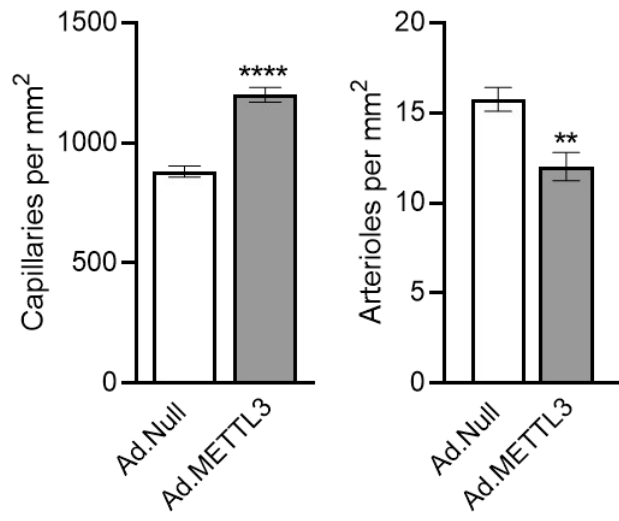
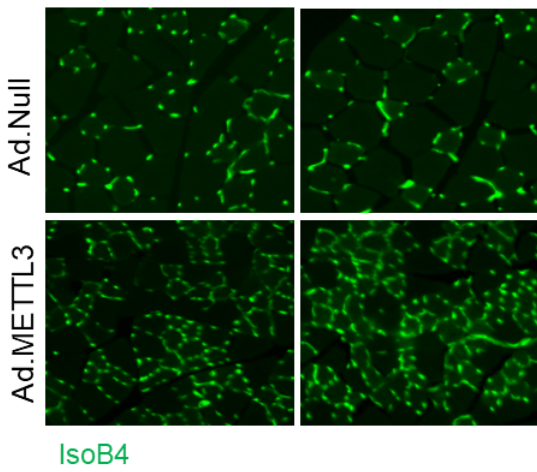
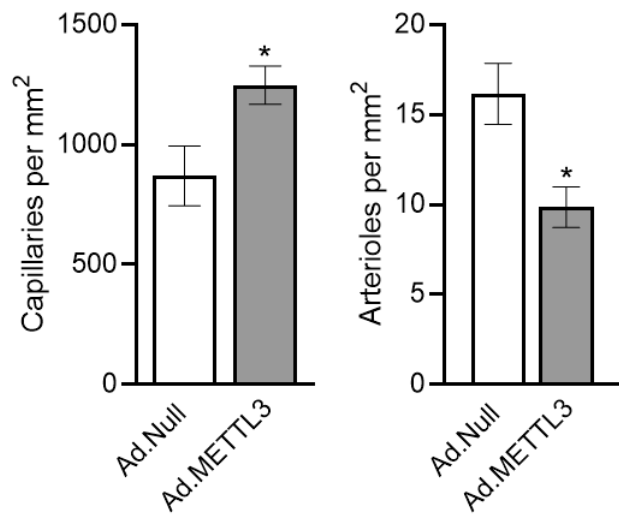
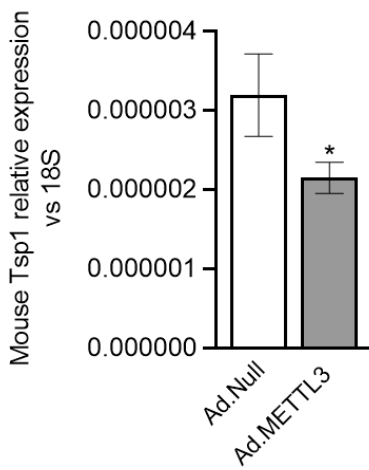
A**B****C****D****E**

Figure 5.5 METTL3 overexpression improves post-ischaemic angiogenesis.

Limb ischemia was surgically induced in male non-diabetic or diabetic CD1 mice by occlusion of the left femoral artery. Immediately after ligation, mice were randomized to receive either Ad.METTL3 or Ad.Null injections into adductor muscle (10^8 plaque-forming units [PFU]/mouse).

Grafts from Ad.METTL3 or Ad.Null ischemic adductor muscles were isolated 21 days after surgery. **(A and C)** Representative microscopy images showing vascular density in **(A)** non-diabetic and **(C)** diabetic groups ($\times 40$ magnification, scale bar 50 μm). Angiogenesis was quantified as isolectin-B4 (IsoB4) positive structures. Cell nuclei in **(A)** were counterstained with DAPI (4',6-diamidino-2-phenylindole). (n= 8 mice in non-DM and n=4 in DM group). **(B and D)** Immunohistological analysis of showing arteriolar density in non-diabetic and diabetic mice injected with Ad.METTL3 or Ad.Null (n = 8 or 4 mice per group, respectively) after limb ischemia, assessed by immunolabelling of α -smooth muscle actin (α SMA) as a marker of VSMCs. Arterioles were quantified according to vessel diameter ($< 20 \mu\text{m}$). **(E)** Tsp1 expression in ischemic adductor muscles, 21 days after limb ischemia surgery and injection with either Ad.METTL3 or Ad.Null, was assessed at mRNA by RT-PCR. Results were normalized to 18S (n=8 in each group). Data presented as mean \pm SEM. Results were assessed by unpaired student t-test. *P<0.05, **P<0.01, ***P<0.01, n.s non-significant vs Ad.Null.

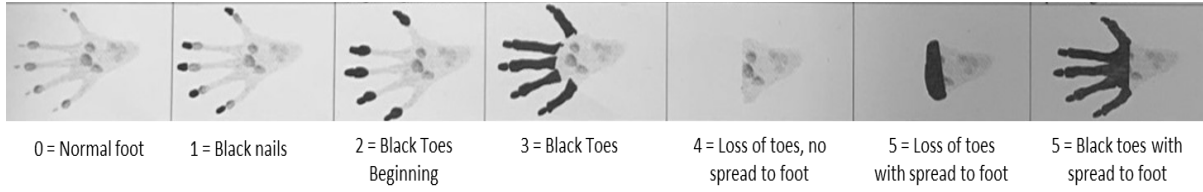
5.2.6 Effects of METTL3 Overexpression on Toe Survival

In the clinical setting, atrophic lower limb muscles show attenuated proangiogenic and regenerative signals and upregulate anabolic and survival pathways, impairing angiogenesis and tissue regeneration [249]. This can lead to ischaemic ulcers, toe necrosis and gangrene, thereby posing a significant risk of limb loss and cardiovascular death. I analysed post-LI toe necrosis as a marker of ischaemia severity to gain preliminary insights into the clinical outcomes of METTL3 replacement. Each animal was closely monitored daily from day 1 to day 7 then at 14- and 21-days post-LI. A score-based system implemented in the Prof. Paolo Madeddu lab (host lab for these experiments) was used to assess the post-operative appearance, clinical signs, unprovoked behaviour, and behavioural responses to external stimuli of both non-DM and DM groups of mice. Foot damage was assigned a score between 0-5 based on visual observations of toe necrosis where 0=normal or unchanged foot, 1= appearance of black nails, 2= appearance of necrotic tissue limited to phalanges bone, 3= necrotic tissue engulfing the metatarsal bone, 4= loss of toes without spread to foot, 5= loss of toes with spread to foot or necrosis spreading to entire foot (refer to figure 5.6A for scoring schematic).

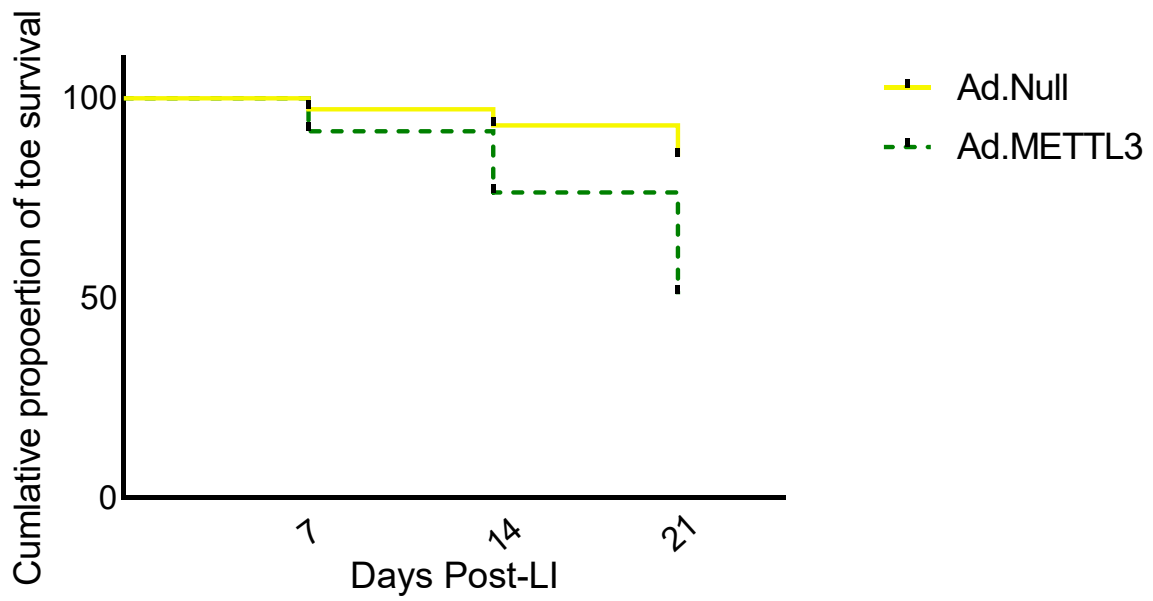
The cumulative proportion of toe survival at 7, 14, and 21 days after the induction of LI was calculated, excluding mice that showed symptoms of femoral nerve damage. Here, I reveal that Ad.METTL3 treatments worsened toe survival in both cohorts of mice, with a more severe outcome observed in diabetic mice (figures 5.6B and D). To extrapolate more information from the raw necrosis scoring data, each animal's scores was plotted as parts of a whole and Ad.METTL3 was compared to Ad.Null for each respective timepoint (7-,14- and 21-days) using a Wilcoxon signed-rank test. Tissue damage was significantly worse in Ad.METTL3 compared to Ad.Null treated ischaemic

limbs at days 7, 14 and 21 with the severity of damage increasing overtime in both non-DM and DM groups (figure 5.6C and E). Hyperglycaemia is known to significantly worsen ischaemic tissue damage and delay cutaneous wound healing; this is indeed highlighted when the DM and non-DM cohorts of mice are compared where I report significantly worse necrotic scores in each corresponding treatment group and timepoint.

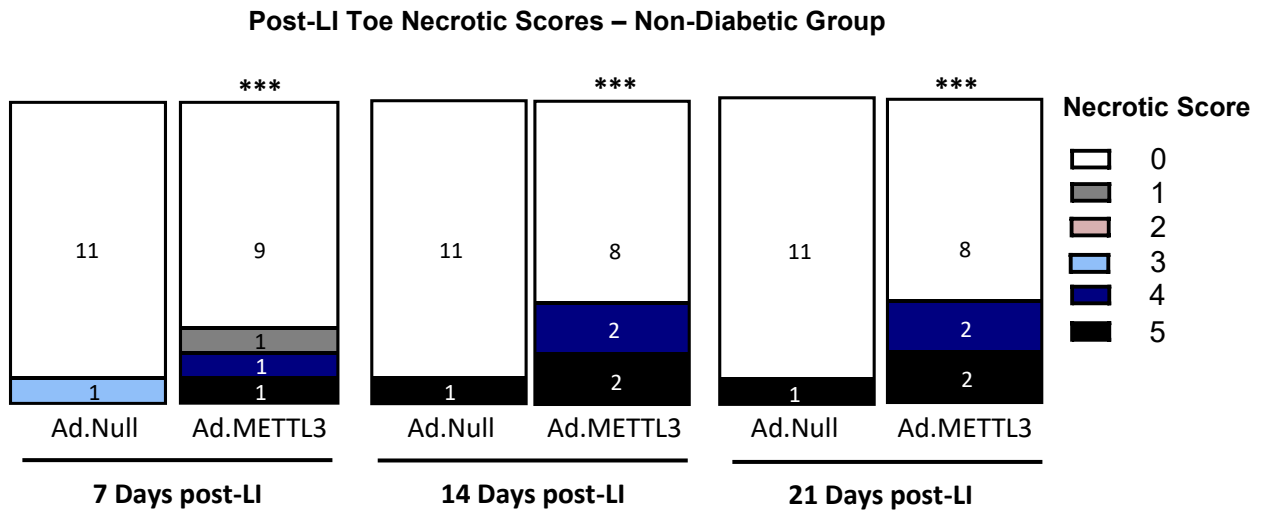
A



B



C



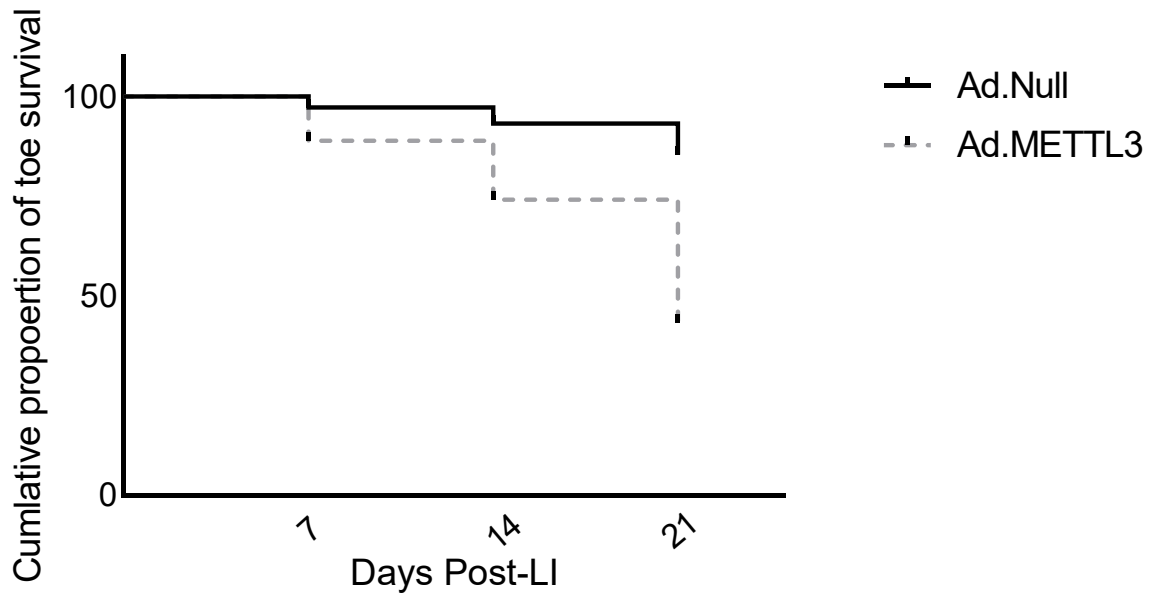
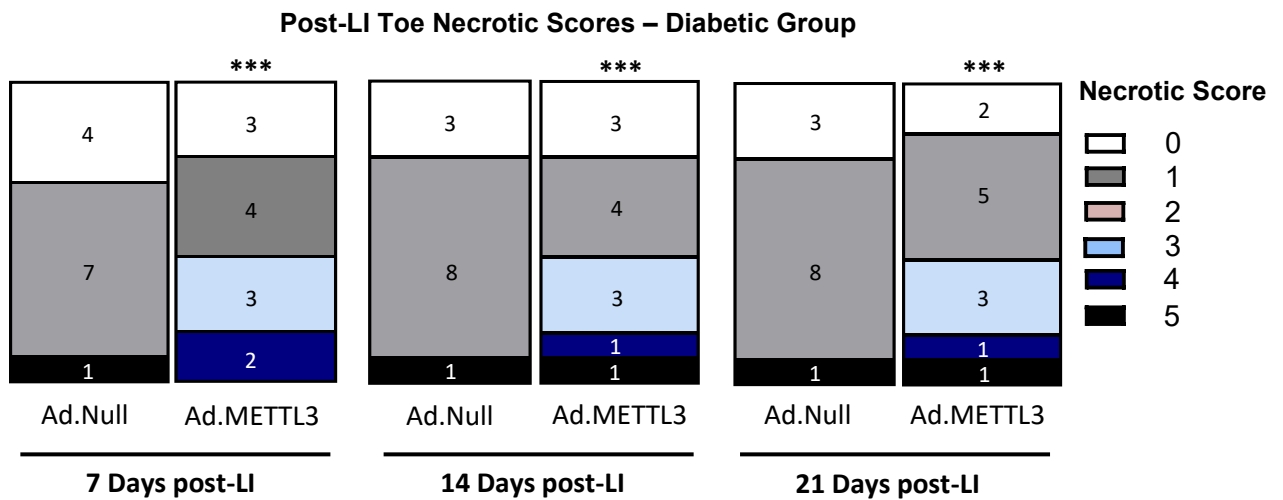
D**E**

Figure 5.6 Effects of METTL3 overexpression on toe survival . Limb ischemia was surgically induced in male non-diabetic or diabetic CD1 mice by occlusion of the left femoral artery. Immediately after ligation, mice were randomized to receive either Ad.METTL3 or Ad.Null injections into adductor muscle (10^8 plaque-forming units [PFU]/mouse). Post-operative toe necrosis was analysed using a visual score-based system outlined in (A). (B and D) Cumulative proportion of toe survival over 21 days of follow-up after ischemia in (B) non-diabetic and (D) diabetic mice injected with Ad.Null or Ad.METTL3, $p = 0.0013$, log rank test. (C and E) Post-LI toe necrotic scores presented as parts of a whole and analysed using Wilcoxon test versus time-matched Ad.Null. Data are presented as mean \pm SEM. All data are presented as mean \pm SEM. (n=12 mice per group).

5.3 Discussion

The mechanisms that lead to diabetic CLI involve a complex interplay of vascular dysfunction, inflammation, and skeletal muscle impairment. The induction and orchestration of new blood vessels is critical for tissue repair in response to injury in CLI. DM induces microangiopathy through the propagation of EC damage while concurrently compromising native reparative responses essential for tissue reperfusion in ischaemic limbs. Insufficient angiogenesis with limited infiltration of inflammatory cells and poor supply of oxygen and nutrients in wound space has an important role in the impaired wound healing process exhibited by CLI patients. DM associated vascular defects therefore contribute to worse clinical outcomes of PAD in diabetics. Evidence presented in chapter 3 of this thesis describes a crucial role of METTL3 in EC function and angiogenesis by modulating the biogenesis of let-7e and the miR-17-92 cluster [168]. Additionally, chapter 4 describes the dysregulation of m6A and METTL3 in diabetic HUVEC and HCMEC and ischaemic limb muscle derived ECs from diabetic mice. Preliminary data by the Emanuelli lab also suggests a reduction of METTL3 in limb muscle samples collected from diabetic patients with CLI (Appendix 1). Thus, this chapter explored the therapeutic modulation of METTL3 as a novel approach for controlling angiogenic responses in the setting of CLI.

In vitro studies were performed on human ECs cultured under hyperglycaemic and ischaemic conditions indicate that the restoration of METTL3 rescues the angiogenic phenotype of diabetic ECs – thus providing an early proof of concept for further *in vivo* interventional studies. To gain an insight into the relevance of the m6A modification in post-LI neovascularisation and BF recovery, I employed a gene therapy approach based on the adenovirus mediated local delivery of Ad.METTL3 in ischaemic muscles. Initial studies aimed to determine the optimal viral concentration for the

overexpression of human METTL3 and the validity of this approach in the delivery of Ad.METTL3 to skeletal muscle ECs. Significant increases in human METTL3 expression were observed following injections with Ad.METTL3 at both 10^8 and 5×10^8 PFU. Additionally, although both viral concentrations showed trends towards an increase in total m6A methylation, higher levels were observed in muscles treated with the lower concentration of Ad.METTL3 (10^8 PFU). This data suggests that while the higher concentration of Ad.METTL3 results in a greater over expression of METTL3, treatment with the lower viral concentration exhibits a higher functional effect. The Ad.METTL3 virus at a concentration of 10^8 PFU was therefore utilised for all further studies.

The evidence presented thus far led us to infer that the supplementation of METTL3 in the setting of CLI would positively impact BF recovery and capillary and arteriole densities, thereby improving LI clinical endpoints. My studies utilising the murine hindlimb ischaemia model reveal a significant improvement in angiogenic revascularization in ischaemic limb muscles overexpressing METTL3, in both non-diabetic and diabetic cohorts. Further investigations involving the transcriptome wide profiling of m6A in diabetic ECs would allow for the elucidation of underlying pathways by which METTL3 promotes neovascularisation. Having demonstrated a role for METTL3 in the regulation of the miR-17-92 cluster of angiogenic miRNAs, it would indeed be of great interest to validate the m6A-miRNAs axis in the context of CLI. Several miRNAs have been identified to regulate the recovery of blood flow following femoral artery ligation. Most relevant to my study, the miR-92a component of the miR-17-92 cluster was shown to increase in ischaemic limb muscles of mice, while its inhibition improved blood flow recovery through the targeting of integrin $\alpha 5$ [250]. A second study revealed that the EC-specific depletion of the miR-17-92 cluster

increased post-LI revascularisation and reperfusion through the repression of WNT-related receptors FZD4 and/or LRP6 [204]. Martello et al., also describe an increase in vascularisation and a reduction in muscle necrosis and apoptosis of ECs following the local administration of miR-26b mimics in ischaemic murine limbs [251]. Additionally, the use of anti-miR-223 and miR-223 knockout mice also improved post-LI reparative angiogenesis. Mechanistically, miR-223 was shown to directly target β 1 integrin which in turn affects the phosphorylation of VEGFR2, FGFR1 and the downstream adaptor protein Akt [252].

Preliminary mechanistic insights into the post-LI proangiogenic role of METTL3 were also provided where I describe a reduction in the angiostatic factor Tsp1 in ischaemic limbs overexpressing METTL3. This is consistent with the data presented in chapter 3 outlining the impact of METTL3 on the functional capacity of let-7e and the miR-17-92 cluster in ECs through the modulation of Tsp1. Interestingly, Tsp1 has been reported to play a deleterious role in CLI and is highly expressed in ischaemic tissue of CLI patients [248, 253]. Tsp-1^{-/-} mice exhibit increased clinical and histological protection from tissue necrosis induced by LI. Tissue protection was associated with a shift in infiltrating macrophages towards a less pro-inflammatory phenotype, increased post-LI angiogenesis, and muscle regeneration [248].

Despite demonstrating that the rescue of METTL3 expression promotes revascularisation, quantification of tissue perfusion relative to the non-ligated contralateral limb revealed no improvements in post-ischaemic blood flow recovery. These findings suggest that the newly formed blood vessels in the Ad.METTL3 treated groups are unable to efficiently deliver blood to the ischaemic limb. Interestingly, during the muscle collection step of these experiments, I regularly observed microhaemorrhages characteristic of a dysregulated vasculature in the ischaemic

adductor muscles of the Ad.METTL3 treated mice. It is therefore plausible that this treatment may indeed promote revascularisation, however the blood vessels formed maybe dysfunctional due to impaired maturation, vascular instability and increased permeability. Although these findings may seem contradictory to previously presented data (section 3.2.6) were an *in vivo* Matrigel experiment revealed a higher percentage of perfused vessels in Ad.METTL3 compared to Ad.Null infected plugs, this discrepancy can be attributed to fundamental differences in the adopted *in vivo* models [168]. The *in vivo* Matrigel assay aims to recapitulate physiological angiogenesis in exogenous cells that form a capillary-like network within the plug which integrates with the endogenous vasculature of host immunodeficient mice. This approach does not account for EC interactions with local cell types, the harsh hyperglycaemic and ischaemic environment and systemic factors such inflammatory responses. Additionally, although these studies reveal a higher percentage of perfused vessels in Ad.METTL3 plugs, they do not provide insights into the integrity of the capillary-like structures, which would be indicated by the proportion of the perfused biotinylated isolectin B4 that remained confined within the newly formed vessels. To evaluate the possibility that Ad.METTL3 treatments result in the formation of unstable or leaky vessels, future studies can adopt a strategy where vascular permeability is measured in an *in vivo* Matrigel plug using two different sized dextran tracers. The lower molecular weight tetramethylrhodamine (TRITC)-dextran would be fully contained within the capillary-like structures and colocalized with the larger molecular weight Fluorescein isothiocyanate (FITC)-tracer in stable and nonleaky vessels [254].

In the peripheral more than in the coronary circulation, arteriogenesis needs to complement angiogenesis for the development of collaterals able to bypass arterial obstructions and ensure reperfusion of the most distal parts of the limb [255]. In the

process of exerting a beneficial effect on angiogenesis, our findings indicate Ad.METTL3 treatments may be exerting a deleterious effect on arteriogenesis, as shown by a decrease in post-LI arteriole density. Although validation experiments demonstrate an overexpression of human METTL3 in ECs isolated from Ad.METTL3 treated ischaemic muscles, the adenovirus utilised does not specifically target ECs and we essentially would not know the proportion of ECs infected. Additionally, while I have elucidated the relevance of METTL3 in the modulation of EC functions, the impact of altering the methylation status of other local cell types is yet to be understood. Arteriogenesis requires precise and temporal coordination of various cell types and cellular processes. Initial EC activation and mobilisation by pro-arteriogenic signals is followed by a complex cascade involving local myocyte signalling, proliferation, migration and attachment of pericytes and VSMCs and monocyte recruitment. Our approach in overexpressing METTL3 may lead to unspecific alterations in the m6A methylome of 100's of transcripts, some of which inevitably contributing to key processes in various cell types conducive to arteriole formation. Previous research has indeed linked METTL3 mediated m6A to vascular smooth muscle cell differentiation [256].

Keeping in mind that the intent of our therapeutic intervention is to mediate angiogenesis through the vascular endothelium, we established a collaboration with Dr Graciela Sala-Newby (University of Bristol) who has begun designing an adenoviral construct, with METTL3 expressed under a VE-cadherin promoter, to improve the endothelial selectivity of transgene expression. Preliminary validation studies of the initial viral extracts have been outlined in Appendix 3. Although the extracts resulted in the successful overexpression of METTL3 in cardiac ECs, this did not translate to an increase in total m6A levels, suggesting a lack of catalytic efficiency of the

overexpressed METTL3 (refer to Appendix 3). It would be of great interest for future studies to utilise a refined form of this virus to overexpress METTL3 specifically in ECs of ischaemic limb muscles using a high-fat diet (HFD) induced T2DM mouse model to more closely mimic the aetiology of human disease.

Impaired wound healing and the subsequent development of ulcerations and necrotic tissue remain as one of the most disabling diabetic complications, leading to amputations, morbidity, and mortality [257]. In fact, necrosis of significant areas of the weight-bearing portion of the foot is identified as one of the key indicators for patients with CLI who would benefit from amputation [258]. It is therefore easy to understand why the majority of preclinical therapeutic efforts to devise approaches that stimulate angiogenesis and arteriogenesis have been directed at the challenge of improving wound healing and minimising necrosis [259]. The therapeutic effects of METTL3 overexpression were therefore studied using post-LI toe necrosis as a clinical endpoint. One of the most striking findings in this study was the dramatic deleterious effect of Ad.METTL3 treatments on toe necrosis and survival. This could be explained by the observed reduction in arteriole density in Ad.METTL3 treated ischaemic limbs. Arterioles have a greater blood-carrying capacity than capillaries where arteriogenesis is responsible for restoring a significant portion of basal blood flow and impairments in collateralization is a prominent cause of delayed healing, ulceration and necrosis [260, 261].

The diabetic cohort also exhibited worse toe necrosis than the non-diabetic cohort of mice, this is in line with findings in most murine models where hyperglycaemia significantly delays wound healing and exacerbates the spread of necrotic tissue [255, 262]. Furthermore, lymphangiogenesis and neovascularisation in the granulation tissue, which are of paramount importance to reinstate tissue integrity, are defective

in diabetic murine models [263]. Impaired revascularisation of the wound bed propagates the formation of foot ulcers and represents a prototypical condition where the adverse effects of hyperglycaemia on the formation of new microvessels manifests [264]. In addition to the effects of underlying hyperglycaemic conditions in the diabetic cohort, toe necrosis is exacerbated by the concomitant limitation of upstream blood flow compounded by the reported effects of Ad.METTL3 treatments on arteriole densities. The progression of tissue necrosis is a condition where neovascularization and inflammation typically coexist with pro-inflammatory markers independently correlating with progression of necrosis and risk of amputation [265]. It would therefore be of benefit for the aforementioned future studies in HFD T2DM mice utilising an EC specific Ad.METTL3 to incorporate the evaluation of histopathological immune features of necrosis, defined by the presence of multi-cellular infiltrates and hypereosinophilic myocytes in sections of ischaemic adductor and gastrocnemius muscles [266].

The overarching aim of the research presented in this chapter is to improve our understanding into the functional effects of METTL3 mediated m6A on revascularisation, reperfusion and recovery in diabetes-induced ischaemic complications of the lower extremities. This study has provided the first evidence of improved angiogenesis in pathogenic ECs following METTL3 supplementation. These findings were reflected in the context of CLI where the exogenous reestablishment of METTL3 expression improved post-ischaemic angiogenesis despite a lack of improvement in blood flow recovery. The unspecific delivery approach for the gene transfer of METTL3 may be responsible for an observed reduction in arteriogenesis and subsequent worsening of toe necrosis. Having shown a clear role for METTL3 in angiogenesis and its dysregulation diabetic ECs, refinement of our delivery approach

through the production of an EC specific vehicle would be crucial in gaining a full understanding of the therapeutic potential of m6A in the setting of diabetic CLI. Most importantly, future studies directed at elucidating the m6A RNA methylation landscape in diabetic and ischaemic ECs would provide fundamental knowledge for the exploitation of m6A as a target for the treatment of CLI. Numerous miRNAs are involved in PAD pathophysiology [267] and having described the involvement of m6A in the processing of angiogenic miRNAs, mapping of the m6A epitranscriptome would allow for identification of specific target miRNAs. This would facilitate the possibility of synergistic regulation of impaired EC mechanisms in patients with PAD.

Chapter 6

Effects of Exogenous METTL3 Supplementation on Post-myocardial Neovascularization and Cardiac Function

6. Effects of Exogenous METTL3 Supplementation on Post-myocardial Neovascularization and Cardiac Function

6.1 Introduction

Although the mortality from CVD is decreasing, IHD represents the leading cause of death worldwide [268]. IHD accounts for 20% of all deaths in Europe and 30% of all deaths over the age of 35 in the US [269, 270]. IHD is a condition characterised by cardiomyocyte damage due to reduced blood supply compared with their metabolic demand. IHD is classically attributable to CAD in which the atherosclerotic obstruction of the epicardial coronary arteries decreases blood flow by more than 50%. Hence, IHD and CAD are often synonymously interchangeable terminologies. Recent clinical, angiographic and autoptic findings indicate a complex and multifaceted aetiology of IHD that is not strictly analogous with CAD. The dysfunction of the coronary microvasculature resulting in impairment of vasomotor tone also evokes IHD independently from the presence of an atherosclerotic plaque [271, 272]. The dynamic nature of IHD results in a variety of clinical manifestations that can simply be divided into chronic coronary syndromes (CCS) or acute coronary syndromes (ACS).

The primary treatment options for IHD consist of cardiovascular risk modification, antithrombotic medication, antianginal medication and revascularisation when applicable. In terms of managing cardiovascular risk, adherence to a healthier lifestyle and cessation of smoking is associated with a reduction of new cardiovascular events in IHD patients [273]. Additionally, lowering LDLs with statins has a major effect on cardiovascular events and death [274]. Antithrombotic therapies suppress the progression of thrombosis, promote dissolution of acute and residual mural thrombus. Antithrombotic drugs are an important treatment option for patients with ACS where their use has dramatically reduced the incidence of MI, stroke, thromboembolism and

death in recent years [275]. Antianginal medications include beta-blockers, long-acting nitrates and calcium channel blockers.

The primary objectives of revascularisation are symptom relief in patients with angina and/or the improvement of prognosis. Percutaneous coronary intervention (PCI) or coronary artery bypass grafting (CABG) may alleviate angina, eliminate ischaemia and adverse clinical manifestations and reduce further cardiovascular events. The choice of revascularization method depends on anatomical coronary pathophysiology. PCI is a procedure which involves the inflation of a balloon within the blocked coronary artery to restore blood flow to the myocardium. PCI have advanced in recent years with the introduction of drug eluting stent into the coronary artery. During CABG surgery, blood vessels originating from the patient are grafted to coronary arteries to bypass the atherosclerotic blockage and increase the blood supply to the myocardium.

CVD is the leading cause of death in the diabetic population, where the prevalence of heart disease accounts for up to 80% of deaths [18, 19]. The Framingham Heart Study published the first prospective study demonstrating a higher incidence of CVD across all age groups for individuals with DM compared to those without [191]. DM worsens coronary arteriosclerosis, increasing the risk of angina and MI, two manifestations of IHD. Additionally, the incapacity of ECs to regulate glucose influx makes them especially susceptible to DM induced damage. Chronic intracellular hyperglycaemia causes EC dysfunction by initiating a self-perpetuating cycle of oxidative stress and aberrant metabolic memory [276]. This propagates microvascular dysfunction and rarefaction due to EC apoptosis and impaired angiogenesis. The resulting coronary microangiopathy reduces myocardial perfusion, making diabetics less able to maintain cardiac function. As a result, IHD in diabetic patients often follows an inexorable course, with the one-year post-MI mortality rate in diabetics being profoundly higher

than those without diabetes [277]. The ability to reduce cardiovascular event rates in the diabetic population by glycaemic control with/out associated lipid lowering approaches, has remained elusive [24]. In this alarming clinical scenario, therapies to maintain and replace the defective microvasculature are urgently needed. The elucidation of novel molecular mechanisms associated with diabetes induced IHD is an important step towards improved therapeutics.

The m6A modification is emerging as a new layer in the developing landscape of posttranscriptional regulation of gene expression and has been shown to be crucial in the regulation of a number of biological processes, while its dysregulation has been implicated in several diseases, including diabetes [182, 193, 218, 278]. GWAS have identified correlations between common SNPs in the FTO region (rs9939609 T>A) with an enhanced susceptibility to CHD [179]. The association of this FTO SNP with CAD and obesity was corroborated by a successive study performed in a Pakistani cohort [180]. A 19-year follow up of the Oulu Project Elucidating Risk of Atherosclerosis (OPERA) studied the relevance of FTO rs9939609 on cardiovascular events and death. FTO rs9939609 indeed predicts CHD, with the AA genotype exhibiting an increased risk of cardiovascular events and death. Additionally, this variant was also identified as an independent risk factor for atherosclerosis. A second SNP within FTO (rs17817449) was correlated with an increased risk of rejection in heart transplant patients [176]. Furthermore, the YTHDF3 polymorphism rs4739066 demonstrated a weak association with MIs in an ethnic Arab population [178]. Moreover, the importance of the m6A modification in cardiomyocytes in the context of heart hypertrophy and failure is recently emerging. METTL3 mediated m6A has been shown to be crucial for maintaining cardiac function and hypertrophic stress responses

[156]. Additionally, the m6A demethylase FTO has also been identified as a critical mediator of cardiac homeostasis and myocardial repair [159].

Of particular importance to the studies outlined in this chapter, the aforementioned unpublished findings by the Emanuelli lab reveal a deregulation of METTL3 in left ventricular biopsies of patients with CAD and T2DM (Appendix 2). Chapter 4 describes a reduction in METTL3 in whole LV tissue and ECs from diabetic mice and in human cardiac ECs cultured in diabetic and ischaemic mimicking conditions. I also highlight a novel role of METTL3 mediated m6A in the regulation of angiogenesis. Loss and gain of function studies reveal METTL3 to be crucial in the modulation of EC processes that are conducive to angiogenesis *in vitro* and *in vivo*. Mechanistically, I show that METTL3 can modulate angiogenesis by mediating the endothelial bioprocessing of the angiogenic miRNAs let-7e and the miR-17-92 cluster. The depletion of endothelial METTL3 results in the nuclear accumulation of pri-let-7e and pri-miR-17-92, a reduction in their functional mature forms and the subsequent increase in their common anti-angiogenic target, Tsp1 [168]. Overexpression of METTL3 also promotes angiogenesis in human ECs exposed to diabetes-mimicking conditions *in vitro*. Additionally, the therapeutic potential of endothelial METTL3 in post-ischaemic reparative angiogenic responses was highlighted in a murine model of LI. ***Based on these evidence, I hypothesise that the post-MI adenovirus mediated supplementation of METTL3 promotes therapeutic angiogenesis and improves cardiac remodelling and function in murine model.***

The aims of the work described in this chapter are to:

- Validate the overexpression of METTL3 in post-MI hearts of mice following adenoviral mediated local gene transfer

- Explore the possibility of improving post-MI revascularisation by restoring METTL3 levels
- Investigate the effects of exogenous METTL3 supplementation on post-MI fibrosis and apoptosis
- Elucidate the effects of exogenous METTL3 supplementation on post-MI cardiac function

College closures resulting from the COVID-19 outbreak caused significant disruption to any animal-based work. As a contingency plan, I successfully applied for a “Short Term Scientific Mission” grant awarded by the European CardioRNA Cost Action to cover the travel costs to a collaborating lab at the University of Otago. Since the pandemic did not impact the possibility to perform animal-based studies in New Zealand, this would have been an excellent opportunity to complete all planned investigations and receive extensive training in relevant techniques while labs in the UK remained closed. Unfortunately, New Zealand closed their borders to all foreign visitors shortly after the award of the grant which has since expired. To circumvent this, Professor Rajesh Katare and his lab member Dhananjie Chandrasekera (University of Otago) kindly performed the experimental procedures outlined in this chapter.

6.2 Results

6.2.1 Validation of Adenovirus Mediated METTL3 Overexpression in the Ischaemic Myocardium

The studies described in this chapter utilised a murine MI model to investigate the functional relevance of Ad.METT3 treatments on myocardial therapeutic angiogenesis and cardiac function in a non-diabetic cohort. MI was induced in 10-week-old male C57BL/6J mice by left anterior descending coronary artery ligation. Immediately after ligation, the animals were randomized to receive either Ad.Null or Ad.METTTL3 intracardiac injections into the peri-infarct border zone (refer to figure 6.1A for experimental outline). Having determined an optimal viral concentration of 10^8 PFU for the overexpression of METTL3 in the hindlimb ischaemia model (refer to sections 5.2.2 and 5.2.3), we opted to proceed using a similar concentration in these MI studies. Western blot analysis of METTL3 in the myocardium at 14 days post-MI was performed to verify successful gene transfer where we observe a 2.5-fold increase in human METTL3 expression at a protein level (figure 6.1B).

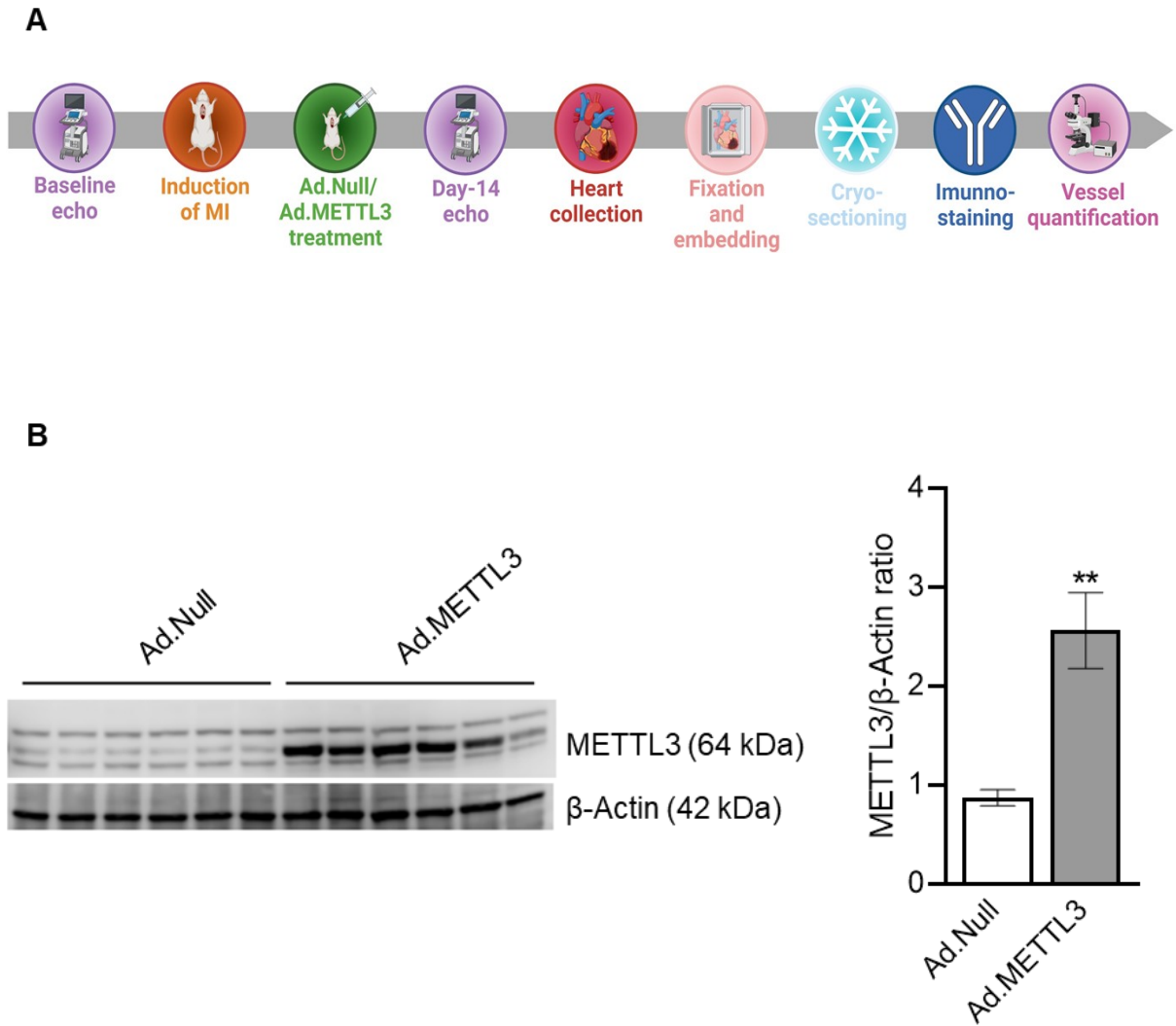


Figure 6.1 Validation of adenoviral mediated METTL3 overexpression in the ischaemic myocardium. (A) Overview of experimental procedure. MI was induced in male C57BL/6J mice by left anterior descending coronary artery ligation. Immediately after ligation, the mice were randomized to receive either Ad.METTL3 or Ad.Null (10^8 PFU/mouse, N=10 each group) intracardiac injection. Baseline echocardiographic readings were taken at base line and at 14-days post MI, at which point the mice where sacrificed and hearts where isolated for immunohistochemical analysis (B) METTL3 protein levels were quantified in the myocardium at 14 days post-MI by western blot analysis. Representative blots are shown, and western blot quantification is expressed as METTL3/ β -Actin ratio (N=6 in each group). B-Actin was used as loading control. Data are expressed as mean \pm SEM. Result was assessed by unpaired Student's t test. *P<0.05, **P<0.01, ***P<0.01, n.s non-significant vs Ad.Null.

6.2.2 Exogenous METTL3 Supplementation Promotes Post-MI

Neovascularisation

To elucidate the therapeutic significance of METTL3 mediated m6A in the ischaemic myocardium, male C57BL/6J mice were surgically induced with MI and received intracardiac injections of either Ad.Null or Ad.METTL3 into the peri-infarct border zone. The animals were sacrificed at day 14 post-MI and hearts were isolated and processed for immunohistochemical analysis of capillary and arteriole densities. The capillaries were visualized by immunofluorescent staining with a fluorochrome-coupled isolectin B4 to stain ECs and the capillary density was assessed relative to the area of cardiomyocytes per high power field area. Ventricular tissue treated with Ad.METTL3 showed significant increases in capillary density compared to infarcted hearts injected with Ad.Null (figure 6.2A and B). Arterioles were also visualised by immunolabelling of α -SMA as a marker of VSMCs. Quantification of arteriole density in the infarcted myocardium of revealed a significant increase in Ad.METTL3 compared to Ad.Null treated hearts (figure 6.2A and C).

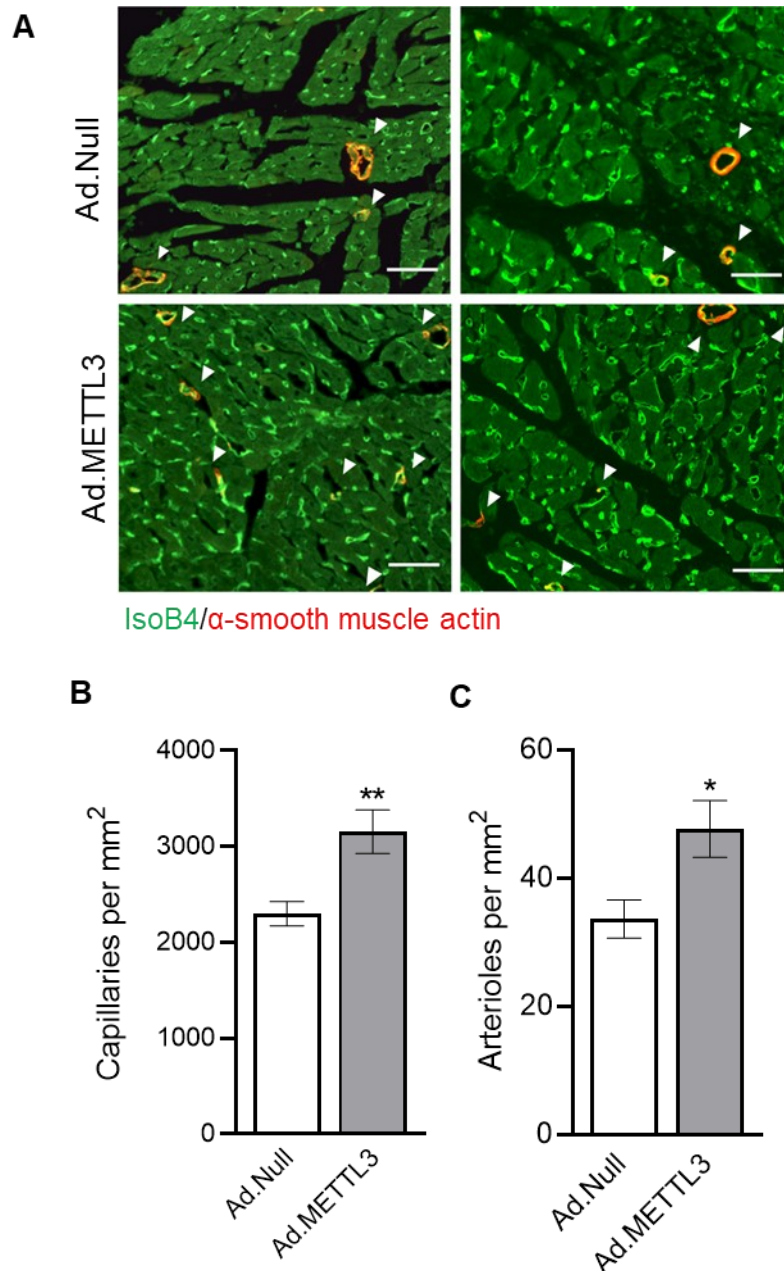


Figure 6.2 Exogenous METTL3 supplementation promotes post-MI neovascularisation. MI was surgically induced in male C57BL/6J mice by occlusion of the left anterior descending coronary artery. Immediately after ligation, mice were randomized to receive either Ad.METTL3 or Ad.Null intracardiac injections (10^8 plaque-forming units [PFU]/mouse, N=10 mice in each group). Ad.METTL3 or Ad.Null treated ischaemic hearts were isolated 14 days post-surgery and processed for immunohistochemical analysis. **(A)** Representative confocal microscopy images showing capillary and arteriole densities ($\times 400$ magnification, scale bar 50 μ m). Capillaries and arterioles were quantified as isolectin-B4 and α -smooth muscle actin positive structures (white arrowheads) respectively. Arterioles were quantified according to vessel diameter (< 20 μ m). Images in **(A)** were co-stained with isolectin-B4 and α -smooth muscle actin. **(B and C)** Graphs showing capillary and arteriole densities respectively. Data presented as mean \pm SEM. Results were assessed by two-way unpaired student t-test. * $P < 0.05$, ** $P < 0.01$, *** $P < 0.001$, n.s non-significant vs Ad.Null.

6.2.3 Post-MI Ad.METTL3 Treatments Reduces Cardiac Apoptosis

Necroscopic analysis on LV transverse sections were performed at day 14 post-MI to study apoptosis and fibrosis. Left ventricular apoptosis, quantified as the number of TUNEL positive capillaries, was significantly reduced following the overexpression of METTL3 compared to Ad.Null treated hearts (figure 6.3A). Cardiac fibrosis is a process of pathological ECM remodelling, resulting in aberrant matrix composition and quality. Initially, post-MI ECM deposition is a protective mechanism and can be beneficial for wound healing and myocardial regeneration. However, excessive and continuous ECM deposition, particularly collagen type I secretion, leads to impaired cardiac function. Fibrosis was determined as the percentage of scarred tissue in the peri-infarct area following Mason's Trichrome staining. No changes in fibrosis were observed in Ad.METTL3 treated hearts compared to those treated with Ad.Null (figure 6.3B).

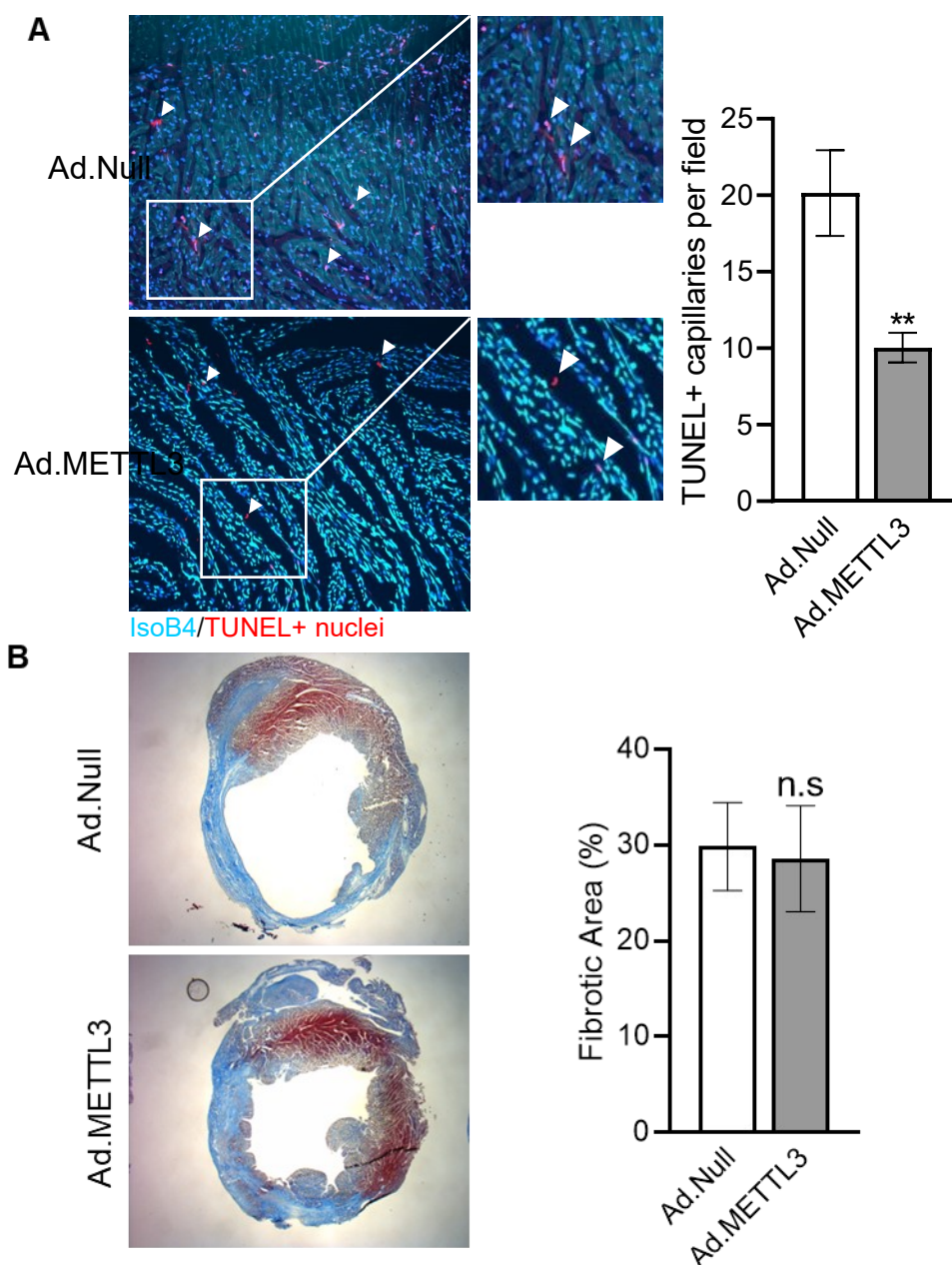
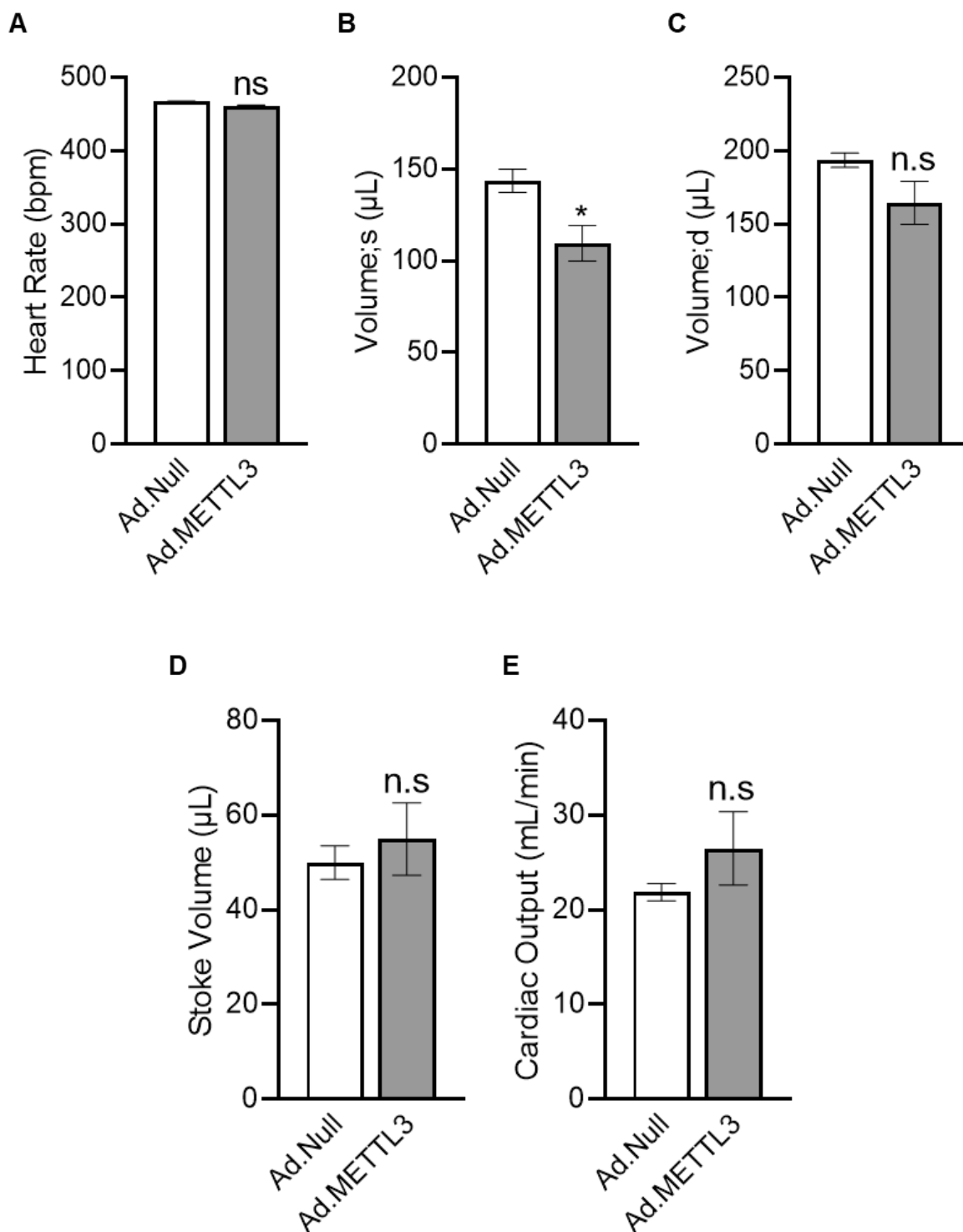


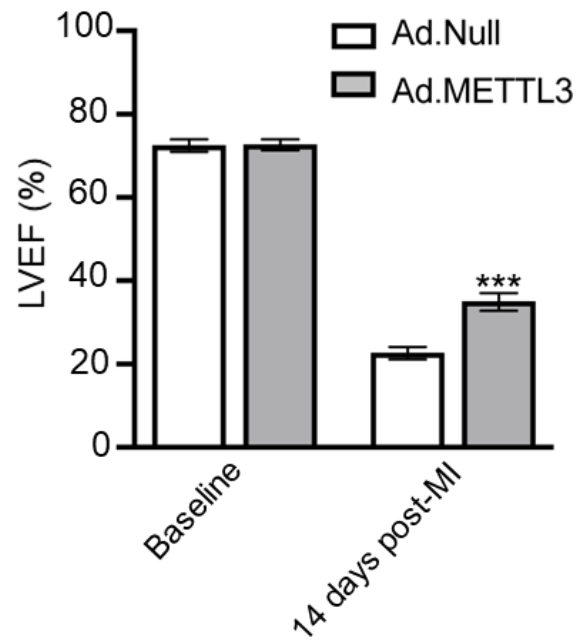
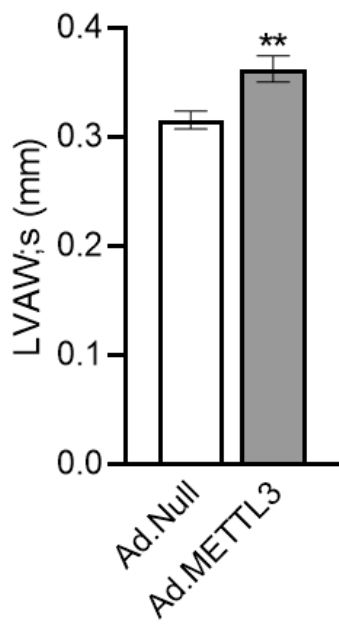
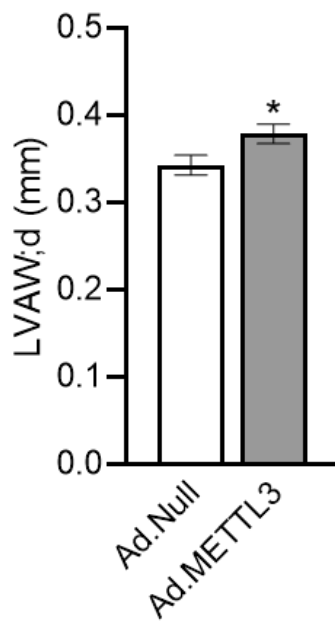
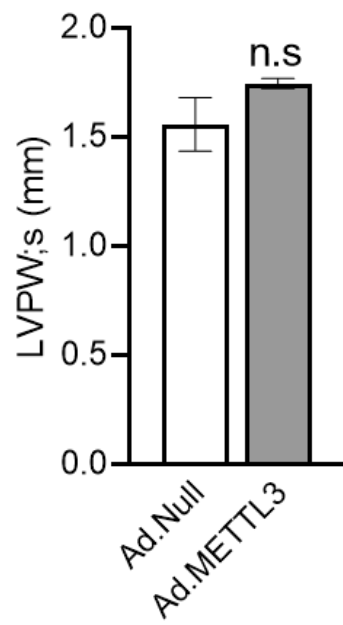
Figure 6.3 Post-MI Ad.METTL3 treatments reduces cardiac apoptosis and fibrosis. MI was surgically induced in male C57BL/6J mice by occlusion of the left anterior descending coronary artery. Immediately after ligation, mice were randomized to receive either Ad.METTL3 or Ad.Null intracardiac injections (10^8 plaque-forming units [PFU]/mouse, N=10 mice in each group). Ad.METTL3 or Ad.Null treated ischaemic hearts were isolated 14 days post-surgery. **(A)** Representative confocal microscopy images showing TUNEL+ capillaries (white arrowheads) ($\times 400$ magnification, scale bar 50 μm). Graph showing number of TUNEL+ capillaries per field. **(B)** Representative brightfield Masson trichrome staining images of LV transverse sections from hearts treated with Ad.Null or Ad.METTL3 at 14 days post-MI. Graph showing fibrotic area in mice treated with Ad.Null or Ad.METTL3. Scar size was quantified as the percentage of total LV area. Data presented as mean \pm SEM. Results were assessed by unpaired student t-test. * $P < 0.05$, ** $P < 0.01$, *** $P < 0.001$, n.s non-significant vs Ad.Null of each respective group.

6.2.4 Post-MI Ad.METTL3 Treatments Attenuates Ischaemia Induced Loss of Cardiac Function

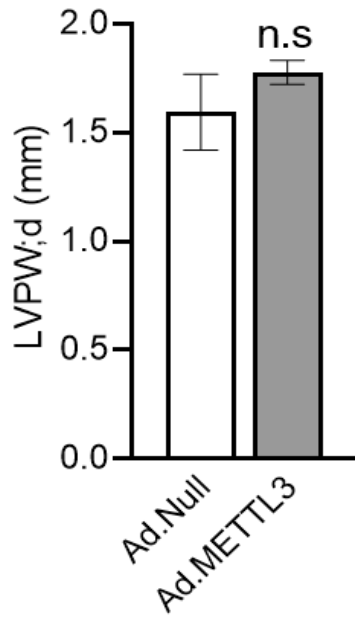
Echocardiographic analysis was performed at day-14 post-MI to gain an insight into the effects of METTL3 overexpression on cardiac function. Ventricular dimensions and function were assessed from averaged measurements of at least 3 consecutive cardiac cycles from short-axis images at mid-papillary level from left parasternal window. We firstly confirm that the cardiac overexpression of METTL3 does not cause a chronotropic effect and that the heart rates of both Ad.Null and Ad.METTL3 treated mice fall into within the recommended range of 400-650 beats/min (figure 6.4A). Ad.METTL3 injected hearts exhibited decreased left ventricular intraventricular volumes at diastole (;d) and systole (;s) (figure 6.4B and C). These hearts also exhibited trends towards an increase in both stroke volume and cardiac output (figure 6.4D and E). The assessment of post-MI left ventricular systolic function is of vital importance as it is closely associated with future patient outcomes [279]. Baseline indexes of left ventricular ejection fraction function did not differ between Ad.Null and Ad.METTL3 treated animals. Most importantly, METTL3 overexpression dramatically improved contractile function, as indicated by an increased percentage of left ventricular ejection fraction (LVEF) (figure 6.4F).

Echocardiographic analysis also revealed an increase in LV anterior wall (LVAW; mm) at diastole and systole in Ad.METTL3 treated hearts (figure 6.4G and H), while no changes were observed in the LV posterior wall (LVPW; mm) (figure 6.4I and J). Additionally, the diameter of the intraventricular cavity was smaller in the METTL3 overexpressing hearts at systole and was unchanged at diastole (figure 6.4K and L). Finally, METTL3 overexpression significantly improved post-MI cardiac function as indicated by an increase in fractional shortening (figure 6.3M).

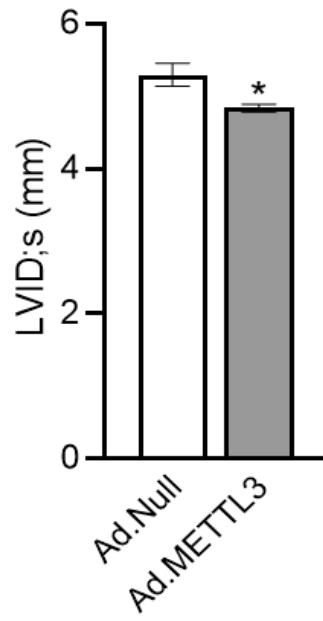


F**G****H****I**

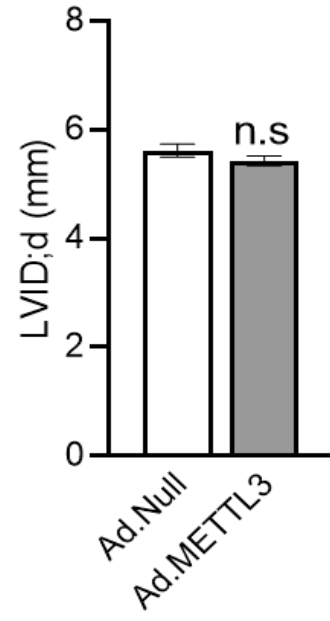
J



K



L



M

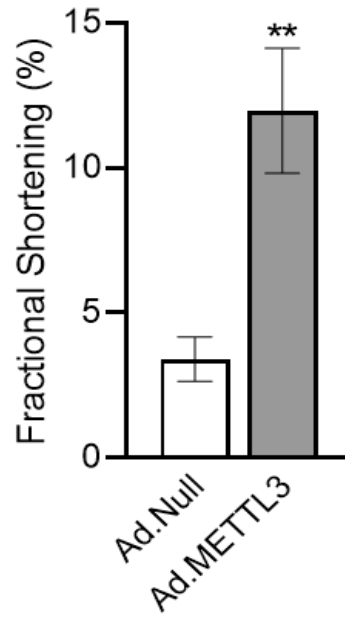


Figure 6.4 Post-MI Ad.METTTL3 treatments attenuates ischaemia induced loss of cardiac function. MI was surgically induced in male C57BL/6J mice by occlusion of the left anterior descending coronary artery. Immediately after ligation, mice were randomized to receive either Ad.METTTL3 or Ad.Null intracardiac injections (10^8 plaque-forming units [PFU]/mouse, N=10 mice in each group). At day 14 post-MI echocardiography was used to assess ventricular dimensions and function from averaged measurements of at least 3 consecutive cardiac cycles. Graphs showing the following echocardiographic variables: **(A)** heart rate (bpm), **(B-C)** LV intraventricular volume (Volume; d/s μ L) at diastole and systole, **(D)** stroke volume (μ L), **(E)** cardiac output (mL/min), **(F)** basal and final percentages of left ventricular ejection fraction (LVEF %), **(G-H)** LV anterior wall dimensions (LVAW; d/s mm) at diastole and systole, **(I-J)** LV posterior wall dimensions (LVPW; d/s mm) at diastole and systole, **(K-L)** dimensions of LV intraventricular cavity (LVID; d/s mm) at diastole and systole and **(M)** percentage of LV fractional shortening. For Ad.Null: N=12 basal, N=8 final; Ad.METTTL3: N=12 basal, N=10 final. Data are expressed as mean \pm SEM. Results in **A-E** and **G-M** were assessed by unpaired Student *t* test, and **(F)** by 2-way ANOVA (Šídák post hoc test). **P*<0.05, ***P*<0.01, ****P*<0.01, *****P*<0.0001 vs Ad.Null infarcted heart.

6.3 Discussion

An MI event is known to inflict significant injury to the coronary microcirculation resulting in vascular collapse and capillary rarefaction in the infarct region. Post-MI cardiac repair requires a robust angiogenic response that is initiated in the infarct border zone and extends into the necrotic infarct core. Unfortunately, the unfavourable prognosis of DM patients with MI is linked to pre-existing microvascular dysfunction and an impaired angiogenic response [280]. I have previously described a deregulation of METTL3 in left ventricular biopsies of patients with CAD and T2DM (Appendix 2). METTL3 is also reduced in whole heart tissue and isolated ECs derived from diabetic mice and in human cardiac microvascular ECs cultured in hyperglycaemic and ischaemic mimicking conditions (refer to section 4.2.4, Chapter 4).

Here, I reveal that the exogenous rescue of METTL3 expression in the infarcted myocardium improves the angiogenic response, as demonstrated by an increase in capillary density. This is in line with the proposed role of METTL3 in the modulation of key EC functions conducive to angiogenesis [168]. These findings also reflect the increase in post-ischaemic capillary formation observed in the murine hind-limb ischaemia model (section 5.2.5, Chapter 5). In possible contrast, Mathiyalagan et al provide evidence that the overexpression of the m6A demethylase FTO, enhances angiogenesis in the ischaemic myocardium as demonstrated by an increase in CD31+ cardiac ECs [159]. However, post-MI angiogenic responses was not the focus of this study and these data were obtained from a small sample size of only 3 mice per group, therefore requiring further validation. It's also important to note that these findings were reported at 4 weeks post-MI as opposed to our 2-week timepoint.

Contrary to the decrease in arteriole density reported in the hind-limb ischaemia model (section 5.2.5, Chapter 5), the post-MI overexpression of METTL3 promotes arteriole formation. It is difficult to surmise the exact cause for this discrepancy in arteriogenic responses, particularly when possible off-target effects of the utilised method for METTL3 overexpression are taken into consideration. The underlying processes exhibited in post-ischaemic revascularisation of cardiac and skeletal muscle are indeed tissue specific. For instance, in the context of MI, surviving epicardial cells in the infarct border zone proliferate to cover the infarct region, while the simultaneous development of a capillary network occurs within the expanded epicardium. Epicardial capillaries acquire smooth muscle cell support and remodel to form arterioles which connect to the coronary vasculature of the underlying myocardium [281]. The remodelling of existing collateral arterioles to revascularize ischaemic tissue relies on precise coordination between varying cell types, which can differ greatly in cardiac and skeletal muscle. Hence a global and unspecific increase in m6A RNA methylation levels can have hugely varying effects in different contexts of ischaemic disease.

Dorn et al., identified a role for METTL3 mediated m6A in cardiac adaptation to stress where an induction of compensated hypertrophic remodelling was described in a METTL3-overexpressing mouse line subjected to cardiac pressure overload. Additionally, the cardiac knockout of METTL3 under similar conditions caused an increase in left ventricular chamber dimensions and ventricular dilation associated with a decrease in fractional shortening [156]. Notably, in this chapter I demonstrate that the post-MI local delivery of Ad.METT3 dramatically improved contractile function, as indicated by a higher percentage of LVEF and fractional shortening without inducing cardiac functional deficits at baseline. Unlike the aforementioned findings in the hindlimb ischaemia model (Chapter 5), these data suggest that the adenoviral

mediated overexpression of METTL3 not only improves post-ischaemic angiogenesis but also exerts a reparative and positive functional effect. On the other hand, a recent study reported a rescue in LVEF and fractional shortening in a mouse model of MI following a reduction in m6A methylation levels through the overexpression of FTO. These studies elucidated the preferential demethylation of specific cardiac contractile transcripts to prevent m6A accelerated degradation and improve their protein expression under ischaemia [159].

EC apoptosis is a typical hallmark of microangiopathy in the diabetic heart and is a driving factor in microvasculature rarefaction. Additionally, in the context of MI, reperfusion therapy is in most cases essential to mitigate permanent damage to the myocardium, however this may cause a paradoxical amplification of EC death and an aggravation of myocardial damage. Here, I report that the post-MI supplementation of METTL3 attenuates endothelial apoptosis as demonstrated by a decrease in TUNEL+ capillaries in Ad.METTL3 compared to Ad.Null treated animals. These findings are in agreement with our *in vitro* data in which the transient depletion of METTL3 in human ECs results in an increase in apoptosis and a reduction in proliferation (refer to section 3.2.1). A number of recent studies however report opposing findings on the apoptotic role of METTL3 and the m6A mark in the ischaemic myocardium. Song et al., describe an increase in m6A RNA methylation levels paralleled by an aberrant upregulation of METTL3 in H/R treated cardiomyocytes and I/R treated murine hearts. The silencing of METTL3 was reported to attenuate I/R injury by enhancing autophagic flux and inhibiting apoptosis in H/R treated cardiomyocytes [131]. A subsequent study utilised a rat MI model to investigate the transcriptome-wide profile of m6A with a focus on mRNAs. The authors observed hypermethylation of mRNA transcripts in the infarcted area and an increase in METTL3 expression. The aberrant deposition of the m6A mark

on *HadH*, *Kcnn1* and *Tet1* transcripts was associated with an increase in apoptosis *in vitro* [282].

Although Chapter 4 of this thesis provides extensive expressional analysis of *METTL3* and m6A in the diabetic murine heart, it would be of great interest to further validate post-MI endogenous *METTL3* expression and m6A methylation levels. Ke et al., explored the relevance of *FTO* in myocardial I/R injury where they identify a downregulation of *FTO* in this setting. *FTO* was shown to be responsible for the demethylation of *YAP1* transcripts and its downregulation contributes to increased myocyte apoptosis upon I/R injury. The overexpression of *FTO* attenuated the H/R-induced apoptosis of cardiomyocytes [283]. Finally, a recent study also identified the upregulation of the m6A methylase *WTAP* in post-MI I/R. Here, *WTAP* was shown to promote cardiac injury by increasing cardiomyocyte apoptosis through the regulation of m6A deposition on *ATF4* transcripts, while its silencing reduced apoptosis [283]. Although these studies may indicate opposing roles of the m6A modification and its regulators in post-MI cell survival, it's important to consider that these investigations were primarily focused on cardiomyocyte apoptosis in the context of I/R injury while our research was specifically aimed at understanding the significance of *METTL3* in the myocardial endothelium and its revascularisation.

Fibrotic scarring of the cardiac muscle is a common occurrence following ischaemic injury to the myocardium. Initially, the deposition of ECM following an MI acts as a protective mechanism and can be beneficial for wound healing and tissue regeneration. However, abnormal proliferation and activation of cardiac fibroblasts and excessive ECM deposition in injured areas of the myocardium results in pathological cardiac fibrosis. Fibrotic tissue exhibits diminished cardiac function due to an impaired ability to conduct impulses and contract, thereby leading to heart failure. An

improvement in post-MI angiogenesis has indeed been associated with reduced adverse fibrotic responses [284]. Interestingly, data presented in this chapter suggest that Ad.METTL3 delivery to the peri-infarct myocardium resulted in no significant improvements of fibrotic area. Conversely, METTL3 overexpression in the heart has been reported to reduce transverse aortic constriction induced fibrosis in two separate studies [156, 160]. METTL3 expression was also reported to increase in cardiac fibrotic tissue and its silencing was shown to alleviate post-MI fibrosis via the reduced activation of cardiac fibroblasts [163]. The overexpression of FTO in mouse MI models also decreased fibrotic scar-size while MeRIP-seq identified FTO regulated fibrotic pathways, further highlighting possible pro-fibrotic effects of increased m6A in the diseased heart [159]. These contradicting findings underline the dynamic role of m6A as a master regulator of large subsets of RNA molecules and considering the complexity and intersection of multiple signalling pathways involved in post-MI responses, it's clear that there is much to be understood about the functions of m6A and its machinery in this setting.

Despite recent advancements and rapidly growing interest in the biological significance of m6A RNA methylation, its involvement in both maintaining cardiac homeostasis and in disease is only recently beginning to be understood. Additionally, the role of METTL3 in the cardiac endothelium and myocardial revascularisation in the context of IHD were up until now completely unexplored. The studies presented in this chapter are the first to demonstrate that the post-MI exogenous supplementation of METTL3 supports neovascularisation in the peri-infarct area and improves cardiac function in the ischaemic heart. Further investigations utilising the murine MI model in animals induced with T2DM through a HFD to mimic the unfavourable prognosis of DM patients with MI would be of great interest. Additionally, studies into the

transcriptome wide distribution of m6A in the diabetes and ischaemia inflicted endothelium is a crucial step towards understanding the mechanisms underlying the positive post-MI response reported here. Nonetheless, our findings provide intriguing new possibilities for the targeting of METTL3, a master regulator of the m6A RNA modification, in improving post-infarction angiogenesis and maintaining cardiac function in the diabetic heart.

Chapter 7

Future Perspectives and Final Conclusions

7 Final Conclusions and Future Perspectives

7.1 Final Conclusions and Future Directions

This thesis focuses on the m6A methylase, METTL3, in the modulation of the angiogenic process and in the setting of diabetes associated ischaemic diseases. Here, I provide compelling evidence that a refined modulation of METTL3 should indeed be considered as an approach for controlling angiogenic responses in the ongoing search for novel regulatory mechanisms that may translate into new therapeutic targets.

Chapter 3 reveals a crucial role for METTL3 in EC function and angiogenesis through the mediation of miRNA processing [168]. Studies have emerged further corroborating this novel role for m6A and its regulators in the modulation of angiogenesis through their action on different RNA species [167, 169, 170, 209]. The discovery of these distinct m6A-related pathways highlights the complexity of this mechanism and its ability to fine-tune gene expression in the regulation of crucial biological processes such as angiogenesis in varying contexts. The particular METTL3 mediated mechanism presented in this thesis was identified using a previously published dataset obtained in a metastatic breast cancer cell line (MDA-MV-231) to extract a list of EC expressed pri-miRNA transcripts methylated by METTL3 [154]. Apart from miRNA processing, m6A RNA methylation also modulates the function of different non-coding RNAs and mRNA metabolism and translation, among other processes. Hence, the levels of METTL3 expression in ECs could also influence potential non-coding RNAs and mRNA transcripts involved in angiogenesis. It is therefore crucial for future studies to profile the transcriptome wide distribution of m6A in METTL3 deficient and control ECs. This will allow for the characterisation of downstream miRNAs and mRNAs primary transcripts related to angiogenesis with differential patterns of m6A

distribution compared to control ECs. LV-METTL3-shRNAs and LV-CT-shRNA utilised in this study can be used to generate a stable METTL3 knockdown in HUVECs while the distribution of m6A can be investigated by MeRIP-seq using published methods [79, 80].

Unfortunately, COVID-19 imposed disruptions to my timeline impeded the culmination of an intriguing series of experiments I had planned. Collaborators of the Emanuelli lab provided the group with mouse embryonic stem cells (mESCs) derived from METTL3-KO animals [287]. Given the well-established role m6A plays in development [92, 286-288] and the newly identified function of METTL3 in angiogenesis, it would be of great interest to use these cells to study the relevance of METTL3/m6A in vasculogenesis and angiogenesis using a previously established protocol by the group for mESC-EC differentiation [296]. These studies would provide fundamental insights into the importance of METTL3 in the development of the vascular system and lead to the development of a valuable research tool through the creation of a line of METTL3-KO mESC-derived ECs. Most importantly, these studies would open an avenue of research into the investigation of stem cell based therapeutic angiogenesis.

Chapter 4 of this study presents promising evidence in line with the initial hypothesis that EC m6A levels and the expression of its regulatory machinery are dysregulated in the diabetic and ischaemic milieu. Here, I show a consistent disruption in the expression of METTL3, and in turn, m6A levels in human ECs exposed to diabetic and ischaemic mimicking conditions, ECs derived from a murine model of diabetic LI and in LV tissue and ECs isolated from diabetic mouse hearts. It would be important to further investigate the levels of m6A and the expression of METTL3 at a protein level in these various models of diabetes and ischaemia. Furthermore, it would be of great interest to explore the levels of m6A and its regulators in infarcted hearts of diabetic

mice. These studies were indeed outlined as future plans in the Early- and Late-Stage Assessments of my PhD, however, were unable to be performed due to COVID-19 closures. To mitigate this, I applied for the aforementioned European CardioRNA Cost Action “Short Term Scientific Mission” grant to perform all remaining animal studies at the University of Otago. To increase the translational value of this work, further expressional analysis of METTL3 and m6A levels would need to be performed in whole muscle and ECs extracted from amputated limbs of diabetic CLI patients. Steps were indeed taken to establish a collaboration with vascular surgeon Dr Janice Tsui (UCL) to provide freshly amputated lower limb tissue for these studies, however COVID-19 imposed restrictions impeded this from coming to fruition. Additionally, qPCR analysis of METTL3 and the measurement of m6A levels in CABG-DM biopsy samples would be important to validate ARCADIA RNA-seq data indicating a reduction in METTL3 transcripts in patient samples (Appendix 2). Nonetheless, the findings presented in chapter 4, in concert with the newly identified role of METTL3 in angiogenesis (chapter 3), opened the intriguing possibility of post-ischaemic rescue of METTL3 as a method to improve diabetic CLI and IHD outcomes.

An important hypothesis of this study is that the exogenous supplementation of METTL3 via local gene transfer would improve post-LI muscular neovascularisation and BF recovery. Chapter 5 of this thesis provides evidence of an increase in post-ischaemic angiogenic responses in METTL3 treated limbs; however, this was also accompanied by a decrease in arteriogenesis, a lack of improvement in limb reperfusion and worsening of toe necrosis. I suggest that the unspecific delivery approach utilised for the gene transfer of METTL3 may be responsible for these unexpected effects. Ongoing efforts aiming to improve the endothelial selectivity of METTL3 transgene expression will be crucial in gaining a better understanding into

the therapeutic potential of METTL3 in the setting of diabetic CLI. Exploring new strategies for revascularization in patients with CLI is of the utmost importance, given that the literature indicates abnormalities in angiogenesis are pervasive to the entire spectrum of diabetes from onset to tissue-specific complications.

Chapter 6 provides compelling evidence suggesting that the overexpression of METTL3 in the infarcted myocardium improves post-ischaemic revascularisation, this was associated with an attenuation of EC death in the peri-infarct border zone and an improvement in cardiac function. Having described a reduction in METTL3 expression and m6A levels ECs from db/db murine hearts, it would be of great interest to further demonstrate the therapeutic potential of METTL3 gene transfer in the post-ischaemic diabetic heart. These studies were indeed planned as part of our collaboration with Professor Rajesh Katare, University of Otago. Although investigations in this thesis utilised an STZ-induced or db/db models of DM, future studies should opt to incorporate a HFD induced model of T2DM. This murine model of T2DM is known to develop cardiac complications at 24-weeks of treatment and has indeed been established in the Emanuelli lab as part of an MSc project I had the opportunity to co-supervise [297]. MI can be surgically induced at the 24-week timepoint followed by treatment with the aforementioned EC-specific Ad.METTL3. This approach will more closely mimic the aetiology of human disease and the unfavourable prognosis of DM patients with IHD, thereby bolstering the translational relevance of these studies.

When considering future directions, it is important to acknowledge efficacy and safety limitations inherent in the utilization of an adenovirus-based approach for the delivery of METTL3. Adenoviral vectors have the capacity to induce substantial transgene expression levels that can greatly surpass the endogenous levels observed in normal physiological conditions. This is particularly relevant when targeting METTL3, a

protein known to modulate the methylation of numerous transcripts involved in diverse cellular processes. The issue of non-physiological overexpression becomes a matter of concern in this context, as it can potentially give rise to off-target effects. Considering the intricacies of the angiogenic process, which necessitates precise regulation and coordination for the revascularization of ischemic tissue, careful control of gene expression is crucial to mitigate the occurrence of adverse events. Additionally, adenoviral vectors can elicit inflammation at the site of delivery due to the high prevalence of pre-existing immunity against common adenovirus serotypes. This immune response may impede the efficient transduction of target cells and potentially lead to adverse effects [36]. Consideration of alternative gene delivery systems would be of great interest for future directions. AAV vectors are a particularly promising option due to their ability to provide a stable and sustained transgene expression profile with minimal immunogenicity [30]. Of particular relevance, a recent study describes the development of an AAV capsid (AAV-BI30) capable of specifically and efficiently transducing ECs in the central nervous system [299]. This approach could indeed pave the way for the development of capsids with cardiac or large-vessel EC tropism.

It will be imperative for future investigations to focus on the elucidation of the mechanisms underlying the positive post-ischaemic revascularisation responses observed in the murine models of diabetic CLI and MI. I have indeed initiated MeRIP-seq studies aiming to characterise the transcriptome wide distribution of m6A in hyperglycaemia and hypoxia inflicted ECs. Here, HUVECs pooled from multiple healthy donors were exposed to HG or a combination of HG and hypoxia for 48-hours (control conditions: NG and normoxia). Total RNA was extracted from these samples and is ready for subsequent processing steps, m6A immunocapturing and sequencing

[298]. These studies will provide novel insights into the differential patterns of m6A distribution at pri-miRNA and mRNA sites in ECs exposed to diabetic and ischaemic mimicking conditions. The pri-miRNAs and other RNA datasets can be integrated in regulatory networks to provide insights into the mechanism of action of identified miRNAs. Additionally, clinical significance of the targets emerging from these studies can then be validated by MeRIP-RT-PCR and mature-miRNA to pri-miRNA ratios can be calculated in whole tissue and ECs extracted from diabetic and ischaemic LV biopsies and CLI patient samples. This will therefore allow for the identification of miRNAs and mRNAs involved in angiogenesis with m6A profiles affected by hyperglycaemia and hypoxia, and in turn reveal targets of potential therapeutic relevance. Judicious and coordinated manipulation of the METTL3-m6A-miRNA axis will concomitantly induce changes in other noncoding RNAs and mRNAs, which can yield additive effects on neovascularisation through cooperative mechanisms.

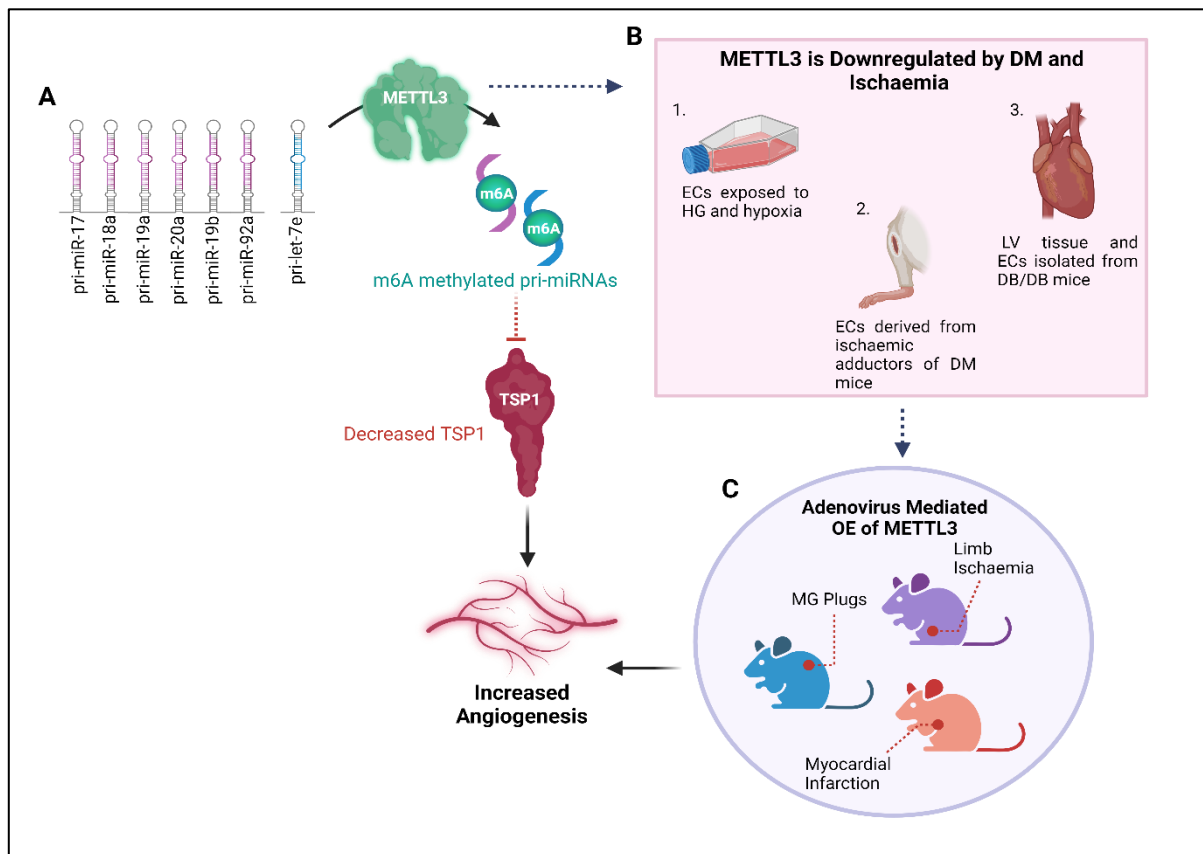


Figure 7.1 General summary of findings. (A) METTL3 mediates the co-transcriptional deposition of m6A on the pri-miR-17-92 cluster and pri-let-7e in ECs. The presence of m6A facilitates the bioprocessing, and in turn, expression of let-7e and the miR-17-92 cluster. These miRNAs repress their common angiostatic target TSP1, thereby improving the angiogenic capacity of ECs. (B) Expressional analysis revealed a dysregulation of m6A and METTL3 in human ECs exposed to diabetic and ischaemic mimicking conditions, ECs derived from a murine model of diabetic LI and in LV tissue and ECs isolated from diabetic mouse hearts. (C) The physiological relevance and therapeutic potential of METTL3 was demonstrated using murine models MG, diabetic limb ischaemia and myocardial infarction. Here, the adenovirus mediated overexpression of METTL3 in ischaemic limb muscles improved post-ischaemic muscular neovascularisation. Additionally, infarcted hearts treated with Ad.METTL3 showed an increase in arteriole and capillary densities while exhibiting improved cardiac function.

7.2 Future Perspectives

The term 'RNA epigenetics' was coined by Chuan He in *Nature Chemical Biology* in 2010 to describe an area of research that has remained stagnant since the initial discovery of chemical modifications of RNA bases in the 1970's [76, 77, 285]. The revelation that the most abundant post-transcriptional modification, m6A, was in fact a dynamic and reversible process, coupled with the development of transcriptome-wide mapping tools for m6A propelled the field of RNA epigenetics into a new frontier of research [78-80]. This fuelled intensive efforts into understanding the biological significance of m6A, thereby uncovering key roles in diverse cellular processes and diseases including development [92, 286], stem cell differentiation [287, 288], viral infection [289] and carcinogenesis [290]. More relevant to this thesis, several studies discerned a role for regulators of m6A in CVD and different cardiovascular risk factors, including diabetes. It is now apparent that changes mediated by various m6A regulatory proteins can indeed disrupt essential cellular pathways, highlighting the indispensability of this modification.

In light of the rapid expansion of the field, the prospect of targeting the epitranscriptome for therapeutics or as a biomarker is not far from reality. Indeed, several biotechnology companies have recently disclosed the development of small-molecule inhibitors of the METTL3-METTL14 complex [291]. Most notable progress has been made in the field of oncology with a selective METTL3 inhibitor, STC-15, moving into phase I clinical trials and the first oral administration in subjects suffering from advanced malignancies taking place in December 2022 (NCT05584111, ClinicalTrials.gov). Although such compounds are eagerly anticipated for testing in the context of ischaemic disease, it is important to consider the varying roles of m6A modifying enzymes across different cardiovascular tissues and their actions in

preserving homeostasis in the cardiovascular system (CVS). The results yielded from preclinical trials of these first-generation compounds will provide fundamental knowledge on the potential of targeting m6A associated pathways. However, applying such approaches for treatment of ischaemic disease might be challenging and will also require careful consideration of cellular, gene and microvesicle therapy approaches.

Further insights into the complexity and function of the m6A mark and its associated machinery may also lead to the attractive prospect of their use as clinical biomarkers with diagnostic or prognostic value. A step beyond this, I envision that machine learning algorithms will provide a new dimensionality in analysing large datasets of epitranscriptional dynamics to enable the use of m6A as a biomarker for diabetes inflicted CVD at a high level of efficiency and accuracy [292]. Although a proof-of-concept has been achieved in a neurology-based study which found that integration of RNA editing events linked to bipolar disorder into machine learning algorithms can assist in its diagnosis, this concept is yet to be tested on large scale diabetes or CVD clinical studies [293].

Despite the progression of the field and the advancements in understanding the significance of the m6A modification and its regulators in the CVS, major challenges continue to impede translational efforts. Firstly, the most utilised detection methods offer limited resolution and are unable to provide multiparametric information, such as location and stoichiometry. Although antibody-based techniques are restricted by their limited specificity, more refined methods such as miCLIP, m6A-LAIC-seq and MAZTER-seq have emerged in recent years (refer section 1.6.3 of thesis for a detailed overview of m6A detection methods). Additionally, all existing methods require a large amount of input RNA, thereby severely limiting the types of experimental and clinical samples that can be used. Given the limited availability of

bio-samples in cardiovascular research, this poses a major hinderance to progress. The multitude of RNA modifications pose another challenge, with over 170 identified to date. Methods for parallel mapping of different modifications in single transcripts to decipher combinatorial code would not only allow us to consider the involvement of other RNA marks in CVD but also unveil possible epigenetic crosstalk of m6A. It is also imperative for future efforts to be directed towards establishing novel approaches for the manipulation of m6A. Current research relies on inhibition of general levels of m6A via the depletion or overexpression of its regulatory machinery. However, specific targeting at a nucleotide level by CRISPR-based RNA editing [294, 295] or synthetically modified RNA oligonucleotides [208] represent attractive approaches. Addressing each of these challenges would be essential in not only building comprehensive fundamental knowledge of m6A in CVD, but also bridging the gap between basic and translational research.

References

1. Ivan, M., et al., *HIF α targeted for VHL-mediated destruction by proline hydroxylation: implications for O₂ sensing*. Science, 2001. **292**(5516): p. 464-8.
2. Koch, S., et al., *Signal transduction by vascular endothelial growth factor receptors*. Biochem J, 2011. **437**(2): p. 169-83.
3. Carmeliet, P. and R.K. Jain, *Molecular mechanisms and clinical applications of angiogenesis*. Nature, 2011. **473**(7347): p. 298-307.
4. Hellstrom, M., et al., *Dll4 signalling through Notch1 regulates formation of tip cells during angiogenesis*. Nature, 2007. **445**(7129): p. 776-80.
5. Gerhardt, H., *VEGF and endothelial guidance in angiogenic sprouting*. Organogenesis, 2008. **4**(4): p. 241-6.
6. Ruhrberg, C., et al., *Spatially restricted patterning cues provided by heparin-binding VEGF-A control blood vessel branching morphogenesis*. Genes Dev, 2002. **16**(20): p. 2684-98.
7. Kamei, M., et al., *Endothelial tubes assemble from intracellular vacuoles in vivo*. Nature, 2006. **442**(7101): p. 453-6.
8. Blum, Y., et al., *Complex cell rearrangements during intersegmental vessel sprouting and vessel fusion in the zebrafish embryo*. Dev Biol, 2008. **316**(2): p. 312-22.
9. Geudens, I. and H. Gerhardt, *Coordinating cell behaviour during blood vessel formation*. Development, 2011. **138**(21): p. 4569-83.
10. Fantin, A., et al., *Tissue macrophages act as cellular chaperones for vascular anastomosis downstream of VEGF-mediated endothelial tip cell induction*. Blood, 2010. **116**(5): p. 829-40.
11. Almagro, S., et al., *The motor protein myosin-X transports VE-cadherin along filopodia to allow the formation of early endothelial cell-cell contacts*. Mol Cell Biol, 2010. **30**(7): p. 1703-17.
12. Wild, S., et al., *Global prevalence of diabetes: estimates for the year 2000 and projections for 2030*. Diabetes Care, 2004. **27**(5): p. 1047-53.
13. Chatterjee, S., K. Khunti, and M.J. Davies, *Type 2 diabetes*. Lancet, 2017. **389**(10085): p. 2239-2251.
14. Seuring, T., O. Archangelidi, and M. Suhrcke, *The Economic Costs of Type 2 Diabetes: A Global Systematic Review*. Pharmacoeconomics, 2015. **33**(8): p. 811-31.
15. DeFronzo, R.A., et al., *Type 2 diabetes mellitus*. Nat Rev Dis Primers, 2015. **1**: p. 15019.
16. Philippe, M.F., et al., *Pancreatic volume and endocrine and exocrine functions in patients with diabetes*. Pancreas, 2011. **40**(3): p. 359-63.
17. Galicia-Garcia, U., et al., *Pathophysiology of Type 2 Diabetes Mellitus*. Int J Mol Sci, 2020. **21**(17).
18. Martin-Timon, I., et al., *Type 2 diabetes and cardiovascular disease: Have all risk factors the same strength?* World J Diabetes, 2014. **5**(4): p. 444-70.
19. Rawal, S., P. Manning, and R. Katare, *Cardiovascular microRNAs: as modulators and diagnostic biomarkers of diabetic heart disease*. Cardiovasc Diabetol, 2014. **13**: p. 44.
20. Nicholls, S.J., et al., *Effect of diabetes on progression of coronary atherosclerosis and arterial remodeling: a pooled analysis of 5 intravascular ultrasound trials*. J Am Coll Cardiol, 2008. **52**(4): p. 255-62.

21. Wang, C.C., M.L. Goalstone, and B. Draznin, *Molecular mechanisms of insulin resistance that impact cardiovascular biology*. Diabetes, 2004. **53**(11): p. 2735-40.
22. Carmena, R., P. Duriez, and J.C. Fruchart, *Atherogenic lipoprotein particles in atherosclerosis*. Circulation, 2004. **109**(23 Suppl 1): p. III2-7.
23. Bornfeldt, K.E., *2013 Russell Ross memorial lecture in vascular biology: cellular and molecular mechanisms of diabetes mellitus-accelerated atherosclerosis*. Arterioscler Thromb Vasc Biol, 2014. **34**(4): p. 705-14.
24. Low Wang, C.C., et al., *Clinical Update: Cardiovascular Disease in Diabetes Mellitus: Atherosclerotic Cardiovascular Disease and Heart Failure in Type 2 Diabetes Mellitus - Mechanisms, Management, and Clinical Considerations*. Circulation, 2016. **133**(24): p. 2459-502.
25. Bornfeldt, K.E. and I. Tabas, *Insulin resistance, hyperglycemia, and atherosclerosis*. Cell Metab, 2011. **14**(5): p. 575-85.
26. Yahagi, K., et al., *Pathology of Human Coronary and Carotid Artery Atherosclerosis and Vascular Calcification in Diabetes Mellitus*. Arterioscler Thromb Vasc Biol, 2017. **37**(2): p. 191-204.
27. Kyrgios, I., et al., *Suboptimal glycaemic control enhances the risk of impaired prothrombotic state in youths with type 1 diabetes mellitus*. Diab Vasc Dis Res, 2014. **11**(3): p. 208-16.
28. Kim, H.K., et al., *High coagulation factor levels and low protein C levels contribute to enhanced thrombin generation in patients with diabetes who do not have macrovascular complications*. J Diabetes Complications, 2014. **28**(3): p. 365-9.
29. Makarevich, P.I., *Therapeutic Angiogenesis: Foundations and Practical Application*. 2017, sine loco: IntechOpen.
30. Johnson, T., et al., *Approaches to therapeutic angiogenesis for ischemic heart disease*. J Mol Med (Berl), 2019. **97**(2): p. 141-151.
31. de Groot, D., G. Pasterkamp, and I.E. Hoefer, *Cardiovascular risk factors and collateral artery formation*. Eur J Clin Invest, 2009. **39**(12): p. 1036-47.
32. Balaji, S., et al., *The Role of Endothelial Progenitor Cells in Postnatal Vasculogenesis: Implications for Therapeutic Neovascularization and Wound Healing*. Adv Wound Care (New Rochelle), 2013. **2**(6): p. 283-295.
33. Lazarous, D.F., et al., *Pharmacodynamics of basic fibroblast growth factor: route of administration determines myocardial and systemic distribution*. Cardiovasc Res, 1997. **36**(1): p. 78-85.
34. Grochot-Przeczek, A., J. Dulak, and A. Jozkowicz, *Therapeutic angiogenesis for revascularization in peripheral artery disease*. Gene, 2013. **525**(2): p. 220-8.
35. Wolff, J.A., et al., *Direct gene transfer into mouse muscle in vivo*. Science, 1990. **247**(4949 Pt 1): p. 1465-8.
36. Yla-Herttuala, S. and K. Alitalo, *Gene transfer as a tool to induce therapeutic vascular growth*. Nat Med, 2003. **9**(6): p. 694-701.
37. Takahashi, T., et al., *Ischemia- and cytokine-induced mobilization of bone marrow-derived endothelial progenitor cells for neovascularization*. Nat Med, 1999. **5**(4): p. 434-8.
38. Asahara, T., et al., *VEGF contributes to postnatal neovascularization by mobilizing bone marrow-derived endothelial progenitor cells*. EMBO J, 1999. **18**(14): p. 3964-72.

39. Takahashi, K. and S. Yamanaka, *Induction of pluripotent stem cells from mouse embryonic and adult fibroblast cultures by defined factors*. Cell, 2006. **126**(4): p. 663-76.
40. Maherali, N., et al., *Directly reprogrammed fibroblasts show global epigenetic remodeling and widespread tissue contribution*. Cell Stem Cell, 2007. **1**(1): p. 55-70.
41. Li, X., et al., *Exosomes derived from endothelial progenitor cells attenuate vascular repair and accelerate reendothelialization by enhancing endothelial function*. Cytotherapy, 2016. **18**(2): p. 253-62.
42. Gray, W.D., et al., *Identification of therapeutic covariant microRNA clusters in hypoxia-treated cardiac progenitor cell exosomes using systems biology*. Circ Res, 2015. **116**(2): p. 255-63.
43. Kang, K., et al., *Exosomes Secreted from CXCR4 Overexpressing Mesenchymal Stem Cells Promote Cardioprotection via Akt Signaling Pathway following Myocardial Infarction*. Stem Cells Int, 2015. **2015**: p. 659890.
44. Ma, J., et al., *Exosomes Derived from Akt-Modified Human Umbilical Cord Mesenchymal Stem Cells Improve Cardiac Regeneration and Promote Angiogenesis via Activating Platelet-Derived Growth Factor D*. Stem Cells Transl Med, 2017. **6**(1): p. 51-59.
45. Bian, S., et al., *Extracellular vesicles derived from human bone marrow mesenchymal stem cells promote angiogenesis in a rat myocardial infarction model*. J Mol Med (Berl), 2014. **92**(4): p. 387-97.
46. Teng, X., et al., *Mesenchymal Stem Cell-Derived Exosomes Improve the Microenvironment of Infarcted Myocardium Contributing to Angiogenesis and Anti-Inflammation*. Cell Physiol Biochem, 2015. **37**(6): p. 2415-24.
47. Zhang, Z., et al., *Pretreatment of Cardiac Stem Cells With Exosomes Derived From Mesenchymal Stem Cells Enhances Myocardial Repair*. J Am Heart Assoc, 2016. **5**(1).
48. Wang, N., et al., *Mesenchymal stem cells-derived extracellular vesicles, via miR-210, improve infarcted cardiac function by promotion of angiogenesis*. Biochim Biophys Acta Mol Basis Dis, 2017. **1863**(8): p. 2085-2092.
49. Khan, M., et al., *Embryonic stem cell-derived exosomes promote endogenous repair mechanisms and enhance cardiac function following myocardial infarction*. Circ Res, 2015. **117**(1): p. 52-64.
50. Kervadec, A., et al., *Cardiovascular progenitor-derived extracellular vesicles recapitulate the beneficial effects of their parent cells in the treatment of chronic heart failure*. J Heart Lung Transplant, 2016. **35**(6): p. 795-807.
51. Barile, L., et al., *Extracellular vesicles from human cardiac progenitor cells inhibit cardiomyocyte apoptosis and improve cardiac function after myocardial infarction*. Cardiovasc Res, 2014. **103**(4): p. 530-41.
52. Tseliou, E., et al., *Fibroblasts Rendered Antifibrotic, Antiapoptotic, and Angiogenic by Priming With Cardiosphere-Derived Extracellular Membrane Vesicles*. J Am Coll Cardiol, 2015. **66**(6): p. 599-611.
53. Agarwal, U., et al., *Experimental, Systems, and Computational Approaches to Understanding the MicroRNA-Mediated Reparative Potential of Cardiac Progenitor Cell-Derived Exosomes From Pediatric Patients*. Circ Res, 2017. **120**(4): p. 701-712.
54. Gallet, R., et al., *Exosomes secreted by cardiosphere-derived cells reduce scarring, attenuate adverse remodelling, and improve function in acute and chronic porcine myocardial infarction*. Eur Heart J, 2017. **38**(3): p. 201-211.

55. Foglio, E., et al., *Exosomal clusterin, identified in the pericardial fluid, improves myocardial performance following MI through epicardial activation, enhanced arteriogenesis and reduced apoptosis*. *Int J Cardiol*, 2015. **197**: p. 333-47.
56. Escudier, B., et al., *Vaccination of metastatic melanoma patients with autologous dendritic cell (DC) derived-exosomes: results of the first phase I clinical trial*. *J Transl Med*, 2005. **3**(1): p. 10.
57. Conlan, R.S., et al., *Exosomes as Reconfigurable Therapeutic Systems*. *Trends Mol Med*, 2017. **23**(7): p. 636-650.
58. Chen, T.S., et al., *Enabling a robust scalable manufacturing process for therapeutic exosomes through oncogenic immortalization of human ESC-derived MSCs*. *J Transl Med*, 2011. **9**: p. 47.
59. Besnier, M., et al., *miR-15a/16 Inhibit Angiogenesis by Targeting the Tie2 Coding Sequence: Therapeutic Potential of a miR-15a/16 Decoy System in Limb Ischemia*. *Mol Ther Nucleic Acids*, 2019. **17**: p. 49-62.
60. Friedman, R.C., et al., *Most mammalian mRNAs are conserved targets of microRNAs*. *Genome Res*, 2009. **19**(1): p. 92-105.
61. Condrat, C.E., et al., *miRNAs as Biomarkers in Disease: Latest Findings Regarding Their Role in Diagnosis and Prognosis*. *Cells*, 2020. **9**(2).
62. Lee, Y., et al., *MicroRNA genes are transcribed by RNA polymerase II*. *EMBO J*, 2004. **23**(20): p. 4051-60.
63. Cai, X., C.H. Hagedorn, and B.R. Cullen, *Human microRNAs are processed from capped, polyadenylated transcripts that can also function as mRNAs*. *RNA*, 2004. **10**(12): p. 1957-66.
64. Han, J., et al., *The Drosha-DGCR8 complex in primary microRNA processing*. *Genes Dev*, 2004. **18**(24): p. 3016-27.
65. Han, J., et al., *Molecular basis for the recognition of primary microRNAs by the Drosha-DGCR8 complex*. *Cell*, 2006. **125**(5): p. 887-901.
66. Bohnsack, M.T., K. Czaplinski, and D. Gorlich, *Exportin 5 is a RanGTP-dependent dsRNA-binding protein that mediates nuclear export of pre-miRNAs*. *RNA*, 2004. **10**(2): p. 185-91.
67. Denli, A.M., et al., *Processing of primary microRNAs by the Microprocessor complex*. *Nature*, 2004. **432**(7014): p. 231-5.
68. Ameres, S.L. and P.D. Zamore, *Diversifying microRNA sequence and function*. *Nat Rev Mol Cell Biol*, 2013. **14**(8): p. 475-88.
69. Treiber, T., N. Treiber, and G. Meister, *Regulation of microRNA biogenesis and its crosstalk with other cellular pathways*. *Nat Rev Mol Cell Biol*, 2019. **20**(1): p. 5-20.
70. Behm-Ansmant, I., et al., *mRNA degradation by miRNAs and GW182 requires both CCR4:NOT deadenylase and DCP1:DCP2 decapping complexes*. *Genes Dev*, 2006. **20**(14): p. 1885-98.
71. Jonas, S. and E. Izaurralde, *Towards a molecular understanding of microRNA-mediated gene silencing*. *Nat Rev Genet*, 2015. **16**(7): p. 421-33.
72. Braun, J.E., E. Huntzinger, and E. Izaurralde, *A molecular link between miRISCs and deadenylases provides new insight into the mechanism of gene silencing by microRNAs*. *Cold Spring Harb Perspect Biol*, 2012. **4**(12).
73. Boccaletto, P., et al., *MODOMICS: a database of RNA modification pathways. 2017 update*. *Nucleic Acids Res*, 2018. **46**(D1): p. D303-D307.
74. Wei, C.M. and B. Moss, *Nucleotide sequences at the N6-methyladenosine sites of HeLa cell messenger ribonucleic acid*. *Biochemistry*, 1977. **16**(8): p. 1672-6.

75. Rottman, F., A.J. Shatkin, and R.P. Perry, *Sequences containing methylated nucleotides at the 5' termini of messenger RNAs: possible implications for processing*. Cell, 1974. **3**(3): p. 197-9.
76. Adams, J.M. and S. Cory, *Modified nucleosides and bizarre 5'-termini in mouse myeloma mRNA*. Nature, 1975. **255**(5503): p. 28-33.
77. Perry, R.P., et al., *The methylated constituents of L cell messenger RNA: evidence for an unusual cluster at the 5' terminus*. Cell, 1975. **4**(4): p. 387-94.
78. Jia, G., et al., *N6-methyladenosine in nuclear RNA is a major substrate of the obesity-associated FTO*. Nat Chem Biol, 2011. **7**(12): p. 885-7.
79. Dominissini, D., et al., *Topology of the human and mouse m6A RNA methylomes revealed by m6A-seq*. Nature, 2012. **485**(7397): p. 201-6.
80. Meyer, K.D., et al., *Comprehensive analysis of mRNA methylation reveals enrichment in 3' UTRs and near stop codons*. Cell, 2012. **149**(7): p. 1635-46.
81. Roost, C., et al., *Structure and thermodynamics of N6-methyladenosine in RNA: a spring-loaded base modification*. J Am Chem Soc, 2015. **137**(5): p. 2107-15.
82. Liu, N., et al., *N(6)-methyladenosine-dependent RNA structural switches regulate RNA-protein interactions*. Nature, 2015. **518**(7540): p. 560-4.
83. Cao, G., et al., *Recent advances in dynamic m6A RNA modification*. Open Biol, 2016. **6**(4): p. 160003.
84. Meyer, K.D. and S.R. Jaffrey, *Rethinking m(6)A Readers, Writers, and Erasers*. Annu Rev Cell Dev Biol, 2017. **33**: p. 319-342.
85. Peer, E., G. Rechavi, and D. Dominissini, *Epitranscriptomics: regulation of mRNA metabolism through modifications*. Curr Opin Chem Biol, 2017. **41**: p. 93-98.
86. Fu, Y., et al., *Gene expression regulation mediated through reversible m(6)A RNA methylation*. Nat Rev Genet, 2014. **15**(5): p. 293-306.
87. Niu, Y., et al., *N6-methyl-adenosine (m6A) in RNA: an old modification with a novel epigenetic function*. Genomics Proteomics Bioinformatics, 2013. **11**(1): p. 8-17.
88. Wang, X., et al., *Structural basis of N(6)-adenosine methylation by the METTL3-METTL14 complex*. Nature, 2016. **534**(7608): p. 575-8.
89. Wang, P., K.A. Doxtader, and Y. Nam, *Structural Basis for Cooperative Function of Mettl3 and Mettl14 Methyltransferases*. Mol Cell, 2016. **63**(2): p. 306-317.
90. Sledz, P. and M. Jinek, *Structural insights into the molecular mechanism of the m(6)A writer complex*. Elife, 2016. **5**.
91. Liu, J., et al., *A METTL3-METTL14 complex mediates mammalian nuclear RNA N6-adenosine methylation*. Nat Chem Biol, 2014. **10**(2): p. 93-5.
92. Wang, Y., et al., *N6-methyladenosine modification destabilizes developmental regulators in embryonic stem cells*. Nat Cell Biol, 2014. **16**(2): p. 191-8.
93. Little, N.A., N.D. Hastie, and R.C. Davies, *Identification of WTAP, a novel Wilms' tumour 1-associating protein*. Hum Mol Genet, 2000. **9**(15): p. 2231-9.
94. Schwartz, S., et al., *Perturbation of m6A writers reveals two distinct classes of mRNA methylation at internal and 5' sites*. Cell Rep, 2014. **8**(1): p. 284-96.
95. Ping, X.L., et al., *Mammalian WTAP is a regulatory subunit of the RNA N6-methyladenosine methyltransferase*. Cell Res, 2014. **24**(2): p. 177-89.
96. Liu, N., et al., *Probing N6-methyladenosine RNA modification status at single nucleotide resolution in mRNA and long noncoding RNA*. RNA, 2013. **19**(12): p. 1848-56.

97. Warda, A.S., et al., *Human METTL16 is a N(6)-methyladenosine (m(6)A) methyltransferase that targets pre-mRNAs and various non-coding RNAs*. EMBO Rep, 2017. **18**(11): p. 2004-2014.
98. Ruszkowska, A., et al., *Structural insights into the RNA methyltransferase domain of METTL16*. Sci Rep, 2018. **8**(1): p. 5311.
99. Doxtader, K.A., et al., *Structural Basis for Regulation of METTL16, an S-Adenosylmethionine Homeostasis Factor*. Mol Cell, 2018. **71**(6): p. 1001-1011 e4.
100. Fu, Y., et al., *FTO-mediated formation of N6-hydroxymethyladenosine and N6-formyladenosine in mammalian RNA*. Nat Commun, 2013. **4**: p. 1798.
101. Dina, C., et al., *Variation in FTO contributes to childhood obesity and severe adult obesity*. Nat Genet, 2007. **39**(6): p. 724-6.
102. Herbert, A., et al., *A common genetic variant is associated with adult and childhood obesity*. Science, 2006. **312**(5771): p. 279-83.
103. Scuteri, A., et al., *Genome-wide association scan shows genetic variants in the FTO gene are associated with obesity-related traits*. PLoS Genet, 2007. **3**(7): p. e115.
104. Gerken, T., et al., *The obesity-associated FTO gene encodes a 2-oxoglutarate-dependent nucleic acid demethylase*. Science, 2007. **318**(5855): p. 1469-72.
105. Jia, G., et al., *Oxidative demethylation of 3-methylthymine and 3-methyluracil in single-stranded DNA and RNA by mouse and human FTO*. FEBS Lett, 2008. **582**(23-24): p. 3313-9.
106. Zheng, G., et al., *ALKBH5 is a mammalian RNA demethylase that impacts RNA metabolism and mouse fertility*. Mol Cell, 2013. **49**(1): p. 18-29.
107. Tang, C., et al., *ALKBH5-dependent m6A demethylation controls splicing and stability of long 3'-UTR mRNAs in male germ cells*. Proc Natl Acad Sci U S A, 2018. **115**(2): p. E325-E333.
108. McTaggart, J.S., et al., *FTO is expressed in neurones throughout the brain and its expression is unaltered by fasting*. PLoS One, 2011. **6**(11): p. e27968.
109. Ho, A.J., et al., *A commonly carried allele of the obesity-related FTO gene is associated with reduced brain volume in the healthy elderly*. Proc Natl Acad Sci U S A, 2010. **107**(18): p. 8404-9.
110. Gao, X., et al., *The fat mass and obesity associated gene FTO functions in the brain to regulate postnatal growth in mice*. PLoS One, 2010. **5**(11): p. e14005.
111. Gulati, P., et al., *Fat mass and obesity-related (FTO) shuttles between the nucleus and cytoplasm*. Biosci Rep, 2014. **34**(5).
112. Zou, S., et al., *N(6)-Methyladenosine: a conformational marker that regulates the substrate specificity of human demethylases FTO and ALKBH5*. Sci Rep, 2016. **6**: p. 25677.
113. Mauer, J., et al., *Reversible methylation of m(6)A(m) in the 5' cap controls mRNA stability*. Nature, 2017. **541**(7637): p. 371-375.
114. Zaccara, S., R.J. Ries, and S.R. Jaffrey, *Reading, writing and erasing mRNA methylation*. Nat Rev Mol Cell Biol, 2019. **20**(10): p. 608-624.
115. Wei, J., et al., *Differential m(6)A, m(6)A(m), and m(1)A Demethylation Mediated by FTO in the Cell Nucleus and Cytoplasm*. Mol Cell, 2018. **71**(6): p. 973-985 e5.
116. Zhang, X., et al., *Structural insights into FTO's catalytic mechanism for the demethylation of multiple RNA substrates*. Proc Natl Acad Sci U S A, 2019. **116**(8): p. 2919-2924.

117. Han, Z., et al., *Crystal structure of the FTO protein reveals basis for its substrate specificity*. Nature, 2010. **464**(7292): p. 1205-9.
118. Wang, T., et al., *Fluorescein Derivatives as Bifunctional Molecules for the Simultaneous Inhibiting and Labeling of FTO Protein*. J Am Chem Soc, 2015. **137**(43): p. 13736-9.
119. Huang, Y., et al., *Meclofenamic acid selectively inhibits FTO demethylation of m6A over ALKBH5*. Nucleic Acids Res, 2015. **43**(1): p. 373-84.
120. Aik, W., et al., *Structural basis for inhibition of the fat mass and obesity associated protein (FTO)*. J Med Chem, 2013. **56**(9): p. 3680-8.
121. Chen, W., et al., *Crystal structure of the RNA demethylase ALKBH5 from zebrafish*. FEBS Lett, 2014. **588**(6): p. 892-8.
122. Aik, W., et al., *Structure of human RNA N(6)-methyladenine demethylase ALKBH5 provides insights into its mechanisms of nucleic acid recognition and demethylation*. Nucleic Acids Res, 2014. **42**(7): p. 4741-54.
123. Wang, X., et al., *N(6)-methyladenosine Modulates Messenger RNA Translation Efficiency*. Cell, 2015. **161**(6): p. 1388-99.
124. Shi, H., et al., *YTHDF3 facilitates translation and decay of N(6)-methyladenosine-modified RNA*. Cell Res, 2017. **27**(3): p. 315-328.
125. Li, A., et al., *Cytoplasmic m(6)A reader YTHDF3 promotes mRNA translation*. Cell Res, 2017. **27**(3): p. 444-447.
126. Xiao, W., et al., *Nuclear m(6)A Reader YTHDC1 Regulates mRNA Splicing*. Mol Cell, 2016. **61**(4): p. 507-519.
127. Roundtree, I.A., et al., *YTHDC1 mediates nuclear export of N(6)-methyladenosine methylated mRNAs*. Elife, 2017. **6**.
128. Kretschmer, J., et al., *The m(6)A reader protein YTHDC2 interacts with the small ribosomal subunit and the 5'-3' exoribonuclease XRN1*. RNA, 2018. **24**(10): p. 1339-1350.
129. Hsu, P.J., et al., *Ythdc2 is an N(6)-methyladenosine binding protein that regulates mammalian spermatogenesis*. Cell Res, 2017. **27**(9): p. 1115-1127.
130. Wu, B., et al., *Molecular basis for the specific and multivariant recognitions of RNA substrates by human hnRNP A2/B1*. Nat Commun, 2018. **9**(1): p. 420.
131. Song, H., et al., *METTL3 and ALKBH5 oppositely regulate m(6)A modification of TFEB mRNA, which dictates the fate of hypoxia/reoxygenation-treated cardiomyocytes*. Autophagy, 2019. **15**(8): p. 1419-1437.
132. Liu, N., et al., *N6-methyladenosine alters RNA structure to regulate binding of a low-complexity protein*. Nucleic Acids Res, 2017. **45**(10): p. 6051-6063.
133. Sweaad, W.K., et al., *Relevance of N6-methyladenosine regulators for transcriptome: Implications for development and the cardiovascular system*. J Mol Cell Cardiol, 2021. **160**: p. 56-70.
134. Zeng, Y., et al., *Refined RIP-seq protocol for epitranscriptome analysis with low input materials*. PLoS Biol, 2018. **16**(9): p. e2006092.
135. McIntyre, A.B.R., et al., *Limits in the detection of m(6)A changes using MeRIP/m(6)A-seq*. Sci Rep, 2020. **10**(1): p. 6590.
136. Liu, S., et al., *REPIC: a database for exploring the N(6)-methyladenosine methylome*. Genome Biol, 2020. **21**(1): p. 100.
137. Chen, K., et al., *High-resolution N(6) -methyladenosine (m(6) A) map using photo-crosslinking-assisted m(6) A sequencing*. Angew Chem Int Ed Engl, 2015. **54**(5): p. 1587-90.
138. Linder, B., et al., *Single-nucleotide-resolution mapping of m6A and m6Am throughout the transcriptome*. Nat Methods, 2015. **12**(8): p. 767-72.

139. Grozhik, A.V., et al., *Mapping m(6)A at Individual-Nucleotide Resolution Using Crosslinking and Immunoprecipitation (miCLIP)*. *Methods Mol Biol*, 2017. **1562**: p. 55-78.
140. Molinie, B., et al., *m(6)A-LAIC-seq reveals the census and complexity of the m(6)A epitranscriptome*. *Nat Methods*, 2016. **13**(8): p. 692-8.
141. Zhang, Z., et al., *Single-base mapping of m(6)A by an antibody-independent method*. *Sci Adv*, 2019. **5**(7): p. eaax0250.
142. Garcia-Campos, M.A., et al., *Deciphering the "m(6)A Code" via Antibody-Independent Quantitative Profiling*. *Cell*, 2019. **178**(3): p. 731-747 e16.
143. Meyer, K.D., *DART-seq: an antibody-free method for global m(6)A detection*. *Nat Methods*, 2019. **16**(12): p. 1275-1280.
144. Zhao, B.S., I.A. Roundtree, and C. He, *Publisher Correction: Post-transcriptional gene regulation by mRNA modifications*. *Nat Rev Mol Cell Biol*, 2018. **19**(12): p. 808.
145. Stoltzfus, C.M. and R.W. Dane, *Accumulation of spliced avian retrovirus mRNA is inhibited in S-adenosylmethionine-depleted chicken embryo fibroblasts*. *J Virol*, 1982. **42**(3): p. 918-31.
146. Camper, S.A., et al., *Effect of undermethylation on mRNA cytoplasmic appearance and half-life*. *Mol Cell Biol*, 1984. **4**(3): p. 538-43.
147. Zhao, X., et al., *FTO-dependent demethylation of N6-methyladenosine regulates mRNA splicing and is required for adipogenesis*. *Cell Res*, 2014. **24**(12): p. 1403-19.
148. Fustin, J.M., et al., *RNA-methylation-dependent RNA processing controls the speed of the circadian clock*. *Cell*, 2013. **155**(4): p. 793-806.
149. Lin, S., et al., *The m(6)A Methyltransferase METTL3 Promotes Translation in Human Cancer Cells*. *Mol Cell*, 2016. **62**(3): p. 335-345.
150. Huang, H., et al., *Recognition of RNA N(6)-methyladenosine by IGF2BP proteins enhances mRNA stability and translation*. *Nat Cell Biol*, 2018. **20**(3): p. 285-295.
151. Meyer, K.D., et al., *5' UTR m(6)A Promotes Cap-Independent Translation*. *Cell*, 2015. **163**(4): p. 999-1010.
152. Wang, X., et al., *N6-methyladenosine-dependent regulation of messenger RNA stability*. *Nature*, 2014. **505**(7481): p. 117-20.
153. Du, H., et al., *YTHDF2 destabilizes m(6)A-containing RNA through direct recruitment of the CCR4-NOT deadenylase complex*. *Nat Commun*, 2016. **7**: p. 12626.
154. Alarcon, C.R., et al., *N6-methyladenosine marks primary microRNAs for processing*. *Nature*, 2015. **519**(7544): p. 482-5.
155. Alarcon, C.R., et al., *HNRNPA2B1 Is a Mediator of m(6)A-Dependent Nuclear RNA Processing Events*. *Cell*, 2015. **162**(6): p. 1299-308.
156. Dorn, L.E., et al., *The N(6)-Methyladenosine mRNA Methylase METTL3 Controls Cardiac Homeostasis and Hypertrophy*. *Circulation*, 2019. **139**(4): p. 533-545.
157. van Berlo, J.H., M. Maillet, and J.D. Molkentin, *Signaling effectors underlying pathologic growth and remodeling of the heart*. *J Clin Invest*, 2013. **123**(1): p. 37-45.
158. Su, Y.R., et al., *Right ventricular protein expression profile in end-stage heart failure*. *Pulm Circ*, 2015. **5**(3): p. 481-97.

159. Mathiyalagan, P., et al., *FTO-Dependent N(6)-Methyladenosine Regulates Cardiac Function During Remodeling and Repair*. *Circulation*, 2019. **139**(4): p. 518-532.
160. Kmietczyk, V., et al., *m(6)A-mRNA methylation regulates cardiac gene expression and cellular growth*. *Life Sci Alliance*, 2019. **2**(2).
161. Berulava, T., et al., *Changes in m6A RNA methylation contribute to heart failure progression by modulating translation*. *Eur J Heart Fail*, 2020. **22**(1): p. 54-66.
162. Zhao, E. and M.J. Czaja, *Transcription factor EB: a central regulator of both the autophagosome and lysosome*. *Hepatology*, 2012. **55**(5): p. 1632-4.
163. Li, T., et al., *Silencing of METTL3 attenuates cardiac fibrosis induced by myocardial infarction via inhibiting the activation of cardiac fibroblasts*. *FASEB J*, 2021. **35**(2): p. e21162.
164. Zhang, C., et al., *m(6)A modulates haematopoietic stem and progenitor cell specification*. *Nature*, 2017. **549**(7671): p. 273-276.
165. Lv, J., et al., *Endothelial-specific m(6)A modulates mouse hematopoietic stem and progenitor cell development via Notch signaling*. *Cell Res*, 2018. **28**(2): p. 249-252.
166. Kruger, N., et al., *Loss of Endothelial FTO Antagonizes Obesity-Induced Metabolic and Vascular Dysfunction*. *Circ Res*, 2020. **126**(2): p. 232-242.
167. Yao, M.D., et al., *Role of METTL3-Dependent N(6)-Methyladenosine mRNA Modification in the Promotion of Angiogenesis*. *Mol Ther*, 2020. **28**(10): p. 2191-2202.
168. Chamorro-Jorganes, A., et al., *METTL3 Regulates Angiogenesis by Modulating let-7e-5p and miRNA-18a-5p Expression in Endothelial Cells*. *Arterioscler Thromb Vasc Biol*, 2021. **41**(6): p. e325-e337.
169. Dong, G., et al., *N6-Methyladenosine Methyltransferase METTL3 Promotes Angiogenesis and Atherosclerosis by Upregulating the JAK2/STAT3 Pathway via m6A Reader IGF2BP1*. *Front Cell Dev Biol*, 2021. **9**: p. 731810.
170. Jiang, W., et al., *The RNA Methyltransferase METTL3 Promotes Endothelial Progenitor Cell Angiogenesis in Mandibular Distraction Osteogenesis via the PI3K/AKT Pathway*. *Front Cell Dev Biol*, 2021. **9**: p. 720925.
171. Wang, L.J., et al., *Wilms' tumour 1-associating protein inhibits endothelial cell angiogenesis by m6A-dependent epigenetic silencing of desmoplakin in brain arteriovenous malformation*. *J Cell Mol Med*, 2020. **24**(9): p. 4981-4991.
172. Zhou, X., et al., *Desmoplakin is required for microvascular tube formation in culture*. *J Cell Sci*, 2004. **117**(Pt 15): p. 3129-40.
173. Garrod, D. and M. Chidgey, *Desmosome structure, composition and function*. *Biochim Biophys Acta*, 2008. **1778**(3): p. 572-87.
174. Nielsen, C.M., et al., *Mouse Models of Cerebral Arteriovenous Malformation*. *Stroke*, 2016. **47**(1): p. 293-300.
175. Jian, D., et al., *METTL14 aggravates endothelial inflammation and atherosclerosis by increasing FOXO1 N6-methyladenosine modifications*. *Theranostics*, 2020. **10**(20): p. 8939-8956.
176. Aijala, M., et al., *The fat mass and obesity-associated (FTO) gene variant rs9939609 predicts long-term incidence of cardiovascular disease and related death independent of the traditional risk factors*. *Ann Med*, 2015. **47**(8): p. 655-63.
177. Hubacek, J.A., et al., *The fat mass and obesity related gene polymorphism influences the risk of rejection in heart transplant patients*. *Clin Transplant*, 2018. **32**(12): p. e13443.

178. Wakil, S.M., et al., *A genome-wide association study reveals susceptibility loci for myocardial infarction/coronary artery disease in Saudi Arabs*. *Atherosclerosis*, 2016. **245**: p. 62-70.
179. Gustavsson, J., et al., *FTO genotype, physical activity, and coronary heart disease risk in Swedish men and women*. *Circ Cardiovasc Genet*, 2014. **7**(2): p. 171-7.
180. Shahid, S.U., et al., *Role of a common variant of Fat Mass and Obesity associated (FTO) gene in obesity and coronary artery disease in subjects from Punjab, Pakistan: a case control study*. *Lipids Health Dis*, 2016. **15**: p. 29.
181. Eckel, R.H., et al., *Prevention Conference VII: Obesity, a worldwide epidemic related to heart disease and stroke: executive summary*. *Circulation*, 2004. **110**(18): p. 2968-75.
182. Frayling, T.M., et al., *A common variant in the FTO gene is associated with body mass index and predisposes to childhood and adult obesity*. *Science*, 2007. **316**(5826): p. 889-94.
183. Hinney, A., et al., *Genome wide association (GWA) study for early onset extreme obesity supports the role of fat mass and obesity associated gene (FTO) variants*. *PLoS One*, 2007. **2**(12): p. e1361.
184. Church, C., et al., *Overexpression of Fto leads to increased food intake and results in obesity*. *Nat Genet*, 2010. **42**(12): p. 1086-92.
185. Fischer, J., et al., *Inactivation of the Fto gene protects from obesity*. *Nature*, 2009. **458**(7240): p. 894-8.
186. Merkestein, M., et al., *FTO influences adipogenesis by regulating mitotic clonal expansion*. *Nat Commun*, 2015. **6**: p. 6792.
187. Wang, X., et al., *m(6)A mRNA methylation controls autophagy and adipogenesis by targeting Atg5 and Atg7*. *Autophagy*, 2020. **16**(7): p. 1221-1235.
188. Wu, R., et al., *FTO regulates adipogenesis by controlling cell cycle progression via m(6)A-YTHDF2 dependent mechanism*. *Biochim Biophys Acta Mol Cell Biol Lipids*, 2018. **1863**(10): p. 1323-1330.
189. Mo, X.B., et al., *Examination of the associations between m(6)A-associated single-nucleotide polymorphisms and blood pressure*. *Hypertens Res*, 2019. **42**(10): p. 1582-1589.
190. Wu, Q., et al., *Epitranscriptomic mechanisms of N6-methyladenosine methylation regulating mammalian hypertension development by determined spontaneously hypertensive rats pericytes*. *Epigenomics*, 2019. **11**(12): p. 1359-1370.
191. Kannel, W.B. and D.L. McGee, *Diabetes and Cardiovascular Disease: The Framingham Study*. *JAMA*, 1979. **241**(19): p. 2035-2038.
192. Norgren, L., et al., *Inter-Society Consensus for the Management of Peripheral Arterial Disease (TASC II)*. *J Vasc Surg*, 2007. **45 Suppl S**: p. S5-67.
193. Shen, F., et al., *Decreased N(6)-methyladenosine in peripheral blood RNA from diabetic patients is associated with FTO expression rather than ALKBH5*. *J Clin Endocrinol Metab*, 2015. **100**(1): p. E148-54.
194. Ford, K.L., et al., *Optimisation of laboratory methods for whole transcriptomic RNA analyses in human left ventricular biopsies and blood samples of clinical relevance*. *PLoS One*, 2019. **14**(3): p. e0213685.
195. Caporali, A., et al., *Deregulation of microRNA-503 contributes to diabetes mellitus-induced impairment of endothelial function and reparative angiogenesis after limb ischemia*. *Circulation*, 2011. **123**(3): p. 282-91.

196. Jeggari, A., D.S. Marks, and E. Larsson, *miRcode: a map of putative microRNA target sites in the long non-coding transcriptome*. *Bioinformatics*, 2012. **28**(15): p. 2062-3.
197. Huang da, W., B.T. Sherman, and R.A. Lempicki, *Systematic and integrative analysis of large gene lists using DAVID bioinformatics resources*. *Nat Protoc*, 2009. **4**(1): p. 44-57.
198. Wang, X., et al., *Corrigendum: Structural basis of N(6)-adenosine methylation by the METTL3-METTL14 complex*. *Nature*, 2017. **542**(7640): p. 260.
199. Bartel, D.P., *MicroRNAs: genomics, biogenesis, mechanism, and function*. *Cell*, 2004. **116**(2): p. 281-97.
200. Fernandez-Hernando, C. and Y. Suarez, *MicroRNAs in endothelial cell homeostasis and vascular disease*. *Curr Opin Hematol*, 2018. **25**(3): p. 227-236.
201. Chen, M., et al., *RNA N6-methyladenosine methyltransferase-like 3 promotes liver cancer progression through YTHDF2-dependent posttranscriptional silencing of SOCS2*. *Hepatology*, 2018. **67**(6): p. 2254-2270.
202. Chamorro-Jorganes, A., et al., *VEGF-Induced Expression of miR-17-92 Cluster in Endothelial Cells Is Mediated by ERK/ELK1 Activation and Regulates Angiogenesis*. *Circ Res*, 2016. **118**(1): p. 38-47.
203. Poliseno, L., et al., *MicroRNAs modulate the angiogenic properties of HUVECs*. *Blood*, 2006. **108**(9): p. 3068-71.
204. Landskroner-Eiger, S., et al., *Endothelial miR-17 approximately 92 cluster negatively regulates arteriogenesis via miRNA-19 repression of WNT signaling*. *Proc Natl Acad Sci U S A*, 2015. **112**(41): p. 12812-7.
205. Iruela-Arispe, M.L., P. Bornstein, and H. Sage, *Thrombospondin exerts an antiangiogenic effect on cord formation by endothelial cells in vitro*. *Proc Natl Acad Sci U S A*, 1991. **88**(11): p. 5026-30.
206. Kuehbacher, A., et al., *Role of Dicer and Drosha for endothelial microRNA expression and angiogenesis*. *Circ Res*, 2007. **101**(1): p. 59-68.
207. Suarez, Y., et al., *Dicer-dependent endothelial microRNAs are necessary for postnatal angiogenesis*. *Proc Natl Acad Sci U S A*, 2008. **105**(37): p. 14082-7.
208. van den Homberg, D.A.L., et al., *N-6-Methyladenosine in Vasoactive microRNAs during Hypoxia; A Novel Role for METTL4*. *Int J Mol Sci*, 2022. **23**(3).
209. Wang, L.J., et al., *N6-methyladenosine methyltransferase METTL3 affects the phenotype of cerebral arteriovenous malformation via modulating Notch signaling pathway*. *J Biomed Sci*, 2020. **27**(1): p. 62.
210. Huang, H., H. Weng, and J. Chen, *m(6)A Modification in Coding and Non-coding RNAs: Roles and Therapeutic Implications in Cancer*. *Cancer Cell*, 2020. **37**(3): p. 270-288.
211. Di Timoteo, G., et al., *Modulation of circRNA Metabolism by m(6)A Modification*. *Cell Rep*, 2020. **31**(6): p. 107641.
212. Paneni, F., et al., *Diabetes and vascular disease: pathophysiology, clinical consequences, and medical therapy: part I*. *Eur Heart J*, 2013. **34**(31): p. 2436-43.
213. Domingueti, C.P., et al., *Diabetes mellitus: The linkage between oxidative stress, inflammation, hypercoagulability and vascular complications*. *J Diabetes Complications*, 2016. **30**(4): p. 738-45.
214. Geraldles, P. and G.L. King, *Activation of protein kinase C isoforms and its impact on diabetic complications*. *Circ Res*, 2010. **106**(8): p. 1319-31.

215. Giannini, C., et al., *Macrovascular angiopathy in children and adolescents with type 1 diabetes*. *Diabetes Metab Res Rev*, 2011. **27**(5): p. 436-60.
216. Caballero, A.E., *Endothelial dysfunction in obesity and insulin resistance: a road to diabetes and heart disease*. *Obes Res*, 2003. **11**(11): p. 1278-89.
217. SMITH, U., et al., *Insulin Signaling and Action in Fat Cells: Associations with Insulin Resistance and Type 2 Diabetes*. *Annals of the New York Academy of Sciences*, 1999. **892**(1): p. 119-126.
218. Yang, Y., et al., *Glucose Is Involved in the Dynamic Regulation of m6A in Patients With Type 2 Diabetes*. *J Clin Endocrinol Metab*, 2019. **104**(3): p. 665-673.
219. Rawal, S., et al., *Down-regulation of proangiogenic microRNA-126 and microRNA-132 are early modulators of diabetic cardiac microangiopathy*. *Cardiovasc Res*, 2017. **113**(1): p. 90-101.
220. Katare, R., et al., *Intravenous gene therapy with PIM-1 via a cardiotropic viral vector halts the progression of diabetic cardiomyopathy through promotion of prosurvival signaling*. *Circ Res*, 2011. **108**(10): p. 1238-51.
221. Nathan, D.M., for the *Diabetes Control and Complications Trial/Epidemiology of Diabetes Interventions and Complications (DCCT/EDIC) Study Research Group*. *Intensive diabetes treatment and cardiovascular disease in patients with type 1 diabetes*. *N Engl J Med*, 2005. **353**: p. 2643-2653.
222. Diabetes, C., et al., *Retinopathy and nephropathy in patients with type 1 diabetes four years after a trial of intensive therapy*. *N Engl J Med*, 2000. **342**(6): p. 381-9.
223. De Jesus, D.F., et al., *m(6)A mRNA Methylation Regulates Human beta-Cell Biology in Physiological States and in Type 2 Diabetes*. *Nat Metab*, 2019. **1**(8): p. 765-774.
224. Vausort, M., et al., *Regulation of N6-Methyladenosine after Myocardial Infarction*. *Cells*, 2022. **11**(15).
225. Xie, W., et al., *METTL3 inhibits hepatic insulin sensitivity via N6-methyladenosine modification of Fasn mRNA and promoting fatty acid metabolism*. *Biochem Biophys Res Commun*, 2019. **518**(1): p. 120-126.
226. Belch, J.J., et al., *Critical issues in peripheral arterial disease detection and management: a call to action*. *Arch Intern Med*, 2003. **163**(8): p. 884-92.
227. Annex, B.H., *Therapeutic angiogenesis for critical limb ischaemia*. *Nat Rev Cardiol*, 2013. **10**(7): p. 387-96.
228. Fowkes, F.G., et al., *Comparison of global estimates of prevalence and risk factors for peripheral artery disease in 2000 and 2010: a systematic review and analysis*. *Lancet*, 2013. **382**(9901): p. 1329-40.
229. Jude, E.B., et al., *Peripheral arterial disease in diabetic and nondiabetic patients: a comparison of severity and outcome*. *Diabetes Care*, 2001. **24**(8): p. 1433-7.
230. Nehler, M.R., et al., *Epidemiology of peripheral arterial disease and critical limb ischemia in an insured national population*. *J Vasc Surg*, 2014. **60**(3): p. 686-95 e2.
231. Teraa, M., et al., *Critical Limb Ischemia: Current Trends and Future Directions*. *J Am Heart Assoc*, 2016. **5**(2).
232. Lawall, H., et al., *Health related quality of life in patients with critical limb ischemia*. *Vasa*, 2012. **41**(2): p. 78-88.
233. Hirsch, A.T., et al., *ACC/AHA 2005 Practice Guidelines for the management of patients with peripheral arterial disease (lower extremity, renal, mesenteric, and*

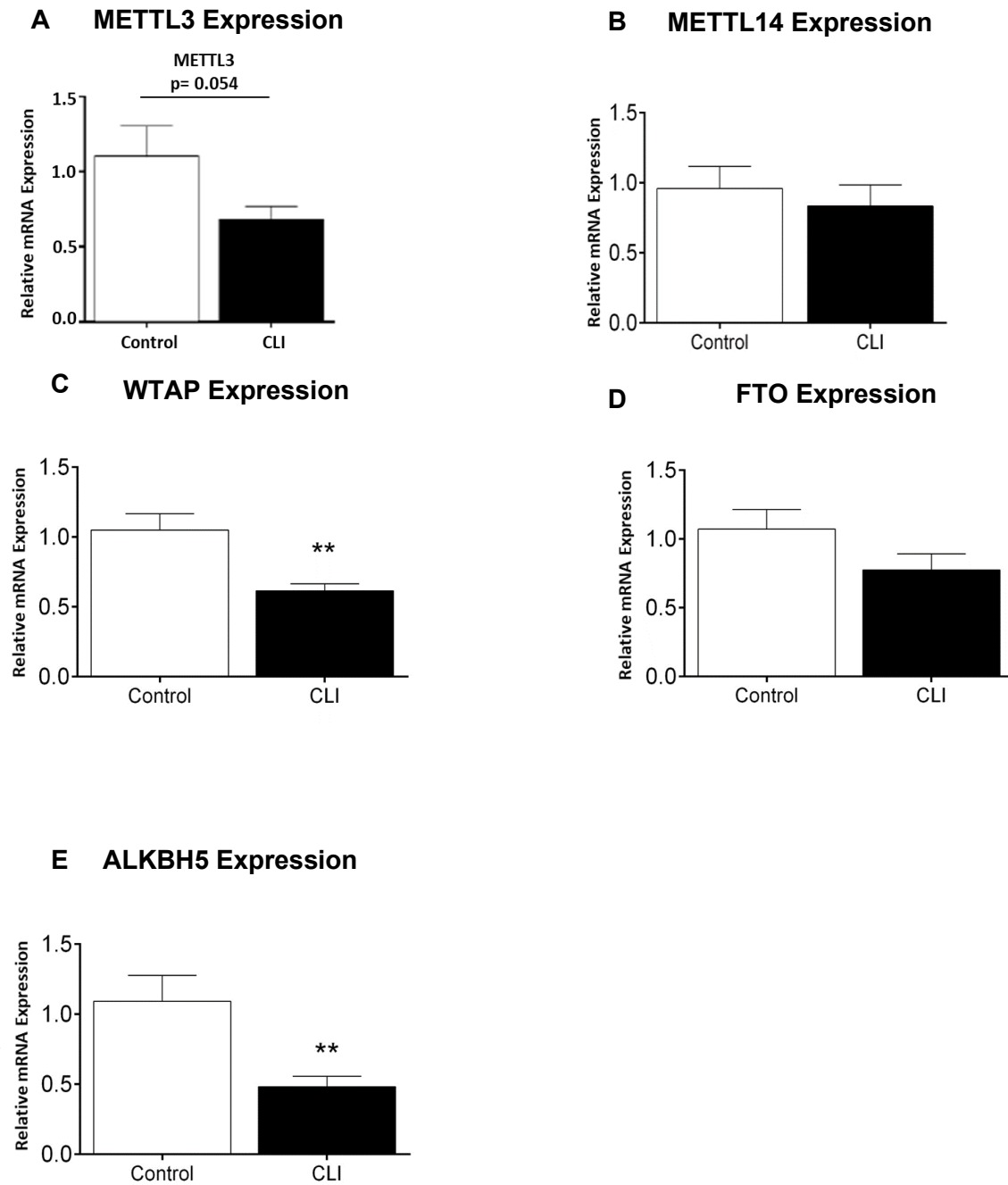
- abdominal aortic): a collaborative report from the American Association for Vascular Surgery/Society for Vascular Surgery, Society for Cardiovascular Angiography and Interventions, Society for Vascular Medicine and Biology, Society of Interventional Radiology, and the ACC/AHA Task Force on Practice Guidelines (Writing Committee to Develop Guidelines for the Management of Patients With Peripheral Arterial Disease): endorsed by the American Association of Cardiovascular and Pulmonary Rehabilitation; National Heart, Lung, and Blood Institute; Society for Vascular Nursing; TransAtlantic Inter-Society Consensus; and Vascular Disease Foundation. Circulation, 2006. 113(11): p. e463-654.*
234. Kinlay, S., *Management of Critical Limb Ischemia*. *Circ Cardiovasc Interv*, 2016. **9**(2): p. e001946.
 235. Laoire, A.N. and F.E.M. Murtagh, *Systematic review of pharmacological therapies for the management of ischaemic pain in patients with non-reconstructable critical limb ischaemia*. *BMJ Support Palliat Care*, 2018. **8**(4): p. 400-410.
 236. Gulcan, E., et al., *Statins may be useful in diabetic foot ulceration treatment and prevention*. *Med Hypotheses*, 2007. **69**(6): p. 1313-5.
 237. Schanzer, A., et al., *Statins are independently associated with reduced mortality in patients undergoing infrainguinal bypass graft surgery for critical limb ischemia*. *J Vasc Surg*, 2008. **47**(4): p. 774-781.
 238. Fernandez, N., et al., *Predictors of failure and success of tibial interventions for critical limb ischemia*. *J Vasc Surg*, 2010. **52**(4): p. 834-42.
 239. Nagaya, N., *Orally active prostacyclin analogue for cardiovascular disease*. *Int Angiol*, 2010. **29**(2 Suppl): p. 14-8.
 240. Creutzig, A., W. Lehmacher, and M. Elze, *Meta-analysis of randomised controlled prostaglandin E1 studies in peripheral arterial occlusive disease stages III and IV*. *Vasa*, 2004. **33**(3): p. 137-44.
 241. Ruffolo, A.J., M. Romano, and A. Ciapponi, *Prostanoids for critical limb ischaemia*. *Cochrane Database Syst Rev*, 2010(1): p. CD006544.
 242. Brass, E.P., et al., *Parenteral therapy with lipo-ecraprost, a lipid-based formulation of a PGE1 analog, does not alter six-month outcomes in patients with critical leg ischemia*. *J Vasc Surg*, 2006. **43**(4): p. 752-9.
 243. Antithrombotic Trialists, C., et al., *Aspirin in the primary and secondary prevention of vascular disease: collaborative meta-analysis of individual participant data from randomised trials*. *Lancet*, 2009. **373**(9678): p. 1849-60.
 244. European Stroke, O., et al., *ESC Guidelines on the diagnosis and treatment of peripheral artery diseases: Document covering atherosclerotic disease of extracranial carotid and vertebral, mesenteric, renal, upper and lower extremity arteries: the Task Force on the Diagnosis and Treatment of Peripheral Artery Diseases of the European Society of Cardiology (ESC)*. *Eur Heart J*, 2011. **32**(22): p. 2851-906.
 245. Rudofker, E.W., S.E. Hogan, and E.J. Armstrong, *Preventing Major Amputations in Patients with Critical Limb Ischemia*. *Curr Cardiol Rep*, 2018. **20**(9): p. 74.
 246. Jones, W.S., et al., *High mortality risks after major lower extremity amputation in Medicare patients with peripheral artery disease*. *Am Heart J*, 2013. **165**(5): p. 809-15, 815 e1.
 247. Dormandy, J., L. Heeck, and S. Vig, *Major amputations: clinical patterns and predictors*. *Semin Vasc Surg*, 1999. **12**(2): p. 154-61.

248. Brechot, N., et al., *Modulation of macrophage activation state protects tissue from necrosis during critical limb ischemia in thrombospondin-1-deficient mice*. PLoS One, 2008. **3**(12): p. e3950.
249. Tuomisto, T.T., et al., *HIF-VEGF-VEGFR-2, TNF-alpha and IGF pathways are upregulated in critical human skeletal muscle ischemia as studied with DNA array*. Atherosclerosis, 2004. **174**(1): p. 111-20.
250. Bonauer, A., et al., *MicroRNA-92a controls angiogenesis and functional recovery of ischemic tissues in mice*. Science, 2009. **324**(5935): p. 1710-3.
251. Martello, A., et al., *Phenotypic miRNA Screen Identifies miR-26b to Promote the Growth and Survival of Endothelial Cells*. Mol Ther Nucleic Acids, 2018. **13**: p. 29-43.
252. Shi, L., et al., *MicroRNA-223 antagonizes angiogenesis by targeting beta1 integrin and preventing growth factor signaling in endothelial cells*. Circ Res, 2013. **113**(12): p. 1320-30.
253. Favier, J., et al., *Critical overexpression of thrombospondin 1 in chronic leg ischaemia*. J Pathol, 2005. **207**(3): p. 358-66.
254. Birdsey, G.M., et al., *The endothelial transcription factor ERG promotes vascular stability and growth through Wnt/beta-catenin signaling*. Dev Cell, 2015. **32**(1): p. 82-96.
255. Fadini, G.P., et al., *Angiogenic Abnormalities in Diabetes Mellitus: Mechanistic and Clinical Aspects*. J Clin Endocrinol Metab, 2019. **104**(11): p. 5431-5444.
256. Lin, J., et al., *Hypoxia Promotes Vascular Smooth Muscle Cell (VSMC) Differentiation of Adipose-Derived Stem Cell (ADSC) by Regulating Mettl3 and Paracrine Factors*. Stem Cells Int, 2020. **2020**: p. 2830565.
257. Schaper, N.C., J. Apelqvist, and K. Bakker, *Reducing lower leg amputations in diabetes: a challenge for patients, healthcare providers and the healthcare system*. Diabetologia, 2012. **55**(7): p. 1869-72.
258. group, T.w., *Management of peripheral arterial disease : Transatlantic inter-society consensus*. J. Vasc. Surg., 2000. **31**: p. S192-S273.
259. Papanas, N. and E. Maltezos, *Advances in treating the ischaemic diabetic foot*. Curr Vasc Pharmacol, 2008. **6**(1): p. 23-8.
260. Abaci, A., et al., *Effect of diabetes mellitus on formation of coronary collateral vessels*. Circulation, 1999. **99**(17): p. 2239-42.
261. Werner, G.S., et al., *Growth factors in the collateral circulation of chronic total coronary occlusions: relation to duration of occlusion and collateral function*. Circulation, 2004. **110**(14): p. 1940-5.
262. Fadini, G.P., et al., *The redox enzyme p66Shc contributes to diabetes and ischemia-induced delay in cutaneous wound healing*. Diabetes, 2010. **59**(9): p. 2306-14.
263. Okizaki, S., et al., *Vascular Endothelial Growth Factor Receptor Type 1 Signaling Prevents Delayed Wound Healing in Diabetes by Attenuating the Production of IL-1beta by Recruited Macrophages*. Am J Pathol, 2016. **186**(6): p. 1481-98.
264. Catrina, S.B. and X. Zheng, *Disturbed hypoxic responses as a pathogenic mechanism of diabetic foot ulcers*. Diabetes Metab Res Rev, 2016. **32** Suppl 1: p. 179-85.
265. Engstrom, G., et al., *Risk of treatment of peripheral arterial disease is related to inflammation-sensitive plasma proteins: a prospective cohort study*. J Vasc Surg, 2004. **40**(6): p. 1101-5.

266. Cotran, R.S., V. Kumar, and R. Stanley, *Robbins pathologic basis of disease*. 2004: WB Saunders CompHny, Philadelphia, USA.
267. Perez-Cremades, D., H.S. Cheng, and M.W. Feinberg, *Noncoding RNAs in Critical Limb Ischemia*. *Arterioscler Thromb Vasc Biol*, 2020. **40**(3): p. 523-533.
268. Severino, P., et al., *Diabetes Mellitus and Ischemic Heart Disease: The Role of Ion Channels*. *Int J Mol Sci*, 2018. **19**(3).
269. Townsend, N., et al., *Cardiovascular disease in Europe: epidemiological update 2016*. *Eur Heart J*, 2016. **37**(42): p. 3232-3245.
270. Benjamin, E.J., et al., *Heart Disease and Stroke Statistics-2017 Update: A Report From the American Heart Association*. *Circulation*, 2017. **135**(10): p. e146-e603.
271. Fedele, F., et al., *Role of genetic polymorphisms of ion channels in the pathophysiology of coronary microvascular dysfunction and ischemic heart disease*. *Basic Res Cardiol*, 2013. **108**(6): p. 387.
272. Fedele, F., et al., *Role of ion channels in coronary microcirculation: a review of the literature*. *Future Cardiol*, 2013. **9**(6): p. 897-905.
273. Chow, C.K., et al., *Association of diet, exercise, and smoking modification with risk of early cardiovascular events after acute coronary syndromes*. *Circulation*, 2010. **121**(6): p. 750-8.
274. Cholesterol Treatment Trialists, C., et al., *Efficacy and safety of more intensive lowering of LDL cholesterol: a meta-analysis of data from 170,000 participants in 26 randomised trials*. *Lancet*, 2010. **376**(9753): p. 1670-81.
275. Bhatheja, R. and D. Mukherjee, *Acute coronary syndromes: unstable angina/non-ST elevation myocardial infarction*. *Crit Care Clin*, 2007. **23**(4): p. 709-35, v.
276. Deedwania, P.C., *Diabetes is a vascular disease: the role of endothelial dysfunction in pathophysiology of cardiovascular disease in diabetes*. *Cardiol Clin*, 2004. **22**(4): p. 505-9, v.
277. Norhammar, A., et al., *Improved but still high short- and long-term mortality rates after myocardial infarction in patients with diabetes mellitus: a time-trend report from the Swedish Register of Information and Knowledge about Swedish Heart Intensive Care Admission*. *Heart*, 2007. **93**(12): p. 1577-83.
278. Scott, L.J., et al., *A genome-wide association study of type 2 diabetes in Finns detects multiple susceptibility variants*. *Science*, 2007. **316**(5829): p. 1341-5.
279. Quinones, M.A., et al., *Echocardiographic predictors of clinical outcome in patients with left ventricular dysfunction enrolled in the SOLVD registry and trials: significance of left ventricular hypertrophy*. *Studies of Left Ventricular Dysfunction*. *J Am Coll Cardiol*, 2000. **35**(5): p. 1237-44.
280. Howangyin, K.Y. and J.S. Silvestre, *Diabetes mellitus and ischemic diseases: molecular mechanisms of vascular repair dysfunction*. *Arterioscler Thromb Vasc Biol*, 2014. **34**(6): p. 1126-35.
281. Nossent, A.Y., *The epitranscriptome: RNA modifications in vascular remodelling*. *Atherosclerosis*, 2022.
282. Zhang, Y., et al., *Validated Impacts of N6-Methyladenosine Methylated mRNAs on Apoptosis and Angiogenesis in Myocardial Infarction Based on MeRIP-Seq Analysis*. *Front Mol Biosci*, 2021. **8**: p. 789923.
283. Ke, W.L., et al., *m(6)A demethylase FTO regulates the apoptosis and inflammation of cardiomyocytes via YAP1 in ischemia-reperfusion injury*. *Bioengineered*, 2022. **13**(3): p. 5443-5452.

284. Wu, X., et al., *Angiogenesis after acute myocardial infarction*. Cardiovasc Res, 2021. **117**(5): p. 1257-1273.
285. He, C., *Grand challenge commentary: RNA epigenetics?* Nat Chem Biol, 2010. **6**(12): p. 863-5.
286. Wen, J., et al., *Zc3h13 Regulates Nuclear RNA m(6)A Methylation and Mouse Embryonic Stem Cell Self-Renewal*. Mol Cell, 2018. **69**(6): p. 1028-1038 e6.
287. Geula, S., et al., *Stem cells. m6A mRNA methylation facilitates resolution of naive pluripotency toward differentiation*. Science, 2015. **347**(6225): p. 1002-6.
288. Batista, P.J., et al., *m(6)A RNA modification controls cell fate transition in mammalian embryonic stem cells*. Cell Stem Cell, 2014. **15**(6): p. 707-19.
289. Tirumuru, N., et al., *N(6)-methyladenosine of HIV-1 RNA regulates viral infection and HIV-1 Gag protein expression*. Elife, 2016. **5**.
290. Dai, D., et al., *N6-methyladenosine links RNA metabolism to cancer progression*. Cell Death Dis, 2018. **9**(2): p. 124.
291. Cully, M., *Chemical inhibitors make their RNA epigenetic mark*. Nat Rev Drug Discov, 2019. **18**(12): p. 892-894.
292. Wan, Y.K., et al., *Beyond sequencing: machine learning algorithms extract biology hidden in Nanopore signal data*. Trends Genet, 2022. **38**(3): p. 246-257.
293. Salvetat, N., et al., *A game changer for bipolar disorder diagnosis using RNA editing-based biomarkers*. Transl Psychiatry, 2022. **12**(1): p. 182.
294. Barbieri, I., et al., *Promoter-bound METTL3 maintains myeloid leukaemia by m(6)A-dependent translation control*. Nature, 2017. **552**(7683): p. 126-131.
295. Merkle, T., et al., *Precise RNA editing by recruiting endogenous ADARs with antisense oligonucleotides*. Nat Biotechnol, 2019. **37**(2): p. 133-138.
296. Descamps, B., et al., *BDNF (Brain-Derived Neurotrophic Factor) Promotes Embryonic Stem Cells Differentiation to Endothelial Cells Via a Molecular Pathway, Including MicroRNA-214, EZH2 (Enhancer of Zeste Homolog 2), and eNOS (Endothelial Nitric Oxide Synthase)*. Arterioscler Thromb Vasc Biol, 2018. **38**(9): p. 2117-2125.
297. Li, H., et al., *Nuclear miR-320 Mediates Diabetes-Induced Cardiac Dysfunction by Activating Transcription of Fatty Acid Metabolic Genes to Cause Lipotoxicity in the Heart*. Circ Res, 2019. **125**(12): p. 1106-1120.
298. Dominissini, D., et al., *Transcriptome-wide mapping of N(6)-methyladenosine by m(6)A-seq based on immunocapturing and massively parallel sequencing*. Nat Protoc, 2013. **8**(1): p. 176-89.
299. Smith, J., et al. *A High-Efficiency AAV for Endothelial Cell Transduction Throughout the Central Nervous System*. Gene Therapy Journal, 2022. **7**(4).

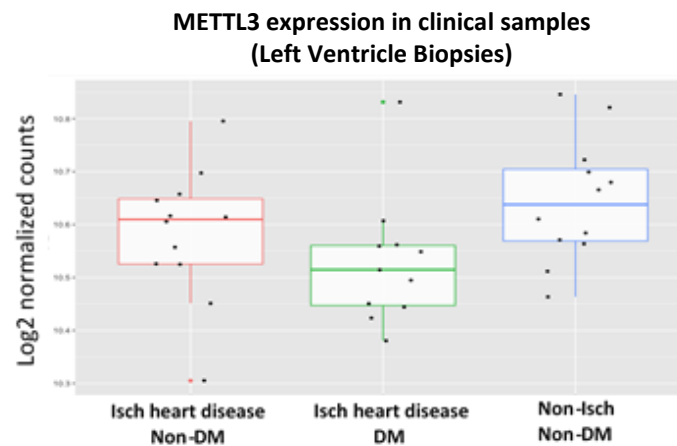
Appendix 1



Appendix 1 Dysregulation of m6A regulatory components in CLI patients.

Unpublished preliminary data from the Emanuelli lab. qRT-PCR analysis of (A) METTL3, (B) METTL14, (C) WTAP, (D) FTO and (E) ALKBH5 in limb muscles of diabetic patients with CLI undergoing lower limb amputation (n=8) and non-diabetic non-ischemic control patients undergoing saphenous vein stripping (n=10). 18s was used as housekeeping gene. All graphical data presented as mean ± SEM. Results were assessed by Mann-Whitney test comparison test applied. *P<0.05, **P<0.01, ***P<0.01, n.s non-significant vs control.

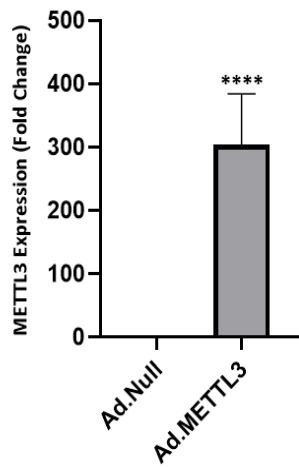
Appendix 2



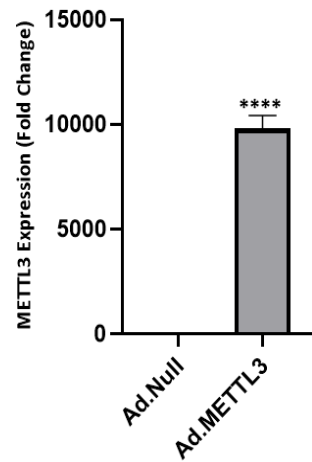
Appendix 2 Clinical expressional analysis of m6A machinery. Unpublished preliminary data from the Emanuelli lab. Transcriptome analysis by RNA-sequencing revealed a reduction in METTL3 levels in LV biopsies collected as part of perspective observational study ARCADIA.

Appendix 3

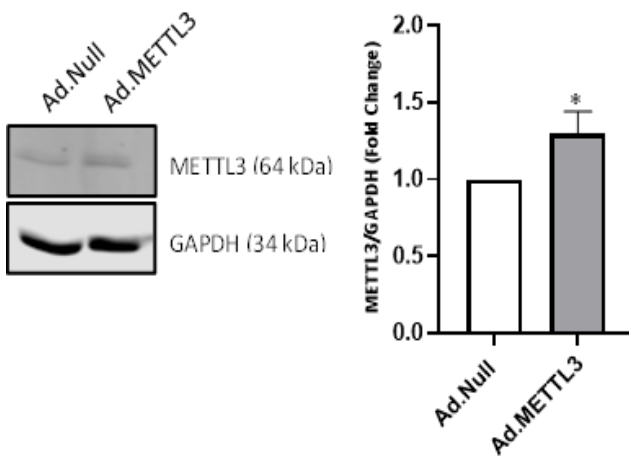
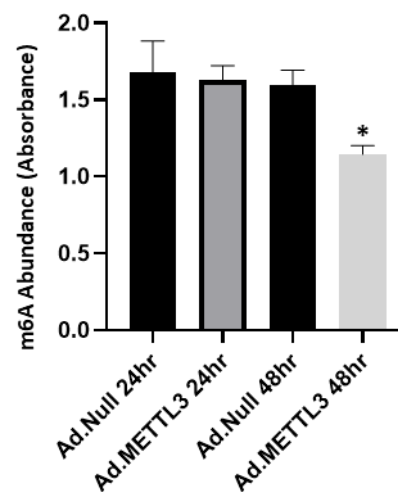
The interventional studies described in chapter 5 indicates that METTL3 overexpression may indeed promote revascularization in ischemic limb muscles, however a decrease in arteriogenesis and a lack of improvement in reperfusion suggests that the newly formed blood vessels are unable to efficiently deliver blood to the ischemic limb. Although validation experiments demonstrate an overexpression of human METTL3 and an increase in m6A in ECs isolated from Ad.METTL3 treated ischemic muscles (B and C), the adenovirus utilised does not specifically target ECs and we essentially would not know the proportion of ECs infected. Additionally, the impact of altering the methylation status of other local cell types is yet to be understood. To overcome this, our collaborator (Dr Graciela Sala-Newby, University of Bristol) worked towards producing an EC specific METTL3 adenovirus to express METTL3 under the VE-cadherin promoter. Preliminary studies presented in this appendix aimed to validate the effects of crude viral extracts on METTL3 expression and m6A levels. A murine cardiac EC line (MCEC-1), kindly provided by Prof. Justin Mason (NHLI Imperial College London), was infected with either Ad.Null or Ad.METTL3 for 24 or 48 hours. Quantitative polymerase chain reaction analysis of METTL3 revealed a 302.88- and 9824.38-fold increase in METTL3 expression at 24 and 48 hours respectively (A and B), while METTL3 protein levels increased by 40% following 24 hours of infection (C). The colorimetric based analysis of total m6A RNA levels indicated no changes in Ad.METTL3 infected cells compared to Ad.Null at the 24-hour timepoint, whereas the infection of MCECs with Ad.METTL3 resulted in a significant decrease in m6A levels at the 48 hours timepoint (D).

A

	Fold Change
Ad.Null	1.0000
Ad.METTL3	302.88

B

	Fold Change
Ad.Null	1.0000
Ad.METTL3	9824.38

C**D**

Appendix 3 Optimisation of Adenovirus for EC Specific Overexpression of METTL3. MCECs were infected with two crude viral extracts of Ad.Null or Ad.METTL3. (A-B) qRT-PCR analysis of METTL3 expression in MCECs following (A) 24 or (B) 48 hours of infection. 18s was used as housekeeping gene (n=3). (B) Quantification of METTL3 protein levels in MCECs was performed by western blot analysis. Representative blots are shown and western blot quantification is expressed as fold change vs Ad.Null (n=3). GAPDH was used as loading control. (C) Global m6A RNA methylation levels in MCECs were quantified using an ELISA based assay following 24- or 48-hours post infection (n=2, performed in triplicates). (A-C) Results were assessed by unpaired student t-test or (D) two-way ANOVA (Tukey's post hoc test). *P<0.05, **P<0.01, ***P<0.01, n.s non-significant vs Ad.Null.

